University of Reading

Rational Design and Optimisation of Polymer Microneedles for Drug Delivery

School of Chemistry, Food and Pharmacy

A thesis submitted for the degree of

Doctor of Philosophy (PhD)

Claudia Chiazor Aguguo

April 2024

DECLARATION OF ORIGINAL AUTHORSHIP

I confirm that this is my own work and the use of all materials from other sources has been properly and fully acknowledged.

Claudia Chiazor Aguguo

ACKNOWLEDGEMENTS

First and foremost, I would like to thank God Almighty for His faithfulness and kindness towards me and for seeing me through this journey. My Heavenly Father, I thank you for teaching, guiding, and providing for me. You brought me to this land, and you have consistently provided the manna and quail for this journey. Words cannot describe how grateful I am. I dedicate this work to you, and I lay it before you for your glory.

I would also like to express my profound appreciation to my parents, Chief Barrister Austin Aguguo and Evangelist Nkeiruka Aguguo. Thank you for your priceless support, for funding my education and for your prayers and care. I am immensely grateful to you, and I am blessed to be yours. Thank you to my wonderful brothers, Austin, Ausbeth and Auberon Aguguo. Thank you for your prayers and support, I really appreciate you all. Thank you to my lovely grandmother, Regina Ewuoma. I am blessed to have you in my life. Thank you for your prayers and your strong words of encouragement that have kept me going.

Massive thanks to my supervisors, Professor Adrian Williams and Professor Vitaliy Khutoryanskiy. I am very pleased to be supervised by you and I'm very grateful for your guidance and support. Thank you for your advice, words of encouragement and for the opportunities you provided. It is a privilege to learn from you.

I would also like to thank Dr Pedro Rivas-Ruiz, Amanpreet Kaur and Nicholas Michael at the University of Reading's Chemical Analysis Facility for their assistance with thermal analysis, scanning electron microscopy and mass spectrometry.

Thank you to my colleagues in Vitaliy's lab for their support with lab equipment, imaging and logistics. I wish you all the best in your future endeavours.

ABSTRACT

Microneedles (MNs) are promising drug delivery systems which enable the delivery of drugs of various physicochemical properties into and across the skin by breaching the skin barrier. Dissolving MNs are a type of MNs which release the incorporated drug by dissolving or degrading in the skin upon contact with the skin's interstitial fluid. Polymers are commonly used to fabricate dissolving MNs, but their mechanical properties limit efficient skin insertion. Therefore, there is a need to identify additional polymers which can create high quality MNs and potentially broaden the applicability of dissolving MNs.

This thesis investigated the feasibility of fabricating dissolving MNs from poly(2-ethyl-oxazoline) (PEOZ) of two molecular weights (50 kDa and 200 kDa) and used polyvinylpyrrolidone (PVP) MNs as a benchmark to evaluate the suitability of PEOZ for fabricating MNs. Findings from the characterisation studies suggest that PEOZ 200 kDa is a promising MN material with comparable performance to PVP whereas sole use of PEOZ 50 kDa is not suitable for MN fabrication.

PEOZ 50 kDa was then blended with poly(vinyl alcohol) (PVA) to assess for miscibility between the polymers in order to improve PEOZ 50 kDa MNs by polymer blending. Polymer miscibility was evaluated by using a combination of various analytical techniques, providing useful insights into polymer miscibility and the potential applications of PEOZ-PVA blends.

This thesis also showcases an innovative approach to treating cutaneous leishmaniasis (CL) by loading paromomycin into dissolving MNs and tailoring the MN composition to the disease. Characterisation studies suggest that the use of paromomycin-containing dissolving MNs is a promising approach to treating CL. Suggestions of additional studies are also proposed to further explore this drug delivery system. Studies towards developing a sensitive assay for quantifying paromomycin in MNs are also described, providing useful insights into paromomycin quantification by liquid chromatography and mass spectrometry.

TABLE OF CONTENTS

LIST OF FIGURES

LIST OF TABLES

CHAPTER 1 – GENERAL INTRODUCTION

1.1 STRUCTURE OF THE HUMAN SKIN

The skin has a surface area of approximately 1.8 m^2 and accounts for approximately 10% of the body mass in an average adult, making it the largest organ in the human body (1). It is a complex organ with a wide range of cell types and structures that enable it to perform its numerous functions, with its primary function being providing protection against the invasion of microorganisms, chemicals, allergens, etc (1-3). The skin comprises of three layers: epidermis, dermis, and hypodermis (Figure 1.1). It also contains hair follicles, sebaceous glands and sweat glands.

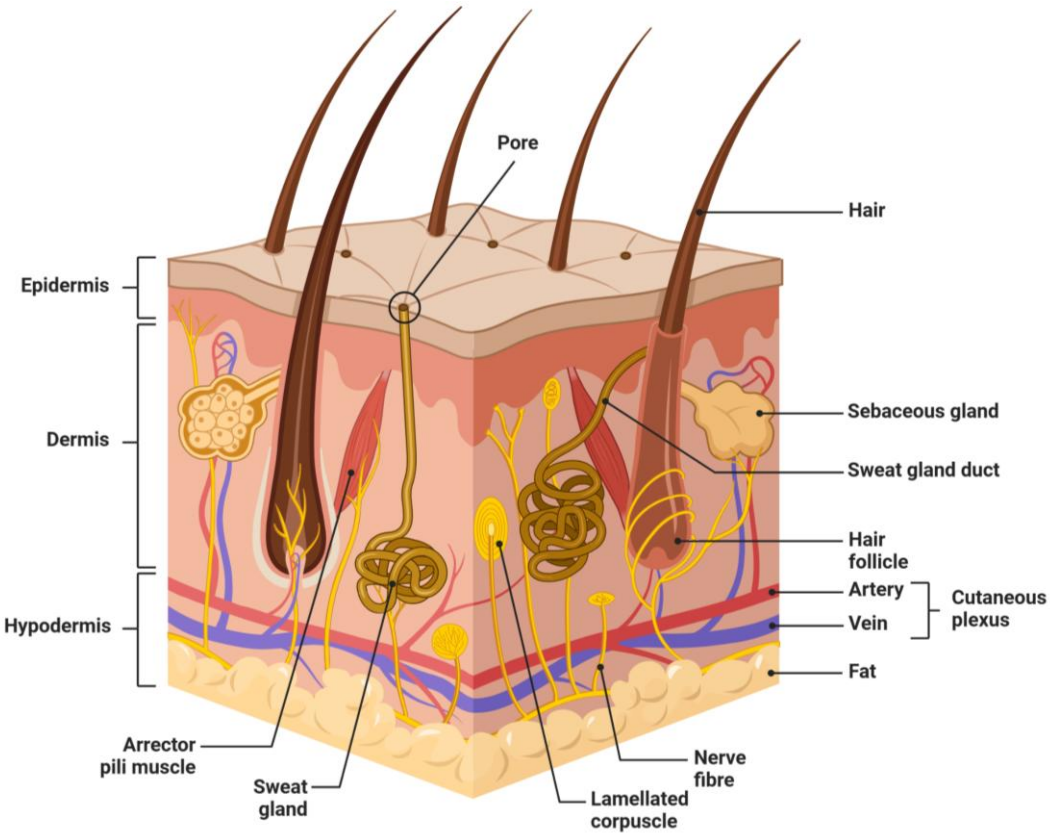

Figure 1.1 Illustration of the structure of human skin. Adapted from Biorender.com (BioRender, USA) template.

1.1.1 EPIDERMIS

The epidermis is the outermost layer of the skin with thickness ranging from 0.05 mm on the eyelids to 0.8 mm on the palms and soles of the feet (4, 5). 95% of the cells in the epidermis are keratinocytes while the remaining 5% are melanocytes, Langerhans cells and Merkel cells (3, 5, 6).

The epidermis is made up of five layers from the skin surface to the interface with the dermis, based on the level of keratinocyte differentiation: *stratum corneum*, *stratum lucidum*, *stratum granulosum*, *stratum spinosum* and *stratum basale*. These layers are then followed by the basement membrane which separates the epidermis from the dermis (1, 6).

The *stratum lucidum*, *stratum granulosum*, *stratum spinosum* and *stratum basale* are generally viable and are often collectively referred to as the viable epidermis which is about 0.13 to 0.18 mm thick (7). The *stratum basale* contains single layer columnar cells and is the only epidermal layer that undergoes proliferation (1). After proliferation, the daughter cells move upwards towards the surface of the skin where they differentiate and finally create the *stratum corneum* (6). Initially, the cells move upwards form the *stratum basale* and change from columnar shape to polygonal shape, forming the *stratum spinosum* which contains differentiated keratinocytes. As the cells migrate further, they form the *stratum granulosum* followed by the *stratum lucidum* where further differentiation takes place resulting in the flattening of the cells and secretion of the contents of lamellar bodies (1, 4, 8). Finally, the cells eventually reach the *stratum corneum,* the outermost layer.

The *stratum corneum* contains terminally differentiated keratinocytes (corneocytes) and a lipid bilayer created by the contents of the lamellar bodies and sebum from the sebaceous glands (1-3, 8). This layer is around 0.005 mm to 0.05 mm thick and is often described as having a “bricks and mortar model” because the corneocytes (the bricks) are surrounded by a lipid bilayer (the mortar). The lipid bilayer contains ceramides,

cholesterol and fatty acids but lack phospholipids unlike the lipid bilayers in other membranes in the body (Figure 1.2). (1, 3, 4, 7, 9).

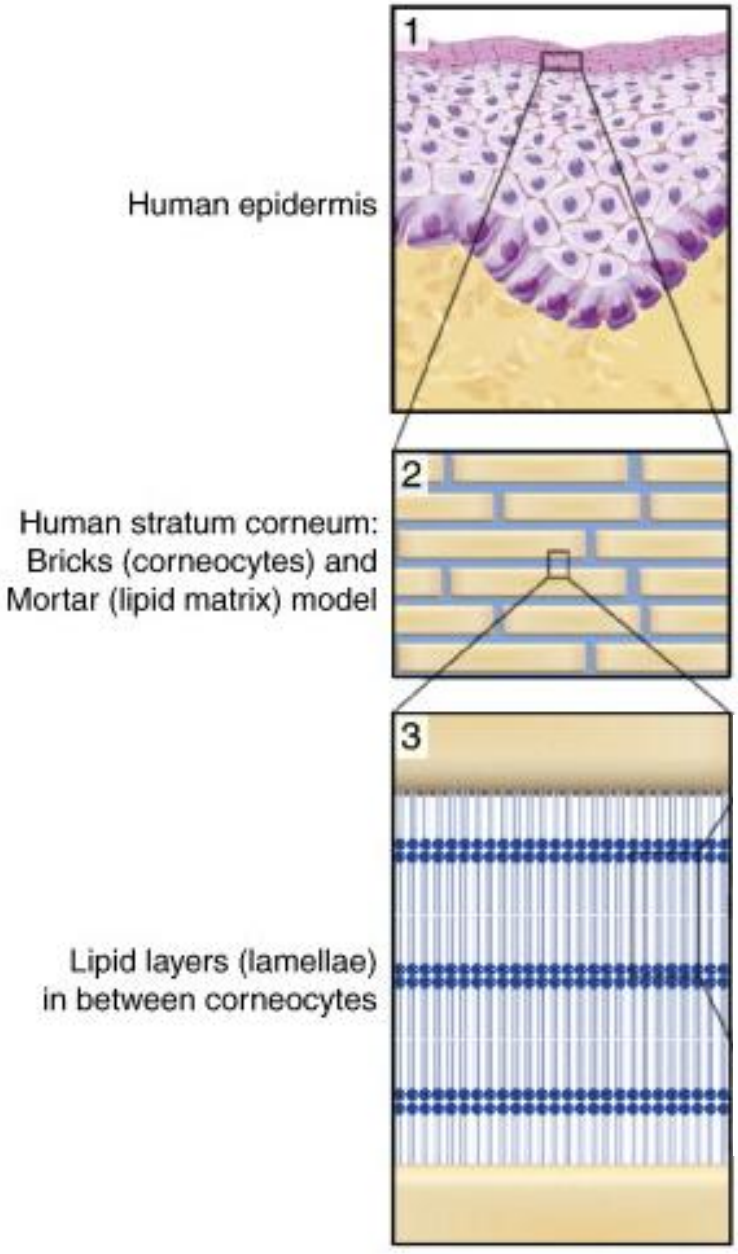

Figure 1.2 Diagrammatic representation of the 1) epidermis 2) bricks and mortar model structure of the stratum corneum 3) lipid bilayer. Image adapted from (10)

1.1.2 DERMIS

The dermis is the main part of the skin, accounting for about 90% of the thickness of the skin with about 2 - 5 mm thickness, depending on the part of the body (1, 4, 5). It provides mechanical strength and flexibility because it is made up of collagen and elastin fibres, in which the lower layer (reticular layer) consists of tightly packed collagen while the upper layer (papillary layer) has loosely packed collagen (1).

The dermis has an aqueous environment and consists of capillaries, sensory nerve endings, hair follicles, sweat glands, macrophages, and lymph vessels, mainly in the reticular layer (6, 7, 11).

1.1.3 HYPODERMIS

The hypodermis, also known as the subcutis, is the innermost layer of the skin which sits next to muscles and bones (5). This layer consists of fat cells and serves as a shock absorber, insulator, nerve signal and vascular conductor, and is involved in energy storage and endocrine purposes (5, 6, 11, 12).

1.2 THE SKIN AS A DRUG DELIVERY SITE

The skin offers a useful site for non- or minimally invasive drug delivery, especially for the treatment of skin diseases, thereby providing a suitable alternative to oral and parenteral dosage forms (7, 13). Topical treatment of skin diseases could maximise therapeutic efficacy by localising the drug at the target site. Additionally, it minimises the risk of first-pass metabolism in the gut and the risk of systemic side effects which could result in poor patient compliance. In most cases, topical skin formulations can be self-administered which is convenient to patients, unlike injections which usually require administration by a trained healthcare professional (5).

However, drug delivery into the skin is challenging due to the *stratum corneum*, the outermost skin layer which consists of densely packed corneocytes in a lipid matrix, as explained in 1.1.1. The *stratum corneum* poses a challenge to drug delivery because it is the skin barrier which protects the body from influx of foreign substances. The passive movement of drugs into the skin is limited to compounds of certain physicochemical properties due to the structure of the *stratum corneum*. The physicochemical properties include a molecular weight less than 500 Daltons, log P between 1 to 3, low degree of ionisation and a minimal number of hydrogen bonding groups (5, 9, 14-16). However, a limited number of drugs meet these criteria, and this could result in limited therapeutic effects due to insufficient drug concentrations at the intended site of action.

Topical skin formulations for drug delivery into the skin are generally classed as liquids, semi-solids, and solids (Figure 1.3).

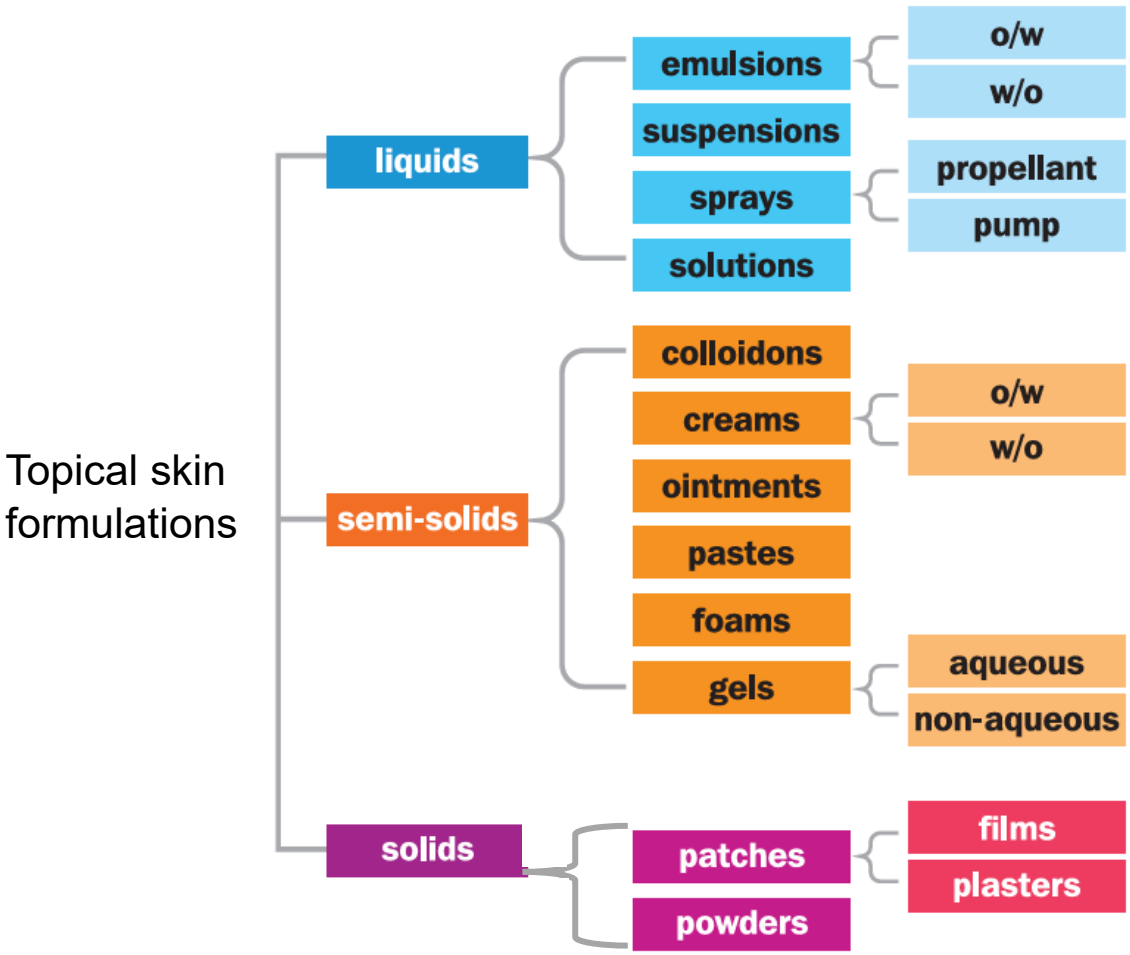

Figure 1.3 An overview of the typical topical skin formulations. Image adapted from (1)

Semi-solid formulations, such as creams, are the most common topical skin formulations possibly due to their ease of use and residence time which is generally longer than that of liquid formulations (1). Creams are two-phase emulsions and could be oil droplets dispersed in water (o/w) or water dispersed in oil (w/o) (9). Formulation design generally involves a drug-centred approach and careful selection of the excipients, such as emulsifiers, for optimal drug release, safety and stability of the formulation (9, 17). Creams, as well as other topical formulations, are generally preferred for conditions where local effect is required or to treat superficial infections due to their low penetrative ability (18, 19).

Topical patches and plasters are also available in the market for localised therapy, such as lidocaine plaster for pain relief (20). There are also transdermal patches which are used to deliver a constant and controlled dose for systemic therapy (9), in which they could be classed based on how the drug is incorporated into the device: patches with the drug in the adhesive, patches with the drug in a matrix, and patches with the drug as a reservoir (1).

Generally, drug delivery using these conventional formulations is typically limited to the drugs which have the physicochemical properties described earlier, and require relatively small quantities for therapeutic efficacy due to the barrier properties of the *stratum corneum* (5, 9, 18). Strategies to improve drug delivery across the *stratum corneum* in topical and transdermal drug delivery are generally classed as chemical and physical methods (1, 14, 21, 22).

An example of a chemical method is the incorporation of penetration enhancers into the formulation (5). These improve permeability of the skin by partitioning into and interacting with the *stratum corneum* in a temporary and reversible manner (21). The main mechanisms of action of penetration enhancers that have been proposed include: disrupting the intercellular lipid bilayer, increasing partitioning of a drug between the formulation and the *stratum corneum*, and interacting with the intercellular proteins in the *stratum corneum* (1, 5, 23). Penetration enhancers are generally classed according to their chemical structures rather than their mechanism of action partly because a penetration enhancer could have more than one mechanism of action (20, 23). Examples include alcohols (e.g. ethanol), fatty acids (e.g. oleic acid), surfactants (e.g. sodium lauryl sulphate), amides (e.g. urea), etc (20, 23). However, common drawbacks with the use of penetration enhancers are skin irritation, limited effectiveness especially for macromolecules, and the process of identifying and selecting the right penetration enhancer for each drug which could be tedious (1, 5, 18, 20). An example is the severe irritation which occurs when paromomycin ointment is applied, and this is believed to be

caused by methylbenzethonium chloride which is a surfactant included in the ointment to act as a penetration enhancer (further information and references are provided in section 1.7.3.1).

Other chemical methods are based on modifying the drug's physicochemical properties to enhance movement through the *stratum corneum*. An example is creating prodrugs usually by chemically attaching a cleavable lipophilic moiety to the drug, as seen in topical corticosteroids (1, 24). However, this approach may not be popular amongst researchers because it involves changing the chemical structure of the drug which could then create a new chemical entity that may need to meet stringent regulatory requirements (24). Additionally, careful consideration is required when choosing the cleavable moieties, as well as the linker where required, so as not to increase the size of the final compound which may in turn hamper movement through the *stratum corneum* (20). Another approach is to create an ion-pair, in which a charged drug is paired with an oppositely charged species to create a neutral pair to enhance movement through the *stratum corneum* (1, 25). However, this approach was unsuccessful in enhancing the penetration of paromomycin for the treatment of cutaneous leishmaniasis, as described in 1.7.3.1.

Physical methods transiently disrupt the *stratum corneum* and/or force drugs across the *stratum corneum* to enhance the passage of drugs, in addition to the potential of targeting the lower layers of the skin (5, 12, 13, 21, 22). The use of hypodermic needles is the oldest physical penetration enhancement technique for drug delivery, but it is associated several drawbacks such as pain, discomfort, needle phobia, as well as the risk of needle-stick injuries and transmission of blood-borne diseases (14, 20, 26).

Novel techniques, such as iontophoresis, ultrasound, needle-free jet injectors, thermal ablation and microneedles, are increasingly gaining attention to address the limitations of existing formulations and to provide advanced types of drug release, such as stimuli-responsive drug release from microneedles (14, 20, 27). Iontophoresis uses electric

current (0.1–1.0 mA/cm^2) to drive the movement of charged drugs into the skin, in which factors such as the magnitude of the applied current, duration of application and molecular weight of the drug can influence the drug delivery (5, 28, 29).

Ultrasound devices utilise ultrasound waves to transiently disrupt the *stratum corneum* and deliver drugs into the skin, but it is associated with undesirable side effects such as minor skin irritation and burns, and the duration of application needs to be carefully selected to avoid damage to the deeper tissues (5, 13, 30).

Needle-free jet injectors utilise a high-velocity jet (usually more than 100 m/s) attached to a spring or compressed gas to deliver drugs (in liquid or powder form) into the skin (5, 31, 32). Fabricating the injectors requires careful consideration to enable ease of use, consistent dosing, dose adjustability and consistent penetration ability to avoid failed injections and excessive penetration which could cause pain (31, 32).

Thermal ablation utilises heat to transiently disrupt the *stratum corneum* to create microchannels for the passage of drugs into the skin, but its use is limited by the complex equipment required (20, 33). Microneedles contain micron-sized projections to enhance drug delivery. Since this thesis is focused on microneedles, further details are described in the subsequent sections.

There have also been promising pre-clinical reports on the combination of physical methods with formulations, such as nanocarriers, gels and creams, to enhance drug delivery into the skin (22, 34, 35). However, some physical methods, such as microneedles, are in early development and require further development to fully realise their potential benefits.

Overall, a “one-size-fits-all” approach is generally unfeasible when selecting a topical formulation and/or a penetration enhancement technique for a drug and/or clinical application, as there is no “perfect” one for every application. So, it is important to tailor the formulation development to factors such as the clinical application, drug, target

patient population, etc, as well as to explore the combination of different strategies to maximise therapeutic efficacy and/or user-friendliness.

Hence, it is logical to further develop and maximise the potential of advanced penetration enhancement techniques which are in early development, such as microneedles, as this could expand the portfolio of drugs that can be efficiently delivered topically. Also, they could create opportunities to be combined with existing formulations to enhance drug delivery and could provide user-friendly drug administration while potentially addressing the current drug formulation gaps for the treatment of skin diseases such as cutaneous leishmaniasis.

1.3 MICRONEEDLES

Microneedles (MNs) are minimally invasive drug delivery systems which contain micron-sized needles, between 250 and 1000 μm long, that are mounted on a base. MNs breach the *stratum corneum* (Figure 1.4 A), without reaching the pain nerve endings, and create transient pores in the skin which enable the delivery of drugs of various physicochemical properties (14, 36). There are various designs of MNs, but they typically contain an array of hundreds to thousands of needles mounted on a backing layer (also known as the base substrate). The MN dimensions could be tailored to the target layer of the skin. The backing layer is usually attached to an adhesive, a syringe, or an applicator (37). An example of an array of MNs is shown in Figure 1.4 B.

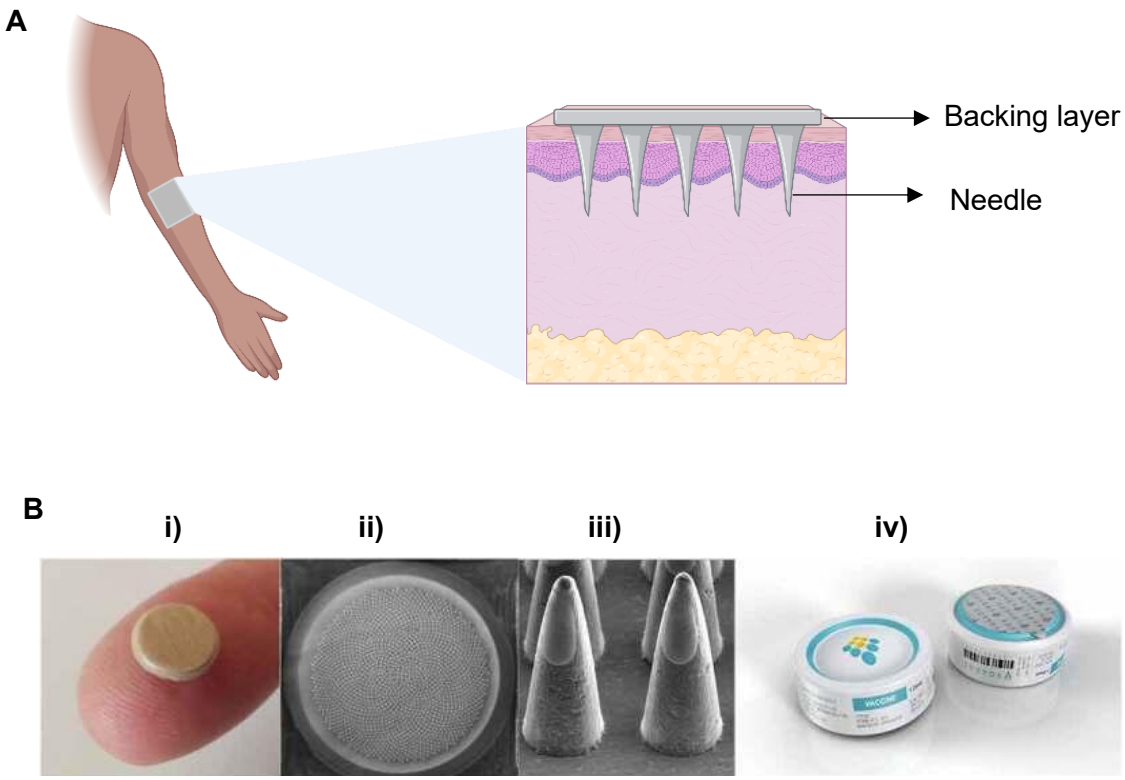

Figure 1.4 A) Illustration of a microneedle array inserted into skin (created with BioRender, USA). B) A vaccine-coated microneedle array that is being developed by a biotechnology company, i) overview ii) close-up view of the array containing approximately 1700 needles, iii) scanning electron microscope image of the needles iv) a microneedle array attached to an applicator (reproduced from (38)).

The first patent for MNs was reported in the 1970s but development of the first MNs was reported in 1998 due to the emergence of suitable technology to create them (39, 40). The initial studies on MNs were mainly based on enhancing the fabrication techniques and materials. Subsequently, advancements in fabrication techniques and the increased awareness of small-scale techniques that are feasible in academic laboratories resulted in a rise in the number of MN research papers and the current trend to further expand the applications of MNs. So far, there has been increasing interest in MN-enhanced topical and systemic delivery of drugs, in which more than 1000 research papers on MNs have been published so far and the number of papers is still rising (41).

The growing interest in MNs is due to the various benefits that MNs provide, as shown in Table 1.1. MNs have the potential to expand the portfolio of drugs that can be delivered into and through the skin, due to bypassing the *stratum corneum* that limits drug delivery to drugs of certain physicochemical characteristics, as described earlier. Additionally, they typically do not cause pain, unlike injections, as shown in several clinical trials, because they are not long enough to reach the pain nerve endings (42-45). MNs also have the potential for self-administration which could reduce the workload of health-care staff and enable cost-effective clinical services by enabling hospital-at-home services, in addition to patient convenience (14, 43, 46). Qualitative studies conducted in various countries have shown positive perceptions towards MNs by members of the public and healthcare staff in the studies (47-50). MNs have also shown promising results for the treatment of skin diseases that require deposition of the drug in the deep layers of the skin which are typically difficult to reach using conventional topical formulations (Figure 1.5) (15, 51, 52). This is useful to target infections located in the deep layers of the skin, including cutaneous leishmaniasis, as described in 1.7.4, which in turn could improve the therapeutic efficacy of antimicrobials administered topically, thus could help reduce the risk of antimicrobial resistance (53-56). Furthermore, Solid MNs could be combined with conventional formulations to enhance drug deposition, as discussed in 1.3.1.1.

Table 1.1 Comparison of the features of cream, transdermal patch and microneedle patch (57, 58)

	Cream	Transdermal Patch	Microneedle patch
Use	Can be self-administered	Can be self-administered	Can be self-administered
Administration	Typically, difficult to apply a standardised dose	Enables the application of a defined dose	Enables the application of a defined dose
Physicochemical properties of the drug	Limited to the properties permitted by the *stratum corneum*	Limited to the properties permitted by the *stratum corneum*	Not limited to the properties permitted by the *stratum corneum*
Drug delivery method	Passive diffusion across the *stratum corneum*	Passive diffusion across the *stratum corneum*	Disruption of the *stratum corneum* to deposit the drug
Drug release	Limited tuneability	Tuneable	Tuneable

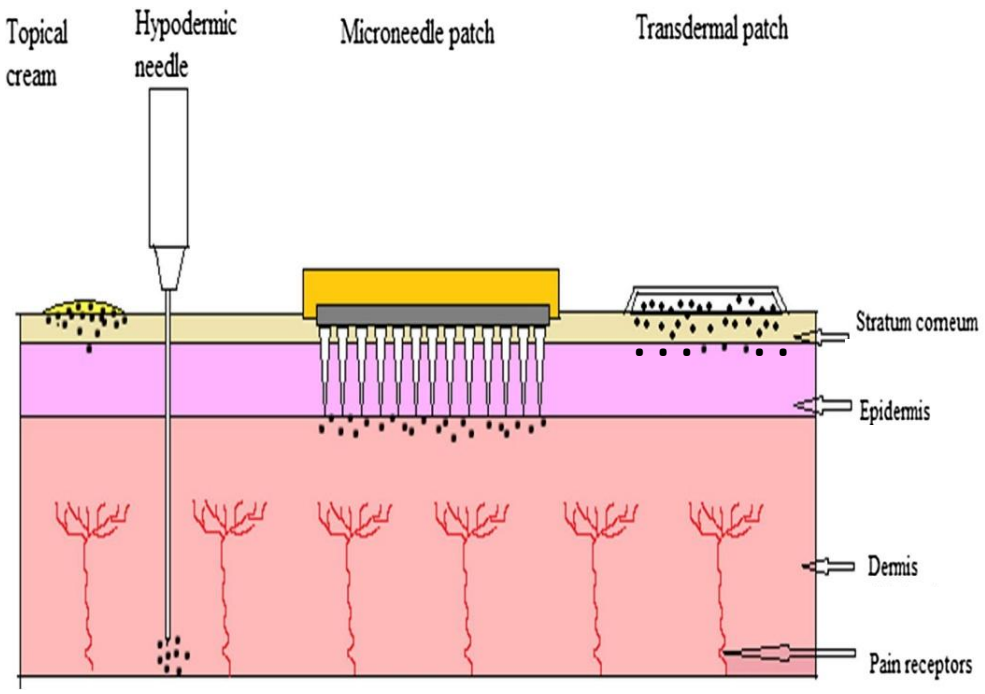

Figure 1.5 Schematic illustration comparing the drug deposition of topical cream, intradermal injection, microneedle patch and transdermal patch within the initial stage of administration. Image adapted from (57).

1.3.1 TYPES OF MICRONEEDLES

MNs are typically classified according to their method of drug release (Figure 1.6)

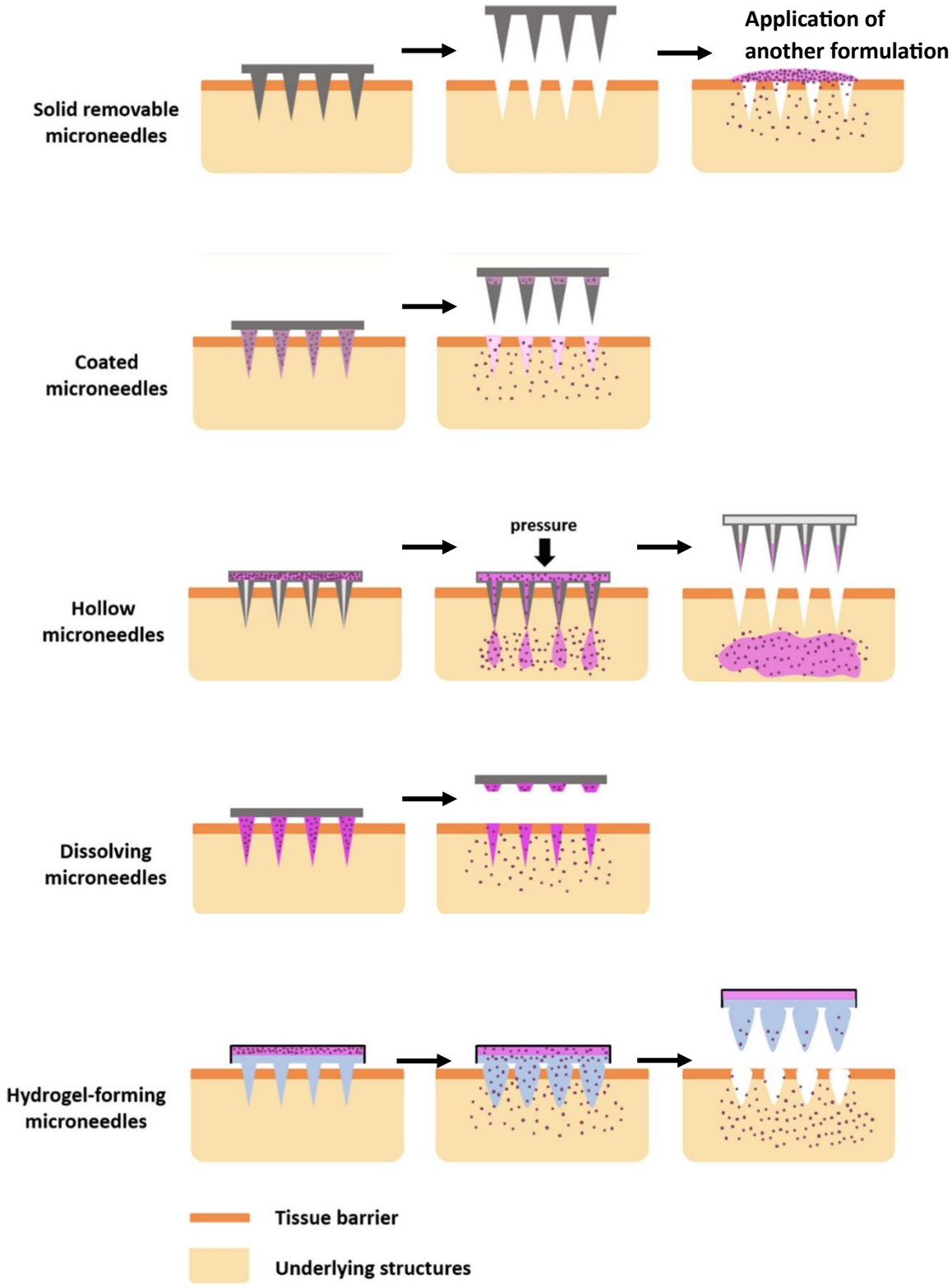

Figure 1.6 Types of microneedles based on the method of drug release. Figure adapted from (59)

1.3.1.1 SOLID MICRONEEDLES

Solid MNs were the first type of MNs reported in the literature for enhanced delivery of drugs through human skin (39). Firstly, the skin is pretreated using solid MNs to create transient pores. Subsequently, the MNs are removed and a drug-containing formulation such as creams, gels, liposomes, etc is applied on the pretreated site (14, 35).

When Nalluri et al. inserted commercially available solid MNs (AdminPatch® and Dermaroller®) into porcine skin prior to the application of sumatriptan solution, they found that the cumulative amount of sumatriptan that permeated increased by 3 to 28 folds, depending on the length of the MNs, in comparison to the cumulative amount that permeated through skin that was not pretreated with solid MNs (60). Similarly, Chen et. al reported enhanced permeation of doxorubicin in liposomes and improved antitumour effect of doxorubicin after skin pretreatment with solid MNs (61).

Solid MNs are promising but their effectiveness depends on the length of time that the pores remain open, in which resealing has been reported to occur within 2 to 48 hours after MN removal (34, 62, 63). Additionally, this technique could be tedious to patients during self-administration as it is a dual step process (40, 64). Nevertheless, solid MNs do not contain drugs therefore they lack the additional manufacturing steps and challenges of drug loading.

1.3.1.2 COATED MICRONEEDLES

These MNs are coated with a drug on the surface of the needles. Upon insertion into the skin, the coating dissolves and deposits the drug in the skin. The MNs are then removed intact from the skin (36, 64). Unlike solid MNs, this involves a one-step application, but it is crucial for the coating process to be uniform and consistent to avoid dosing inaccuracy and variation between the MNs (65). The size of the needles limits the amount of drug that can be loaded and the increased thickness of the needles due to

the coating, could affect the mechanical properties of the MNs so, coated MNs are generally studied for potent drugs and vaccines, as these typically require relatively small doses for an effect (36, 40, 66). In this regard, MNs made from polylactic acid were coated with bleomycin and were studied for the treatment of warts (67). In this human study, the MNs showed similar therapeutic efficacy with cryotherapy but significantly less pain compared to cryotherapy.

1.3.1.3 HOLLOW MICRONEEDLES

Hollow MNs have a hole in the centre for the passage of drug solutions into the skin. Approximately 1.5 mL of drug solution can be delivered through these MNs, and controlled release is achievable by adjusting the pressure which in turn affects the flow rate (57, 64, 68). Upon insertion, compression of the dermal tissues around the needles resists drug flow and can block the opening at the tips but attempts have been made to resolve these issues (40). To avoid blockage at the tip, a group created hollow MNs with openings on the side of the needles instead of the centre (69). It has also been reported that resistance to flow could be minimised by retracting the needles slightly above the initial depth of insertion (70, 71). The flow rate could also be increased by creating MNs with larger holes in the centre, however, this is associated with poor mechanical properties (64). Overall, hollow MNs are generally suited for administration by trained healthcare professionals.

There are currently hollow MNs available in the market which have been approved by the US Food and Drug Administration (FDA), such as MicronJet™ (72). Hollow MNs have also been studied for the extraction of interstitial fluid in the skin for diagnostic purposes (73).

Additionally, recent reports of hollow MNs explored loading drugs in the solid state rather than drug solutions, so as to remove the need for cold chain storage. This design is

usually achieved by creating hollow cavities in MNs made from polymers and filling the cavities with powdered drugs, as a hybrid of dissolving MNs. It has been explored for vaccines and drugs such as finasteride, insulin and tofacitinib (74-77).

1.3.1.4 DISSOLVING MICRONEEDLES

Dissolving MNs are typically designed as a patch and are loaded with a drug or another delivery system within the needles. Upon contact with the interstitial fluid in the skin, the needles dissolve or degrade inside the skin and then release the drug or formulation. This occurs because the needles are made from sugars or polymers that are water-soluble or biodegradable. Controlled drug release is achievable with this type of MNs by choosing materials which dissolve or degrade at the desired rate. Biodegradable materials, such as poly(lactic-co-glycolic acid), typically result in sustained release which could last for months while immediate release is observed when water-soluble materials, such as hyaluronic acid, are used (78, 79). Dissolving MNs have enhanced the penetration of drugs of various physicochemical properties, including small and large molecular drugs (52, 80-82).

The various benefits associated with dissolving MNs have made this type of MNs to be popular amongst researchers. Dissolving MNs generally do not generate sharps waste since the needles dissolve or degrade in the skin. Another reason for the growing interest in dissolving MNs is the versatility they provide not only for controlled drug release but also for the incorporation of other drug delivery systems, such as nanoparticles (83-85).

Dissolving MNs could also be designed for rapid separation of the backing layer from the needles. This enables implantation of the needles and the constituent drug in the skin while the backing layer can be removed within few minutes of application. This is then followed by sustained drug release over few days or months from the implanted needles. This could be convenient for patients as the MN patch would not need to remain

on the skin for a long time (78, 86). The potential for synergistic effects by the polymer and drug has also been proposed. For example, Fonseca et. al reported a dissolving MN composed of needles made from hyaluronic acid and a backing layer made from bacterial nanocellulose loaded with rutin, an anti-ageing agent. The aim was to deliver rutin using the pores created by the hyaluronic acid needles, while hyaluronic acid smoothens the skin (87).

Despite these advantages, dissolving MNs are not without limitations. Firstly, the dissolving MNs generally have low mechanical strength due to the use of polymers (88), in which moisture absorption by hygroscopic polymers can cause further weakening. This usually leads to buckling of the needles upon insertion or incomplete insertion which could result in drug wastage and inconsistent dosing.

Consequently, several attempts have been done to address these issues. For instance, combinations of polymers have been used to improve the mechanical properties of the MNs mainly by optimising the polymer composition to obtain optimal mechanical properties and drug release. Another strategy is incorporating the drug in the needles, while the backing layer contains plain solution of the same polymer used in making the needles or of a different polymer that enhances the mechanical properties of the backing layer. This method has been shown to improve the skin penetrability of dissolving MNs (89). A consequence of this is that the size of the needles in a MN patch limits the amount of drug loaded in the MN, in which several studies have loaded around tens of nanograms to less than 1 milligram of drug, depending on the dimensions and total number of needles in the array (50, 90). However, this is mainly suitable for potent drugs and vaccines. Common strategies that have been reported to address the issue of low drug loading are increasing the MN patch size, incorporating other drug-loaded delivery systems, such as nanoparticles or fabricating the needles from the drug alone (50, 82, 90-92).

1.3.1.5 HYDROGEL FORMING MICRONEEDLES

Hydrogel forming MNs, which were first reported in 2012, are the latest type of MNs. These MNs are solid when dry but swell and soften upon uptake of interstitial fluid in the skin, due to their hydrophilic nature (93). The drug can be incorporated in the crosslinked polymer matrix or placed in a reservoir attached to the backing layer of the MNs, in which the drug diffuses through the aqueous pathways created by the swollen hydrogels. The latter provides the opportunity for high drug loading unlike dissolving MNs. These MNs can also be created without a drug to extract interstitial fluid for disease diagnosis and monitoring because the fluid contains clinically relevant biomarkers (94). Hydrogel forming MNs have several advantages which make them of interest to drug developers. Firstly, adjusting the polymer crosslinking ratio could provide controlled drug release. Secondly, there is less risk of accumulation of the polymers used in making them because the polymers are not deposited in the skin (93). Additionally, they cannot be reused post-administration due to softening of the needles, thereby, preventing the generation of sharps waste and the risk of needle stick injury (93, 95).

The first hydrogel forming MNs were created using Gantrez® crosslinked with PEG, and these showed slow swelling ability (93). The same group of researchers then showed that the swelling size could be increased by adding sodium carbonate (95). However, there is a need to discover other polymers to make hydrogel forming MNs, as unsuitability between the commonly used polymers and some drugs have been reported, for example, the incompatibility of Gantrez® with certain ionic drugs (96). Consequently, researchers are exploring the use of other polymers to fabricate hydrogel forming MNs but the majority of the studies involve chemically modifying polymers for crosslinking and to improve their swelling ability (94). A subset of this type of MN is porous MNs which contain pores distributed within the needles. These MNs require careful selection of the fabricating materials because their porous structure typically renders them fragile which in turn limits their use (97).

1.3.2 MATERIALS FOR FABRICATING MICRONEEDLES

An ideal material for MN fabrication should have good mechanical properties for skin penetration and handling, be inert, easily manufacturable, readily obtainable, stable under storage conditions, cost-effective and biocompatible. Materials such as silicon, metals, and polymers, have been reported for fabricating MNs.

1.3.2.1 SILICON AND SILICA GLASS

Silicon, which was used to fabricate the first MNs, has good mechanical properties, and can be created in various shapes and sizes (39, 40). It has been used to create solid, hollow, and coated MNs. Silicon MNs are usually fabricated by lithography and wet/dry etching. Briefly, silicon dioxide is coated on silicon wafer followed by layering of a photoresist material which enables the transfer of a pattern from a photomask using UV light. Subsequently, the wet etching using a chemical etching or dry etching using reactive ion etching or ion beam milling is performed, generating the MNs (40). However, this fabrication process is costly and involves various steps and specialist equipment, making it an undesirable option for low cost and efficient large-scale manufacturing (40, 98, 99).

Silica glass is an inert material which has also been used for fabricating MNs. Its toughness is comparable to silicon and its transparent nature makes is beneficial for visualisation, hence suitable for hollow MNs (40), in which silica glass hollow MNs were first designed to create MNs for laboratory experiments (100). Manufacturing silica glass MNs generally involves hand-pulling which is tedious and could create non-uniform MNs (98).

Although MNs made from silicon and silica glass can penetrate the skin, they are brittle and could break during insertion. Furthermore, they are neither water-soluble nor biodegradable, hence they could remain in the skin if not completely cleared by epidermal turnover (40, 98). Raghavan et.al reported that coating gold on the tips of

silicon MNs improved the biocompatibility of the MNs (101) but there was no biocompatibility test in their study, such as cell culture assays, to support their claim of improved biocompatibility.

1.3.2.2 METALS AND CERAMICS

Metals, such as stainless steel and titanium, have been used to create solid, hollow, and coated MNs (15, 102). Although some metals are biocompatible and are commonly used for manufacturing medical devices, their susceptibility to corrosion poses an issue (98) and they provide limited opportunity to control drug release from MNs.

Ceramics, such as alumina, have also been used to fabricate MNs. Alumina is resistant to corrosion due to the strong bonding between aluminium and oxygen (17). It is also biocompatible but brittle (103).

1.3.2.3 SIMPLE SUGARS

Sugars, such as maltose, are water-soluble materials which have been used to make dissolving MNs. They are relatively inexpensive and are biocompatible, but their mechanical properties are poor for efficient skin insertion.

Maltose was used to produce the first sugar dissolving MNs. In the study, dissolving MNs made from maltose disintegrated within few hours of storage at 50% humidity (104). In another study, Donnelly et. al. reported difficulties in fabricating dissolving MNs from galactose (105). The issues highlighted were poor flow of molten galactose due to its viscosity, destruction of the incorporated drug due to the use of high temperature, breakage of the MNs during handling, poor stability of the MNs within few hours of storage at ambient conditions and blockage of the pores in the skin by the semi-dissolved galactose. The authors then concluded that carbohydrate-based MNs are not suitable alternatives to silicon and metal MNs. However, this was one of the early reports

of MNs when viscous sugar and polymer melts were used to fabricate MNs. Current reports use aqueous sugar solutions to address the issue of viscosity.

Nevertheless, the brittle nature of the simple sugars that have been studied makes them unsuitable to be used as sole materials for MNs. Therefore, they are usually combined with other sugars or polymers to obtain MNs with sufficient mechanical properties for skin insertion and when loading macromolecules into MNs because sugars are known to stabilise macromolecules (106-109).

1.3.2.4 POLYMERS

Polymers are amongst the common materials used for MN fabrication (14). This is likely due to the numerous benefits that they provide, such as biocompatibility, biodegradability of some polymers and the opportunity for controlled drug release, which in turn could contribute to the versatility of MNs as drug delivery systems. Polymers are commonly used to fabricate dissolving and hydrogel forming MNs and a few have been used to fabricate solid, coated, and hollow MN (15, 40, 110, 111). So far, polymers have also been used to fabricate MNs with advanced drug release mechanisms such as stimuli-responsive release (e.g., glucose, pH, temperature), and a combination of bolus and sustained drug release (85, 112-114).

Table 1.2 shows examples of polymers that have been reported in the literature for MN fabrication both as sole materials and in combination with other polymers.

Table 1.2 Overview of polymers reported for microneedle fabrication and some of the microneedles they have been used to fabricate.

Polymer	Type of MN	Properties and rationale for use	Reference
Poly (vinylpyrrolidone) (PVP)	DMN HfMN	• Rapid dissolution • Enables the formulation of hydrophilic and hydrophobic drugs • Produces brittle MNs, especially low molecular weight PVP, so it is typically combined with plasticizers or other polymers.	(96, 115-117)
Poly (vinyl alcohol) (PVA)	DMN HfMN	• Rapid dissolution • Provides crosslinking and blending opportunities for HfMN fabrication and for enhancing mechanical properties of MNs. •It is typically combined with other materials for MN fabrication but there are very few reports of using PVA as a sole MN material, in which the MNs exhibited sufficient skin insertion ability.	(52, 96, 118-120)
Hyaluronic acid	DMN HfMN	• Rapid dissolution • Low risk of accumulation because it is naturally degraded in humans. • Good swelling capacity and can be crosslinked. • Cosmetic function and wound healing ability. • Viscosity could limit micromoulding. • MNs with good skin insertion ability with a penetration efficiency of about 100% in pig skin.	(79, 94, 121, 122)
Chitosan	DMN HfMN	• Sustained drug release. • Can be crosslinked to create HfMNs. • Possesses wound healing properties • Viscosity could limit micromoulding • MNs exhibit good skin insertion ability with a penetration efficiency of approximately 100% in pig skin.	(123, 124)

MN- microneedle, DMN – dissolving microneedles, HfMN – hydrogel forming microneedles

Sodium alginate	DMN	• Rapid dissolution • MNs have insufficient skin insertion ability but can be enhanced by chemical crosslinking or blending with other materials.	(85, 108)
Carboxymet-hylcellulose (CMC)	DMN	• Rapid dissolution • Combined with other materials to provide sufficient skin insertion ability.	(90, 107, 125)
Pullulan (PL)	DMN HfMN	• Crosslinking ability and good swelling capacity • PL MNs were found to have a low total moisture content (<7% in thermogravimetric analysis at 10°C/min) which favoured storage stability of the MNs and possibly their mechanical properties. • MNs exhibit good skin insertion without breaking, with a penetration depth that is consistent with 50-60% of the needle length.	(80, 124, 126)
Poly (methyl vinyl ether-co-maleic acid) (Gantrez®)	DMN HfMN	• Able to create DMNs and HfMNs • Creates MNs with well-defined shapes and sufficient strength for skin insertion. Penetration efficiency of ~100% in pig skin without breaking and ~10% needle height reduction due to bending after axial force compression against a metal block. • Limited compatibility with a range of drugs due to its ionic nature and the need to select the right grade for the intended use. • Non-degradable polymer with a high molecular weight (1500 kDa) which could pose a risk of accumulation if the DMN is used repeatedly. • Poor swelling ability so requires additives to fabricate HfMN.	(110, 127-129)

DMN – dissolving microneedles, HfMN – hydrogel forming microneedles

Zein	DMN	• Good swelling ability. • Enables the encapsulation of hydrophobic and hydrophilic drugs. • Formed brittle MNs when used alone so required the addition of plasticizers.	(130, 131)
Poly (lactic-co-glycolic acid) (PLGA), poly (glycolic acid) (PGA) and poly (lactic acid) (PLA)	DMN CMN	• Sustained drug release • Potential for tuneable drug release by adjusting the ratio of PGA to PLA in PLGA. • MN fabrication is typically done using polymer melts which could be unsuitable for temperature-sensitive drugs. • MNs possess sufficient skin insertion ability.	(40, 132-134)
Acrylate	SMN	• Used in medical devices and is durable • MNs insert into pig skin without breaking	(111, 135)
SU-8	HMN	• Used in fabricating microfluidic devices and implantable devices. • Suitable for MN fabrication by lithography. • MNs inserted into mouse skin without breaking.	(98, 136)
Silk fibroin	DMN	• Potential for tuneable release • Stabilises biomacromolecules e.g. vaccines • Requires multiple treatments prior to use • MNs inserted into skin with ~100% efficiency	(128, 137)
BIS Poly (N-isopropylacr-ylamide) (PNIPAm)	DMN	• Potential for stimuli-responsive drug release • MNs had poor mechanical properties (>20% height reduction after compression with a texture analyser) so it was blended with another polymer.	(27)

DMN – dissolving microneedles, HfMN – hydrogel forming microneedles, CMN – coated microneedles, SMN – solid microneedles, HMN – hollow microneedles

The polymers that have been reported in the literature for MN fabrication are generally selected due to their safety profile, biocompatibility and previous use in drug delivery and medical devices (40, 138). Table 1.2 describes the features of individual polymers that favour and limit their use as MN materials.

The rules for polymer selection for MN fabrication are currently not strictly defined so polymer selection is often context-dependent and multi-faceted, in which it typically involves a consideration of mechanical properties, as well as other factors such as the intended MN design, the application and the fabrication method (36, 37, 40, 139).

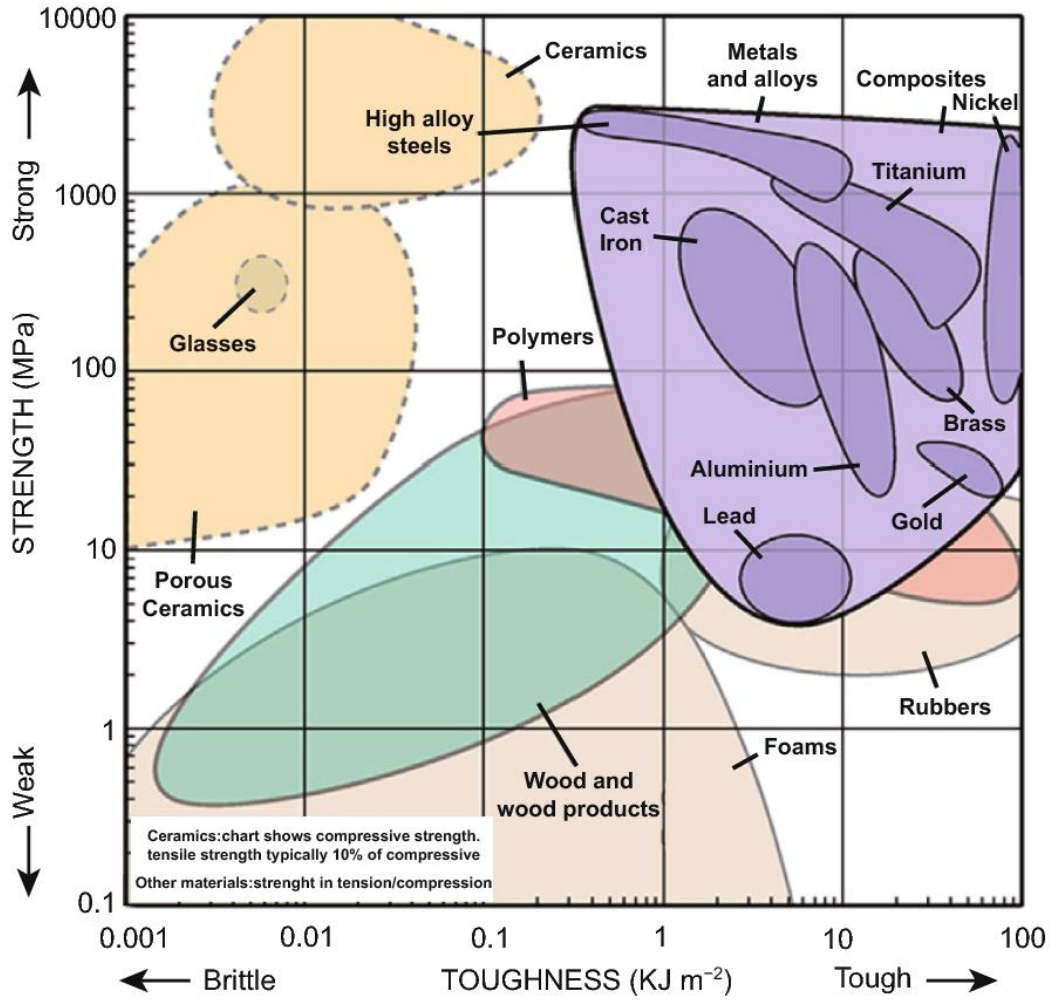

Figure 1.7 Strength versus toughness graphs for various materials, including the common ones used in fabricating microneedles. Image adapted from (40).

Materials for MNs require sufficient strength and toughness to enable the MNs to remain intact during handling, puncture the skin without failing, as well as withstand the skin's elasticity for optimum penetration, particularly to avoid the risk of inaccurate or inconsistent dosing if all the needles in the MN patch fail to puncture the skin and/or reach the intended depth (36, 140, 141). Hence, from a materials science perspective, metals are generally more attractive than polymers for MN fabrication, as seen in Figure 1.7 (40, 98, 131, 141). Additionally, adsorbed moisture and drug loading have been reported to weaken polymeric MNs (79, 80, 142).

However, polymers offer various benefits which contribute to the versatility of MNs, as described earlier. Varying the needle shape or dimensions is a known method of improving the mechanical properties of MNs, including polymeric MNs and metal MNs (90, 123). This method typically requires diverse mould designs or fabrication methods such as micromilling and 3D printing that enable diverse MN designs (15, 138, 143), but these are not easily accessible to all researchers.

Additionally, it is challenging for a single polymer to meet the demands of sufficient mechanical properties for successful skin insertion, as well as other criteria for the intended MN design and application (140, 144). Therefore, other strategies are usually employed to enhance the mechanical properties of polymer-based MNs, such as polymer blending, chemical crosslinking, etc (15, 108, 140, 145).

Examples of other factors that influence polymer selection are polymer-drug compatibility, appropriate fluidity for fabrication by micromoulding, unique properties of the polymer such as wound healing properties, as well as the desired type of drug release such as sustained, burst, dual release or stimuli-responsive, which is usually determined by the intended application (27, 37, 51, 52, 81, 146).

In the opinion of the author of this thesis, the current pre-clinical studies on MNs in the literature can be broadly classified into three types: i) the application of MNs, ii) MN fabrication methods and materials, iii) studying and improving MN insertion in the skin.

When MNs are studied for their application (whether disease or drug), various polymers that have been reported to create MNs are usually tested and then the polymer(s), including the ratio between polymers when more than one polymer is used, that meet certain criteria is/are selected for the application (52, 82, 144, 146). As MNs are still in early development, there are no standardised quality criteria for drug-containing MNs. Therefore, polymer selection is currently defined by the researchers on an ad hoc basis and could be based on factors such as mechanical properties, polymer-drug compatibility, MN morphology after incorporating the drug, the effect of the polymer on the disease, etc.

With regards to MN fabrication methods and materials, studies in this category typically report new or improved fabrication methods. They also report the use of new MN materials (especially polymers) due to the need for additional polymers for fabricating MNs and diversifying MN drug release (15, 27, 64, 123, 128).

MN development presents several conflicting constraints that must be addressed for optimal design and application (37) and no single polymer currently satisfies all the criteria for every MN design and application based on the author's opinion. It is important to identify other polymers and explore the quality of MNs created from the unexplored polymers, whether used as sole MN materials or in combination with other polymers. This could in turn expand MN applications and the portfolio of drugs that can be formulated in MNs, as well as provide additional options for polymer blending for enhancing mechanical properties. It could also potentially offer unique drug release mechanisms and diversify the type of hydrogel forming MNs that could be created by exploiting the crosslinking properties of the unexplored polymers (147).

Polymers are used to fabricate dissolving and hydrogel forming MNs and the most common polymer used in fabricating drug-loaded dissolving MNs is polyvinylpyrrolidone (PVP) (128). PVP is a synthetic polymer which has been extensively studied for

biomedical applications because it is biocompatible, non-ionic, generally safe, and versatile, exhibiting solubility in water and some organic solvents (148).

PVP was first proposed as a MN material due to its characteristics and established use in drug delivery. Firstly, it was suggested that the rigid rings in its monomer could provide tight polymer chains for sufficient mechanical properties that favour efficient skin insertion (149, 150). Additionally, it has an established safety profile, and its rapid dissolution provides fast drug release which is beneficial for conditions that require a quick therapeutic effect (148, 150). Furthermore, it typically does not require harsh MN fabrication conditions, and this is suitable for sensitive compounds such as proteins (149, 150).

Earlier studies used low molecular weight PVP due to its relatively rapid renal clearance and thus a lower risk of accumulation in the body compared to high molecular weight PVP. However, its use as a sole material for MNs is limited by poor mechanical properties for skin insertion. Although high molecular weight PVP generally has better mechanical properties than low molecular weight PVP (151), its viscosity limits its widespread use for MN fabrication. Therefore, a common composition is a combination of low molecular weight PVP with poly(vinyl alcohol) for improved mechanical properties due to hydrogen bonding between the polymers (120).

The most common method for fabricating polymeric dissolving and hydrogel forming MNs is micro-moulding (98, 152). This could be because dissolving and hydrogel forming MNs have so far received more attention from academic researchers than from industrial researchers (41), thereby favouring the use of micro-moulding, a cheap and convenient method for laboratory experiments (153).

Micro-moulding involves creating moulds containing cavities that are inverse shapes of the desired master template, such as a solid MN made from metals. The moulds are then used to fabricate MNs which are replicas of the master template. Micro-moulding could be performed by hot embossing, injection moulding or casting, with the most

common being casting (40). During casting, drug-free or drug-containing polymer solutions are poured into the cavities of the mould. Subsequently, application of pressure or centrifugation is performed to enable filling of the cavities, then the resulting MNs are removed after drying. Thermal crosslinking can also be performed after casting in the mould to produce hydrogel forming MNs (93).

Polydimethylsiloxane (PDMS) is commonly used for making moulds in MN fabrication and this is because it is inert, flexible and has a low surface tension which allows it to attach properly to the master template for adequate reproducibility (40, 98, 106).

An ideal material for MN fabrication by micro-moulding has adequate fluidity to flow well into the mould and fill the cavities. Additionally, it does not create brittle MNs which break upon removal from the mould. It is apparent that various polymers can be used to fabricate MNs, however, the mechanical properties of polymers are generally not as good as metals, as described earlier.

So, typical strategies are to modify the polymer or use blends of polymers to improve the mechanical properties, as described earlier. Polymer blending could also provide the additional benefit of tuneable drug release by adjusting the ratio of the component polymers (120). It is preferred that the combined polymers blend properly to reduce the risk of inconsistent fabrication and inaccurate dosing. However, several polymers generally do not form miscible blends with other polymers (154) so there are currently limited options for polymer blending to fabricate high quality MNs with tailored properties.

There is a need to identify other polymers that could fabricate high quality MNs, ideally when used as sole MN materials, and to explore unique mechanisms of drug release that the unexplored polymers could offer. Identifying other polymers for MN fabrication could also expand the options of available polymers to blend for MN fabrication. Furthermore, identifying other polymers could also expand the portfolio of drugs that can be loaded in MNs and the breadth of the applicability of MNs, especially as the available options of polymers for efficient MN fabrication with several drugs are limited (128).

When a polymer is to be explored for MN fabrication, it is logical to initially fabricate dissolving MNs because this type of MN generally does not require chemical modification or crosslinking of the polymer, unlike hydrogel forming MNs. Therefore, sole use of the polymer for dissolving MN fabrication could enable investigation of the polymer's performance as a MN material. Hence, this work will evaluate the suitability of a promising polymer which has not been explored for MN fabrication by fabricating dissolving MNs made from the polymer and characterising the MNs.

1.4 POLY(2-OXAZOLINES) AS MICRONEEDLE MATERIALS

1.4.1 POLY(2-OXAZOLINES)

Poly(2-oxazolines) (POZ) is a class of non-ionic and synthetic polymers which is receiving a growing interest in biomedical applications because the polymers are biocompatible, tuneable and have stealth properties (155-157). For example, a POZ-based medical device, ETHIZIA™ Hemostatic Sealing Patch, by Ethicon (Johnson and Johnson), recently obtained CE mark approval as an adjunctive treatment of haemostasis (158).

POZs are synthesised by cationic ring opening polymerisation of 2-oxalozines, yielding the general structure shown in Figure 1.8. POZs exhibit physical and chemical properties that are unique to the alkyl chain length of each type of POZ. Additionally, the structure and properties of POZs can be tuned by functionalising the monomers and/or the reagents used during polymerisation (157, 159-161).

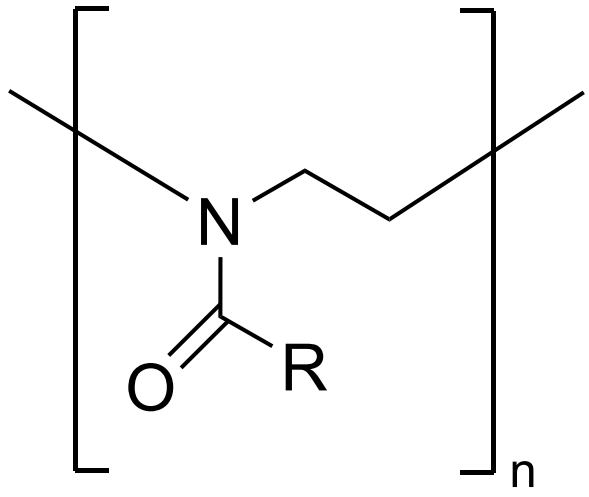

Figure 1.8 General chemical structure of poly(2-oxazolines). R is an alkyl group which varies depending on the type of poly(2-oxazoline). Created using ChemDraw (PerkinElmer, USA).

1.4.2 POLY(2-OXAZOLINES) IN DRUG DELIVERY

The unique properties of POZ favour the development of a wide variation of POZ-based materials for drug delivery and the formulation of a wide range of drugs of various physicochemical properties (161, 162). Hence, these polymers have attracted the interest of researchers in the field.

POZs have been explored as materials for developing films (163), conjugates with proteins and low molecular weight drug compounds (164, 165), micelles (166), lipid nanocapsules (167), tablets (161), hydrogels (168), coatings on nanoparticles (169), amorphous solid dispersions (170), and peptidomimetics (171).

The most researched and commercially available POZ is poly(2-ethyl-oxazoline) (PEOZ). PEOZ (Figure 1.9) is an amorphous polymer that is soluble in water and in some organic solvents (172). In addition to the various pre-clinical studies exploring the use of PEOZ in drug delivery, there is a Phase 1 clinical trial studying a conjugate of PEOZ and rotigotine for symptomatic treatment of Parkinson's Disease (173).

1.4.3 THE POTENTIAL OF POLY(2-OXAZOLINES) AS MICRONEEDLE MATERIALS

Despite the growing interest in POZs and their numerous applications reported in literature, there is currently no report on fabricating MNs from POZs. To date, the only reports associated with both POZs and MNs are a patent where a PEOZ-drug conjugate was loaded into a PVP MN (174) and a research study where PEOZ-coated insulin was coated on a metal MN (175).

As mentioned earlier, there is a need to identify more polymers that can be used for MN fabrication. The properties of POZs support them as suitable candidates to explore as MN materials. Firstly, their tuneability could enable the development of unique MN delivery systems with tailored release rates. Secondly, they could expand the portfolio of drugs that can be formulated into MN and potentially improve the loading efficiency of

certain drugs by enabling the solubilisation of a variety of drugs of various physicochemical properties (161), especially as PEOZ is soluble in both water and some organic solvents.

As PEOZ is the only commercially available POZ and the most studied one with various information of its capability in drug delivery, it is logical to first explore PEOZ as a MN material. However, there is limited information on the mechanical properties of PEOZ (159). This is mainly because the functions of most of the PEOZ-based drug delivery systems in the literature do not rely on their mechanical properties. Therefore, detailed studies on its mechanical properties are required to assess the suitability of PEOZ for MN fabrication. Additionally, since PVP is the most common polymer used in fabricating MNs and both PEOZ and PVP (Figure 1.9) are tertiary amides, it is logical to use PVP MNs as a benchmark to compare with PEOZ MNs so as to evaluate the suitability of PEOZ for fabricating MNs.

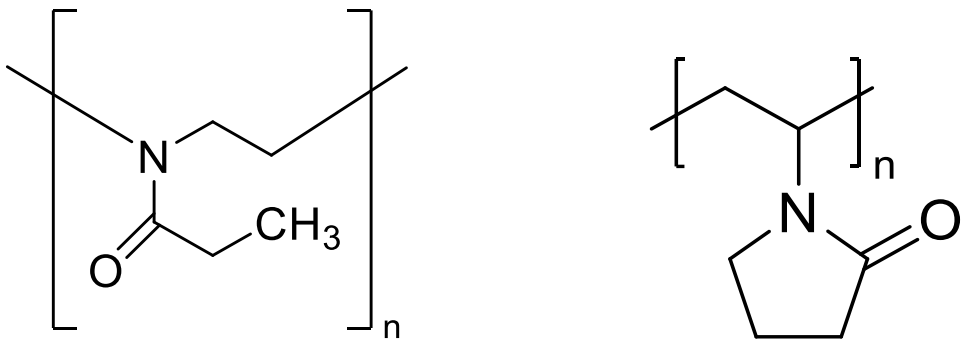

Poly(2-ethyl-2-oxazoline) (PEOZ) **Polyvinylpyrrolidone (PVP)**

Figure 1.9 Chemical structures of poly(2-ethyl-2-oxazoline) and polyvinylpyrrolidone. Created using ChemDraw (PerkinElmer, USA).

1.5 APPLICATIONS OF MICRONEEDLES

MNs were initially designed with the aim of improving the skin penetration of drugs by pre-treating the skin with solid MNs and as alternatives to hypodermic needles using hollow MNs (36). Currently, MNs have gained a lot of interest from researchers, resulting in several reports in journals and patents of numerous applications of MNs beyond their initial reported use (Figure 1.10).

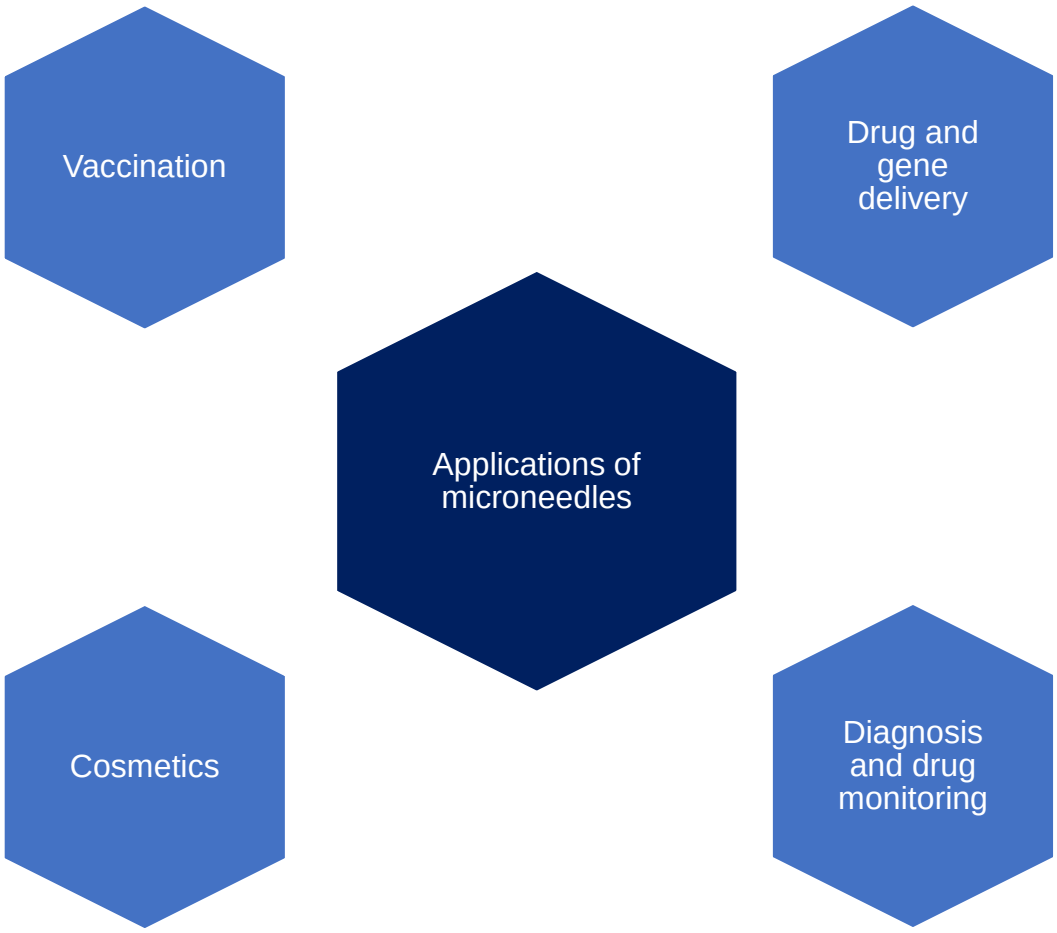

Figure 1.10 Applications of microneedles in humans

The presence of immune cells in the skin makes the skin a suitable site for vaccination. Vaccination using MNs offers various benefits such as self-administration, potential for non-cold chain storage, dose-sparing effect and comparable or superior efficacy to vaccination using conventional injections (36, 38, 40, 113, 176-178). The COVID-19 pandemic increased the awareness of barriers to the clinical translation and equitable access to innovative medical technologies, thereby intensifying collaboration to maximise the potential of these technologies. Consequently, there has been an increase in the number of pre-clinical and clinical studies on the use of MNs, as well as in the number of public-private partnerships to accelerate the commercialisation of MNs (46, 179), especially for vaccine delivery. For example, Vaxxas Ltd, a biotechnology company in Australia, recently announced positive results of Phase 1 clinic studies of their MN patch for measles and rubella vaccine, license agreements with a pharmaceutical industry partner, as well as funding from charity organisations to facilitate the development of their proprietary MN technology (38, 180, 181).

MNs are also used for cosmetic purposes, such as to improve skin texture and to stimulate hair growth. There are several solid MNs in the market that are used for cosmetic purposes such as Dermaroller®, as well as dissolving MNs made from hyaluronic acid, for example MicroHyala® (182-184). There are also pre-clinical and clinical studies which investigated the use of MNs loaded with cosmeceutical compounds (75, 185-187).

Another application of MN is for disease diagnosis and the monitoring of drug concentrations. The skin's interstitial fluid contains analytes that are useful for disease diagnosis and monitoring, for example glucose. Several studies have explored MNs as diagnostic and disease monitoring tools primarily for diabetes, cancer, and infectious diseases (94, 188-190). MNs can be used to either extract interstitial fluid from the skin for analysis *ex vivo* or can be modified to selectively bind biomarkers in the interstitial fluid (36). For example, Jiang et. al developed a hollow MN to extract interstitial fluid

from the skin for the detection of histidine-rich protein 2 which is a biomarker for malaria (73). Whereas Kim et.al developed coated MNs containing antibodies for the detection of tuberculosis-associated biomarkers (191). MNs have also been used to measure drug concentrations in the body to aid adequate drug dosing for therapeutic efficacy and for regular drug monitoring to ensure patient safety (192).

The most reported application of MNs is for drug delivery into and through the skin (topical and transdermal drug delivery) (41). Although MNs were originally created to enhance drug penetration into the skin, as mentioned earlier, the use of MNs in drug delivery has evolved into administration in other organs such as the eyes and mouth (59, 193). Studies have shown the use of MNs to deliver low molecular weight drugs such as ibuprofen and doxorubicin (82, 117) and high molecular weight drugs such as insulin, human growth hormone and monoclonal antibodies (36, 80). MNs have also been reported to have the potential to treat skin diseases which require deposition of the drug in the deep layers of the skin which are difficult to reach using conventional topical formulations (15, 51).

MNs could be designed to either be drug-free or loaded with a drug. Currently, there are drug-free MNs that are commercially available while drug-loaded MNs are still in development. MNs recently received increased attention by funders, pharmaceutical companies, and policymakers due to the increased awareness of the need for innovative medical technologies during the COVID-19 pandemic. This has led to further research partnerships and investments which could facilitate the commercialisation of drug-loaded MNs (46).

1.6 LEISHMANIASIS

Leishmaniasis is a vector-borne disease which is ranked as the second mostly deadly parasitic disease, after malaria (194, 195). It is caused by several species of *Leishmania* parasites which are transmitted to humans through sandfly bites (196, 197).

When a *Leishmania*-infected sandfly bites a non-infected human, the parasites enter the macrophages in the human cells and undergo a morphological change from a flagellated form (promastigote) to a non-flagellated form (amastigotes). The amastigotes then multiply and are released following the bursting of the macrophages (198, 199). (Figure 1.11). The presence of these amastigotes is responsible for the symptoms associated with leishmaniasis (195, 197, 198).

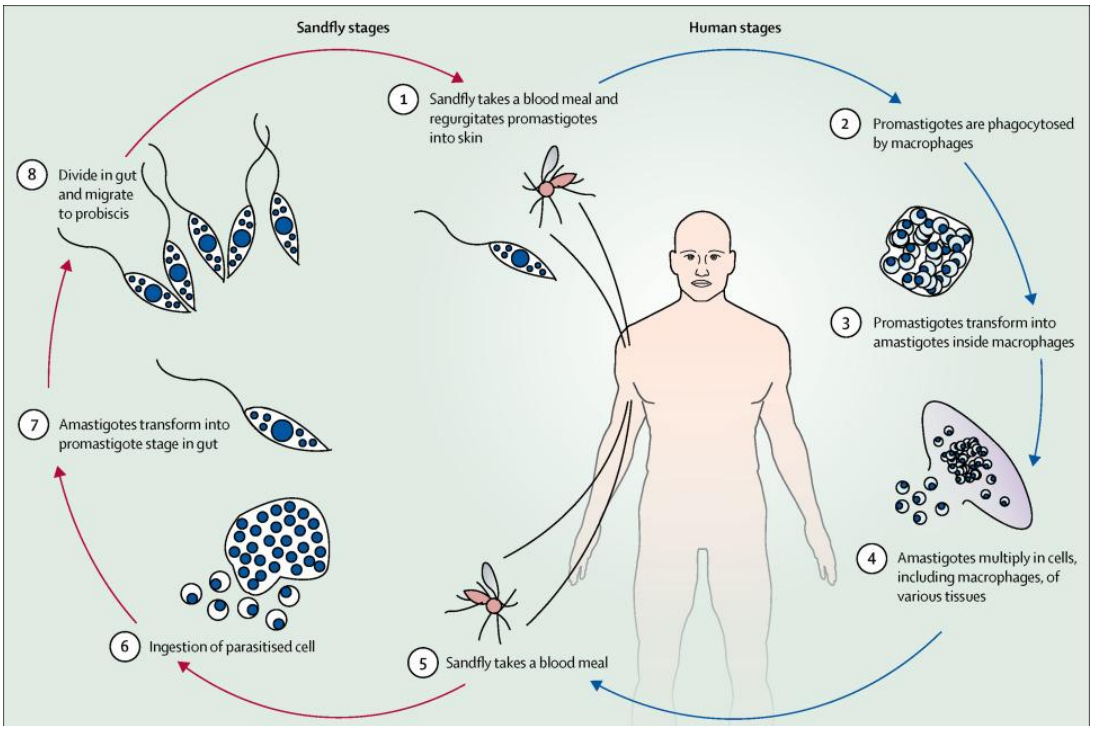

Figure 1.11 Life cycle of *Leishmania* in a sandfly vector and a human host. Reproduced from (196).

Leishmaniasis is prevalent mainly in tropical and temperate countries, and it is regarded as a poverty-related disease which is associated with several factors that increase the risk of being infected (195, 196, 200). Some of the risk factors include poor domestic sanitary conditions which serve as breeding sites for sandflies, disease transmission between people in overcrowded houses, and malnutrition which is linked to disease progression (200).

Leishmaniasis is caused by more than 20 species of *Leishmania* and the geographic distribution of leishmaniasis is divided into Old World and New World, based on the location of the region (Table 1.3) (196, 197).

Table 1.3 Regions in the world where leishmaniasis is prevalent (197)

Category	Description
Old World	Eastern Hemisphere such as Asia, the Middle East, Southern Europe, and Africa
New World	Western Hemisphere such as the USA, South America, Central America, and Mexico

Additionally, there are increasing reports of new cases of leishmaniasis, including in areas where it was historically not endemic. This could be as a result of travel and migration, as well as climate change, in which the World Health Organization (WHO) classifies leishmaniasis as a climate-sensitive disease because its spread is enhanced by temperature changes which enable the survival of the sandfly vectors (200-202).

The clinical presentation of leishmaniasis is mainly based on the type of *Leishmania* species present, in which there are three main types of the disease (196, 197, 200):

- Visceral leishmaniasis is the deadliest form of the disease which causes systemic infection resulting in fever, weight loss and anaemia, and enlargement of the spleen and liver (197, 200).
- Mucosal leishmaniasis which affects the mucosal linings in the nose, throat and mouth and results in lesions, bleeding, excessive secretions, and inflammation in the affected areas (197, 200).
- Cutaneous leishmaniasis, the most common form of leishmaniasis, presents as lesions and ulcers on the skin (194, 200).

In view of this thesis, the rest of this review will focus on cutaneous leishmaniasis, as it is a skin-related disease.

1.7 CUTANEOUS LEISHMANIASIS

1.7.1 EPIDEMIOLOGY OF CUTANEOUS LEISHMANIASIS

Cutaneous leishmaniasis (CL) is the most common form of leishmaniasis with an annual global incidence of 600 000 to 1 million cases and is endemic in 90 countries, according to 2022 data from the WHO (Figure 1.12) (200). It is likely that these values are an underestimate due to underreporting of new cases to the WHO (200, 202).

There are more than 17 species of *Leishmania* parasites that cause CL (202). As mentioned earlier, the geographical distribution of all types of leishmaniasis is grouped into two categories: Old World and New World (Table 1.3). In the case of CL, the main species that cause CL in the Old World region are *L. major*. *L. tropica* and *L.aethiopica* while the main species in the New World region are *L. mexicana*, *L. braziliensis*, *L. panamensis* and *L. guyanensis* (203, 204).

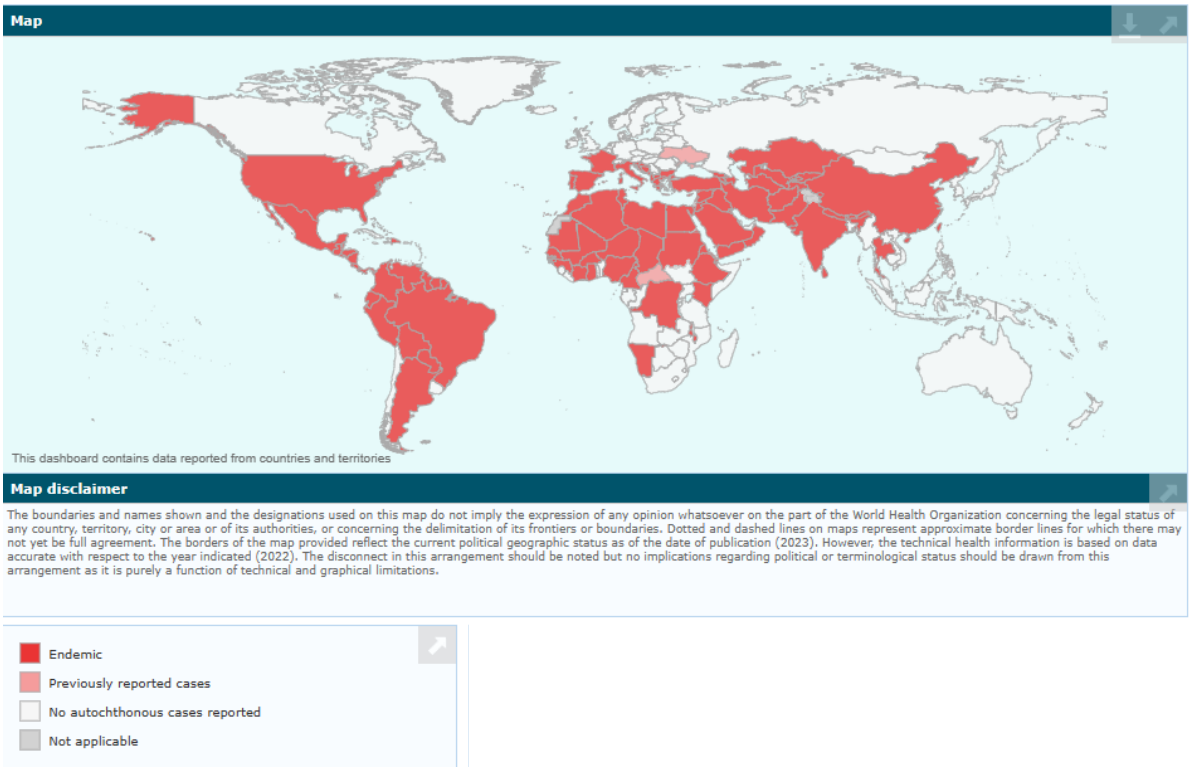

Figure 1.12 Status of endemicity of cutaneous leishmaniasis in 2022, based on reports to the World Health Organization. Picture adapted from (205).

1.7.2 CLINICAL PRESENTATION OF CUTANEOUS LEISHMANIASIS

CL typically presents as skin lesions which often start as papules at the site(s) of bite, followed by enlargement into nodules, epidermal thickening, sometimes with progression into ulcers, and finally fibrotic scars (202, 203, 206-210). The clinical presentation of CL depends on the *Leishmania species*, co-morbidities, and immunity of the human host (204). Some species cause single or multiple skin lesions which self-heal within 3 to 18 months and result in disfiguring scars, whereas some species cause disseminated lesions which can take years to heal (196, 206). In addition, some species cause CL that further progresses into mucocutaneous leishmaniasis in the nose, mouth, and throat especially when CL is not treated early and properly (194, 204). This can result in partial or complete destruction of the mucosal membranes in the nose, mouth and throat (211).

The skin lesions and scarring from CL, as well as the progression into mucocutaneous leishmaniasis, tend to result in disfigurement, especially when it is not treated early and properly. This in turn is associated with social and economic consequences due to stigma, discrimination and social isolation experienced by the sufferers, primarily females, in addition to exclusion from work and school (211-214).

1.7.3 TREATMENT OF CUTANEOUS LEISHMANIASIS

Early therapeutic intervention generally accelerates healing, prevents scarring, and reduces complications of CL. As there is no current vaccine against CL, pharmacological and non-pharmacological therapies are the main ways of managing the disease (Figure 1.13). However, the current drugs are considered 'out-dated' and are associated with limited efficacy and several toxic side effects such as liver toxicity, nausea, stomach upset, cardiotoxicity and kidney failure, especially from systemic administration (196, 198, 204).

The WHO recommends topical treatment for the treatment of uncomplicated CL, as it is convenient to use and it localises treatment at the infection site, which leads to enhanced efficacy and lowers the risk of systemic side effects (202, 203, 215). However, conventional topical formulations are inadequate for CL treatment due to various reasons. Firstly, the physicochemical properties of the majority of the current drugs for treating CL do not meet the criteria (19) required for effective passive penetration through the *stratum corneum*, as described in 1.2. Secondly, skin affected with CL contains a thickened epidermis and necrotic tissue which presents a further obstacle to drug delivery (25, 111, 216). Additionally, the presence of *Leishmania* parasites within the macrophages in the lower region of the skin poses a further obstacle because the drug needs to reach this region of the skin for sufficient efficacy (19, 217, 218).

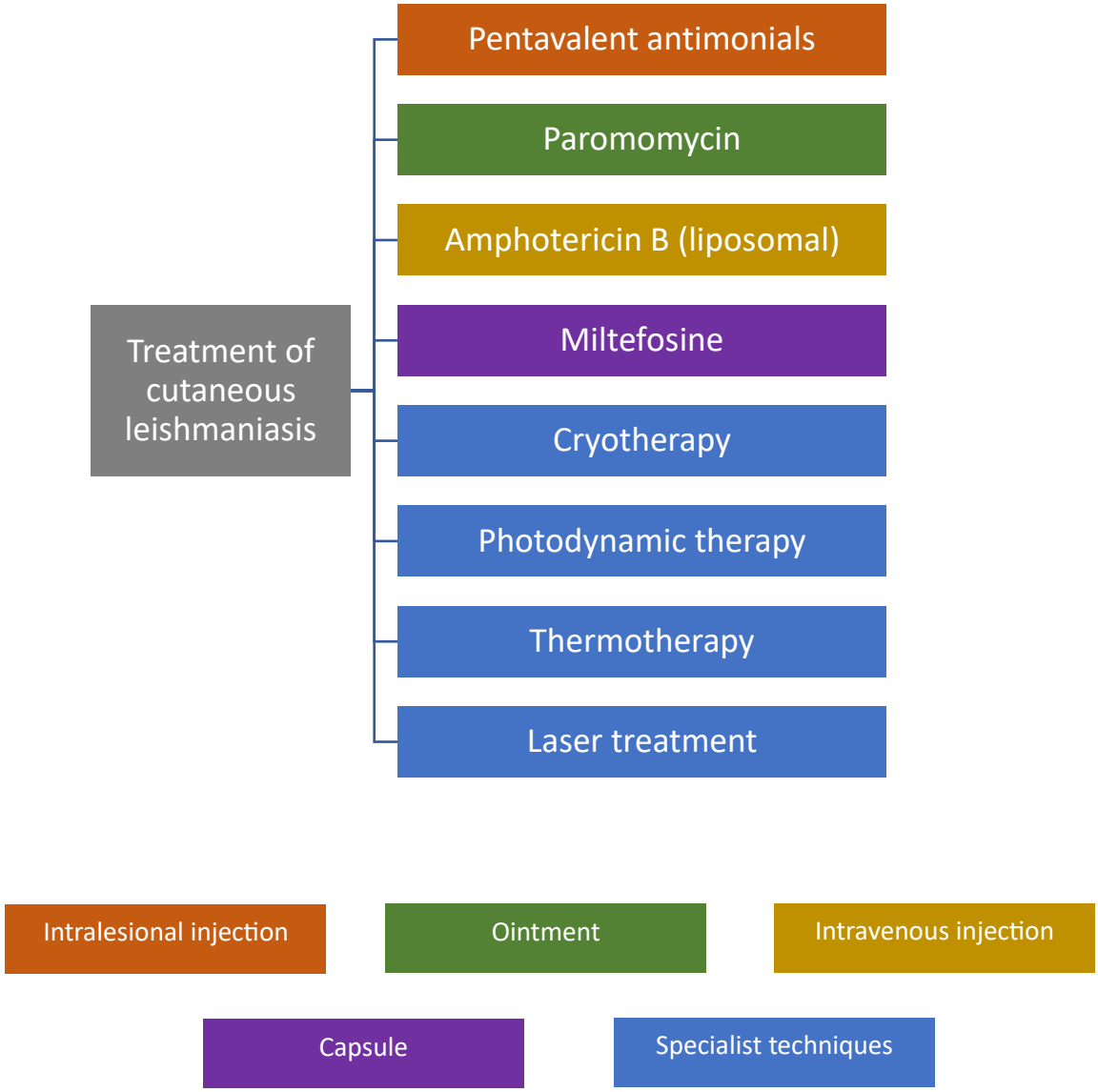

Figure 1.13 Overview of the current treatments of cutaneous leishmaniasis.

Intralesional administration of pentavalent antimonials, such as sodium stibogluconate and meglumine antimonate, is the most common treatment of CL (202). The use of pentavalent antimonials became the first treatment of leishmaniasis over 60 years ago, in which the administration was changed from systemic administration to intralesional injections for CL treatment to reduce the risk of their toxic side effects (19, 198). The efficacy of pentavalent antimonials has been reported to be between 60 to 70% and less

than 50% in some cases, due to the wide range of *Leishmania* species and increasing parasite resistance to treatment, amongst other factors (211, 215).

CL treatment using intralesional pentavalent antimonials involves 3 to 7 weeks of injections in a hospital or clinic (211). Not only is this treatment regime expensive and challenging to the healthcare systems in the low-resource CL-prevalent countries but it is also painful and discomforting to the patients, resulting in poor compliance (211, 219). Furthermore, the patients in rural areas need to travel long distances to access this prolonged treatment, resulting in high economic burden and early treatment discontinuation by the patients (220-222).

Paromomycin is the only drug available in a topical skin formulation (ointment) for the treatment of CL. However, its therapeutic efficacy is hampered by its hydrophilic nature and size which limit passive penetration of a therapeutic amount of the drug into the skin.

Other topical treatments of CL are photodynamic therapy, cryotherapy, and thermotherapy. These have shown promising results in the literature, including in combination with antileishmanial drugs (203, 223). However, they require operation by trained healthcare staff and the use of specialist equipment which are not cost-effective and readily available in many low-resource CL-prevalent countries (203, 207).

Therefore, there is a need to develop topical skin formulations that are affordable, patient-friendly, safe, and effective in treating CL. This is affirmed by a qualitative study where patients with CL stressed the need for effective, convenient, and less painful treatments (222). Furthermore, the Drugs for Neglected Diseases Initiative (DNDi) also highlighted the urgent need for new CL treatments that accelerate the healing lesions without scarring and can be self-administered (211).

In order to aid the research and development of CL treatments, DNDi created the target product profile (TPP) of new CL treatments (Table 1.4).

Table 1.4 Target product profile of new cutaneous leishmaniasis treatments. Adapted from (224).

	Ideal	Acceptable
Target species	All species of *Leishmania*	*L.tropica* or *L.braziliensis*
Safety/tolerability	Well tolerated All adverse reactions (AR)s ≤ Grade 1	Safety monitoring at primary health care level. No major safety concerns: Well tolerated in >95% of patients treated. Systemic AR ≤ Grade 3 in <5%. Local AR ≤ Grade 2 in <30% No treatment-induced mortality
Contraindication	None	Can be assessed at primary health care level.
Efficacy	>95% patients with complete clinical cure, defined as 100% epithelialization/flattening of lesion(s) at 3 months from treatment onset. Minimal scar. No relapse or development of *L. recidivans* or mucocutaneous leishmaniasis. Parasitological endpoint not required	60% epithelialization/flattening of lesion(s) for *L. tropica* and 70% for *L. braziliensis* patients with complete cure. Scar no worse than natural healing. <5% rate of relapse or development of *L. recidivans* or mucocutaneous leishmaniasis at 1 year.
Formulation	Topical/oral	Non-parenteral or few doses if parenteral.
Treatment regimen	Topical ≤ 14 days Oral < 7 days	Topical: 28 days Oral: twice daily for 28 days Parenteral ≤ 3 injections

Target population	No restrictions	>9 months of age. No efficacy in immune-compromised patients. Not for use in pregnancy.
Stability	No cold chain At least 3 years at 37º C	2 years at 4 - 8º C
Cost	To be defined	To be defined

The current drugs used in treating CL were not originally developed for CL rather they were either developed for visceral leishmaniasis or other infectious diseases (204). Therefore, the design of topical skin formulations that are suitable for CL treatment was not prioritised. In view of the increasing global burden of CL, the current trend is developing new formulations of either the current antileishmanial drugs or of new antileishmanial drug candidates that are in clinical development.

However, there is slow progress in the field, and this is mainly due to the variable efficacy and the limited ability of the formulations in the studies to effectively deliver therapeutic levels of the drugs to the lower region of the skin where the parasites reside. For example, an amphotericin B cream developed in a study showed poor efficacy in clinical trials and the authors suspect that it is due to poor penetration (225). Similar findings were observed in an *in vivo* study of a film forming system for topical application containing an antileishmanial drug candidate, DNDi-0690 (218). A limited number of pre-clinical studies of drug-loaded nanocarriers have been reported in the literature for CL treatment but the majority of them were either tested *in vitro* alone or were administered intraperitoneally for *in vivo* studies.

1.7.3.1 PAROMOMYCIN

This section of the review will focus on paromomycin and the studies in the literature aimed at improving its formulation for the treatment of CL.

Paromomycin (Figure 1.14) is an aminoglycoside which is isolated from *Streptomyces* spp (226, 227). Its chemical structure consists of a 4,5-disubstituted 2-deoxystreptamine ring connected to sugars which contain hydroxyl and amino groups (228, 229). Paromomycin has a broad spectrum antibacterial activity, as well as activity against *Leishmania* parasites (230). Its mechanism of action against *Leishmania* is not fully understood but proposed theories include the inhibition of protein synthesis in *Leishmania* by binding to the parasites' ribosomes, as well as the disruption of cell metabolism (230-234).

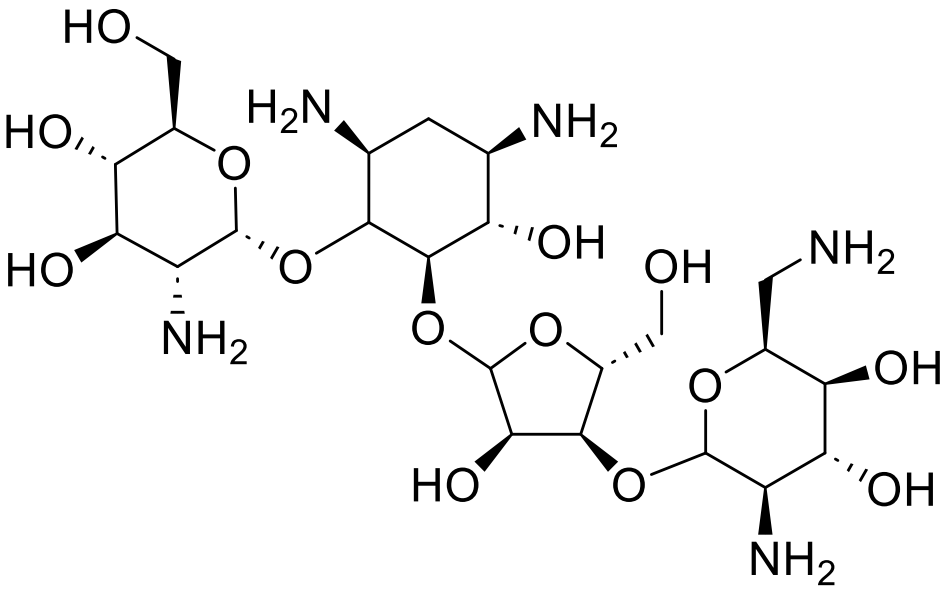

Figure 1.14 Chemical structure of paromomycin. Created using ChemDraw (PerkinElmer, USA).

Paromomycin is a Biopharmaceutical Classification System (BCS) class III drug, with high water solubility and a log P of -8.7 (19). It is available commercially as paromomycin sulphate, with the sulphate accounting for approximately 10% of the product (227). The molecular weight of paromomycin is 615 Da while that of the salt form is 714 Da. These physicochemical properties of paromomycin are outside the criteria for passive movement of drugs into the skin due to the selective nature of the *stratum corneum,* as described in 1.2. Additionally, parenteral administration of paromomycin is associated with ototoxicity and nephrotoxicity (227, 235). Therefore, an adequate topical formulation of paromomycin is required for the effective treatment of CL.

The only marketed topical formulation of paromomycin is Leshcutan®, an ointment containing 15% w/w paromomycin sulphate and 12% w/w methylbenzethonium chloride (MBCl), which is administered twice daily for 20 days to treat CL (203, 236). It is not approved by the FDA, but it is marketed in Israel and could be purchased online as an unlicensed product in other countries (230, 236).

The use of paromomycin ointment for the treatment of CL was first reported in 1984 by El-On et. al. (237). The authors reported that an ointment containing 15% w/w paromomycin sulphate and 12% w/w MBCl resulted in lesion healing in BALB/c mice infected with *L. major*. Subsequently, a randomised, double-blind, cross-over clinical trial was conducted in Israel with 43 patients with CL caused by *L. major* to further investigate the ointment for CL treatment (238). This study showed a 74% cure rate in the group treated with paromomycin ointment and a 26% cure rate in the placebo group. However, adverse reactions occurred in some patients in the treatment group which is likely due to MBCl (further details are provided later).

Subsequent clinical trials conducted in other countries, such as Iran, Guatemala, and Turkey, reported variable efficacy of Leshcutan® for CL treatment, with cure rates ranging from 37% to 85%, in which higher cure rates were generally seen in patients with ulcerated lesions from CL caused by *L. major*, which is the species in the clinical

trial in Israel mentioned earlier (239-243). It has been suggested that a reason for this could be that the ointment is more effective in ulcerated lesions (limited skin barrier) on CL-infected skin, which is typical of CL caused by *L. major* (236, 241, 244, 245). Whereas poor efficacy of the ointment is seen in CL caused by other *Leishmania* species which typically present as non-ulcerated lesions with thickened and hardened skin, particularly at the early stage of the disease when early therapeutic intervention is recommended to prevent permanent disfigurement (236, 241, 244, 245). This could be attributed to the limited ability of the ointment to effectively penetrate the skin barrier and deposit therapeutic amounts of paromomycin in the lower region of the skin where the parasites reside (19, 111, 216, 218, 237), as mentioned earlier in section 1.7.3.

Additionally, adverse reactions, such as severe irritation and burning sensation, were observed in the clinical trials, including treatment cessation in some cases, and this is suspected to be associated with MBCl, a surfactant and preservative usually used in cosmetics at concentrations below 1% (202, 236, 238, 241, 246). MBCl was incorporated into Leshcutan® to enhance delivery into the skin as a penetration enhancer, and a high concentration was used because this improved the efficacy of the ointment (237, 238). However, the adverse reactions limit routine use of Leshcutan® in clinical practice (202, 215, 230, 236, 247).

Consequently, several efforts were made to address the shortcomings of Leshcutan® by developing alternative formulations of paromomycin. Another ointment was developed to replace MBCl with urea (15% w/w paromomycin sulphate and 10% w/w urea) but clinical trials reported lack of efficacy against CL although with lower adverse effects than the ointment containing MBCl (202, 230, 248, 249). Further development of the ointment was not progressed further due to its lack of apparent efficacy against CL.

A cream containing paromomycin and gentamicin was also developed because it was proposed that gentamicin, another aminoglycoside, enhanced the efficacy of paromomycin, in addition to the need to develop a more suitable topical formulation than

Leshcutan® (250). A phase 2 clinical trial in Tunisia and France (n = 92) reported a cure rate of 94% compared to 71% in placebo (251). This was then followed by a phase 3 clinical trial in Tunisia (n = 375) which reported a cure rate of 81% compared to 58% in placebo but with a comparable cure rate to a cream containing paromomycin alone (250). Also, a phase 3 clinical trial in Panama (n = 399) reported a cure rate of 79% but non-superiority of the paromomycin and gentamicin cream to paromomycin alone (252). However, the lesions were debrided before the cream was applied during these clinical trials and this may have influenced the findings of these studies because it may enhance drug movement into skin. Additionally, debridement could be discomforting to the patients. This cream is not currently commercially available and there is limited information on its status.

It is apparent that there is a need to develop a new formulation of paromomycin to optimise the treatment of CL, especially for early-stage non-ulcerated CL caused by *Leishmania* species other than *L. major*, to reduce the global burden of the disease (245, 253). An ideal formulation of paromomycin for CL treatment should not only enable deposition of the drug into the lower region of the skin, but also sustain delivery for a suitable period to enable adequate exposure of paromomycin in the target site since paromomycin exhibits rapid clearance from the skin (217).

There are various reports in the literature about advanced formulations of paromomycin but the majority of these were developed for visceral leishmaniasis, due to the initial trend of developing new treatments for visceral leishmaniasis (19). In an *ex vivo* study which aimed to enhance paromomycin delivery into the skin for CL treatment, ion pairing of paromomycin with various acids was performed to alter its physicochemical properties for skin penetration (25). Both paromomycin and the paromomycin ion pairs did not penetrate intact skin but they penetrated when the *stratum corneum* was removed, suggesting the limiting effect of the *stratum corneum* to penetration due to the molecular

weight of paromomycin and its salts (> 500 Da). So, paromomycin ion pairs are not ideal formulations for early-stage CL based on the findings of the study.

Paromomycin loaded in drug delivery systems such as liposomes, solid lipid nanoparticles, polymer nanoparticles, transfersomes and hydrogels have also been evaluated in *in vitro* and *in vivo* studies for the treatment of CL (217, 254-258). These formulations have generally shown promising antileishmanial activity in *in vitro* studies. However, there are mixed results with respect to their efficacy *in vivo* owing mainly to limited penetration into intact skin and rapid clearance of paromomycin from the skin.

Physical penetration enhancers have the potential to improve drug penetration into the skin, as described in 1.2. A study reported that penetration of paromomycin solution in pig skin increased by 7 to 40 folds due to the use of iontophoresis, depending on the applied current (29). However, further studies are required to further assess its feasibility. It is rather surprising that there are no reports of microneedles to deliver paromomycin for the treatment of CL despite the reported ability of microneedles to enhance skin delivery of drugs of various physicochemical properties, as well as the additional benefits they could offer to the treatment of CL.

1.7.4 MICRONEEDLES FOR THE TREATMENT OF CUTANEOUS LEISHMANIASIS

As mentioned in 1.5, microneedles have shown promising results for topical drug delivery, including for the treatment of skin diseases, as well as for drugs of various molecular weights (14).

In addition to the advantage of local drug administration which reduces the risk of systemic side effects, microneedles have several features which have the potential to improve the treatment of cutaneous leishmaniasis (CL) and thus could contribute to the reduction of the global burden of the disease. The height of the microneedles could enable targeting of the lower region of the skin where the *Leishmania* parasites reside, thereby enhancing the therapeutic effect of the drug. Additionally, the administration of microneedles is generally painless and enables self-administration, which in turn could enhance treatment accessibility and patient satisfaction, as well as reduce the workload of healthcare professionals in the resource-strained CL-prevalent countries, unlike the use of painful intralesional injections which typically require administration by trained healthcare professionals, as described in 1.7.3. As microneedles have been shown to enable non-cold chain storage of various drugs and vaccines, as described earlier, it is plausible they could remove the need for cold chain storage of CL treatments unlike liposomal amphotericin B which requires cold chain storage which could be costly for low- and middle-income countries. Overall, microneedles have features which align with the preferences of patients with CL, as described earlier. Microneedles also align with some aspects of DNDi's target product profile of new CL treatments, as described in Table 1.4, especially formulation type and storage.

Furthermore, the use of dissolving microneedles could reduce the risk of needle stick injuries which could transmit blood-borne infections, a serious problem affecting many of the CL-endemic countries (259). This is because this type of microneedles releases the loaded drug by dissolving or degrading in the skin without generating sharps waste, as described in 1.3.1.4. Also, the drug release rate from the dissolving microneedles

could be tuned due to the type of polymer(s) used in developing the microneedles (36). This could enable controlled release of the drug at the target site, resulting in adequate exposure of the drug to the parasites.

Therefore, it is logical to explore the use of microneedles for the treatment of CL. However, despite the potential benefits of microneedles, there are very few reports in the literature of microneedles for CL treatment. Currently, the majority of the reports in the literature are based on solid microneedles while there is only one report of drug-containing dissolving microneedles for CL treatment. In the first report of microneedles for CL treatment, *in vivo* studies were conducted to investigate solid microneedles for enhancing skin penetration of amphotericin B solution for CL treatment (111). The studies were conducted using murine models, each infected with a distinct *Leishmania* species and at different stages of the disease (early and late stages). The authors found that in early-stage CL, solid microneedles combined with amphotericin B solution exhibited better activity, with regards to nodule suppression and parasite burden, than amphotericin B solution alone and with comparable activity to the commercially available liposomal amphotericin B which was administered intraperitoneally in this study. However, the combination of solid microneedles with amphotericin B solution was not effective against late-stage CL (disseminated and large nodules) which are generally treated by a combination of topical and systemic treatments (203).

As mentioned earlier, early therapeutic intervention accelerates healing, prevents scarring, and reduces complications of CL. The promising findings in the first report of microneedles for CL treatment showcase the potential of microneedles for CL treatment, as they align with the current guidelines which recommend the use of topical treatment for uncomplicated CL with relatively small lesions (19, 203, 215).

Other reports of solid microneedles for CL treatment include the use of solid microneedles to enhance the skin penetration of amphotericin B-loaded transferosomes, and the combination of solid microneedles with radiofrequency (62, 260).

A study conducted by Zare et.al. is the only report of drug-containing dissolving microneedles for CL treatment at the time of writing this thesis. In this study, microneedles made from polyvinylpyrrolidone and carboxymethylcellulose were loaded with amphotericin B and evaluated for CL treatment (125). The microneedles showed promising results for skin penetration and *in vitro* antileishmanial activity, but additional tests are required to further assess the feasibility of amphotericin B-loaded microneedles for CL treatment.

Exploring the formulation of other antileishmanial drugs, such as paromomycin, into dissolving microneedles for CL treatment is warranted, as this could enable treatment against various forms of CL. This is vital because CL is a complex disease with varying symptoms caused by different *Leishmania* species, which results in variation in the antileishmanial activities of the current drugs. So, it is logical to develop and optimise other drug-containing dissolving microneedles to address the unmet needs in CL treatment and to improve treatment outcomes.

There is currently no report of paromomycin-containing dissolving microneedles for CL treatment. As mentioned earlier, paromomycin is the only antileishmanial drug formulated in a topical product (ointment) and its efficacy is hampered by its limited ability to reach the region of skin where the *Leishmania* parasites reside. Therefore, the development of paromomycin-containing microneedles is warranted because the drug requires a new topical formulation for improved efficacy. As the development of dissolving microneedles requires a tailored approach rather than a ‘one size fits all’ approach for all drugs and diseases, this thesis will describe studies directed towards developing paromomycin-containing microneedles for CL treatment.

1.8 AIMS AND OBJECTIVES

The aim of this work is to fabricate and evaluate dissolving microneedles which consist of novel compositions i.e. a new fabrication material (PEOZ), as well as paromomycin, an antileishmanial drug which has not been loaded in microneedles. This is in order to maximise the potential and applicability of microneedles and to improve the efficacy and patient-centricity of the treatment of cutaneous leishmaniasis. The objectives of this work are as follows:

- To explore the feasibility of fabricating dissolving microneedles from PEOZ and using PVP as a benchmark to evaluate the performance of PEOZ microneedles. An in-house fabrication protocol will be developed for this work followed by fabrication of PEOZ microneedles and PVP microneedles. Subsequently, the microneedles will be characterised by microscopic visualisation, compression tests, insertion tests and *in vitro* drug release tests.
- To investigate the miscibility between PEOZ and another polymer in order to optimise PEOZ microneedles for improved performance, based on the findings of the feasibility studies. Miscibility between the polymers will be evaluated using microscopy, thermal analyses, and infrared spectroscopy.
- To explore the feasibility of loading paromomycin into dissolving microneedles to deposit paromomycin in the lower region of the skin where *Leishmania* parasites reside. Paromomycin-loaded microneedles will be fabricated and characterised and compared with drug-free dissolving microneedles.
- To develop an in-house sensitive assay for quantifying paromomycin in microneedles in order to conduct drug release tests. This will be done by adapting published protocols which combined liquid chromatography with mass spectrometry (LC-MS).

CHAPTER 2 – POLY(2-ETHYL-2-OXAZOLINE) AS A MICRONEEDLE MATERIAL

2.1 INTRODUCTION

This chapter describes the first report, to the best of the author's knowledge, of fabricating MNs from PEOZ of two molecular weights and comparing the MNs with those made from two molecular weights of PVP.

The reasons for investigating PEOZ as a material for MNs and comparing with PVP are described in 1.4. In this study, the morphology, and physical characteristics of the MNs were examined, as well as the drug release behaviour from the MNs, using sodium fluorescein as a model drug. PEOZ 50 kDa and 200 kDa were used in this work and compared with PVP 55 kDa and 360 kDa, which are the closest molecular weights to those of PEOZ in the market.

This chapter also describes the steps taken to develop an in-house method of fabricating MNs. Initially, the author performed and adapted methods described in the literature to build expertise in fabricating MNs, as well as to develop a suitable fabrication method for this work. Additionally, different moulds were used and compared, including a custom-made mould, prior to selecting an appropriate mould for fabricating MNs.

2.2 MATERIALS AND METHODS

2.2.1 MATERIALS

PEOZ 50 kDa was purchased from Alfa Aesar, UK. PEOZ 200 kDa, PVP 55 kDa, PVP 360 kDa, polydimethylsiloxane (PDMS) (Sylgard® 184) elastomer kit and sodium fluorescein were purchased from Sigma Aldrich, UK. Titanium microneedles (DermaStamp), containing 35 needles (1000 μm high), were purchased from Amazon UK. Phosphate buffered saline (PBS) tablets, 3mL syringes and needles were purchased from Fisher Scientific, UK.

2.2.2 METHOD DEVELOPMENT OF MICRONEEDLE FABRICATION

2.2.2.1 PREPARATION OF A CUSTOM-MADE MOULD

DermaStamp was used as the master template to manufacture the mould. Firstly, the polymeric base and curing agent in the elastomer kit were thoroughly mixed at a ratio of 10:1 w/w. The master template was then inserted into the mixture at a 45 degrees angle. The mixture and master template were placed under vacuum at 800 mbar for an hour to remove entrapped air. Subsequently, the mixture was transferred to a container which had aluminium foil inside to enable removal of the mould. Then, the master template was inserted and held in place perpendicularly to the container. After curing at 80°C for an hour, the master template and the resulting PDMS mould were placed in an ice bath, followed by separation of the master template from the mould (15).

2.2.2.2 MICRONEEDLE FABRICATION USING A CUSTOM-MADE MOULD

PVP microneedles were fabricated by micro-moulding, using adapted methods reported in the literature (79, 117). A two-step moulding process was used to fabricate MNs with inverse shapes of the PDMS mould (Figure 2.1). PDMS inserts were made in 50mL centrifuge tubes to enable alignment of the PDMS mould inside the tubes for centrifugation (Figure 2.2 A).

20% w/v PVP 360 kDa in deionised water was prepared and the resulting gel was kept to rest for 2 hours at room temperature to enable the air bubbles to settle. 100mg of the gel was then poured in the custom-made PDMS mould prepared in 2.2.2.1, followed by centrifugation at 1808 x g for 1 hour and removal of excess solution on the mould. Then, 150 mg of the gel was poured into the mould to form the backing layer. This was followed by further centrifugation at 1808 x g for 10 mins and drying in a silica gel-containing desiccator at room temperature for 48 hours. A separate batch of MNs was prepared and dried for 24 hours to identify the optimal drying time. The resulting MNs were then

separated from the mould and viewed under an optical microscope (GX microscope with a HiChrome microscope camera from GT Vision Ltd, UK).

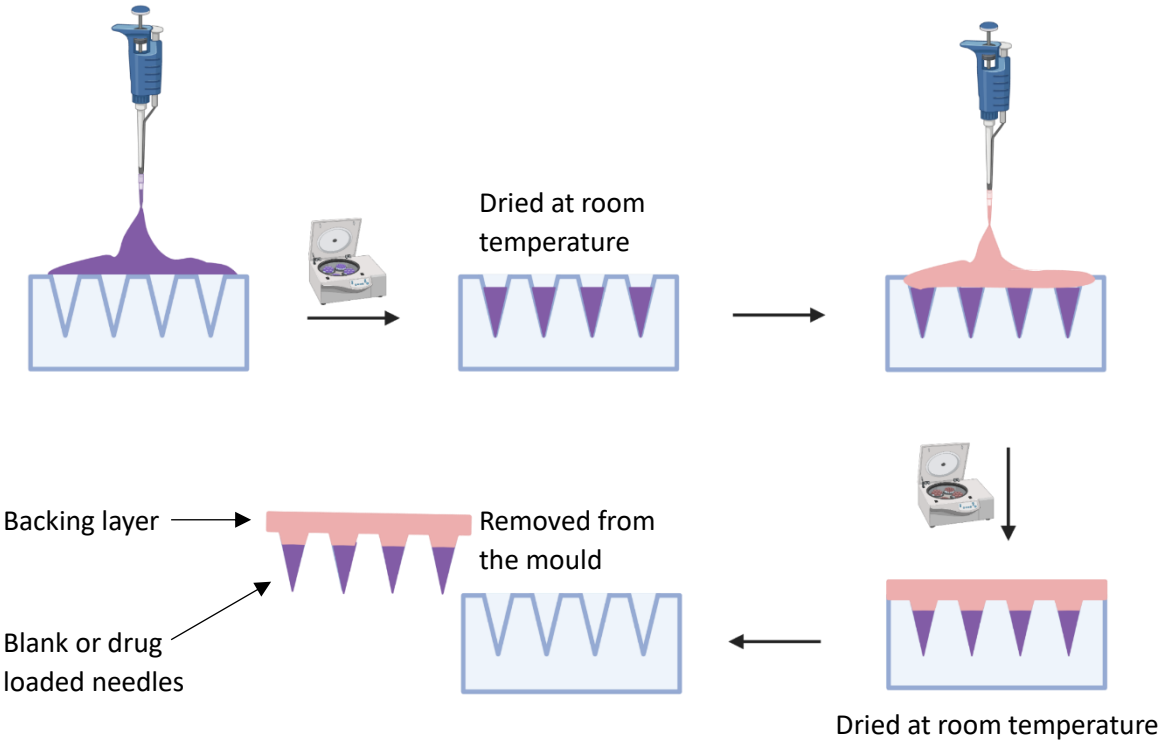

Figure 2.1 Illustration of microneedle fabrication by micro-moulding (not drawn to scale). Created with Biorender.com (BioRender, USA).

2.2.2.3 MICRONEEDLE FABRICATION USING A COMMERCIAL MOULD

PVP MNs were fabricated using the micro-moulding process shown in Figure 2.1 and a commercial PDMS mould (Figure 2.2 B), containing an array of 10 x 10 pyramidal cavities 500µm high, purchased from Micropoint Technologies Ltd, Singapore. 20% w/v of PVP in deionised water was prepared and 70 mg of the resulting gel was poured into the PDMS mould. The mould was then centrifugated at 1808 x g for 1 hour to fill the cavities. After that, the excess gel on the surface of the mould was removed and the mould was then dried for 16 hours at room temperature in a desiccator containing silica gel. Subsequently, 20% w/v of PVP 360 kDa was prepared and 90mg of the gel was

poured into the mould, followed by centrifugation at 1808 x g for 10 minutes to form the backing layer. This was followed by drying for 24 hours at room temperature in a desiccator containing silica gel.

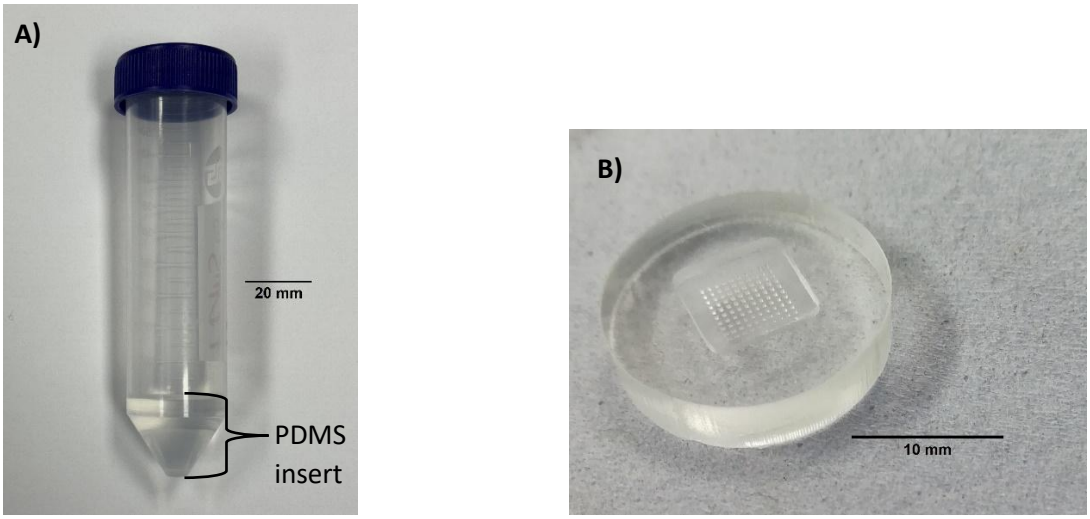

Figure 2.2 A) A centrifuge tube containing PDMS insert B) Commercial PDMS mould taken using a Samsung phone camera (Samsung, South Korea).

2.2.3 FABRICATION OF PEOZ MNs AND PVP MNs

1g of PEOZ 50 kDa, PVP 55 kDa, PEOZ 200 kDa or PVP 360 kDa were dissolved separately in 5mL of deionised water to produce 20% w/v solutions (gel in the case of PVP 360 kDa). Then, 60 µL of the resulting solutions or 70 mg of the resulting gel (in the case of PVP 360 kDa) were poured into the commercial PDMS mould to fabricate four types of MNs using the methods described in 2.2.2.3, with the needles made from one of the polymers while PVP 360 kDa was used to make the backing layer of all the MNs.

Sodium fluorescein loaded MNs were prepared using the same method and quantities described above but with needles made from 1mg/mL of sodium fluorescein plus 20% w/v aqueous solution of PEOZ 200 kDa or gel of PVP 360 kDa.

2.2.4 PHYSICAL CHARACTERISATION OF MICRONEEDLES

2.2.4.1 VISUAL INSPECTION

The MNs were visualised using an optical microscope (GX microscope with a HiChrome microscope camera, from GT Vision Ltd, UK) and a scanning electron microscope (SEM) (FEI Quanta 600 FEG from FEI Ltd, UK) which was operated at 20 kV in high vacuum mode. For SEM imaging, MNs were placed on an aluminium stub with carbon double-sided tape and coated with gold (Edwards coating system from Edwards Ltd, UK) to make the MNs conductive. Dimensions of the MNs were measured using ImageJ software (National Institutes of Health, USA).

2.2.4.2 EVALUATION OF MECHANICAL PROPERTIES

Compression testing was performed on the MNs using a TA.XT2 texture analyser (Stable Micro Systems, UK) fixed with a 5kg load cell and a cylindrical aluminium probe (20 mm diameter) from Stable Micro Systems, UK. The instrument was set to compression mode with a test speed of 0.5 mm/s. Both the pre-test and post-test speeds were 0.5 mm/s and the trigger force was 0.049 N. Each MN patch was placed on a flat metal block (8cm x 8cm) and then the instrument's movable probe applied an axial force on the MN patch until the probe reached 0.4 mm from the needle tip (Figure 2.3). A force-distance curve was then obtained from Exponent TA.XT software (Stable Micro Systems, UK).

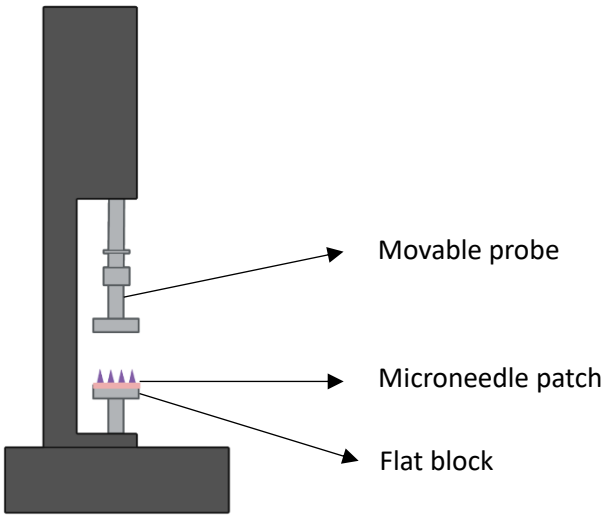

Figure 2.3 Illustration of compression testing of microneedles using a texture analyser (not drawn to scale). Created with Biorender.com (BioRender, USA).

2.2.4.3 INSERTION TEST

Preliminary insertion tests were conducted by using 8 folded sheets of Parafilm® M (thickness of each sheet = 126 µm) as an artificial skin simulant (15, 52, 261, 262) .Each MN patch was manually inserted into the Parafilm sheets and held for 30 seconds using thumb pressure (Figure 2.4). After insertion, each sheet was viewed under an optical microscope (details stated earlier) to count the number of holes created. The penetration efficiency of the MNs on each sheet was calculated using equation 2.1. SEM images of the MNs after insertion were obtained as described in 2.2.4.1.

$$\text{Penetration efficiency (\%)} = \frac{\text{Number of holes in Parafilm® M}}{\text{Number of needles in the array}} \times 100 \qquad (2.1)$$

The estimated penetration depth of each MN patch was calculated by adding the thickness of the sheets pierced by the MNs. Each sheet is 126 µm thick, so the penetration depth increases by 126 µm as the MNs pierce each additional sheet.

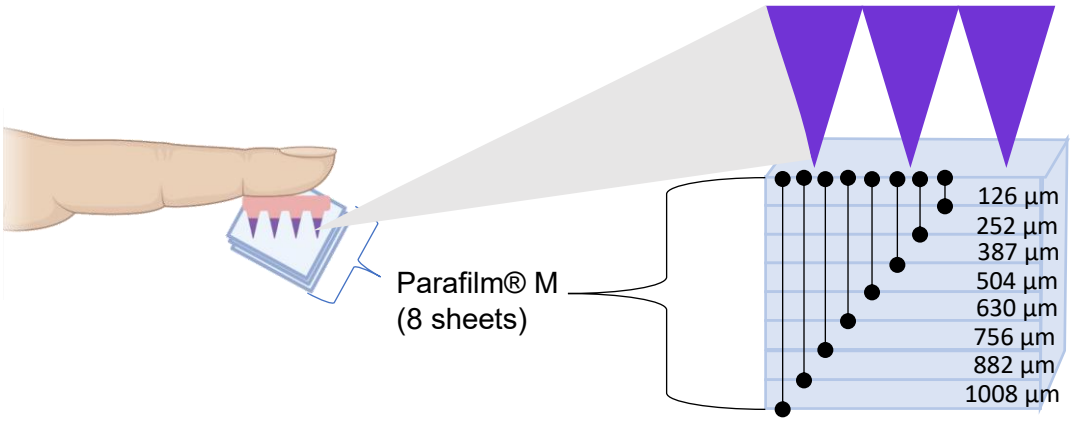

Figure 2.4 Illustration of microneedles being inserted into 8 layers of Parafilm® M, a skin simulant (not drawn to scale). Created with Biorender.com (BioRender, USA).

2.2.5 QUANTIFICATION OF SODIUM FLUORESCEIN

PBS was prepared by dissolving 10 PBS tablets in 800mL of ultrapure water in a 1L volumetric flask, followed by adjustment of the pH to 7.4 and making the solution up to 1 L. A stock solution of 1 mg/mL of sodium fluorescein in PBS was prepared and further diluted to make three sets of standard solutions ranging from 0.005 to 0.03 µg/mL. The fluorescence intensity of each standard solution was measured using a Varian Eclipse fluorescence spectrophotometer (Varian Inc, USA) at emission and excitation wavelengths of 512 nm and 494 nm respectively. A calibration curve was then created by plotting the intensity against the concentrations of the standard solutions. Sodium fluorescein was quantified using a regression line equation generated from Microsoft Excel (Microsoft, USA).

2.2.6 *IN VITRO* DRUG RELEASE STUDY

PEOZ 200 kDa MN and PVP 360 kDa MN, both loaded with sodium fluorescein, were used for the *in vitro* drug release study.

The drug release study was initially attempted using an unjacketed glass Franz diffusion cell (20mm orifice diameter, 3.14 cm^2 orifice area, 15mL receptor volume from PermeGear, Inc. USA). Firstly, a cellulose-based Visking dialysis membrane with a molecular weight cut-off of 12 kDa - 14 kDa and a pore size of 24 Angstrom (Medicell Membranes Ltd, UK) was trimmed to fit the orifice, rinsed with PBS and soaked in PBS for 20 minutes. Then, a magnetic stirring bar was placed inside the receptor chamber of the Franz cell and the receptor chamber was then filled with PBS followed by using the cellulose membrane to cover the entire orifice of the chamber. The donor chamber was subsequently placed on top of the receptor chamber and the two chambers were clamped using a stainless steel Cell Clamp (Medicell Membranes Ltd, UK). The Franz cell was then placed in a water bath containing water and was magnetically stirred at

400 rpm at 37° ± 1°C. Subsequently, the MN patch was placed inside the donor chamber using a pair of tweezers, with the needles facing downwards towards the receptor chamber and touching the cellulose-based membrane. Then, 2mL was removed from the receptor chamber through the sampling port at different time intervals (0, 2, 5, 10, 15, 20, 30, 60 and 120 minutes) using a 3mL syringe attached to a needle and was then replaced with 2mL of fresh PBS (maintained at the same temperature) at each time using an unused syringe and needle. The fluorescence intensity of each 2mL aliquot was then measured, as described in 2.2.5.

An alternative experimental design was then used for the drug release study. Each MN patch was immersed in a glass container containing 15mL of PBS which was magnetically stirred at 400 rpm and maintained at 37° ± 1°C using a water bath. Then, 2mL was removed from the dissolution medium at different time intervals (0, 2, 5, 10, 15, 20 and 30 minutes) and replaced with 2mL of fresh PBS (maintained at the same temperature) at each time (81, 263-265). The fluorescence intensity of each 2mL aliquot was measured, as described in 2.2.5, and the concentrations were obtained from the calibration curve equation. The cumulative sodium fluorescein released was then calculated by taking the PBS volume into account.

The total sodium fluorescein content in a MN patch was measured by adapting methods reported in the literature (144, 266). Six MN patches (three each of PEOZ 200 kDa MNs and PVP 360 kDa MNs) were dissolved separately in 15mL PBS using a magnetic stirrer run at 400 rpm for 1 hour at 37 ± 1°C using a water bath. Then a 2mL aliquot was removed and analysed as described in 2.2.5. The results are expressed as mean ± SD (n=3).

The percentage cumulative release, defined as the percentage of the cumulative released to the total sodium fluorescein in a MN patch, was plotted against time. Then, the release data of sodium fluorescein from PEOZ 200 kDa MNs and PVP 360 kDa MNs

were fitted to three kinetic models (first order model, zero order model and Higuchi model) using Microsoft Excel (Microsoft, USA) as described below (267, 268). Data points up to the first 100% release were used.

- First order model - Plotted the logarithm of % cumulative remaining against time.
- Zero order model - Plotted % cumulative released against time.
- Higuchi model – Plotted % cumulative released against square root of time.

2.2.7 STATISTICAL ANALYSIS

IBM SPSS® Statistics (IBM, USA) was used for statistical tests. Data are presented as mean ± SD of triplicates. Independent samples t-test was used to compare two groups and one-way analysis of variance (ANOVA) with Tukey's post hoc test was used to compare three or more groups due to their equal variances, as confirmed by Levene's test of homogeneity of variances. Differences were regarded as statistically significant if $p < 0.05$.

2.3 RESULTS

2.3.1 METHOD DEVELOPMENT FOR MICRONEEDLE FABRICATION

2.3.1.1 PREPARATION OF A CUSTOM-MADE MOULD

The initial PDMS moulds that were prepared lacked uniformity due to the presence of air bubbles particularly in the cavities which could in turn affect the needle integrity. Initially, the mixture of polymeric base and curing agent was placed under vacuum to remove air bubbles, as described in 2.2. However, air bubbles were created once the master template was inserted. Prolonging the duration of degassing under vacuum did not resolve the problem. So, the preparation method was adjusted to reduce the likelihood of creating air bubbles. This was done by wetting the master template and tilting the master template to prevent air entrapment, followed by placing both the master template and mixture under vacuum. Although these changes did not prevent the formation of air bubbles entirely, the number of holes as a result of air bubbles in the cavities was less than that of the initial moulds that were made.

The resulting PDMS mould (Figure 2.5) had an irregular surface due to the use of aluminium foil in the preparation process, although aluminium foil aided separation of the mould from the container. The success rate of creating moulds without voids was low, making the process tedious with unpredictable outcomes. Furthermore, the thickness of the backing layer could not be controlled, resulting in variation in each batch of moulds.

A)

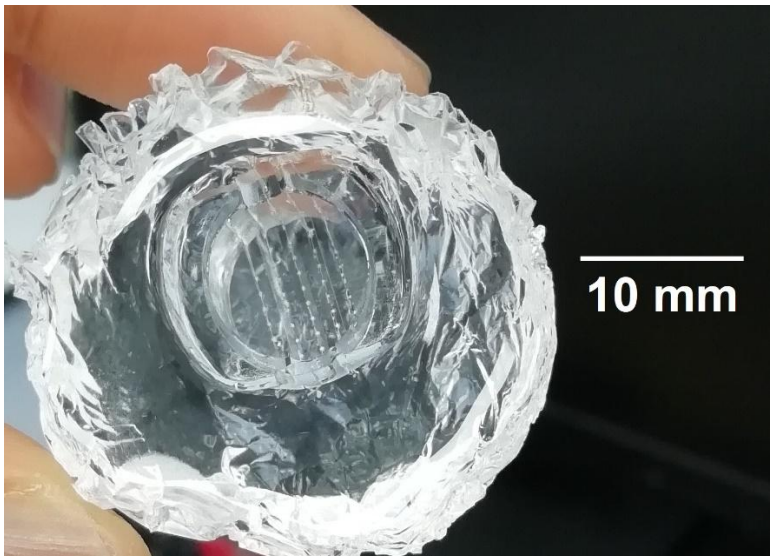

B)

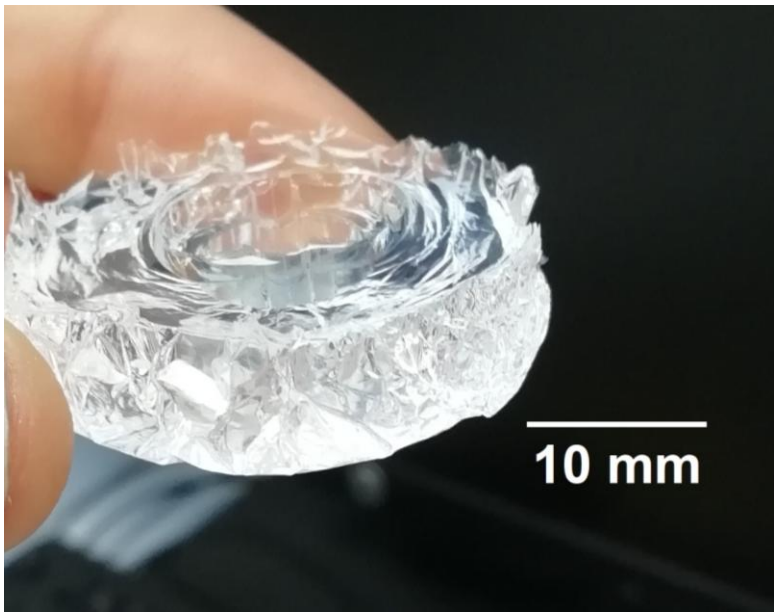

Figure 2.5: A) PDMS mould (top view) B) PDMS mould (side view). Taken using a Samsung phone camera (Samsung, South Korea).

2.3.1.2 MICRONEEDLE FABRICATION USING A CUSTOM-MADE MOULD

PVP MNs (Figure 2.6 A) were made with shapes similar to the master template (Figure 2.6 B). The tip-to-tip distance between the needles was 770 ± 3 μm and the height and base width were 873 ± 13 μm and 117 ± 5 μm respectively. All 35 needles formed with

well-defined conical shapes, but there were voids in the backing layer. Also, MN patches with holes in the needles were discarded. There was an observable difference in the thickness of the backing layer across each MN batch due to the uneven surface of PDMS moulds. Additionally, a drying time of 24 hours was insufficient because the MN patch, especially the backing layer, was stuck to the mould and had not completely solidified. Whereas 48 hours of drying produced an intact MN patch which was easily detachable from the mould.

A)

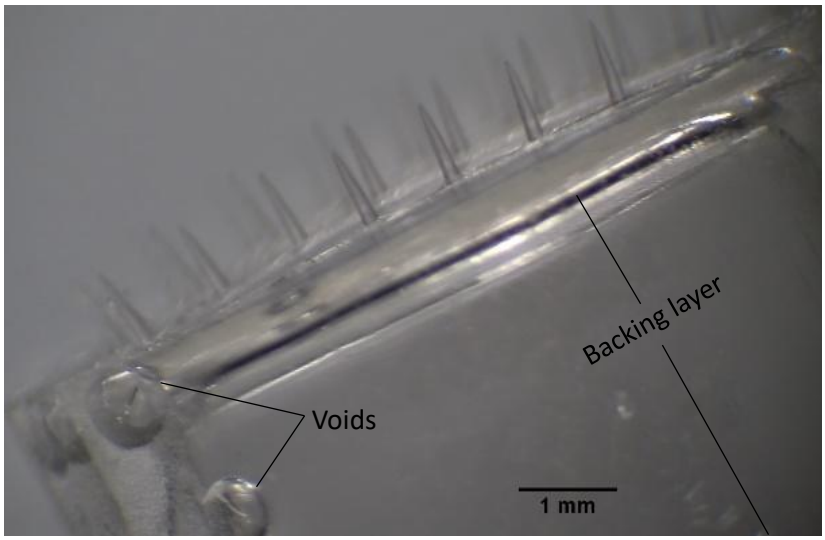

B)

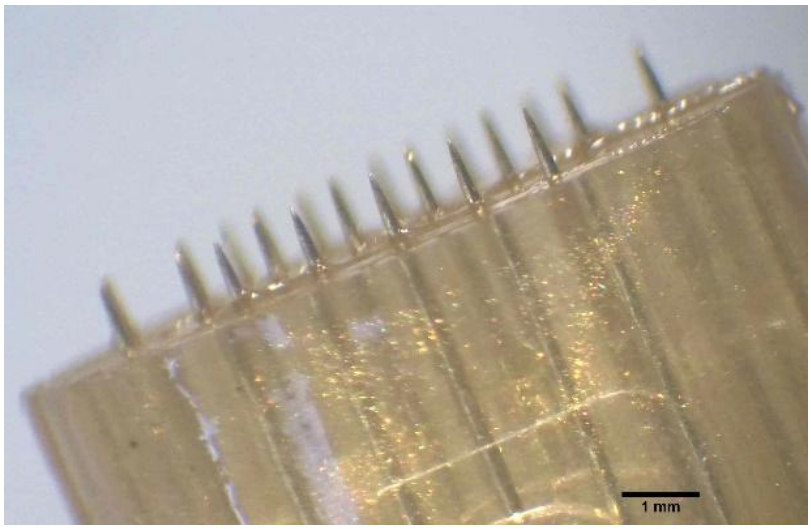

Figure 2.6: A) PVP microneedles (1.5X) B) Master template (1X) Scale bar = 1mm.

2.3.1.3 MICRONEEDLE FABRICATION USING A COMMERCIAL MOULD

The commercial PDMS mould (Figure 2.7 A) contains 100 inverted pyramidal cavities. As seen in Figure 2.7 B, which is the internal region of the mould's cavity under SEM, the mould has a layered surface from the base to the tip. The dimensions of the cavities are shown in Figure 2.7 C. The PVP MN patches made from the mould had 100 pyramidal microneedles inverse of the mould, and backing layers with smooth surfaces and uniform thickness across batches and did not break upon handling (Figure 2.7 D).

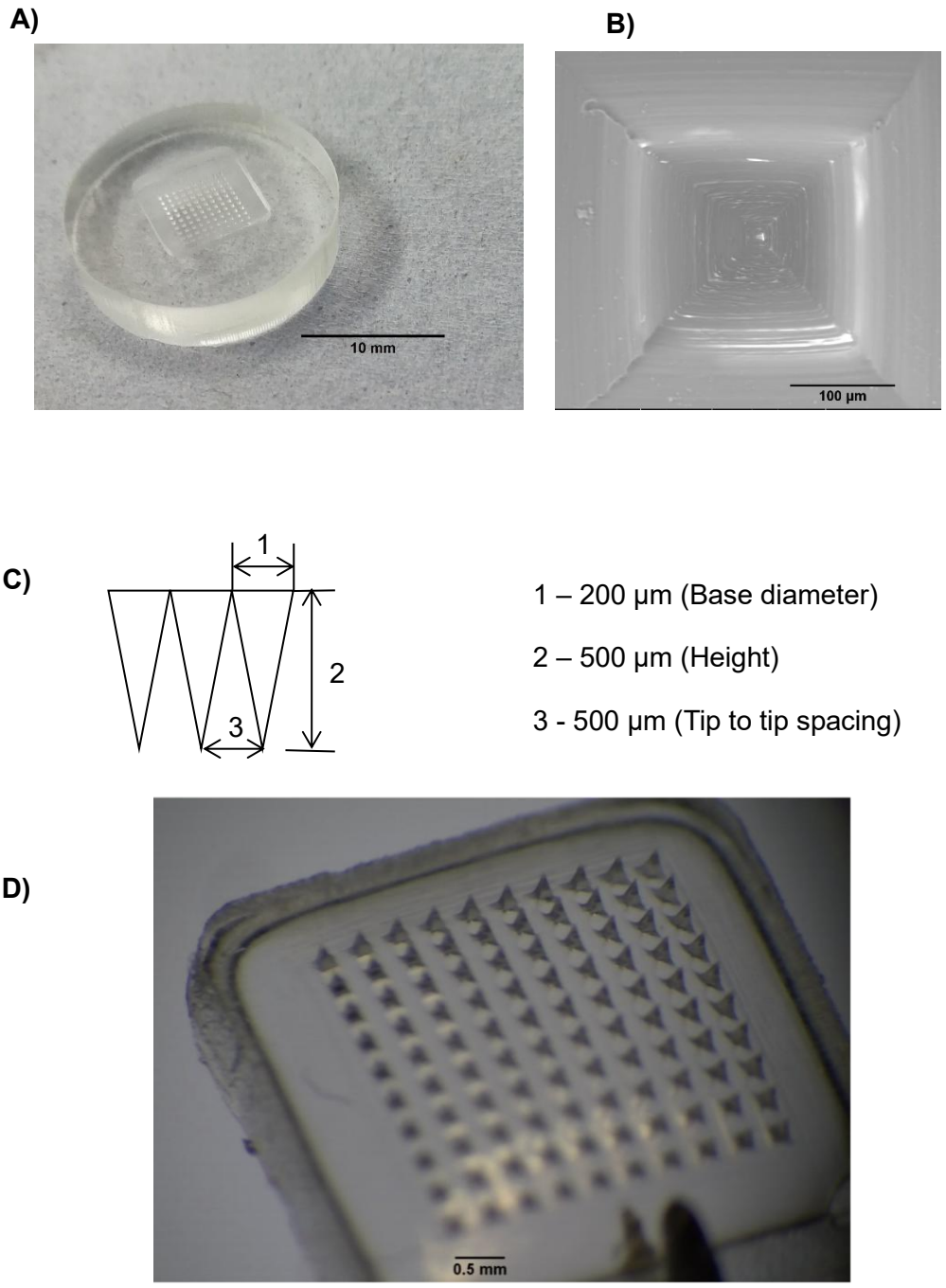

Figure 2.7: A) Commercial PDMS mould (Samsung phone camera, Samsung, South Korea) B) SEM image of the mould cavity from the top (700X) C) Dimensions of the mould D) Optical microscope image of PVP microneedles (1.5X).

2.3.2 FABRICATION AND VISUAL INSPECTION OF PEOZ MNs and PVP MNs

Four types of MNs were then fabricated using the commercial mould, namely, PEOZ 50 kDa MNs, PVP 55 kDa MNs, PEOZ 200 kDa MNs and PVP 360 kDa MNs. Each type of MNs had 100 pyramidal needles with well-defined tips (Figure 2.8). When PEOZ 50 kDa was used as the backing layer for PEOZ 50 kDa MNs, the MN patch was thin and fragile and broke upon handling. Since PVP 360 kDa produced a good backing layer during the method development in 2.2.2, it was used to create the backing layer for the four types of MNs in order to have a consistent and robust base to enable characterisation of the needles in each patch which were made from the four polymers.

As shown in Table 2.1, the heights of the MNs were less than the height of the mould. In PVP 360 kDa MNs, the needles in the middle of the patch looked sharper than those on the sides. Each type of MNs had needles with layered surfaces similar to the mould, however, PEOZ 50 kDa MNs also had broken patches on the needles (Figure 2.8).

Table 2.1 Dimensions of PEOZ microneedles and PVP microneedles. Data shown as mean ± SD of triplicates.

MN type	Height (μm)	Base width (μm)	Tip diameter (μm)	Tip to tip spacing (μm)
PEOZ 50 kDa	384 ± 4	202 ± 3	8 ± 1	492 ± 3
PVP 55 kDa	388 ± 3	203 ± 2	5 ± 2	493 ± 1
PEOZ 200 kDa	385 ± 2	203 ± 3	4 ± 1	493 ± 2
PVP 360 kDa	383 ± 12	201 ± 3	7 ± 4	493 ± 2

No statistically significant difference was observed between the above listed dimensions of the four groups of microneedles. ANOVA test with Tukey's post hoc test.

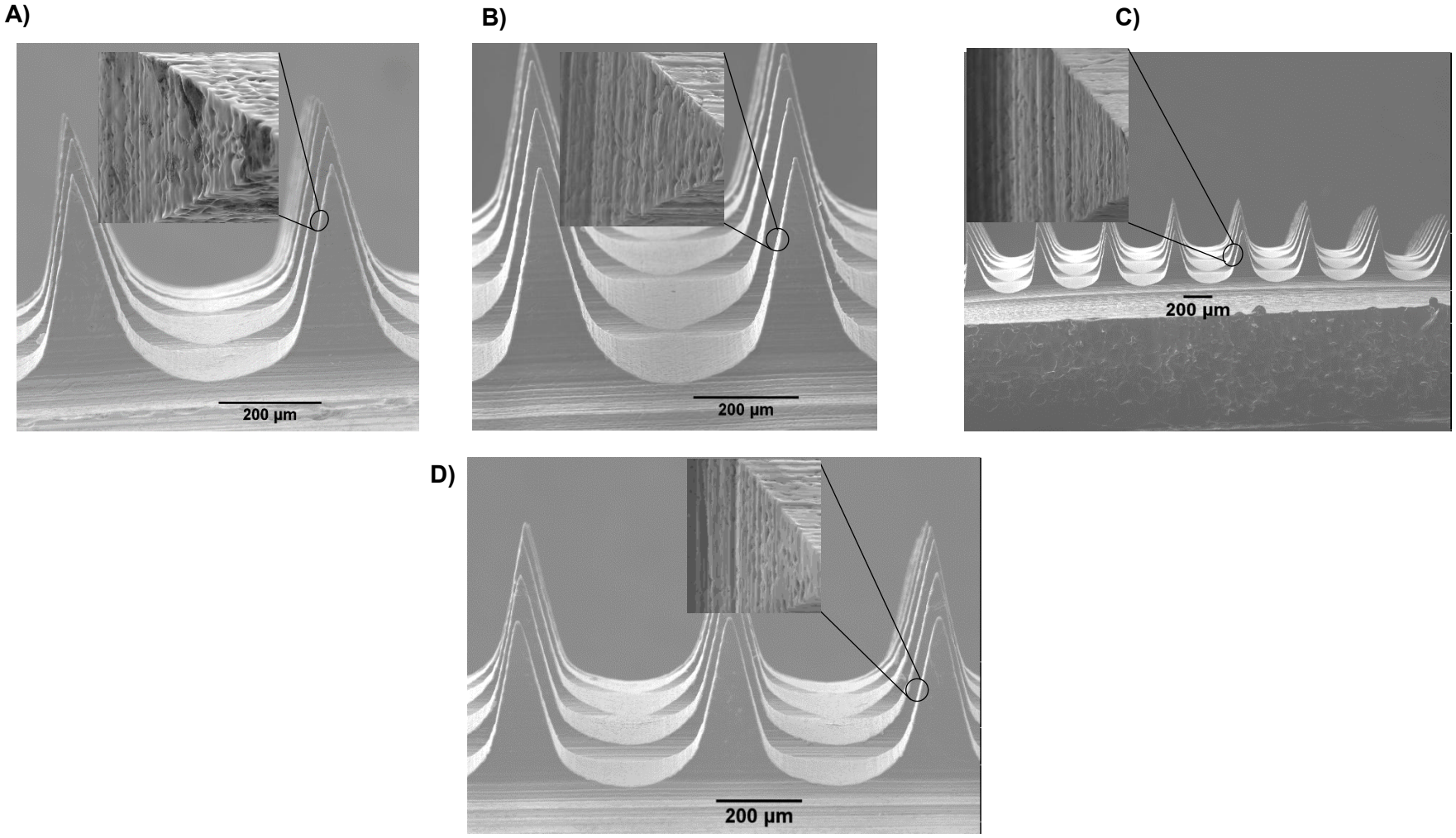

Figure 2.8 SEM images of microneedles made from A) PEOZ 50 kDa B) PVP 55 kDa C) PEOZ 200 kDa D) PVP 360 kDa. A and B are X300 magnification, C is X70 magnification and D is X200 magnification. Magnified surfaces are X2000 viewed from the top.

2.3.3 EVALUATION OF MECHANICAL PROPERTIES

Figure 2.9 A shows the force-distance curves of the MNs while Figure 2.9 B shows the maximum force required to compress each type of MN to 0.4 mm. The MNs showed similar mechanical behaviour, as there was no sudden drop in the curve until the end of the experiment while the compression force increased with distance.

However, resistance to compression increased with polymer molecular weight for both PEOZ and PVP. PEOZ 50 kDa MNs showed the lowest resistance to compression but there was no statistically significant difference between the maximum force required to compress it and that of PVP 55 kDa MNs.

Visualisation under a microscope showed that the MNs did not break and the backing layer of each type of MN remained intact at the end of the experiment.

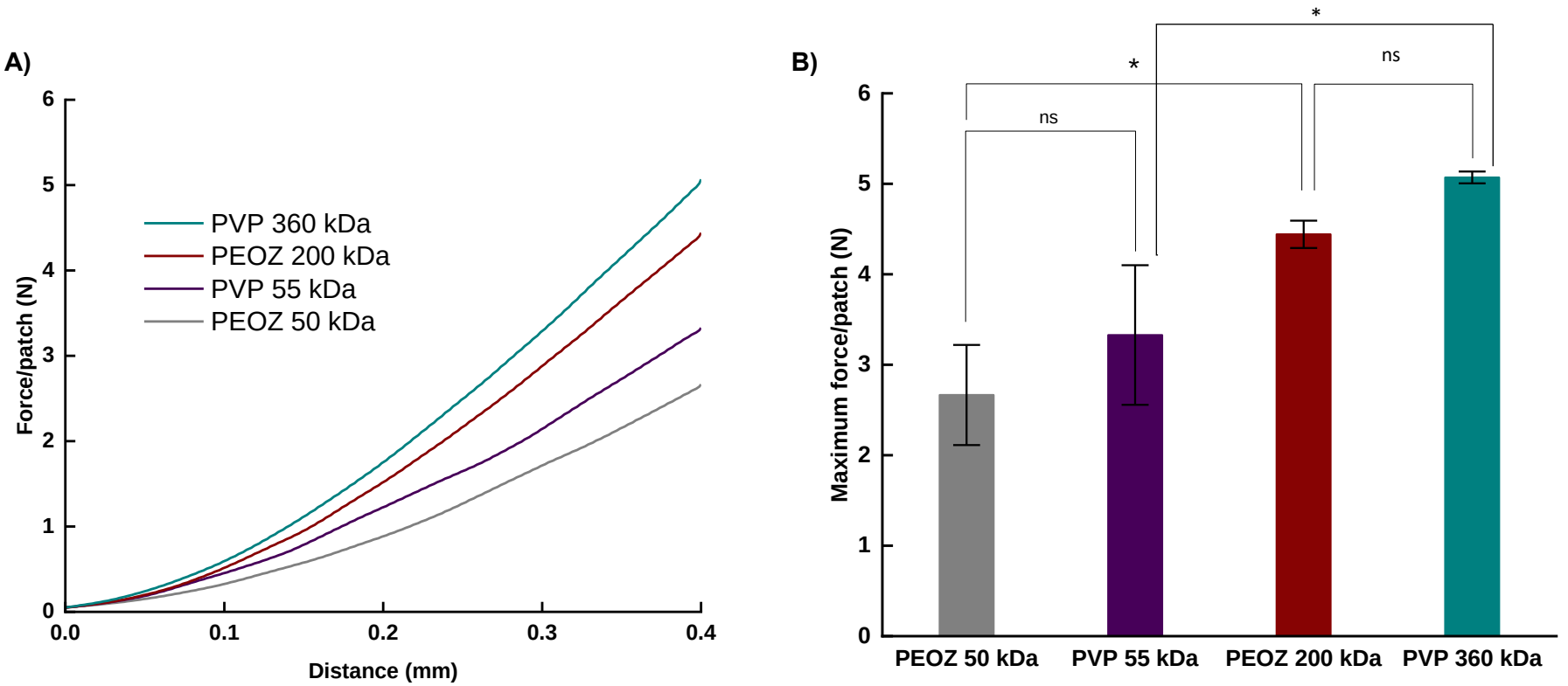

Figure 2.9 A) Force-distance curves of PEOZ and PVP microneedles after the application of an axial force. B) Maximum force required to compress the needles to 0.4 mm (obtained from the force-distance curves), data presented as mean ± SD of triplicates. * = p<0.05, ns = p>0.05. ANOVA with Tukey's post hoc test.

2.3.4 INSERTION TEST

The penetration efficiency of the MNs reduced as the depth of the skin model increased (Figure 2.10). The needles in each type of MNs punctured the first and second layers of Parafilm® M, however only PEOZ 200 kDa and PVP 360 kDa reached the third layer.

The penetration efficiencies of the four types of MNs were similar in the first sheet (approximately 100%) but this changed in the second sheet, with the MNs made from high molecular weight PEOZ and PVP having higher penetration efficiencies than those made from the low molecular weight PEOZ and PVP, which is consistent with the results of the compression test. PVP 55 kDa MN showed higher penetration efficiency in the second sheet than PEOZ 50 kDa but this is not statistically significant. Additionally, PVP 360 kDa MN showed higher penetration efficiency than PEOZ 200 kDa in the second and third sheets but the differences were not statistically significant.

Images of the MNs after insertion are shown in Figure 2.11. The backing layer in the four types of MNs remained intact and did not break after insertion. MNs made from PEOZ 200 kDa and PVP 360 kDa did not break or bend after insertion and their tips remained intact. However, some needles of PVP 55 kDa MNs and PEOZ 50 kDa MNs broke at the tips while the others bent. The % height reduction in the bent PEOZ 50 kDa MNs and PVP 55 kDa MNs (measured in similar sections in each MN patch) were 30 ± 5 % and 10 ± 2 % respectively with a statistically significant difference (Independent samples t-test was used because only two groups of MNs exhibited height reduction post-insertion).

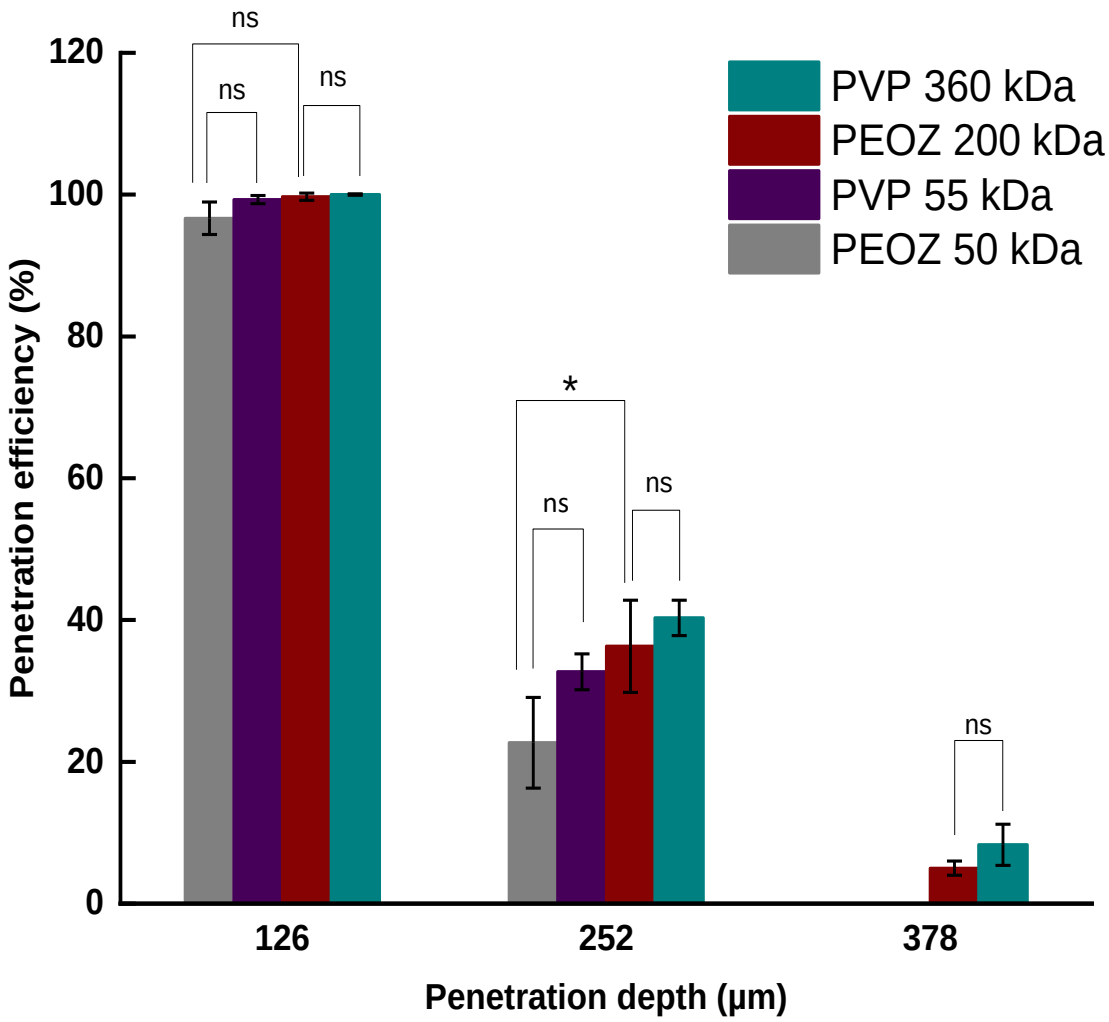

Figure 2.10 Penetration efficiency of the microneedles at different depths in Parafilm® M. Data presented as mean ± SD of n=3. * = p<0.05, ns = p>0.05. ANOVA with Tukey's post hoc test.

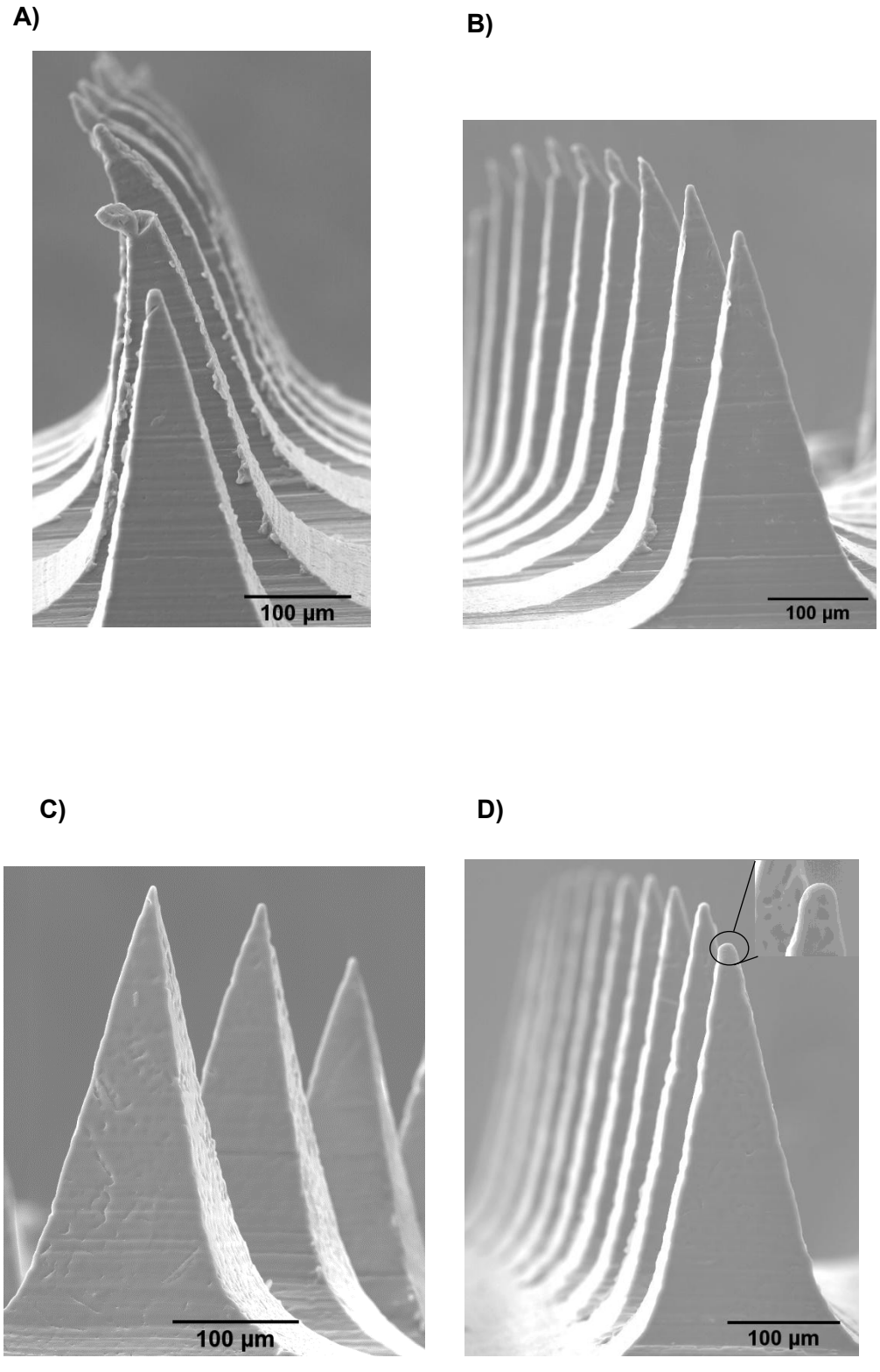

Figure 2.11 SEM images of microneedles after insertion into Parafilm® M A) PEOZ 50 kDa B) PVP 55 kDa C) PEOZ 200 kDa D) PVP 360 kDa. A-D X500 magnification.

2.3.5 QUANTIFICATION OF SODIUM FLUORESCEIN

The calibration curve (Figure 2.12) shows a linear relationship between fluorescence intensity and the concentration of sodium fluorescein in the concentration range studied (0.005 – 0.03 µg/mL). The equation of the regression line is y = 7417.1x + 3.4857, where y is the intensity, x is the concentration of sodium fluorescein, and the correlation coefficient (R^2) is 0.9994. The limit of detection (LOD) and limit of quantification (LOQ) are 0.002 µg/mL and 0.005 µg/mL respectively, calculated using the equations below:

$$LOD = \frac{3.3\,\sigma}{S} \quad (2.2) \qquad LOQ = \frac{10\,\sigma}{S} \quad (2.3)$$

Where σ = standard deviation of the response and S = slope of the calibration curve.

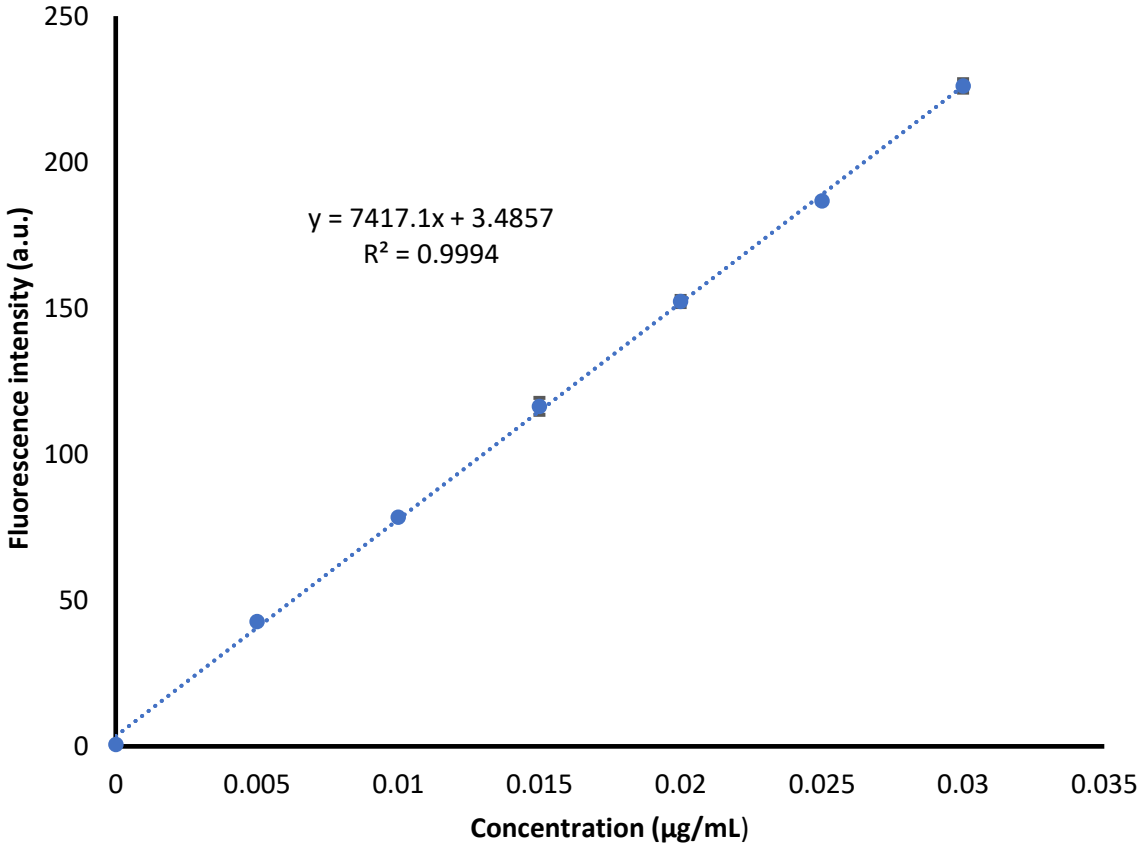

Figure 2.12 Calibration curve of sodium fluorescein. Data points and error bars are mean ± SD of triplicates. The error bars are smaller than the data points.

2.3.6 *IN VITRO* DRUG RELEASE STUDY

PEOZ 200 kDa MNs and PVP 360 kDa MNs were used in this study due to their performance in the characterisation studies. The theoretical amount of sodium fluorescein in each patch MN patch is 0.5 µg/patch based on the volume of the needles in the patch and the sodium fluorescein concentration in the polymer solution. Quantitative analysis showed that the total sodium fluorescein content was 0.48 ± 0.02 µg/patch and 0.46 ± 0.01 µg/patch in PEOZ 200 kDa MNs and PVP 360 kDa MNs respectively (mean ± SD, n=3), and there was no statistically significant difference between these values (Independent samples t-test). These findings are consistent with studies in the literature which reported 92% to 98% drug recovery from MNs (144, 266), further details are in the discussion section.

Details about the rationale for attempting the Franz diffusion cell experiment for the *in vitro* release study are provided in the discussion section. The Franz diffusion cell experiment was conducted three times for each type of MN, but the fluorescence intensities of the aliquots obtained throughout the three experiments were very low and not distinguishable from the background signal.

In the first experiment, residues of the backing layer remained on the membrane inside the donor chamber. Then, the experiment was repeated but with a 3g weight (2mL flat bottom autosampler vial with a cap, Scientific Laboratory Supplies, UK) placed on the MN patch in the donor chamber, based on the method reported in the literature (269). By the end of the experiment (60 minutes), there was no residue of the backing layer for both types of MNs. Despite this, the intensities of the aliquots were still low, rather a green solution was seen on the membrane and on the bottom of the vial, which is likely sodium fluorescein.

Subsequently, training was sought from technical experts to ensure that the experiment was arranged correctly. The experiment was then repeated (with a vial placed on the MN patch), and the duration of the experiment was extended to 120 minutes. However, the

intensities were similar to the intensities of the previous experiments and a green solution was still present on the membrane and on the bottom of the vial.

Therefore, an alternative experimental design was used for the study, in which the MN patches were immersed in the release medium, as described in 2.2.6. The release profiles of sodium fluorescein from both PEOZ 200 kDa MNs and PVP 360 kDa MNs in PBS are shown in Figure 2.13. In PEOZ 200 kDa MNs, less than 40% of the sodium fluorescein was released within the first 5 minutes, followed by the release of approximately 100% within 20 minutes. In contrast, PVP 360 kDa MNs showed faster release, with more than 80% of sodium fluorescein being released within the first 5 minutes and the remaining within 10 minutes. The MNs were observed throughout the study, and it was seen that the needles dissolved within the first few minutes while the backing layers of both MNs changed to gel-like substances at the start of the experiment before they dissolved entirely within approximately 20 minutes for both MNs.

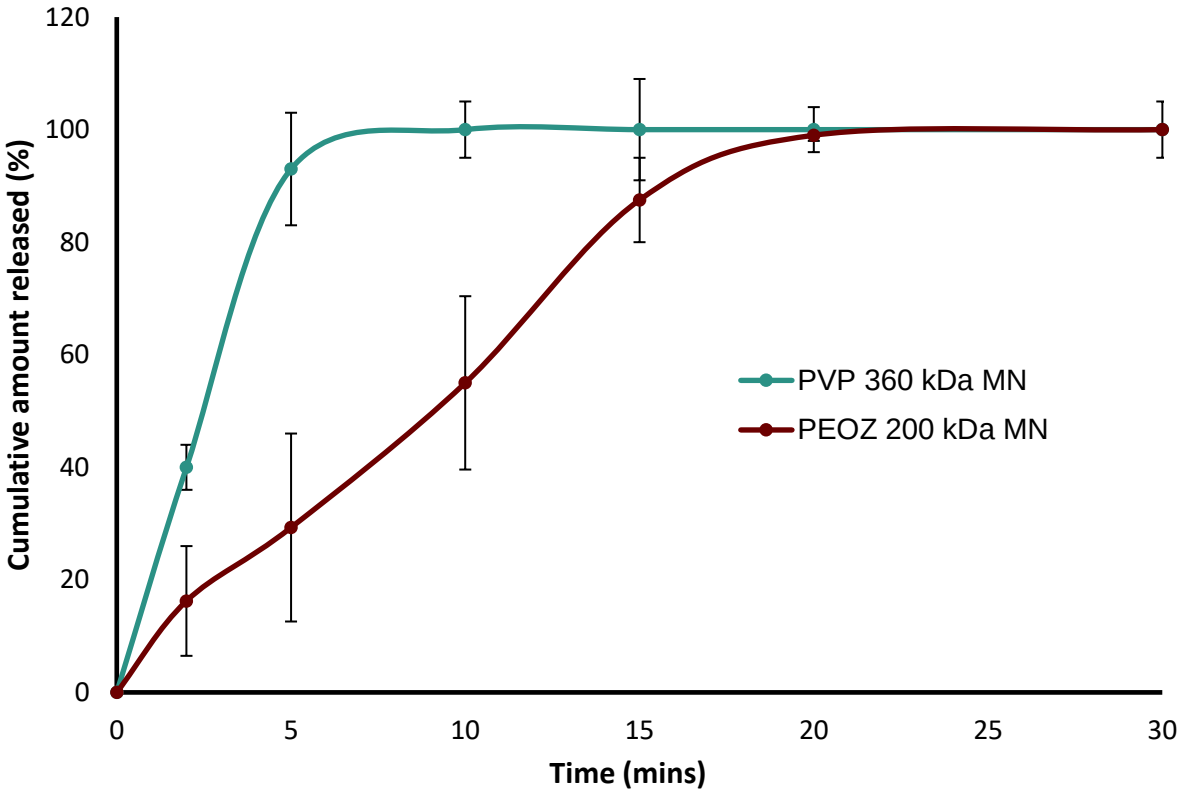

Figure 2.13 *In vitro* release profiles of sodium fluorescein from microneedles made from PVP 360 kDa and PEOZ 200 kDa in phosphate buffer saline. Data points and error bars are mean ± SD of triplicates.

Figures 2.14 and 2.15 show the graphs generated from the kinetic modelling of the *in vitro* release test data while Table 2.2 shows the correlation coefficients of the models.

Table 2.2 Correlation coefficient (R^2) values of kinetic models for sodium fluorescein released from PEOZ 200 kDa microneedles and PVP 360 kDa microneedles.

Microneedle (MN)	First order model	Zero order model	Higuchi model
PEOZ 200 kDa MN	0.8629	0.9852	0.9424
PVP 360 kDa MN	0.9799	0.8122	0.9387

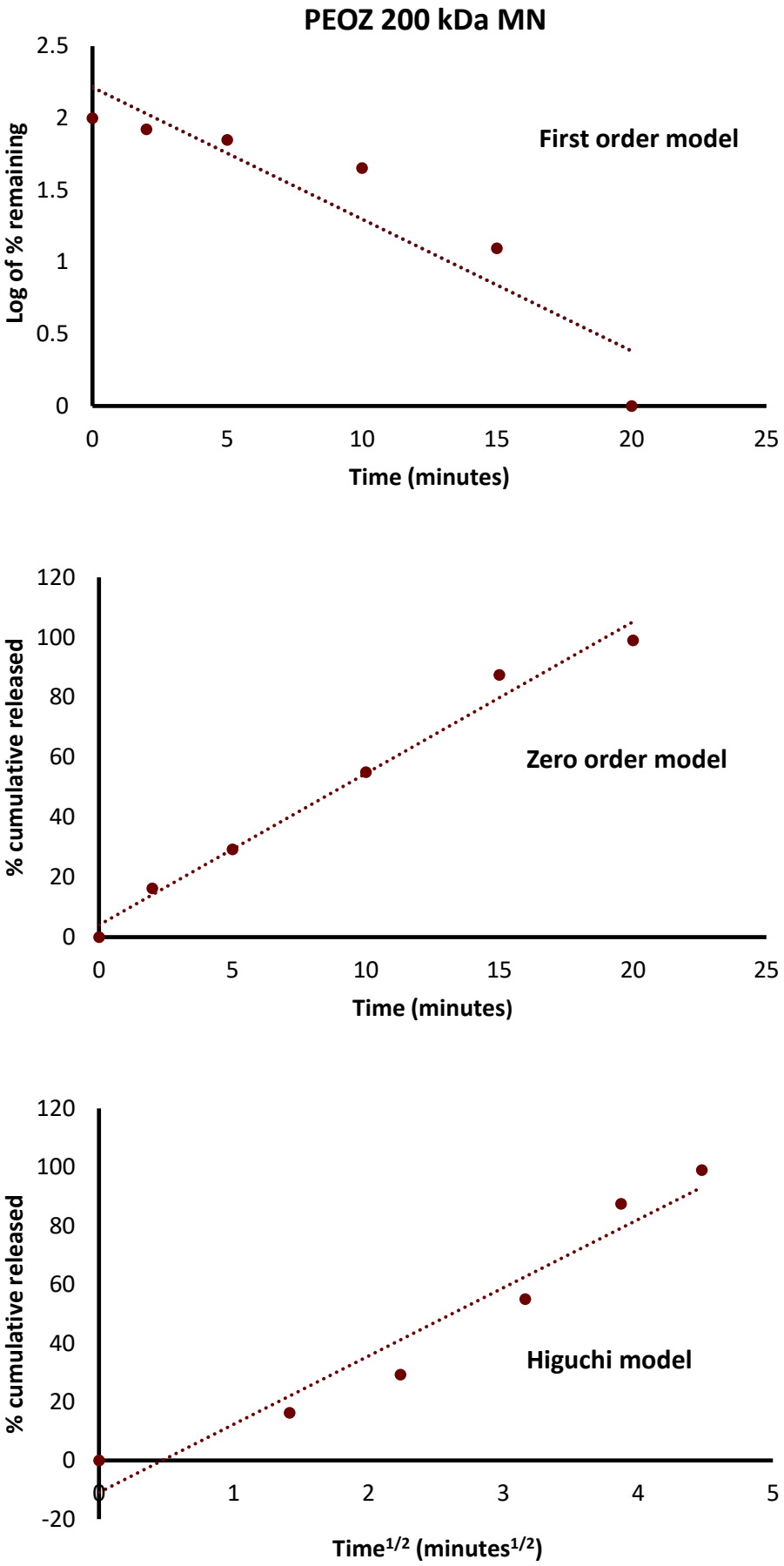

Figure 2.14 Mathematical modelling graphs of sodium fluorescein released from PEOZ 200 kDa MN in phosphate buffer saline.

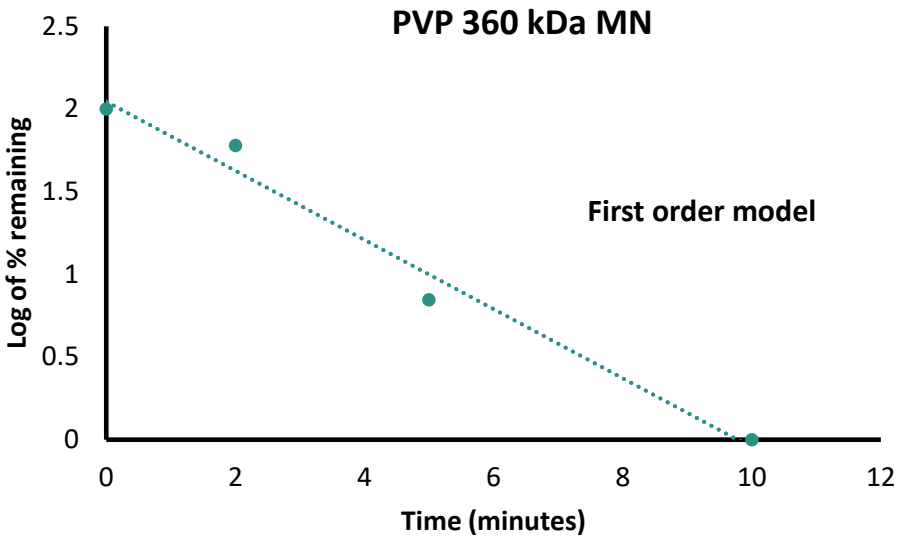

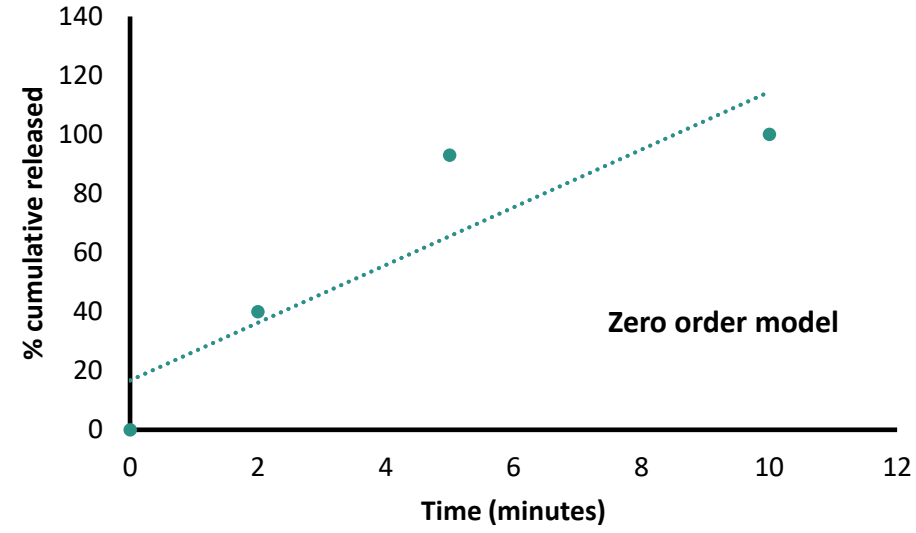

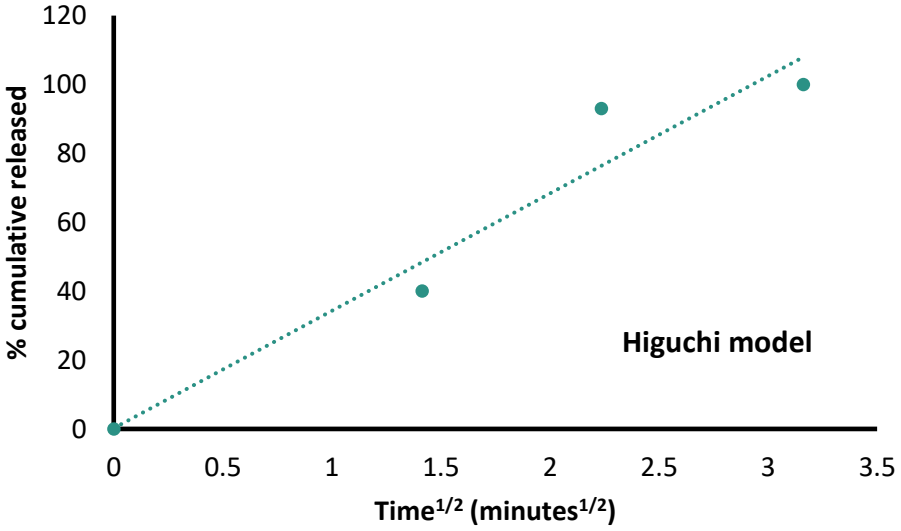

Figure 2.15 Mathematical modelling graphs of sodium fluorescein released from PVP 360 kDa MN in phosphate buffer saline.

2.4 DISCUSSION

This chapter describes the first report of fabricating and characterising MNs made from PEOZ (50 kDa and 200 kDa) and comparing them with those made from PVP (55 kDa and 360 kDa). A fabrication method was initially developed by adapting methods in the literature and attempts were made to create a custom-made PDMS mould prior to using a commercial PDMS mould for PEOZ MN and PVP MN fabrication.

The fabrication process was not complex and enabled small scale MN fabrication in an academic laboratory. The flexibility of PDMS enabled the detachment of MN patches after drying. However, as seen in the MNs that were fabricated from the custom-made moulds, it is vital to use well-prepared and uniform moulds as these could affect the quality of the MNs. The structure of the DermaStamp master template made it challenging to produce suitable moulds due to the required manoeuvring of the master template to remove and avoid the introduction of air bubbles after inserting it into the PDMS mixture. Although wetting the master template reduced the number of air bubbles, the overall process had poor production efficiency and led to several unsuccessful attempts to produce suitable moulds. It was also challenging to control the thickness of the backing layer as this was affected by the position of the master template when inserted into the mixture. The presence of voids and inconsistency in the thickness of the backing layer are not ideal as these could affect the performance of the MNs and create batch-to-batch variation.

PVP MNs with similar structure to the master template were fabricated by micro-moulding. The height of MNs was less than that of the master template and this could be due to water loss on drying, in which other studies have shown a height loss ranging from 5-20% in polymeric MNs (108, 120, 126). A drying time of 24 hours was not sufficient to fabricate MNs using the custom-made mould. The drying time could be due to the long duration of water evaporation from the viscous high molecular weight gel (270), in addition to the thickness of the backing layer.

Nevertheless, optimisation of the fabrication process, such as adjusting drying time, removing bubbles from the PDMS, etc, yielded MNs. However, the mould was changed to a commercially available PDMS mould to ensure consistency because the height of the needles in the DermaStamp master template varied between batches, in addition to the aforementioned issues.

The PDMS moulds were changed to a set of commercially available moulds which have been used in the literature to create good quality MNs (126, 271-273). The PDMS moulds with 100 needle cavities made the fabrication process more efficient and reproducible than when the previous moulds were used and they could enable increased drug loading due to the increased number of needle cavities. Factors such as fabrication material, needle geometry, dimensions, and the state of the backing layer can influence the mechanical properties of MNs (90, 123, 138). So, it was important to ensure that the shape, dimensions and backing layer thickness were controlled and variability was minimal to evaluate PEOZ as a MN material. The two most common MN shapes reported in the literature are pyramidal and conical shapes (90). Moulds which create pyramidal MNs were chosen because pyramidal MNs have been reported to have better mechanical properties than conical MNs, which could be because pyramids have a larger surface area than cones with a similar base diameter (90, 143). Some studies have reported the use of other shapes such as obelisk (274). Although these have been reported to improve the mechanical properties and drug loading of the MNs, they generally require advanced manufacturing techniques such as 3D printing and micromilling which were not accessible in this study.

A good MN material creates needles that replicate the shape and number of needles in the mould or master template, as well as create uniform needles with well-defined tips. This is important for dose uniformity and adequate skin insertion. MNs, each made from 50 kDa and 200 kDa PEOZ, were fabricated for the first time and compared with 55 kDa PVP MNs and 360 kDa PVP MNs. The MNs were fabricated by micro-moulding using

the commercially available mould. It was interesting to see that 200 kDa PEOZ did not form a viscous gel when dissolved in water, rather it formed a solution despite being of a high molecular weight. In contrast, 360 kDa PVP formed a viscous gel which required settling to remove bubbles prior to casting in the mould. Viscosity of polymer solutions could pose an issue in MN fabrication by micro-moulding, as it generally interferes with complete filling of the mould cavities which reflects on the needle tips and dimensions.

PEOZ 50 kDa and 200 kDa, as well as PVP 55 kDa and 360 kDa, formed 100 needles, with pyramidal shapes, well-defined tips and dimensions similar to the mould. However, the cracked areas on PEOZ 50 kDa MNs suggest that PEOZ 50 kDa alone is not ideal for fabricating MNs. The cracks could be due to the brittle nature of PEOZ 50 kDa which has been reported in films made from it (163).

Several researchers have shown that PDMS moulds from Micropoint Technologies Ltd create good quality MNs which are suitable for drug loading and skin insertion. However, there is no information on the internal structure of the mould cavities. As shown in Figure 2.7 B, the mould cavities are layered, and this was reflected in the MN structure. This layered structure of MNs was also seen in the literature (79, 271) and there is no evidence that this structure has adverse effects on MN integrity and function.

It is important that the MN backing layer has appropriate strength and flexibility to enable proper application on the skin (40). Since PEOZ 50 kDa created a thin and fragile backing layer, PVP 360 kDa was used to make the backing layer of the four types of MNs to maintain consistency for characterisation of the needles. It is common for the backing layer of MNs to be made from materials that are different from those used in making the needles, in order to enhance the mechanical properties (15, 52, 89).

The heights of the MNs fabricated in this study are within the range for bypassing the *stratum corneum* without reaching the pain receptors in the dermis, and the tip diameters and spacing between the needles are similar to those in the literature which are known to be suitable for skin insertion (147).

The heights of the four types of MNs were lower than that of the mould and this phenomenon, which is common in polymeric MNs made from moulding, could be due to water evaporation during drying (108, 151). The height reduction in the PEOZ 50 kDa and 200 kDa MN is similar to that reported in the literature, as mentioned earlier. This suggests that the use of PEOZ 50 kDa and 200 kDa does not negatively impact the dimensions of MNs made by micro-moulding.

Although the height of PVP 360 kDa MNs was similar to the heights of the other MNs, the dimensions of the needles in the PVP 360 kDa MNs seemed to lack consistency across the patch. This could be attributed to the viscosity of PVP 360 kDa which may have resulted in non-uniform filling of each mould cavity during fabrication. The potential inconsistency in the dimensions of PVP 360 kDa MNs, as well as the morphology of the MNs made by the custom-made mould, show the limitation of micro-moulding as a fabrication method for MNs, as the resulting MNs are affected by the features of the moulds and by the dispensing and filling of the mould cavities, especially for viscous polymers. Several attempts have been proposed in the literature to enable complete filling of the mould cavities and to improve the reproducibility of micro-moulding, especially for viscous polymer solutions, for both small-scale and large-scale MN fabrication (38, 106, 275, 276).

It is imperative for MNs to have adequate mechanical properties to overcome resistance from the skin during insertion and to insert into the skin without breaking. Application of an axial force to compress MNs is a common method of studying mechanical properties of MNs. In the compression study, the texture analyser applied an axial force to the MNs to measure the force required to move the probe as a function of distance. The similarity in the shape of the force-distance curves of PEOZ MNs and PVP MNs in this study suggest that they show similar mechanical behaviour i.e., a continuous curve without a distinct drop which is typical of pyramidal MNs made from polymers. The continuity of the curve and increase in force with distance indicate that the needles gradually

deformed rather than breaking abruptly unlike conical MNs (90, 277). Visualisation under a microscope showed that the MNs did not break within the force range of the experiment, which is consistent with the shape of the curves.

The results also indicate that resistance to compression increased with an increase in molecular weight for both PEOZ MNs and PVP MNs. This is in agreement with other reports of PVP MNs, polyvinyl alcohol MNs, and hyaluronic acid MNs (151, 277-280). This phenomenon could be due to the presence of increased interactions between polymer chains in high molecular weight polymers compared with those in low molecular weight polymers, resulting in stronger chain entanglements which could in turn lead to higher resistance to deformation (281).

Conversely, a study compared 10 kDa, 74 kDa, 290 kDa hyaluronic acid MNs and found that compressive strength reduced with an increase in molecular weight, with 10 kDa showing the highest resistance to compression (282). The authors suggested that this could be due to tighter packing of the low molecular weight polymer chains during drying. Whilst the argument is plausible, the wide variation in the heights of the MNs in their study may have influenced their results, especially as the results of the compression test in the study were not consistent with the results of the insertion test.

The molecular weights of PEOZ and PVP used in this study were chosen based on the closest matching ones available in the market. So, the slight variation in molecular weights between PEOZ and PVP may have influenced the observed numerically higher values in PVP MNs than PEOZ MNs in the compression test. Furthermore, the rigid ring in PVP's monomer may give PVP tighter chains than PEOZ which may favour PVP's resistance to compression (150). However, there was no statistically significant difference between the maximum forces of compression for PEOZ MNs and PVP MNs, in both the high and low molecular weights.

The PEOZ MNs and PVP MNs in this study required forces between 2.8 – 4.8 N to compress them to 0.4 mm. Bhatnagar et. al and Zhu et. al. reported forces of

approximately 8 N and 28 N to compress PVP 360 kDa MNs and hyaluronic acid MNs to 0.4 mm respectively (79, 117). It is very likely that these forces are higher than those seen in this study because of the marked difference in MN height, patch size and tip diameter between the MNs in this study and theirs. Although compression testing is commonly used to measure MN mechanical properties, variation in the experiment conditions, patch size, needle dimensions and geometry used by different authors pose a challenge in comparing reported properties of MNs because these parameters influence the results.

Attempts have been made to identify a method of assessing MNs and determining if they are suitable for skin insertion. One common method uses insertion forces reported in the literature as a threshold value to determine if the compression or failure force of the MNs is greater than the insertion force. The maximum force that MNs can tolerate, or the failure force, should be higher than the force applied during insertion into skin. Hence, several authors tend to assume that their MNs are suitable if the MNs can tolerate forces higher than reported insertion forces in the literature, but insertion values reported in literature are conflicting. One commonly cited report used in the MN research field is by Davis et. al. who found that insertion force varies linearly with tip cross-sectional area, and ranges between 0.08 – 3.04 N per needle for manual insertion without an applicator (283). The study was done by inserting a single metal MN, with tip radii between 30 – 80 μm, into 3 male volunteers. However, some researchers suggest that this should be used with caution because the failure force of a single MN may not reflect that of an array of MNs (40, 152, 284). Economidou et. al. reported an insertion force of 0.035 N per needle for pyramidal MNs in a study where a 7x7 MN patch with 1000 μm needles was inserted into porcine skin using a texture analyser (143).

In contrast, Yan et. al. suggested that it is not reliable to judge MNs by comparing compression/failure force with insertion force due to their study which showed variation in the insertion profiles of different MNs which had a similar compression force (285).

On the other hand, Larrañeta et. al. found that the average force exerted on a MN patch by thumb pressure is approximately 20 N (261). This finding then led to a different type of MN characterisation by this group where MNs are compared by measuring their percentage height reduction after axial force compression but there is no clear guide on the acceptable threshold for MN height reduction after compression.

In view of these differing approaches, quality specifications for MNs set by regulatory bodies are required to aid in characterising and assessing the mechanical properties of MNs, as this could facilitate evaluation of new MN materials such as PEOZ used in this study, as well as the translation of drug-loaded MNs for clinical use.

Although the axial force compression test gives insights into the behaviour of MNs during compression, it does not fully reflect insertion into the skin since the MNs were compressed against a rigid metal block which results in localisation of the force on the needle tips. During skin insertion, the forces experienced by the MNs on the soft and viscoelastic tissue are spread across a larger area on the MN patch (80, 135). Additionally, the test assumes that all needles in a patch compress at the same rate which is not always the case as there could be variation between needles in the same patch (286).

Nevertheless, the test gave insights into the ability of PEOZ MNs to resist compression and how they compare to PVP MNs. However, further tests were done to investigate the skin insertion ability of the MNs and if they can withstand insertion by hand.

Parafilm® M, a mix of hydrocarbon wax and a polyolefin, is a skin simulant validated by Larrañeta et. al for MN insertion studies (261) and has been adopted by several researchers in the MN research field. Eight sheets of Parafilm® M were folded to create a skin simulant with approximately 1 mm thickness, mimicking full thickness skin. The first sheet corresponds to a penetration depth of 126 μm and the next sheets after it correspond to an additional depth of 126 μm. This enables an estimation of the penetration depth of the MNs while the number of holes created in each sheet relates to

the MNs' penetration efficiency at each depth. This test is a common method of evaluating MN skin insertion. However, this work took an additional step to examine the MN morphology before and after insertion. Most studies on MNs report the MN morphology before and after compression but this was done in the insertion test in this study because it is a closer mimic to skin insertion than compression against a rigid block and it could give information about whether the MNs could maintain their integrity after manual insertion.

The penetration efficiency of the MNs dropped as the depth increased. This is due to the elasticity of Parafilm® M which mimics the viscoelastic nature of skin and its resistance to insertion, resulting in the penetration depth being less than the needle height. Studies have shown that MNs penetrate to about 10 – 80% of their full height (15, 126, 287). The four types of MNs in this study had approximately 100% penetration efficiency in the first Parafilm® M sheet, indicating that they can bypass the stratum corneum which is approximately 5-50 μm thick (7, 261).

The findings of the insertion test suggest that the insertion performance of the MNs improved with an increase in molecular weight, which is consistent with the findings of the compression test. This could be due to the reasons explained earlier about polymer chain interactions. Approximately 40% of PEOZ 200 kDa MNs and PVP 360 kDa MNs punctured the second sheet which corresponds to a depth of 252 μm and less than 10% of both the PEOZ 200 kDa MNs and PVP 360 kDa MNs reached the third sheet. Since the penetration efficiencies on the third sheet are less than 20% for both types of MNs (261), the penetration depth of PEOZ 200 kDa MNs and PVP 360 kDa MNs is estimated to be between 252 – 378 μm.

The insertion test suggests that the penetration depths and efficiencies of PEOZ 200 kDa MNs and PVP 360 kDa MNs are comparable, and this is consistent with the compression test which showed the lack of a statistically significant difference between their maximum forces of compression. Most importantly, PEOZ 200 kDa MNs and PVP

360 kDa MNs remained essentially intact after insertion. This suggests that the MNs can withstand the skin's resistive forces during insertion, as well as the force applied by thumb pressure.

The insertion test also showed that PEOZ 50 kDa MNs performed poorly, because they deformed markedly, including fractures in some needles, after insertion. Both PEOZ 50 kDa MNs and PVP 55 kDa MNs penetrated up to the second sheet (252 μm) and there was no statistically significant difference between their penetration efficiencies on the second sheet. These results are consistent with the results of the compression test. Needle deformation also occurred in PVP 55 kDa MNs post-insertion, and this suggests their limited ability to resist the skin's resistive forces during insertion which is not ideal. Other studies that used low molecular weight PVP to fabricate MNs utilised polymer blending to create good quality MNs (120, 280, 288). This could also be explored for PEOZ 50 kDa. Overall, these results strongly suggest that PEOZ 50 kDa is not suitable as a sole material for fabricating MNs.

It is also worth noting that the degree of deformation in both PEOZ 50 kDa MNs and PVP 55 kDa MNs varied between needles in each patch. For example, the needles on the sides tended to deform less than those in the middle. This could be due to variation in the mechanical properties of the needles in each patch or variation in the distribution of the insertion force across the patch (139, 286). Overall, these results show the benefit of using more than one characterisation method to a gain a comprehensive view of the suitability of a polymer for MN fabrication.

MNs were also evaluated using an *in vitro* release test with sodium fluorescein as a model drug and fluorescence spectrophotometry as the assay. Sodium fluorescein was selected because it is water soluble, can be easily detected (including at low concentrations) and provides an opportunity to visualise its distribution on the MNs (289-292). Fluorescence spectrophotometry was used due to its high sensitivity which makes

it suitable for MNs because the drugs in MNs are usually present in low amounts due to the size of the MNs.

The difference between the theoretical amount of sodium fluorescein and the measured amount of sodium fluorescein in the MN patches in this study aligns with findings in the literature (references in 2.3.6). The small observed difference could be attributed to loss during fabrication which is expected in a small-scale laboratory manufacturing performed manually by an individual. Analysis of each step in the fabrication process could help identify potential strategies to minimise loss. It is also interesting to see that the sodium fluorescein content in PEOZ 200kDa MNs and PVP 360 kDa MNs were comparable despite the potential of limited solubilisation of sodium fluorescein in the viscous PVP 360 kDa gel which was expected to have resulted in further loss of sodium fluorescein during fabrication. Overall, the findings suggest reliability of the MNs for drug delivery.

It is important that a drug delivery system releases its encapsulated drug after administration. So, an *in vitro* drug release test was done to further explore PEOZ 200 kDa as a MN material, with PVP 360 kDa as the comparator, due to the promising results in the previous tests.

A literature review was conducted to inform the experimental design of the *in vitro* drug release study in this work, and it became apparent that there is no standardised method for evaluating *in vitro* drug release in MNs, at the time of writing this thesis. However, there are few reports in the literature that aimed to develop methods that are tailored to MNs. In majority of the reports that were found, the MN patch was immersed in the release medium without a membrane and the drug release was measured at different time intervals (81, 115, 117, 263-265, 293, 294).

In vitro release tests for transdermal patches are typically conducted using a United States Pharmacopeia (USP) apparatus such as the paddle over disk method (USP apparatus 5) where the patch is placed on a disk inside a release medium which is stirred using a paddle and then drug release over the entire surface of the patch is evaluated

(295-297). *In vitro* release tests for semi-solid formulations are typically performed using an open chamber diffusion cell system, such as Franz diffusion cell, with an inert synthetic membrane which is typically used as a mechanical support which separates the formulation from the release medium (1, 298-300). Alternatively, *in vitro* release tests for semi-solid formulations can be performed by immersing the formulation in the release medium (301, 302). It has been suggested that the Franz diffusion cell experimental design is suitable for MNs because it resembles MN insertion in the skin where the needles are in contact with the interstitial fluid before the fluid reaches the backing layer (269).

Another experimental design reported in the literature for MNs is the immersion of the MN patch in a bag made from a dialysis membrane, followed by immersing the bag in the release medium (279) but this is quite similar to the USP method for transdermal patches described earlier because the needles and backing layer are in contact with the release medium at the same time.

Other studies modified the dialysis bag method by scrapping the needles from the MN patch and immersing the needles in a dialysis bag (a cellulose-based dialysis membrane), followed by sealing the bag and immersing it in a bottle containing the release medium (303, 304). This method enables the evaluation of drug release from the needles alone, but the authors of one of the studies reported that the drug release from this method was faster than the drug release from *ex vivo* and *in vivo* experiments due to reasons described later in this section. Additionally, it is preferable to include the backing layer in the experiment because if the drug migrated to the backing layer, the fluid will migrate to the backing layer after the dissolution of the needles which will then result in the release of the drug from the backing layer during application on the skin (81, 87, 269).

Another study proposed the use of a sheet of Parafilm® M to create a pouch around the MN patch (269). In this method, the MN is inserted into a sheet of Parafilm® M and the

sheet is then wrapped around the patch and thermally sealed to cover the base and expose the needles alone to the release medium prior to the release medium reaching the backing layer afterwards. Then, the Parafilm® M-wrapped MN patch is immersed in a container containing the release medium. However, the efficiency of this method for measuring drug release is dependent on the penetration ability of the MNs in Parafilm® M, i.e. they should remain intact to prevent drug loss, based on the findings of the study. The method is also not suitable for MNs that have backing layers that swell to a size that causes the Parafilm® M sheet to break, based on the findings of the study. Additionally, as Parafilm® M has been reported as a skin simulant for MN insertion studies, as described earlier, this experimental design could resemble an *in vitro* permeation test rather than a release test and the authors in the study found that the release profile obtained from this design was comparable to that obtained from a Franz diffusion cell experiment using a sheet of Parafilm® M as the membrane. Furthermore, Parafilm® M may act as a rate-limiting membrane due to its hydrophobic nature which may slow down contact between the MN patch and the aqueous release medium which may in turn reduce the rate of drug release.

In view of these, the *in vitro* release study was conducted using a Franz diffusion cell system with a cellulose-based membrane (299). However, it is surprising that sodium fluorescein was not released in detectable amounts throughout the experiment, despite adjusting the design and prolonging the duration of the experiment. It is interesting to see that placing a weight on the MN patch resulted in the dissolution of the entire patch including the backing layer, as this suggests that it enhanced contact between the patch and the membrane. However, the reason for the limited release of sodium fluorescein into the receptor chamber is unclear.

The membrane exhibits an elastic and loose gel-like structure when wet and this may make it difficult for the needles to puncture the membrane and/or embed within the created pores in the membrane in order to be in contact with the release medium and

this may have then limited drug release into the receptor chamber. It has been reported that MNs retracted within 1 minute after insertion into a silicone membrane (based on an evaluation using optical coherence tomography) whereas this did not occur in Parafilm® M (269, 305). The authors then suggested that needle retraction could explain the poor drug permeation observed in an *in vitro* permeation test which was performed using silicone membrane compared to when Parafilm and pig skin were used.

It could also be that there was an air bubble entrapped between the membrane and the receptor chamber in this work which may have obstructed the release of sodium fluorescein into the chamber. The author of this thesis acknowledged their limited expertise in setting up this experiment so training was sought from technical experts but there were no changes in the outcome of the experiment.

Therefore, an alternative experimental design was used, in which the entire MN patch was immersed in PBS and the release of sodium fluorescein was measured at different time intervals, which is similar to the USP method for transdermal patches mentioned earlier. This experimental design used in this work was based on the methods used in several reports in the literature, as described earlier. With regards to the potential for overestimation or underestimation of drug release using this method, it is plausible that this depends on the distribution of sodium fluorescein within the patch, i.e. if the sodium fluorescein is in the needles alone or if some of it migrated to the backing layer. So, even with the backing layer being in contact with the release medium at the same time as the needles, the amount of sodium fluorescein released may not be over-estimated if the backing layer did not contain any drug. However, this may not be the case due to drug migration to the backing layer, as described later in this section. On the other hand, the swelling of the backing layer during the experiment may result in retention of moisture at the interface between the needles and the backing layer and/or create pores in the backing layer through which sodium fluorescein can pass through, which in turn may result in faster drug release than in the skin (294).

Overall, there is a need for a standardised experimental design for *in vitro* release tests for MNs, which could be combined with *in vitro* permeation tests to facilitate MN development. However, it is worth noting that the drug release rate observed in the *in vitro* release tests for MNs in the literature is generally higher than that observed in *ex vivo* and *in vivo* studies, including the *in vitro* experimental design described earlier, where drug release from the needles alone was evaluated after separating the needles from the backing layer (115, 293, 304). This could be due to the inherently variable and complex nature of the human skin which makes it challenging to mimic and to correlate findings from *in vitro* tests with *in vivo* performance for topical and transdermal formulations (293, 298, 301, 306).

Several *in vitro* drug release tests on polymeric MNs have shown that MNs made from water soluble polymers exhibit rapid drug release. For example, carboxymethylcellulose MNs and hyaluronic acid MNs released more than 80% of their encapsulated drugs (diclofenac sodium and amifostine respectively) within 20 minutes of immersion in PBS (307, 308). As expected, sodium fluorescein in this work was released rapidly from both PEOZ 200 kDa MN and PVP 360 kDa MN, owing to the water solubility of sodium fluorescein and the polymers.

Initially, the needles dissolved within few minutes of immersion in PBS followed by dissolution of the backing layer. This could be because the needles and backing layer differ in thickness and surface area. Generally, the factors that affect the dissolution rate of solids, including pharmaceutical compounds, could be explained using the Noyes-Whitney equation (equation 2.4) when the rate-limiting step of the dissolution is the diffusion of the solid molecules through the diffusion layer (9, 309).

$$\frac{dm}{dt} = \frac{DA\,(C_s - C)}{h} \qquad (2.4)$$

Where dm/dt is the dissolution rate, D is the diffusion coefficient of the solute, A is the surface area of the solute in contact with the solvent, C_s is the saturation solubility of the solute in solution in the diffusion layer, C is the concentration of the solute in the bulk solution and h is the thickness of the diffusion layer around the solute.

Based on the equation, the needles are expected to have a faster dissolution rate than the backing layer, as they have a higher surface area which enables more contact with the dissolution medium to facilitate dissolution. However, the needles and backing layer are both made from polymers and the Noyes-Whitney equation does not fully align with polymers because polymer dissolution is more complex than non-polymers (310). Hence, other factors could be taken in account such as the unique process of polymer dissolution.

In the case of polymers, swelling occurs followed by chain disentanglement resulting in a transition from a glassy state to a rubbery state, and finally dissolution. Generally, the swelling forms two interfaces, the glassy - rubbery interface and the rubbery - solvent interface. These interfaces then reduce as the solvent further penetrates the polymer to enable dissolution (310, 311). This phenomenon could be the reason for the formation of a thick gel-like substance in the backing layer before it dissolved. Therefore, it could be that swelling occurred in both the needles and backing layer followed by polymer chain disentanglement for dissolution, but these may have occurred slowly in the backing layer due to its dimensions and denser packing which may have limited solvent penetration and chain disentanglement in comparison to the needles. It is not surprising that the needles in this work dissolved rapidly before the backing layer, as this is consistent with findings in the literature, such as 50% reduction in PVP needle length within 10 seconds due to dissolution in mice skin and the backing layer still undissolved at this stage (81, 115, 312).

The sodium fluorescein release behaviour observed from PVP 360 kDa MNs is consistent with findings in the literature (81, 115, 117) but it is interesting to see that the release rate from PEOZ 200 kDa MNs was lower than that of PVP 360 kDa MNs. This could be due to variation in the distribution of sodium fluorescein in the PEOZ 200 kDa and PVP 360 kDa MN patches. PVP 360 kDa may have had more sodium fluorescein on its outer surface than PEOZ 200 kDa during drying or some of the sodium fluorescein in PEOZ 200 kDa MNs may have migrated to the backing layer, a common phenomenon in MNs (52, 81, 89, 313, 314), which may then result in a slow release due to the slower dissolution occurring in the backing layer than in the needles, as mentioned earlier (81, 269). Efforts were made to visualise the distribution of sodium fluorescein within the MNs using a fluorescence microscope and confocal microscope, but these were not successful due to poor resolution in the available fluorescence microscope and inaccessibility to the local confocal microscope due to policy restrictions.

Furthermore, the release rate of sodium fluorescein from PEOZ 200 kDa MN in this study could relate to the dissolution rate of PEOZ *per se* in formulations, which has shown surprising results in the literature. Hoogenboom et. al. reported the first use of PEOZ as a matrix material to prepare tablets by hot melt extrusion and injection moulding. The authors were surprised to see that tablets made from PEOZ 200 kDa exhibited a slower than expected dissolution rate (60 minutes to dissolve by 50%) despite the high-water solubility of PEOZ. The authors suggested that this could be due to the high pressure used in injection moulding which may have caused high entanglement of the polymer chains (161). In this work, efforts were made to visualise the rate at which the PEOZ 200 kDa needles dissolved *in situ* by inserting them in skin and viewing under a confocal microscope, but this was not feasible in this study, as mentioned earlier. However, such an experiment could be done in future to examine the dissolution rate of the PEOZ MNs.

The release data of sodium fluorescein from PEOZ 200 kDa MNs and PVP 360 kDa MNs were fitted to three common mathematical models (first order model, zero order

model and Higuchi model) to evaluate the drug release. It should be noted that the very rapid dissolution rate of PVP MNs meant that only three data points could be acquired and so fitting of the data is not ideal. Notwithstanding this, the model with the highest correlation coefficient was considered to be the one which best aligns with the release mechanism.

The sodium fluorescein release from PEOZ 200 kDa MNs and PVP 360 kDa MNs were best modelled with zero order and first order respectively. Zero order release shows a drug delivery system which releases its encapsulated drug at a constant rate irrespective of the drug concentration. This is beneficial for certain therapies where drug concentration is required to be constant (315, 316). First order release occurs in a system where the release rate depends on the amount of drug remaining (267, 317). Mathematical modelling has been employed in the literature for MNs, in which drug release from some polymeric MNs were typically found to be consistent with first order and zero order models (318-320).

The Higuchi model, the oldest and most used model in the literature for pharmaceutical formulations, was proposed in the 1960s by Higuchi to describe drug release from matrix systems based on his drug release study on an ointment containing finely dispersed drugs (311, 321-323). The model describes a direct proportional relationship between the amount of drug and the square root of time, as shown below:

$$Q_t = \sqrt{Dt(2A - C_s)\,C_s} \qquad 2.5$$

Where, Q_t is the amount of drug released per unit exposed area after time t, A is initial amount of drug in the matrix, C_s is the solubility of the drug in the matrix, in which $A >> C_s$, and D is the diffusivity of the drug (311, 321, 324).

Based on the Higuchi model, the encapsulated drug diffuses from the matrix into the release medium which is kept under perfect sink conditions (by the skin in the case of the original study by Higuchi) (321, 324, 325).

The model is based on the following assumptions (311, 321, 323, 325, 326):

i) The initial drug concentration in the matrix is much higher than the drug's solubility in the matrix (by a factor of 10 or more) and there is a pseudo-steady-state condition during the release process.
ii) The diffusivity of the drug is constant, and drug diffusion occurs in one dimension when described mathematically.
iii) The drug particles are uniformly distributed in the matrix and are smaller than the thickness of the system.
iv) Matrix swelling and dissolution during drug release are negligible.
v) Perfect sink conditions are maintained, for example by the skin.

The model was originally used to describe drug release from a planar matrix system but several researchers, including Higuchi, have modified and extended the original equation to evaluate matrix systems of other shapes, such as spherical systems (321, 323, 324, 327).

It is likely that the Higuchi model is very popular amongst researchers due to its simplicity and well-established use for a long period of time (311, 324). However, Peppas et. al. highlighted the potentially incorrect use of this model to evaluate a wide range of drug delivery systems, including tablets, which deviate from the assumptions of the model (323, 325). Examples of common errors highlighted by the authors include using the model for drug delivery systems that swell or dissolve, for three-dimensional systems, over-simplification of the drug delivery process without accounting for other factors such as excipients, etc. Additionally, potential changes in the MN structure with time, which could be due to polymer swelling, dissolution, breakdown, etc, may result in a non-constant diffusivity of the drug, so models that account for a time-dependent change in

diffusivity may be more suitable for drug release that is primarily diffusion-dependent (328). Despite the limitations of the model, Peppas et. al. mentioned that for drug delivery systems that deviate from Higuchi's assumptions, the model could still give a rough idea of the underlying release mechanism of the systems, but the interpretation should be viewed with caution and preferably complemented with additional advanced mathematical models (323).

The Higuchi model was used in this work to get a preliminary idea of the underlying release mechanism of the MNs in this work, as this may help in comparing them, especially PEOZ MNs (new material), with other MNs in the literature. The model has been used in several reports in the literature to evaluate drug release in MNs (308, 320, 329, 330). Therefore, the aim of using this model in this work is to get a preliminary understanding of the release mechanism at the initial development stage of PEOZ MNs although the author of this work notes the model's limitations and did not intend to use any observed fit with the model to solely describe the release mechanisms of the MNs in this work.

It is worth noting that the models used in this work may not fully explain the release mechanisms in MNs, and this could be due to the structural features of MNs which these models generally do not account for (293, 331). An example is the geometry of the needles which influences the surface area exposed to the release medium at each position of the needles and this may result in non-uniform drug release, which in turn could affect the goodness of fit to a simple mathematical model that assumes that the drug flows in an ideal and uniform manner (311, 323, 332). Additionally, non-uniform needle dimensions or drug distribution, particularly in MNs fabricated in non-industrial settings, may result in variation in the drug release, which generally deviates from the simple mathematical drug release models (311). Furthermore, the swelling of polymers before dissolving, the formation of cracks or pores in the matrix system (needles and backing layer in this case) upon contact with the release medium due to polymer

swelling, or multiple release mechanisms occurring simultaneously, are potential events which could occur during drug release from polymeric drug delivery systems, which in turn could cause a deviation from the “ideal” systems that simple mathematical models are based on, as well as could make it complex to model such phenomena mathematically (311, 332, 333). Also, it is likely challenging to accurately detect multiple release mechanisms that are occurring simultaneously when the release is very rapid such as the release rate that was observed in this work.

It has been highlighted in the literature that there is a need for mathematical models that are tailored to MNs due to the aforementioned factors and several other reasons that have been raised by researchers in the MN field (293, 331). There is currently no model that accurately suits all formulations, and it is challenging and complex to develop perfect models for each formulation which accounts for all the relevant physicochemical and physiological parameters for each formulation that can be modelled by mathematical concepts (333, 334). However, mathematical modelling of MNs, for drug release and other characteristics such as skin insertion, is still in its infancy and a few researchers have looked into developing MN-specific models, including models that account for parameters such as polymer properties (e.g. size of the polymer chain) and the relationship between structural parameters like geometry, needle density, and their resulting effects on drug release (331, 332, 335).

Overall, the findings in this work suggest that PEOZ 200 kDa is a promising MN material due to its fluidity for micro-moulding, as well as its ability to form well-defined needles, overcome compression, insert into a skin simulant without breaking and release its loaded drug *in-vitro* in PBS. However, additional tests are required to gain further insights, such as evaluating its use for a clinical application, conducting skin irritation tests, and investigating the effect of humidity on the needles, as well as its ability to maintain the needle integrity and stability of its constituent drug upon storage. Suggestions for future work on PEOZ 200 kDa MNs are mentioned in Chapter 5.

CHAPTER 3 – INVESTIGATING MISCIBILITY BETWEEN POLY(2-ETHYL-2-OXAZOLINE AND POLY(VINYL ALCOHOL) FOR MICRONEEDLE FABRICATION

3.1 INTRODUCTION

This chapter describes the optimisation of low molecular weight PEOZ (50 kDa) for MN fabrication using polymer blending. The findings in Chapter 2 suggest that PEOZ 50 kDa is unsuitable as a sole material for fabricating MNs due to insufficient mechanical properties, unlike PEOZ 200 kDa. Although PEOZ 200 kDa showed promising results for MN fabrication, its use may be limited to therapies which require single administration rather than prolonged or frequent administration. This is to reduce the risk of accumulation since the clearance of PEOZ from the body relies on renal excretion and high molecular weight PEOZ exhibits prolonged clearance compared to low molecular weight PEOZ (336).

In order to improve the mechanical properties of PEOZ 50 kDa for MN fabrication, it could be blended with another polymer or could be chemically crosslinked. Chemical crosslinking of PEOZ could require various tedious steps, including purification to remove impurities, thereby further complicating the MN fabrication process. Polymer blending, a common strategy in the literature for MNs, offers a low cost and less time-consuming opportunity to optimise polymers to obtain the desired properties of the MNs (120, 163, 337, 338). Therefore, it could be beneficial to blend PEOZ 50 kDa with another polymer to enhance its mechanical properties for MN fabrication.

The polymer blends that have been used to fabricate dissolving MNs to date are composed of polymers that are widely known to be miscible and have been successfully blended for various applications. Hence, the common trend is to use such blends for MN fabrication. This could be because MNs are still relatively in early phase development so fabricating MNs, especially dissolving MNs, from immiscible blends may hinder their

regulatory approval owing to stringent requirements to prove prolonged stability and uniform mechanical properties and drug distribution.

There are few polymers that have been studied for miscibility with PEOZ and most of these polymers have not been used to fabricate MNs, based on a review of the literature. (163, 339, 340). Ideally, the polymer to be blended with PEOZ would have proven ability to create MNs, so as to improve the likelihood of developing high quality MNs when blended with PEOZ.

Poly(vinyl alcohol) (PVA) (Figure 3.1) is a biocompatible, water-soluble and FDA-approved synthetic polymer which has been used extensively for biomedical applications (341-343). PVA has also been used as a MN material, usually in combination with another polymer, for the enhancement of mechanical properties, such as through hydrogen bonding with low molecular weight PVP (52, 84, 279, 344).

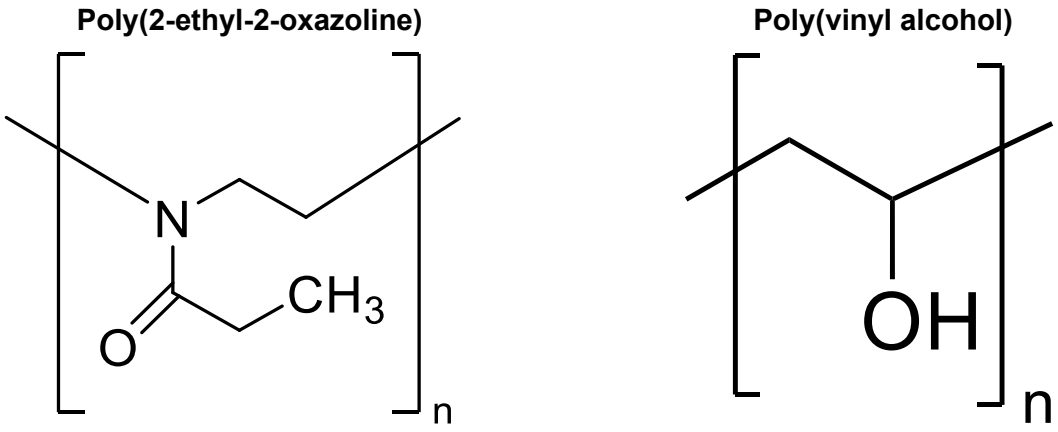

Figure 3.1 Chemical structures of poly(2-ethyl-2-oxazoline) and poly(vinyl alcohol). Created using ChemDraw (PerkinElmer, USA).

Polymer miscibility is driven by favourable intermolecular interactions between the polymers (345). Miscibility between PVA and other polymers, such as PVP, has been shown to be driven by hydrogen bonding between the hydroxyl groups in PVA and the proton-accepting groups in the other polymer (338, 346, 347). PEOZ has been reported

to interact by hydrogen bonding with polymers that contain hydroxyl or carboxylic groups, mainly through the carbonyl oxygen in its side chains (163, 340). Therefore, it is hypothesised in this work that PEOZ will be miscible with PVA due to hydrogen bonding.

There are conflicting reports on the miscibility between PEOZ and PVA in the literature. Parada et.al reported immiscibility between the polymers across the composition range that was studied, based only on results from differential scanning calorimetry (345). In contrast, when Rajashekara et. al compared various ratios of PEOZ and PVA, they reported that the polymers are miscible when the ratio of PEOZ:PVA was 30:70 % wt based on UV and FT-IR studies (348). However, this work is limited because the conclusions were not based on data from the functional group of PEOZ that is expected to be involved in hydrogen bonding. Additionally, Okada et. al reported that the polymers are miscible only when 10 kDa PEOZ is used (349), and this could be attributed to a less packed polymer chain which may favour interactions between the polymers, but this conflicts with the findings of Rajashekara et. al. (348) who reported miscibility between PVA and 500 kDa PEOZ.

Nevertheless, these studies lack comprehensive analysis at molecular level to support their findings. Also, the studies were performed using PVA with 99 - 100% degree of hydrolysis but the majority of PVA-based MNs in the literature were fabricated using PVA with 87 - 89% degree of hydrolysis due to its physical characteristics which favour MN performance, particularly for dissolving MNs (118, 279, 344, 350). One of the common reasons for selecting PVA for MN fabrication is for rapid drug release due to its rapid dissolution in water (40, 98). However, the degree of hydrolysis is known to affect the solubility of PVA in water (351, 352). A study evaluated MNs made from two grades of PVA with different degrees of hydrolysis: i) 97 – 100% and ii) 87 – 89% (350). It was found that MNs made from PVA with a degree of hydrolysis of 87 – 89% completely dissolved in PBS within 60 minutes. Whereas those made from PVA with a degree of hydrolysis of 97 – 100% did not dissolve within the duration of the experiment rather

exhibited prolonged swelling which is generally not preferred for dissolving MNs that are made for rapid drug release. The study also reported that the higher the degree of hydrolysis, the higher the stiffness of the MNs, resulting in brittle MNs, in which the authors suggested that it could be attributed to the increased hydrogen bonding within the PVA chains due to the increased amount of hydroxyl groups.

Typically, the higher the degree of hydrolysis in PVA, particularly above 90%, the lower the aqueous solubility due to the increased amount of hydroxyl groups in the polymer which form rigid complexes due to hydrogen bonding (351-354). One would expect the increase in the amount of hydroxyl groups to favour hydrogen bonding with water molecules for dissolution and this is plausible. However, PVA with 99% degree of hydrolysis has stronger cohesive forces of interactions than PVA with 88% degree of hydrolysis (355). It is likely that the stronger the bonding within PVA chains, the higher the energy required to break the bonds for dissolution, hence, interfering with hydrogen bonding with water molecules and thereby reducing aqueous solubility as the degree of hydrolysis increases (352). This could also be associated with the need for a temperature above 90°C to dissolve PVA with a degree of hydrolysis above 90% within 30 to 120 mins while PVA with 88% degree of hydrolysis typically requires 70 to 90°C to dissolve within a similar timeframe, depending on the molecular weight (356).

This work aims to conduct a comprehensive miscibility study of PEOZ and PVA using a combination of analytical techniques to bridge the gap in the literature about miscibility between the polymers and for potential application of the blends in MN fabrication. Miscibility studies will be conducted using PEOZ and PVA mixed at different ratios to determine if there is miscibility across the ratios in this study. This could also bring the opportunity to evaluate if varying the PVA:PEOZ ratio affects MN mechanical properties and drug release rate, as was seen in PVA-PVP MNs (120).

3.2 MATERIALS AND METHODS

3.2.1 MATERIALS

PEOZ 50 kDa and PVA 31 kDa – 50 kDa (87-89% hydrolysed) were purchased from Alfa Aesar, UK and Sigma Aldrich, UK respectively.

3.2.2 CASTING OF FILMS

20% w/v aqueous solutions of PVA and PEOZ were prepared separately by dissolving the required amounts in deionised water for 3 hours at 90°C for PVA and for 1 hour at 25°C for PEOZ, under magnetic stirring. PVA solution was left to cool to 25°C before mixing with PEOZ solution.

Three PVA and PEOZ blend solutions were then prepared by mixing PVA and PEOZ solutions in various proportions, with a total polymer concentration of 20% w/v, and magnetically stirring the solutions at 25°C for 16 hours. The resulting blend solutions were viscous and transparent under visual inspection.

The aqueous solutions of the polymer blends and the homopolymers were poured into separate 90 mm Petri dishes and dried in a convection oven at 35°C for 2 days. Subsequently, the resulting films were separated from the Petri dishes followed by storage in sealed plastic pouches in a desiccator. The films were also dried in a vacuum oven for 16 hours at 40°C and 800 mbar before DSC experiments.

Films made from the polymer blends are denoted herein as PVA:PEOZ 75:25, PVA:PEOZ 50:50 and PVA:PEOZ 25:75, which correspond to the proportion by weight of each polymer in the blend.

3.2.3 SEM IMAGING OF FILMS

The films were cryofractured using liquid nitrogen to obtain the cross-sections. Then, the film surfaces and cross-sections were coated with gold (Edwards coating system, Edwards Ltd, UK) and placed on aluminium stubs with carbon double-sided tapes. The

morphology of the surfaces and cross-sections of the films were then examined using FEI Quanta 600 FEG environmental SEM (FEI Ltd, UK), operated at 20 kV in high vacuum mode. The diameters of the structures on the films were measured using ImageJ software (National Institutes of Health, USA).

3.2.4 DIFFERENTIAL SCANNING CALORIMETRY (DSC)

DSC was conducted using a DSC Q2000 (TA instruments, USA) which was calibrated with indium.

3.2.4.1 CONVENTIONAL DSC

4 – 5 mg of the films were placed in hermetically sealed pierced Tzero aluminium pans. The procedure was performed under nitrogen gas and with an empty sealed pan as the reference. The pans were heated to 100°C at 10°C/min followed by cooling at 20°C/min to 0°C and finally heating at 10°C/min to 130°C/min.

3.2.4.2 MODULATED DSC

5 – 7 mg of the films were placed in hermetically sealed standard aluminium pans and an empty sealed pan was used as the reference. Modulated DSC was performed under nitrogen gas using a temperature modulation of ± 0.8°C every 60 seconds and a heating ramp of 5°C/min (357). TA Instruments Universal Analysis software (TA instruments, USA) was used for the analysis. Glass transition temperature (Tg) was measured from the mid temperature in the step change in the reversing heat flow curve. The step change in heat capacity at Tg (ΔC_p) was also measured from the reversing heat flow curve.

3.2.5 THERMOGRAVIMETRIC ANALYSIS (TGA)

TGA of the films (2 - 4 mg) was performed using a TGA Q50 (TA instruments, USA) at a heating rate of 10°C/min over a range of 25 - 600°C under nitrogen gas (flow rate at 40 mL/min and 60 mL/min for the balance and sample respectively). TA Instruments Universal Analysis software (TA instruments, USA) was used for the analysis.

3.2.6 FOURIER TRANSFORM INFRARED (FT-IR) SPECTROSCOPY

FT-IR spectra of the films were measured using PerkinElmer FTIR spectrometer with an ATR (attenuated total reflectance) attachment (PerkinElmer, USA). The spectra were measured between 4200 and 650 cm^{-1} at a resolution of 4 cm^{-1} with data presented as the average of 16 scans per run.

3.2.7 STATISTICAL ANALYSIS

IBM SPSS® Statistics (IBM, USA) was used for the statistical tests. Data are presented as mean ± SD of triplicates. Independent samples t-test was used to compare two groups and one-way analysis of variance (ANOVA) with Tukey's post hoc test was used to compare three or more groups due to their equal variances, as confirmed by Levene's test of homogeneity of variances. Differences were regarded as statistically significant if $p < 0.05$.

3.3 RESULTS

3.3.1 FILM MORPHOLOGY

PVA formed a flexible transparent film with a well-defined shape which was a replica of the Petri dish and was easily detachable from the Petri dish without breaking. Whereas PEOZ formed a brittle transparent film with an irregular shape which broke upon detachment and handling. This is consistent with earlier findings in Chapter 2 where PEOZ 50 kDa MNs had poor mechanical properties.

The films of the blends exhibited intermediate behaviour of the individual polymers, in which flexibility and film forming ability reduced as the amount of PVA in the blend reduced. PVA:PEOZ 50:50 and 25:75 films were opaque whereas the PVA:PEOZ 75:25 film was transparent. SEM images of the film surfaces and cross-sections of PVA films and PEOZ films are shown in Figure 3.2 while the SEM images of the blend films are shown in Figures 3.3 to 3.5

PVA

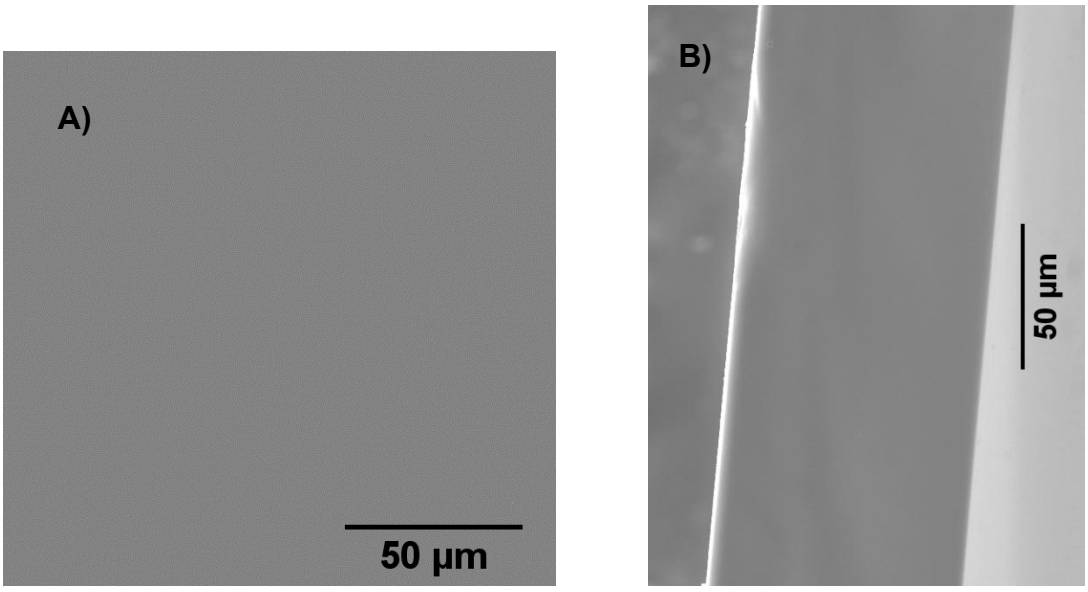

PEOZ

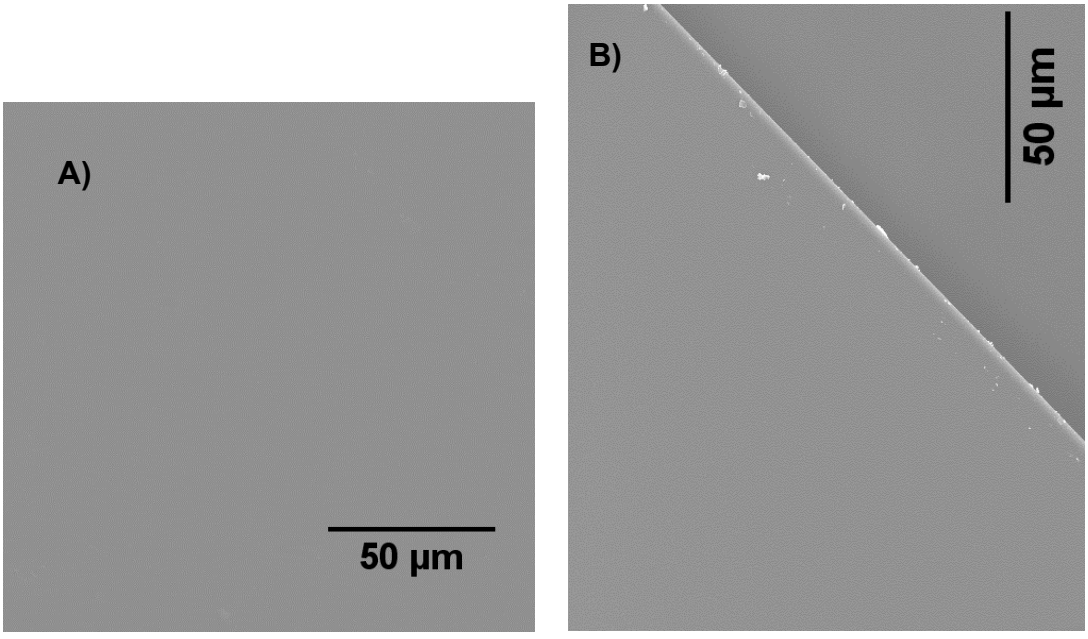

Figure 3.2 SEM images of PVA and PEOZ films A) surface B) cross-section. A and B X1000

PVA:PEOZ 50:50

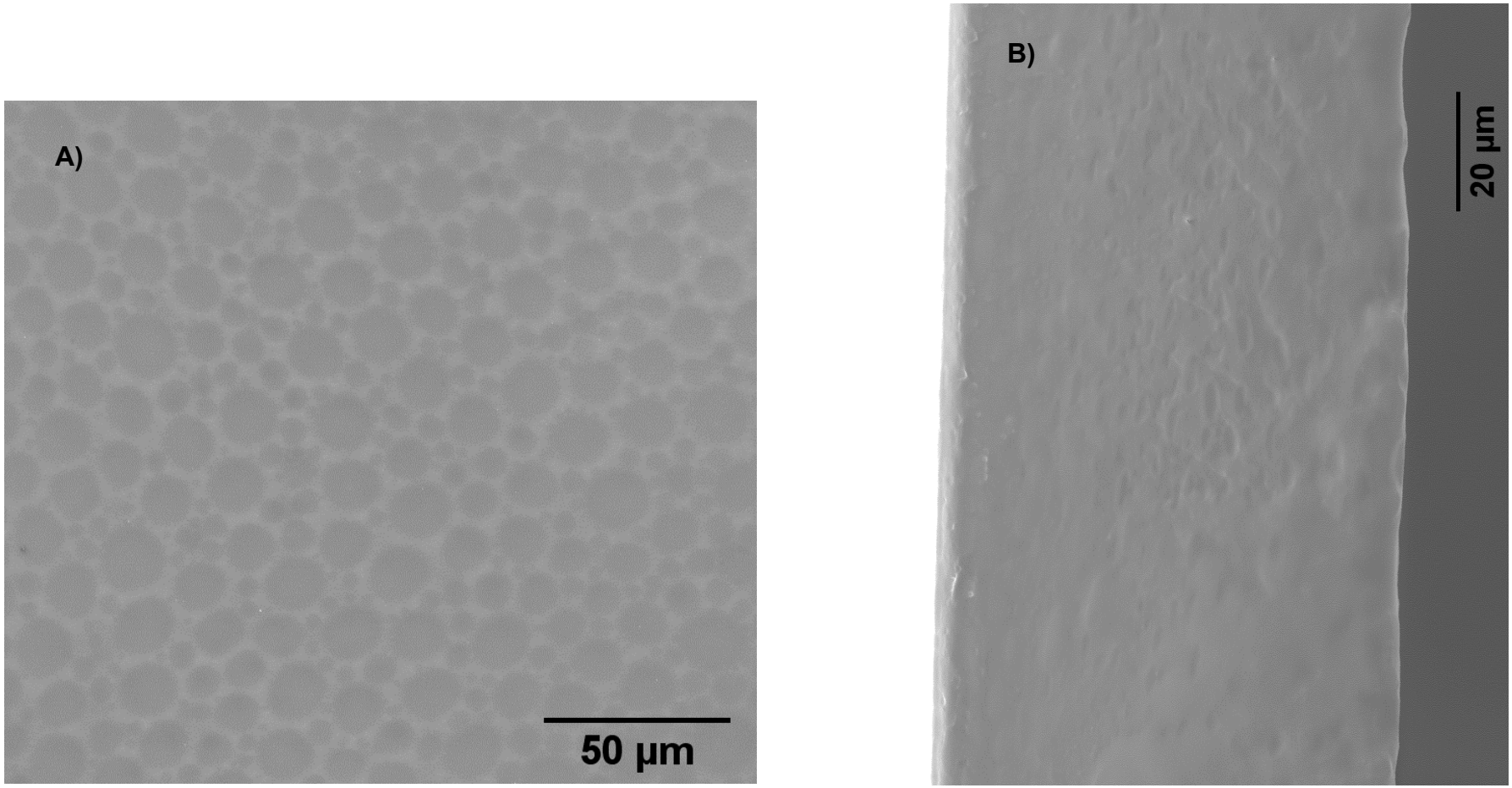

Figure 3.3 SEM images of PVA:PEOZ 50:50 A) surface X1000 B) cross-section X2000

PVA:PEOZ 25:75

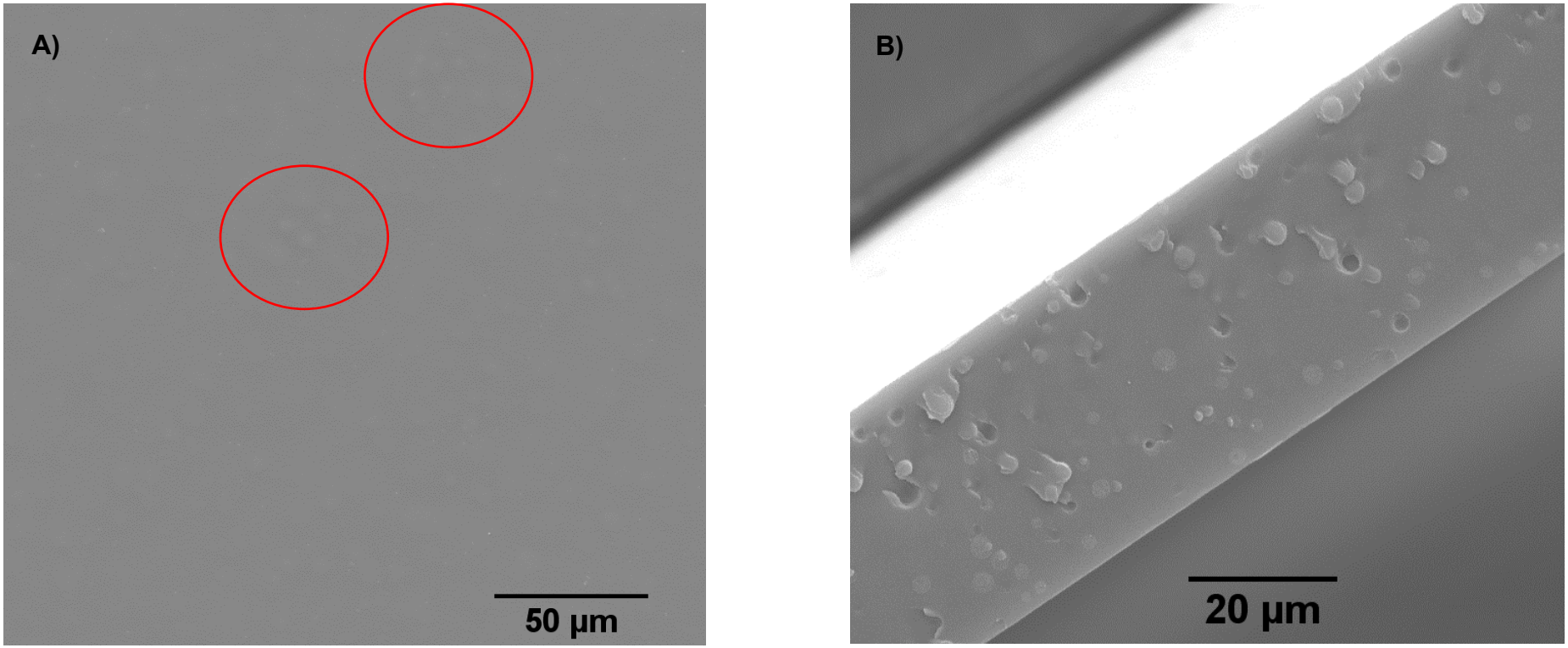

Figure 3.4 SEM images of PVA:PEOZ 25:75 A) surface X1000 B) cross-section X2000. Red circles in A show some of the globular structures on the surface.

PVA:PEOZ 75:25

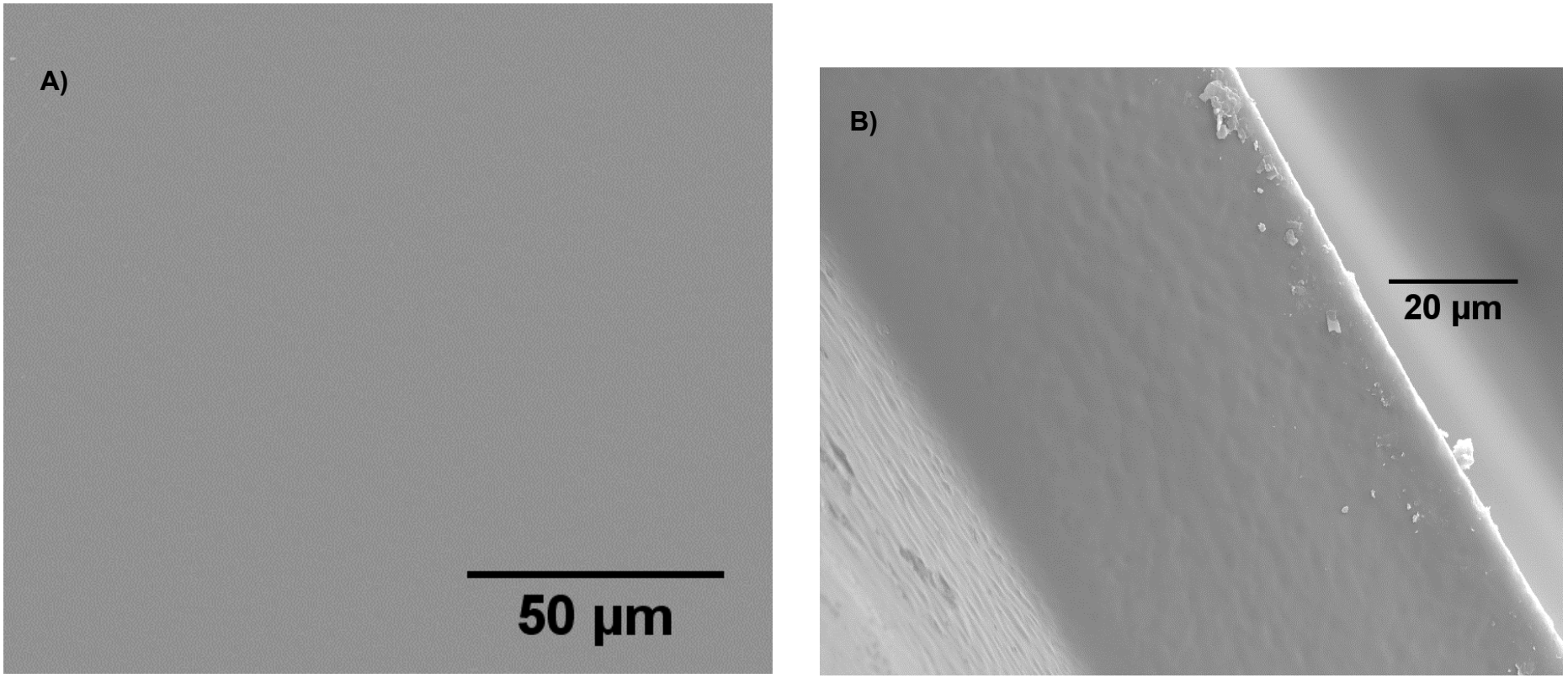

Figure 3.5 SEM images of PVA:PEOZ 75:25 A) surface X1000 B) cross-section X2000

SEM analysis showed that PVA and PEOZ each produced films with homogenous morphologies in both their surfaces and cross-sections while the morphologies of the blend films suggest phase separation.

The PVA:PEOZ 50:50 film contained spherical structures (diameter ranging from 2 to 13 μm) dispersed in a continuous phase (Figure 3.3). There were also spherical structures in the PVA:PEOZ 25:75 film (Figure 3.4) but with more uniformity than those in the 50:50 blend and a diameter of about 2 μm. The PVA:PEOZ 75:25 film had a smoother surface than the other blends but with irregular striations or round structures close together in the cross-section (Figure 3.5). The particles on the side of the PVA:PEOZ 75:25 cross-section are due to fractures during cryofracturing.

3.3.2 DSC (CONVENTIONAL AND MODULATED)

Initially, DSC analysis was conducted using conventional DSC, but this was not sensitive enough to obtain a clear and obvious glass transition for PVA, as shown in Figure 3.6. The following adjustments were then made to the DSC method but there was no improvement in the DSC curve:

1. increase in the sample size,
2. increase in the heating rate from 10°C/min to 20°C/min, and
3. rapid cooling

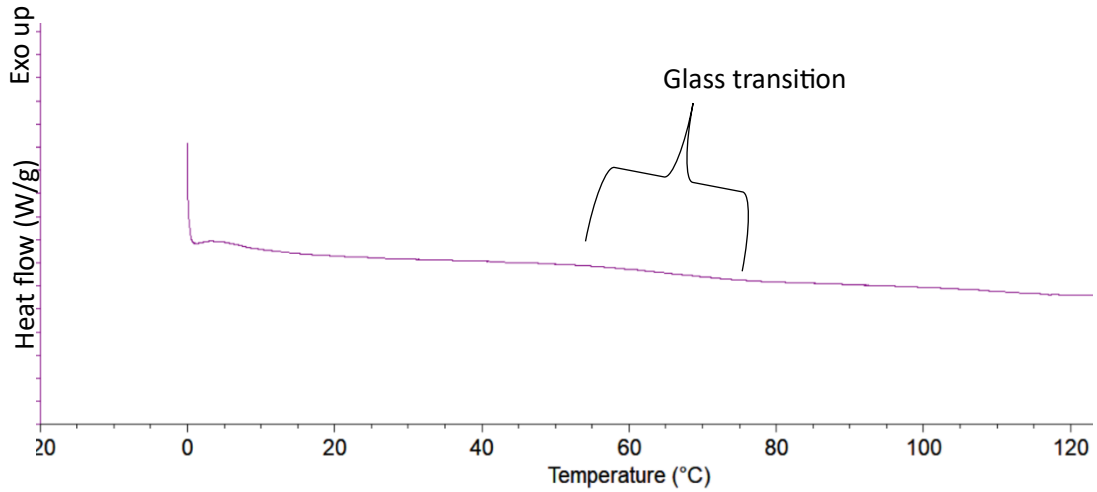

Figure 3.6 Conventional DSC thermogram of the second heating cycle of PVA film at 10°C/min.

Therefore, modulated DSC was conducted based on methods described in the literature (357) and the pan was changed from a Tzero aluminium pan to a standard aluminium pan to enable an increase in sample size from approximately 4 mg to 7 mg and to enhance contact between the samples and the bottom of the pans.

Figure 3.7 shows the modulated DSC thermograms of PVA, PEOZ and the blend films and Table 3.1 shows the Tg of each film.

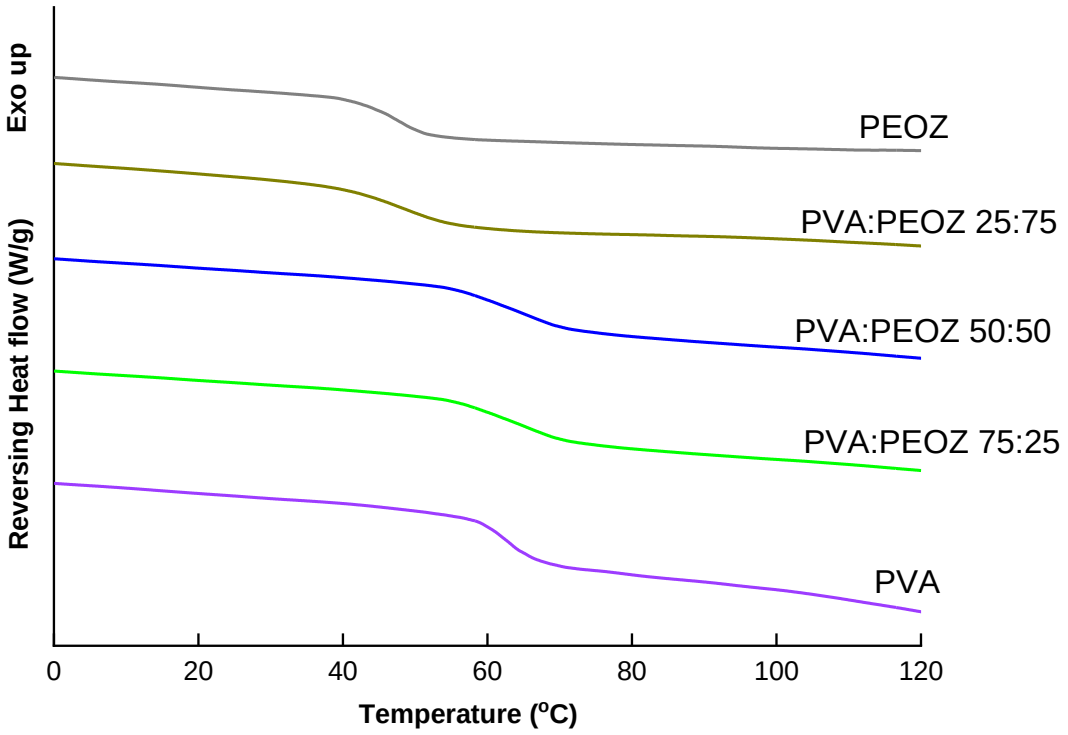

Figure 3.7 Modulated DSC thermograms of PVA, PEOZ and blend films using a temperature modulation of ± 0.8°C every 60 seconds and a heating ramp of 5°C/min.

Table 3.1 The glass transition temperatures (Tg) of films made from PVA, PEOZ and PVA-PEOZ blends obtained from modulated DSC (temperature modulation of ± 0.8°C every 60 seconds and a heating ramp of 5°C/min). Data shown as mean ± SD of triplicates.

Film	Tg (°C)
PEOZ	47.7 ± 0.5
PVA:PEOZ 25:75	48.2 ± 1.1
PVA:PEOZ 50:50	64.3 ± 0.7
PVA:PEOZ 75:25	62.7 ± 2.2
PVA	63.2 ± 0.3

There is no statistically significant difference between the Tgs of the single polymers and the Tgs of the blends where they are present in a higher proportion than the other polymer. There is also no statistically significant difference between the Tg of PVA and the Tg of the PVA:PEOZ 50:50 blend. ANOVA test with Tukey's post hoc test.

Both the PVA and PEOZ exhibited relatively sharp glass transitions, with PVA having a Tg higher than that of PEOZ by about 15 degrees. The temperature range for the glass transition of each blend is broader than that of the single polymers. Additionally, the Tgs of PVA:PEOZ 25:75 and PVA:PEOZ 75:25 are similar to the Tgs of PEOZ and PVA respectively. Whereas, the Tg of PVA:PEOZ 50:50 is similar to the Tg of PVA rather than an intermediate of the Tgs of PVA and PEOZ.

Since there is a small difference between the Tgs of PVA and PEOZ, there could be an overlap of peaks if there are two Tgs present in the blends. Therefore, the derivatives of the reversing heat flow data were plotted against temperature to analyse the number of

thermal events within the temperature range where the glass transitions of PVA and PEOZ occurred. Figure 3.8 shows that each blend has only one step change from baseline with peak temperatures that are similar to the Tgs in Table 3.1. None of the blends seemed to have more than one Tg and PVA:PEOZ 25:75 exhibited glass transition at a similar temperature to PEOZ while that of the 50:50 and 75:25 blends occurred at temperatures similar to that of PVA, which is similar to the original thermograms in Figure 3.7.

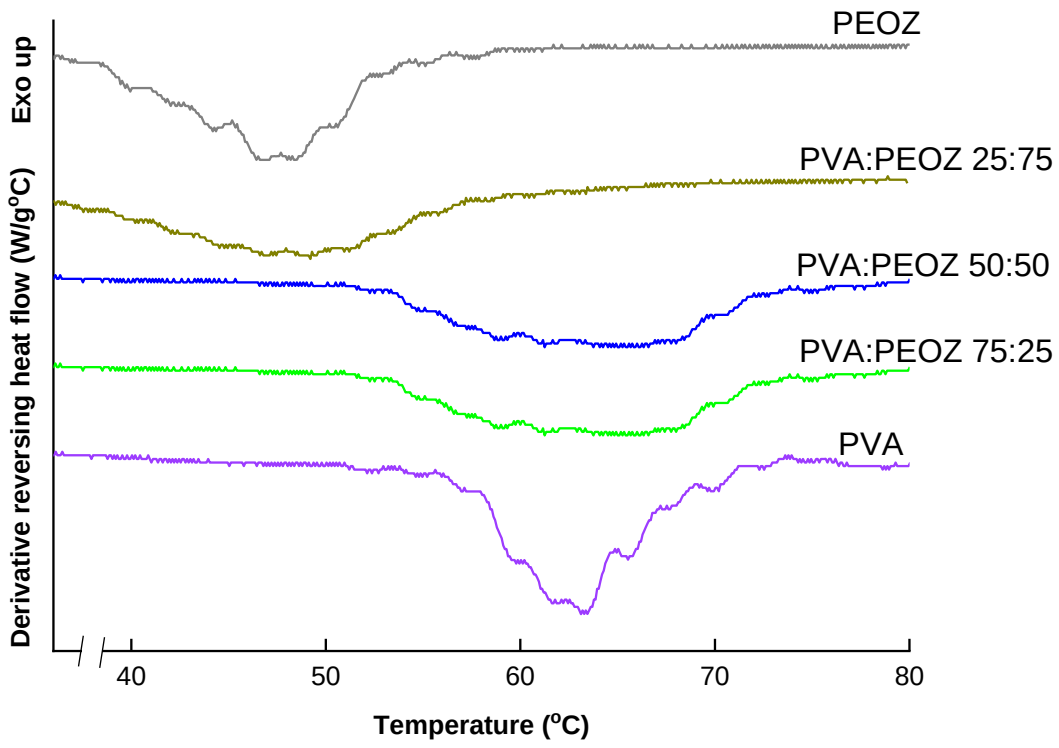

Figure 3.8 Modulated DSC thermograms of the derivatives of the reversible heating flow between 36°C and 80°C.

3.3.3 THERMOGRAVIMETRIC ANALYSIS (TGA)

The TGA curves (Figure 3.9A) and Table 3.2 show the percentage weight loss of PEOZ, PVA and the blends with respect to temperature, while the differential thermogravimetry (DTG) curves show the number of events that occurred (Figure 3.9B).

The TGA curve of PEOZ exhibited two step changes. The first stage is associated with the loss of free and bound water while the second stage which started from around 323°C is due to degradation of PEOZ. The TGA curve of PVA exhibited three step changes. Similar to PEOZ, the first stage is consistent with the loss of free and bound water. The second and third stages which started around 246°C and 401°C respectively, are due to the degradation of PVA, the release of volatile byproducts of PVA degradation and degradation of the polyene residue (358-361).

The TGA curves of the blends are intermediates of those of the single polymers, with the degradation temperatures of the blends corresponding to the proportion of the polymers. The first drop in the curves of the blends is consistent with loss of free and bound water. The next drop presented with onset temperatures between those of PVA and PEOZ, with the temperature increasing as the amount of PEOZ increased. However, the split peaks in DTG curves of the blends are consistent with the degradation temperatures of both PVA and PEOZ, in which the split peaks are more prominent in PVA:POZ 50:50.

Table 3.2 also shows the percentage weight loss around the first step change in the TGA curves up to approximately 120°C, which is analogous to the loss of free and bound water (163). Although the weight loss at this stage seemed to vary between the films, there was no statistically significant difference between them.

Table 3.2 Moisture content and onset temperature of degradation between 200 – 350°C of PEOZ, PVA and their blends. Data shown as mean ± SD of triplicates.

Film	Moisture content (% weight loss up to 120°C)	Onset degradation temperature (°C)
PEOZ	$4.7 \pm 1.5 \times 10^{-3}$	323.4 ± 2.6
PVA:PEOZ 25:75	$4.6 \pm 2.4 \times 10^{-3}$	269.0 ± 2.6
PVA:PEOZ 50:50	$4.7 \pm 2.0 \times 10^{-3}$	257.5 ± 2.1
PVA:PEOZ 75:25	$5.5 \pm 6.1 \times 10^{-3}$	250.8 ± 4.2
PVA	$5.0 \pm 4.5 \times 10^{-3}$	246.0 ± 2.0

There is no statistically significant difference between the moisture content of the five groups.

There is a statistically significant difference between the onset degradation temperature of PEOZ and the temperatures of the blends.

There is a statistically significant difference between the onset degradation temperature of PVA and the blends except PVA:PEOZ 75:25.

ANOVA test with Tukey's post hoc test.

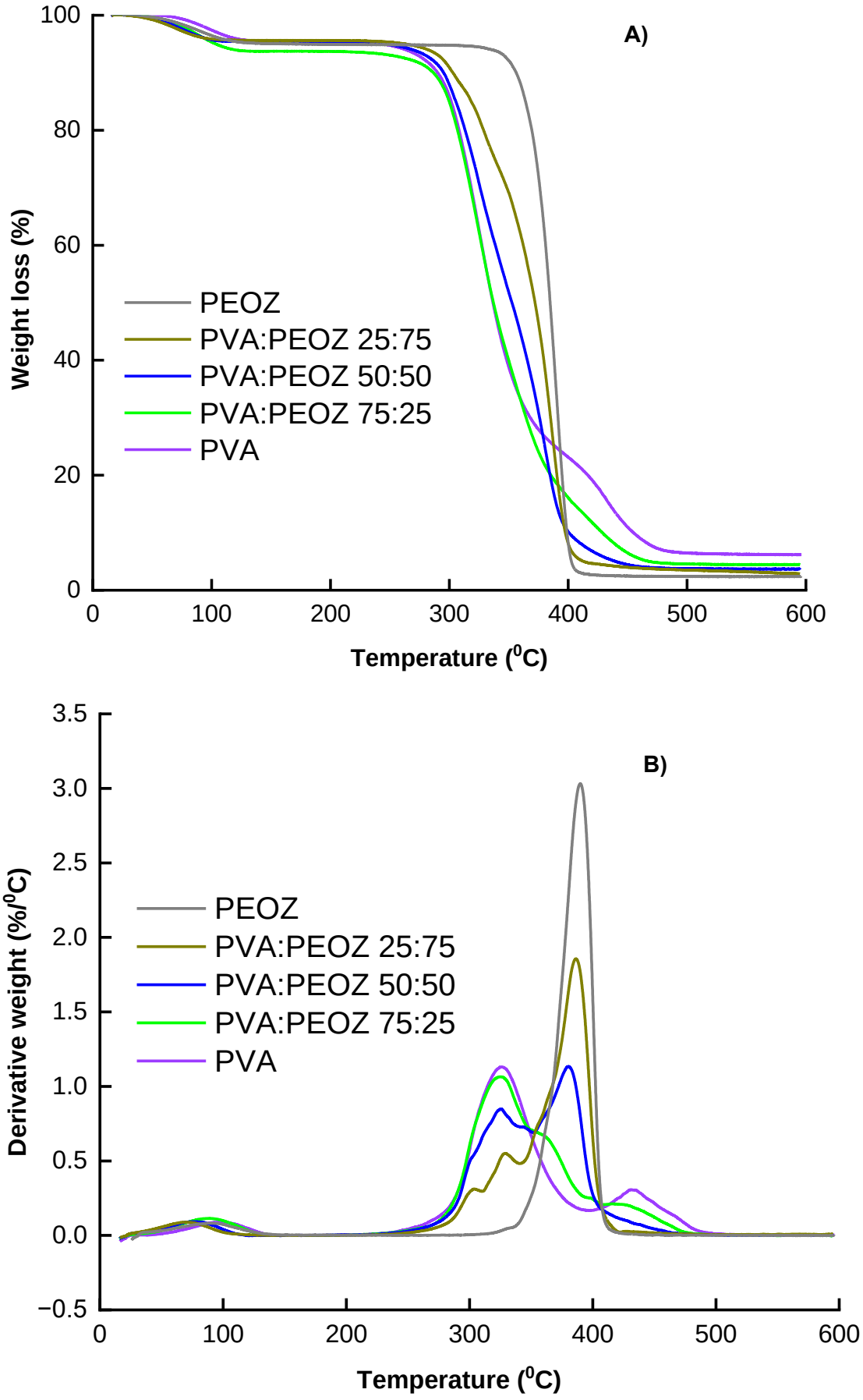

Figure 3.9 A) TGA curves and B) DTG curves of films of PEOZ, PVA and PVA-PEOZ blends.

3.3.4 FOURIER TRANSFORM INFRARED (FT-IR) SPECTROSCOPY

The FT-IR spectra of PVA, PEOZ and the blends are shown in Figure 3.10

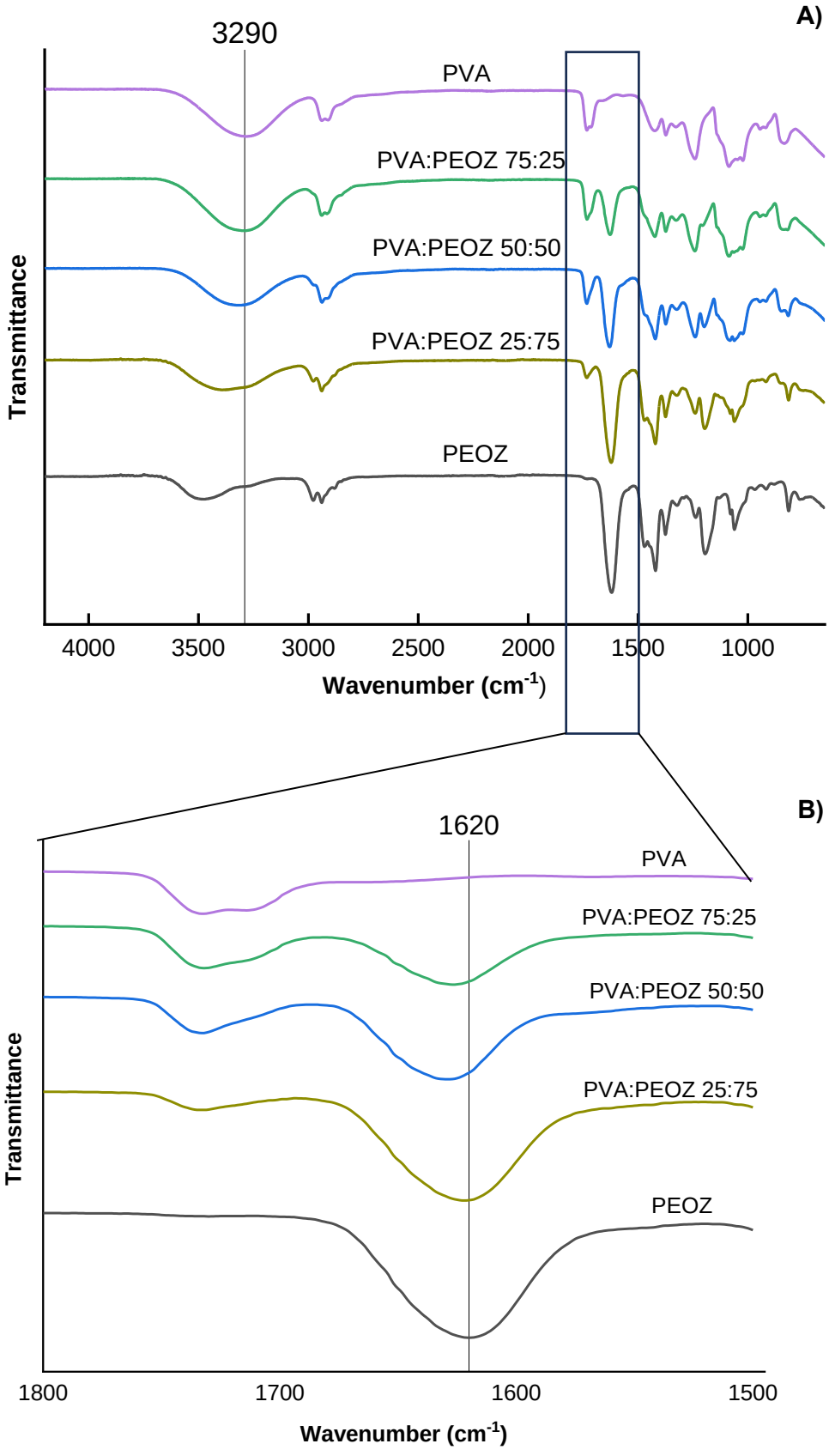

Figure 3.10 A) FTIR spectra of PEOZ, PVA and blend films B) Enlarged view of the FTIR spectra between 1500 and 1800 cm^{-1}.

The assignments of the main peaks of neat PVA and PEOZ are shown in Table 3.3

Table 3.3 FT-IR peak assignments of PVA and PEOZ (362-366)

Polymer	Wavenumber (cm^{-1})	Peak assignment
PVA	3100 - 3550	O-H stretching
	2938	C-H stretching
	1732	C=O stretching
	1422	C-H bending
PEOZ	2939	C-H stretching
	1620	C=O amide stretching
	1420	C-H bending

The broad peak between 3100 to 3550 cm^{-1} in PVA is consistent with the stretching modes of the hydroxyl groups in the polymer which undergo intramolecular hydrogen bonding (363). As mentioned earlier, PVA with 87-89% degree of hydrolysis was used in this work. Thus, the peak around 1732 cm^{-1} is consistent with the carbonyl group present in the acetate group in the polymer (364). The spectrum of PEOZ contains a peak centred around 3486 cm^{-1} which is consistent with hydroxyl groups from adsorbed atmospheric moisture in the film (163, 367).

The spectra of the blends contain the peaks of both PVA and PEOZ, with the peak intensity of each polymer correlating with the proportion of the polymer in the blend. No obvious change was observed in the peak assigned to PVA's hydroxyl group in the spectra of the blends. Interestingly, the intensity of the shoulder on PVA's C=O peak reduced as the concentration of PEOZ increased in the blends. Figure 3.10B shows a magnified view of the peaks between 1500 and 1800 cm^{-1}. Similar to the peak for the hydroxyl group, there was no appreciable change in the peak assigned to PEOZ's C=O, except a minimal shift to a higher wavenumber in the PVA:PEOZ 50:50 blend.

3.4 DISCUSSION

This chapter assessed miscibility between PVA and PEOZ using a combination of analytical techniques with the aim of developing a blend that has suitable properties to fabricate MNs.

Polymer blends can be classed as fully miscible, partially miscible, or immiscible, and the likelihood of polymer-polymer miscibility depends on the value of the change in Gibbs free energy of mixing (ΔG_{mix}) (368-370).

ΔG_{mix} is generally derived by:

$$\Delta G_{mix} = \Delta H_{mix} - T\Delta S_{mix} \qquad (3.1)$$

Where ΔH_{mix} is the change in enthalpy during mixing, T is the temperature and ΔS_{mix} is the change in entropy during mixing.

Generally, ΔG needs to be less than zero for a reaction to be thermodynamically favourable (369, 371). A ΔG_{mix} value less than zero favours polymer-polymer miscibility, thus a negative value of ΔH_{mix} and a positive value of ΔS_{mix} are generally required (368, 372). Since the effect of ΔS_{mix} in polymer-polymer miscibility is negligible due to the high molecular weight of polymer molecules, the main contributor in the value of ΔG_{mix} is the ΔH_{mix} (370, 372, 373). ΔH_{mix} is usually negative when there are strong specific intermolecular interactions between the polymers, such as hydrogen bonding (369, 372).

A common model used to evaluate polymer mixing is the Flory-Huggins Theory which was originally derived to provide a thermodynamic understanding of polymers in solutions but has been extended to understand mixing in other polymer systems such as drug-polymer and polymer-polymer miscibility studies (374-377). This theory for binary systems assumes a lattice model where the cells in the lattice are occupied by segments of the polymer chains or solvent molecules, in which each segment is present in adjacent positions to the other, but polymer molecules typically occupy more than one cell in the lattice due to their size (369, 375, 377). The entropy of mixing is then due to

the number of possible arrangements, and this could be derived from the volume fraction of each component to that of the lattice (369, 375, 377). Flory-Huggins Theory expands the general ΔG_{mix} equation by combining entropy and enthalpy contributions in a manner that is specific to polymers based on the lattice model, as shown in equation 3.2.

$$\frac{\Delta G_{mix}}{RT} = \frac{\emptyset_1}{N_1 v_1} \ln \emptyset_1 + \frac{\emptyset_2}{N_2 v_2} \ln \emptyset_2 + \frac{\chi}{v} \emptyset_1 \emptyset_2 \quad (3.2)$$

Where ΔG_{mix} is the change in Gibbs free energy of mixing, R is the gas constant, T is the temperature, $\emptyset_1$ and $\emptyset_2$ are the volume fractions and N_1 and N_2 are the degrees of polymerisation for polymer 1 and 2 respectively, v_1, and v_2 are the average molar volumes of the repeating units of polymer 1 and 2, v is the reference volume (usually taken as the smallest of v_1, or v_2) and χ is the Flory-Huggins interaction parameter which describes the enthalpic interactions of the polymers (369, 377, 378).

The first two sections on the right side of the equation are the entropic terms while the last section is the enthalpic term which includes the Flory-Huggins interaction parameter (χ) that describes the enthalpic interactions of the polymers (369, 376, 378).

Entropic contribution to the change in Gibbs free energy of mixing in polymers is negligible compared to the enthalpic contribution due to the lower number of possible arrangements in the lattice from the large molecules unlike in low molecular weight compounds (369, 371, 379). Therefore, the main driver of miscibility, in the case of polymer blends, is the enthalpic contribution which needs to be exothermic. For the mixing to be exothermic, strong specific interactions, such as hydrogen bonding, need to occur between the polymers, ideally more prominent than the interactions between the molecules in each individual polymer (369, 371).

The Flory-Huggins interaction parameter (χ) can be used to predict miscibility as it is in the enthalpic section of the Flory-Huggins equation for ΔG_{mix} (equation 3.2). A negative or low positive (very close to zero) value of χ for a polymer blend indicates strong interactions between the polymers and based on equation 3.2, this could result in a low value of ΔG_{mix} which favours miscibility. Whereas a high positive value of χ indicates

strong cohesive forces in each polymer in the blend which could result in a high value of ΔG_{mix}, hence does not favour miscibility (377, 380, 381). The critical interaction parameter (χ_c) is the thermodynamic boundary between miscibility and immiscibility of a given polymer system (381) and it can be derived from equation 3.3. It has been reported that miscibility occurs when $\chi < \chi_c$ (377, 378, 382-384).

$$\chi_c = \frac{1}{2}\left\{\frac{1}{\sqrt{N_1}} + \frac{1}{\sqrt{N_2}}\right\}^2 \qquad (3.3)$$

Where χ_c is the critical interaction parameter, N_1 and N_2 are the degrees of polymerisation of polymer 1 and 2 respectively (383, 385).

Figure 3.11 shows the effect of χ on the change in Gibbs free energy of mixing based on predictive simulations from a study where χ_c was 0.6 (377).

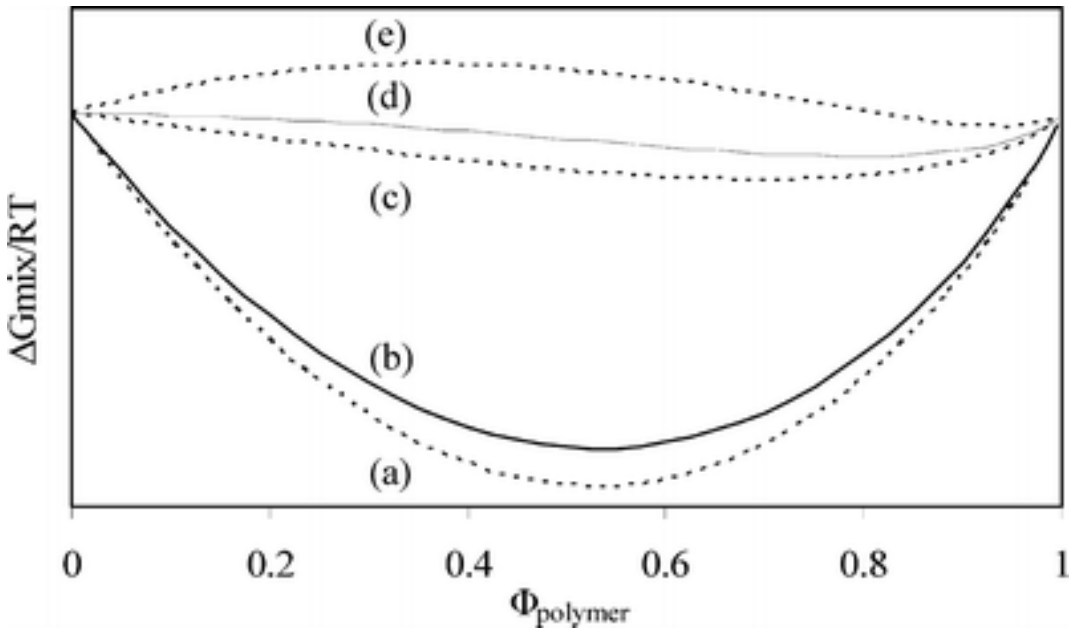

Figure 3.11 The change in free energy of mixing as a function of volume fraction a polymer in a drug-polymer system as predicted using Flory–Huggins lattice theory with different values of the interaction parameter. The interaction parameter used was (a) −4.2, (b) −3.8, (c) 0.5, (d) 1.0, and (e) 2.0. Image adapted from (377).

The value of χ for polymer blends can be obtained by experimental techniques such as ellipsometry, osmotic pressure measurements, melting point depression and scattering techniques such as small-angle neutron scattering or indirectly by using solubility parameters to estimate χ (377, 381-383, 386, 387).

Hildebrand solubility parameter (δ), which was originally developed for non-polar liquids, describes the strength of intermolecular forces between atoms or molecules in a material (370, 388-390). It is related to the cohesive energy density (CED) of a material, as shown in equation 3.4 and the CED is the energy required to separate the atoms or molecules in a unit volume of a material to infinite distance resulting in no interactions between the atoms or molecules (310, 382, 388, 391, 392).

$$\delta = \sqrt{CED} = \sqrt{\frac{\Delta E_V}{V_m}} \qquad (3.4)$$

Where δ is the Hildebrand solubility parameter, CED is the cohesive energy density, ΔE_V is the energy of vaporisation and V_m is the molar volume of the material (392)

Based on the principle of "like dissolves like", polymers with similar δ values are expected to be miscible because it is implied that if the interactions in one polymer are similar to the interactions in the other polymer, then there is a likelihood of a low enthalpy of mixing between the polymers, thereby favouring miscibility (380, 384, 388, 392). It has been reported that immiscibility between polymers is expected when the difference between the values of their δ is greater than 2 $MPa^{1/2}$ (383, 384, 391, 393). For example, a study reported phase separation in a blend of polystyrene (PS) and poly(3-hexylthiophene) (P3HT) and the authors predicted this because the values of δ for PS and P3HT were 17.9 $MPa^{1/2}$ and 14.8 $MPa^{1/2}$ respectively and the value of χ for the blend was 0.48 at 23 °C which was higher than the χ_c (0.015) (394).

The value of χ for polymer blends can be estimated based on the relationship between χ and δ, as shown in equation 3.5

$$\chi = \frac{V}{RT}(\delta_1 - \delta_2)^2 \qquad (3.5)$$

Where χ is the Flory Huggins interaction parameter, V is the mean of the molar volumes of polymers 1 and 2, R is the universal gas constant, T is the temperature and δ_1 and δ_2 are the Hildebrand solubility parameters of polymers 1 and 2 respectively (310, 382, 394).

However, the Hildebrand solubility parameter does not account for specific interactions, such as hydrogen bonding, as well as potential effects of crystallinity and cross-linking in polymers, in which there have been cases of conflicting results between miscibility prediction based on the relationship between δ and χ and miscibility studies on the blends by experimental techniques (310, 377, 382). Hansen solubility parameters was proposed by Hansen to account for specific interactions by incorporating three parameters to represent dispersion interactions (δ_D), polar interactions (δ_P) and hydrogen bonding (δ_H) (395). These can then be used to find δ (equation 3.6) to enable the prediction of miscibility between polymers (370, 396).

$$\delta = \sqrt{\delta_D^2 + \delta_P^2 + \delta_H^2} \qquad (3.6)$$

Where δ is the Hildebrand solubility parameter, δ_D , δ_P and δ_H are the Hansen solubility parameters based on dispersion, polar and hydrogen bonding interactions respectively.

Solubility parameters can be obtained from the energy of vaporisation, but this is not suitable for polymers because polymers tend to decompose before vaporisation can occur (154, 310, 392, 397). Therefore, indirect methods are generally used such as

solvent testing, group contribution methods and molecular dynamic simulations (310, 380, 382, 383, 386, 389).

Therefore, a potentially useful approach for selecting polymers for blending is to compare the values of δ of each polymer. As mentioned in 3.1, it is hypothesised in this work that PEOZ will be miscible with PVA due to the availability of hydrogen bonding groups in both polymers. However, the literature value of δ for PVA with 88% degree of hydrolysis is 26.1 $MPa^{1/2}$ (obtained by molecular dynamic simulations) (398). Whereas that of PEOZ is 23.49 $MPa^{1/2}$ (obtained by group contribution methods) (399). Based on these values, PVA and PEOZ would be immiscible because the dissimilar interactions in the polymers suggest that interactions between PVA and PEOZ would not result in a low ΔH_{mix}, hence a high ΔG_{mix}. However, it is worth noting that these values are from different studies and the value of δ could depend on the technique used in determining it (382).

Another approach in utilising solubility parameters to select polymer blends is by plotting the value of $(\delta_1 - \delta_2)^2$ (for polymers 1 and 2) against the composition of one of the polymers in the blend to identify miscibility windows (400). The authors who proposed this method stated that the blend composition which gives a value of $(\delta_1 - \delta_2)^2$ below an experimentally determined threshold is miscible. However, this method was developed for blends which contain at least one co-polymer.

PEOZ was reported to be immiscible with poly(2-n-propyl-2-oxazoline) (PPOZ) despite PEOZ having a relatively similar value of δ with PPOZ (22.66 $MPa^{1/2}$ obtained by group contribution methods) (399). The authors of the miscibility study reported that immiscibility was driven by the variation between the side chains of PEOZ and PPOZ which hindered cross-interactions between the polymers, as well as by the molecular weight of the polymers. Steric effects of side chains are not accounted for in solubility parameters (390). Additionally, the use of solubility parameters has been reported to be less reliable for polymer blends than for polymer solutions because a polymer could cause the other polymer to interact or arrange its chains in a manner different from when

the other polymer is in a pure solution, in which this could vary based on the intrinsic properties of each polymer (154, 382). This shows the complexity of predicting polymer behaviour compared to small molecular compounds. Furthermore, using the solubility parameter approach to predict χ, hence miscibility, is limited because equation 3.5 involves squared differences which by default could produce a positive value of χ so a pair of polymers that have strong interactions between them may be predicted to be immiscible (154, 395). With regards to molecular weight which influenced immiscibility between PEOZ and PPOZ, its effect indirectly influences the value of ΔG_{mix} through equation 3.2 (370, 399).

Miscible polymer blends exhibit a homogenous morphology at molecular level (373). SEM was used in this work to study the morphologies of the films of PVA-PEOZ blends, as well as the films of the individual polymers, PVA and PEOZ. The morphologies of PVA and PEOZ in this work are consistent with findings in literature (163, 401, 402). PVA:PEOZ 50:50 and PVA:PEOZ 25:75 films showed phase separation with spherical structures dispersed in a continuous phase. Interestingly, the size of the spherical structures reduced when the proportion of PVA reduced from 50% to 25%. The PVA:PEOZ 75:25 film had a smooth surface with irregular spherical structures in the cross-section. The smooth surface could indicate miscibility in this composition but the spheres in the cross-section suggest heterogeneity in the arrangement of both polymers in the blend. The spheres in PVA:PEOZ 75:25 could be PEOZ dispersed in a PVA continuous phase. Similar observation of phase separation was seen in a study where PVA was blended with poly(ethylene oxide) (PEO) (403). Similarly, in another study, phase separation was observed in microscopic images when PEOZ was blended with poly(2-n-propyl-2-oxazoline) (PPOZ) (399). By labelling PEOZ with a fluorescent dye, the authors visualised the morphologies of different compositions of the PEOZ and PPOZ blends and found that green spherical domains were dispersed in a non-fluorescent continuous phase when the proportion of PEOZ was 30%, and non-

fluorescent spherical domains were dispersed in a green fluorescent phase when the proportion of PEOZ was 70%.

DSC is a common technique for assessing miscibility between polymers, in which the presence of one glass transition temperature (Tg) in the polymer blend suggests miscibility between the polymers (163, 404-406). Initially, conventional DSC was used in this work, but this was limited by its poor sensitivity in detecting the Tg of PVA despite changes to the sample size and methods. So, modulated DSC was then used because it provides a more sensitive detection of Tg than conventional DSC (407-410).

The Tgs of PVA and PEOZ in this work are consistent with reports by other researchers (357, 411). Although there was no obvious indication of more than one Tg in the blends, their Tgs were rather unexpected. The glass transitions of the three blends were broad and the Tgs of the PVA:PEOZ 25:75 and 75:25 blends were similar to the Tg of the polymer present in a higher proportion than the other. Interestingly, the Tg of PVA:PEOZ 50:50 was broad and similar to that of PVA which may suggest that the polymer chains were arranged in a manner that enabled the interactions within PVA to dominate the glass transition of the blend or other reasons described in later. Broad glass transitions and Tg of polymer blends which match the major polymer component could indicate lack of complete miscibility between the polymers (406, 412, 413).

Models such as the Fox equation (equation 3.7) and Gordon-Taylor equation (equation 3.8), which show the dependence of the Tgs of blends on the polymer composition, can be used to predict the Tgs of polymer blends (414, 415).

Fox equation $$\frac{1}{Tg} = \frac{w_1}{Tg_1} + \frac{w_2}{Tg_2}$$ 3.7

Gordon-Taylor equation $$Tg = \frac{w_1 Tg_1 + kw_2 Tg_2}{w_1 + kw_2}$$ 3.8

Where w_1 and w_2 are the weight fractions of PVA and PEOZ respectively, Tg_1 and Tg_2 are the glass transition temperatures of the PVA and PEOZ respectively, Tg is the glass transition temperature of the blend and k is the ratio of the step change in the heat capacity at Tg of PEOZ to that of PVA ($k = \Delta Cp_2/\Delta Cp_1$) (345, 414, 416, 417).

Figure 3.12 shows how the Tgs of the blends obtained in this study compare with the Tgs calculated from the Fox and Gordon-Taylor equations.

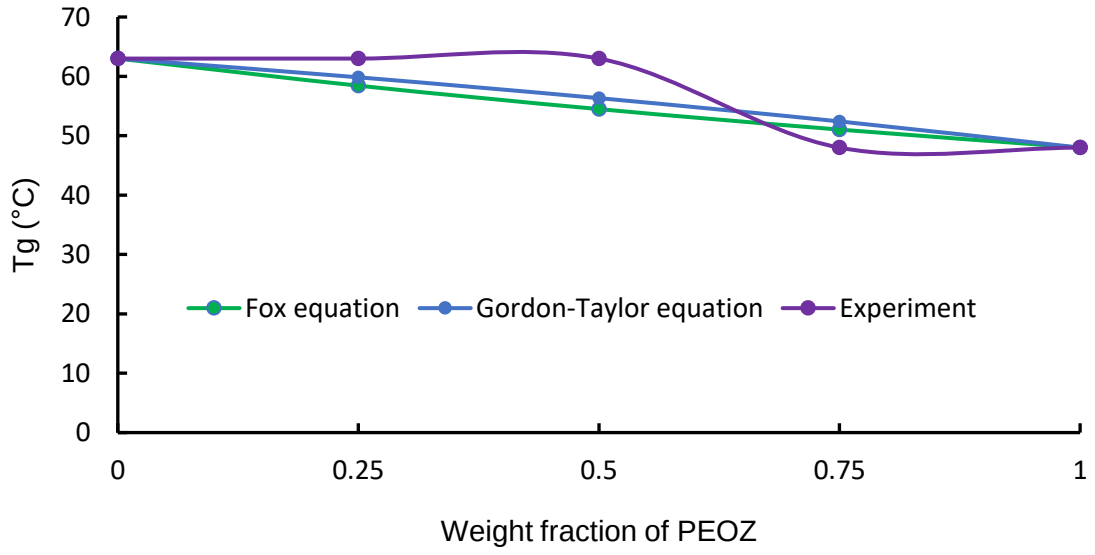

Figure 3.12 Theoretical and experimental glass transition temperatures of PVA-PEOZ blends as a function of PEOZ content.

It is expected that the Tgs of the blends are intermediates of the Tgs of the individual polymers (163, 339), with the Tg being dependent on the polymer composition as predicted by the models in equations 3.7 and 3.8. Figure 3.12 shows deviation from the predicted Tgs of the blends with limited correlation between Tg and polymer composition (R^2 = 0.75, Microsoft Excel, Microsoft USA). The deviation could be due to the phase separation in the blends, as seen in the SEM images, or due to interactions between the polymers that may not exhibit ideal mixing behaviour which the models are based on. The models assume ideal polymer mixing and do not take into account specific interactions between the polymers, potential changes in volume of the system upon mixing and potential structural arrangements that are unique to each polymer and its respective molecular weight in a given blend (387, 416, 418-421).

An alternative model such as the Kwei equation (equation 3.9) could be evaluated for its suitability with the blends in this study. This model was proposed to account for interactions between polymers, such as hydrogen bonding, by modifying the Gordon-Taylor equation to include q which is a parameter that shows the strength of the interactions between the polymers in the blend, in which a high and positive q value indicates strong interactions between the polymers (417, 418, 422, 423).

A modified version of the Kwei equation (equation 3.10) has also been proposed to account for self-association in the constituent polymers (417) which may be relevant for PVA due to its prominent self-associating behaviour (354). The modified equation assumes that the effective weight fraction of the self-associating polymer that is available to interact with the other polymer is lower than its actual weight fraction due to self-association.

Kwei equation

$$Tg = \frac{w_1 Tg_1 + kw_2 Tg_2}{w_1 + kw_2} + qw_1 w_2 \quad (3.9)$$

Kwei equation modified

$$Tg = \frac{w_1 Tg_1 + kw_2 Tg_2}{w_1 + kw_2} + qw_1^{2-\alpha} w_2^{\alpha} \quad (3.10)$$

Where w_1 and w_2 are the weight fractions of the polymers 1 and 2 respectively, Tg_1 and Tg_2 are the glass transition temperatures of polymers 1 and 2 respectively, Tg is the glass transition temperature of the blend, k is the ratio of the changes in heat capacity at Tg of the polymers, and α represents self-association in polymer 2 (obtained by mathematical fitting) and it is assumed that α >1 and $w_2^{\alpha} < w_2$) (417).

The Kwei equation and the modified version require advanced modelling tools to find the variable parameters, such as q, using experimental data but these tools were not accessible in this work so the equations could not be attempted. However, the low variation between the Tgs of the blends and the individual polymers may influence the reliability of the modelling to find the value of q, and the phase separation in the blends may make the predictive models unsuitable in this work because they generally align with blends that are not phase separated (418).

Furthermore, it has been reported that polymer blends that exhibit phase separation tend to be associated with an S-shaped Tg versus polymer composition curve which deviates from the predicted Tg values, and the inflection point in the curve aligns with the point at which phase inversion occurs (423). It is interesting to see that the curve obtained in this work (Figure 3.12) resembles an S-shaped curve and it is likely that the sections before and after the inflection point align with when the continuous phase is the major polymer component in the blend. However, in the case of the 50:50 blend, this may explain the reason for its similar Tg with PVA because it could be that the continuous phase in this blend is PVA.

The general assumption in polymer science is that polymer blends are miscible if the blends have a single Tg. However, this has proven to not always be the case in some polymer blends, as the glass transition could be affected by the analytical technique, superposition of the glass transitions of the constituent polymers, or the complex arrangement of the polymer chains when blended, amongst other possible reasons (390, 424). For example, when a copolymer of lignin and caprolactone was blended with poly(vinyl chloride), a single Tg was observed but phase separation was also observed which suggests immiscibility (390, 425). Additionally, it has been stated that two polymers could be classified as immiscible if the Tg of their blend is similar to that of one of the constituent polymers despite there being a single Tg (406, 412).

As mentioned earlier, there were unsuccessful attempts to use conventional DSC, even with variations in the protocol, so modulated DSC was used because it has been reported to be more sensitive than conventional DSC (408, 424). This is likely because modulated DSC uses a linear ramp and a sinusoidal heating rate which enables the separation of reversible thermal events that depend on heat capacity, such as glass transition, and non-reversible ones that are related to kinetic events, such as crystallisation (408, 413).

However, it is worth noting that since modulated DSC involves non-isothermal conditions, the oscillations may drive conformational changes in the polymer chains beyond the normal behaviour of the polymer chains in their ground state which may result in favourable mixing (426).

An alternative approach to modulated DSC to increase sensitivity in order to find the Tg is the use of a fast heating rate at or above 100°C/min (427). This is because it can be challenging to observe glass transitions using standard conditions in conventional DSC because the signal for glass transition is generally “weak”, so a high heating rate results in an increase in the heat flow over a shorter period, which in turn makes the transition more apparent, thereby improving sensitivity (413, 427). However, this technique is

typically associated with thermal lag to the sample and the potential of uneven distribution of heat in the sample which could distort the measured signal (428, 429). Furthermore, the fast heating could affect thermal events in the sample because the heating rate could be too fast for the large polymer chains to adjust their chain arrangements in the manner which they usually would when heat is applied, in which certain thermal events in some materials have been reported to be hindered when this fast heating technique was used (430).

Additionally, the use of DSC, usually conventional DSC, generally requires an initial heating, usually above the Tg, to remove thermal history followed by cooling and a second heating for the analysis, but these could then result in changes in the nature or thermal behaviour of the blends, for example due to changes in the arrangements or mobility of the polymer chains (412, 413, 431). Hence, there is no technique without limitations.

Nevertheless, modulated DSC has been reported in the literature to be able to indicate the lack of complete miscibility between polymers, including blends that had more than one Tg. As stated earlier, a study showed that PEOZ and poly(2-n-propyl-2-oxazoline) are immiscible and phase separation occurred in the blends (399). The polymer blends were analysed using modulated DSC and this showed two distinct Tgs. Modulated DSC also indicated partial miscibility between poly(methyl methacrylate) and poly(epichlorohydrin) based on two Tgs in one of the blends (432). Additionally, another study which used modulated DSC to assess polymer-polymer miscibility showed that the Tg of hydroxypropyl methyl cellulose was unchanged when it was blended with hydroxypropyl cellulose, which indicates immiscibility (412). However, the relatively similar Tg values of PVA and PEOZ (a difference of less than 20°C) in this work may make it challenging to effectively assess miscibility through measuring Tg because the broad single Tg in the blends may be two overlapping Tgs (386, 424) which may not be obvious despite assessing the derivative curves. Therefore, the findings of this work

emphasise the benefits of utilising more than one analytical method to assess polymer-polymer miscibility and provides valuable insights which support claims in the literature that the sole dependence of a single Tg in polymer blends is not a reliable proof of complete polymer-polymer miscibility (385, 390).

TGA was performed in this work to examine the thermal stability of the blends and how they compare with the individual polymers. The TGA profiles of the individual polymers in this work are in agreement with reports in the literature (163, 361, 362, 433).

Since PEOZ is more thermally stable PVA, the blends exhibited thermal behaviour that was an intermediate between PEOZ and PVA. Additionally, the onset temperature of degradation that occurred between 200 and 400°C in the blends increased as the amount of PEOZ increased. This suggests that PEOZ improved the thermal stability of the blends. However, the DTG curves showed multiple events occurring in this temperature range which most likely aligns with the degradation of PEOZ and PVA occurring close to each other. Some researchers have stated that the DTG curves of blends of miscible polymers present as a single degradation peak around the temperature range for the main degradation of the constituent polymers (404, 434). A study found that polymer blends which exhibited phase separation under SEM also had two degradation peaks close to each other in the DTG curve which were consistent with the degradation of the constituent polymers (434). The findings of their study is similar to results in this thesis especially in the case of PVA:PEOZ 50:50 which had the most prominent split peaks in the DTG and phase separation under SEM but this could also be as a result of the proportion of the polymers in the 50:50 blend compared to the other blends. Overall, despite the increase in the thermal stability of the blends due to PEOZ, their thermal behaviours suggest poor homogeneity in the blends because the constituent polymers seemed to degrade distinctly from each other rather than uniformly.

The films of PVA, PEOZ and the blends had comparable moisture content based on the percentage weight loss in the TGA data. The percentage weight loss associated with water loss in the PVA and PEOZ films in this work is consistent with reports in the literature (163, 435). However, it is plausible that the moisture content may differ from that of films when the polymers are used to fabricate microneedles due to differences in the processing conditions, such as temperature and drying times, amongst other reasons.

FT-IR spectroscopy was used to examine interactions between PVA and PEOZ, as it is a widely used technique which provides useful information on any intermolecular interactions that exist in polymer blends (345, 354). The FT-IR spectra of PVA and PEOZ in this work are consistent with those in the literature (163, 344, 362, 365).

The intensities of the characteristic peaks of PVA and PEOZ in the blends were consistent with the compositions of the polymers in each blend. There were no significant changes in the peak positions and shapes of PVA's O-H and PEOZ's C=O groups in most of the blends, and these are the groups expected to interact by hydrogen bonding, as described earlier. This is similar to the findings in another study (345). It was expected that the peak due to the O-H groups will broaden and shift and the peak due to C=O will form a shoulder on the peak at a lower wavenumber (339, 347, 361, 364, 406, 411). The peak associated with C=O in the PVA:PEOZ 50:50 blend apparently shifted to a higher wavenumber by about 3cm^{-1} but without an associated change in the peak associated with the O-H group. It is worth noting that this is the blend whose morphology contained the largest globules dispersed in a continuous phase. It is possible that there may have been a change in the arrangement of PEOZ chains which may have affected the polarity of the C=O bond (340).

As described above, the PVA used in this study has a degree of hydrolysis of 87-89% and so contains a small proportion of poly(vinyl acetate) which presents as a C=O peak in the FT-IR spectra around 1732 cm^{-1}. This group is known to interact by intramolecular

hydrogen bonding with O-H groups in PVA (354). It is interesting to see that the shoulder on this C=O peak decreases in intensity as the amount of PEOZ increases. This could be because PEOZ disrupts its interaction with the O-H groups or the reduction in intensity could be related to the composition of PVA in the blend. Nevertheless, the FT-IR spectra suggest that there is no evidence of strong interactions between the polymers.

Overall, the results of the analytical experiments in this work suggest that there is no strong evidence of full miscibility between PVA and PEOZ across the range of compositions studied. Several polymer scientists have noted that many polymer blends are not miscible due to weak interactions between the polymers, as well as their high molecular weights (in comparison to small compounds) which hinder sufficient intermolecular interactions for miscibility (373, 436). In the case of PVA and PEOZ, the strong self-association that occurs in PVA may have hindered favourable enthalpic interactions between PVA and PEOZ to facilitate complete miscibility, based on the change in Gibbs free energy equation described earlier (354).

Although PVA and PEOZ blends formed films in this work, the author of this work prefers to use miscible polymer blends to fabricate microneedles. This is mainly because the phase separation observed in the films may result in uneven drug distribution or non-uniform skin insertion properties in a microneedle patch, which could in turn lead to inconsistent dosing and unreliable skin insertion. For example, a study showed that the use of immiscible polymers created phase separated films and microneedles with non-homogenous morphologies and the authors highlighted the potential implications of this on drug delivery (437). Another study showed that microneedles with non-homogenous drug distribution had poor mechanical strength (438). Additionally, inconsistent drug levels from batches of a microneedle patch for migraine treatment was noted as one of the reasons for the recent rejection of the microneedle patch by the FDA, in which there was uncertainty about the aspect of the manufacturing process and/or materials that led to this issue (439). It may have been beneficial to conduct a drug distribution analysis on

microneedles made from PVA-PEOZ blend to examine if phase separation influenced drug distribution on the microneedles. However, as stated in Chapter 2, attempts were made in this work to evaluate drug distribution in microneedles using fluorescence and confocal microscopes, but this was not possible due to the lack of suitable microscopes with sufficient resolution.

Additionally, the presence of phase separation may require additional manufacturing processes to ensure controlled and consistent morphology, especially with regards to the size of the globules in the dispersed phase, including throughout the shelf-life of the formulation. This could in turn add to the complexity and cost of manufacturing. As drug-loaded microneedles are still in early phase development, it would be preferable to use optimal fabrication materials and manufacturing processes so as not to hinder their regulatory approval. The author of this work believes that it is preferable to achieve complete homogeneity in microneedles, or at least a degree of homogeneity defined by regulatory standards. Alternatively, it would be beneficial to demonstrate that inhomogeneity in microneedles has little or no effect on the drug exposure levels, clinical outcomes and stability of the microneedles upon storage.

The formation of films does not necessarily guarantee that the polymer blends will produce microneedles with sufficient mechanical properties for skin insertion. In this work, low molecular weight PEOZ formed brittle films that withstood manual handling for SEM analysis but demonstrated poor performance in the insertion test in chapter 2. It is also important to note that SEM analysis requires a small sample size, and the material does not experience the same forces experienced during skin insertion.

However, the PVA-PEOZ blends in this work could benefit from further studies to explore potential applications. For example, an immiscible blend of PEOZ and PPOZ was proposed as a potential material for making electrospun nanofibers for tissue engineering (399). The blends could also be beneficial for fabricating a different type of microneedles, as described in chapter 5. Furthermore, the potential of the blends in this

work could be further enhanced by incorporating compatibilizers or nanoparticles into the blends, which is a common practice in polymer science to control the morphologies of immiscible polymer blends while exploring or tailoring the blends to an application (373, 436, 440, 441) but this could increase the complexity and cost of manufacturing.

This work also shows the importance of using more than one technique to investigate miscibility between polymers because the behaviour of polymers is complex, and one technique alone may not give sufficient details of the behaviour at molecular level. Miscibility was only examined at solid state in this work due to the intended application of the blends. Miscibility in the solution state is beyond the scope of this work, but this could be explored as a future study, including assessing the effects of solvents and temperature (354, 390, 397, 442).

As explained earlier, the aim of this work is to blend low molecular weight PEOZ and PVA for MN fabrication to enhance the mechanical properties of PEOZ MNs. However, the findings from the analytical tests suggest the unsuitability of PVA-PEOZ blends for the fabrication of dissolving MNs due to poor miscibility. Although there is potential to explore alternative methods of enhancing the mechanical properties of low molecular weight PEOZ MNs, such as via chemical modification, a different polymer was used in the next chapter.

CHAPTER 4 – DEVELOPING PAROMOMYCIN-BASED MICRONEEDLES FOR THE TREATMENT OF CUTANEOUS LEISHMANIASIS

4.1 INTRODUCTION

This chapter describes the fabrication of dissolving microneedles (MNs) containing paromomycin (PM) as an innovative approach to treating cutaneous leishmaniasis (CL). It also describes studies directed towards developing a new and sensitive method of quantifying PM in MNs using liquid chromatography and mass spectrometry.

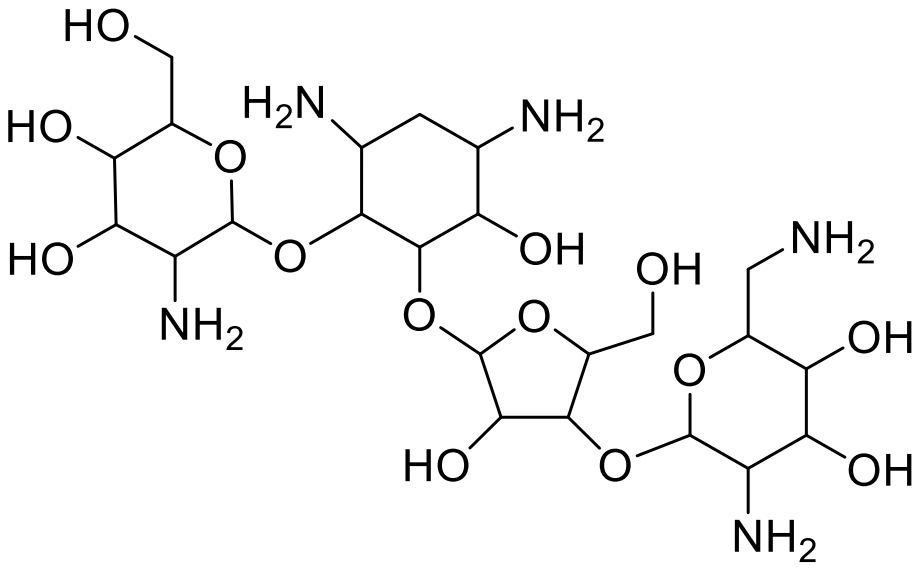

Figure 4.1 Chemical structure of paromomycin. Created using ChemDraw (PerkinElmer, USA).

4.1.1 PAROMOMYCIN BASED MICRONEEDLES

This work focused on fabricating two types of dissolving MNs; one with the needles made solely from PM and another with PM loaded in chitosan needles.

MN fabrication has progressed over the years from using silicon to polymers. This transformation in the field is mainly due to the need to improve MN quality and manufacturing, as well as due to serendipity. Further advancement in materials for MN fabrication is imminent such as the use of drugs alone to fabricate MNs. This approach was initially proposed to mitigate the issue of low drug loading (90), which is a longstanding drawback of dissolving MNs, as stated in 1.3.

Additionally, polymeric MNs generally require high amounts of polymers to achieve sufficient mechanical strength for skin insertion and this could amount to 50 – 100mg in a 10cm^2 patch (93, 95). The sole use of drugs to fabricate MNs could minimise deposition of polymers in the skin, as well as reduce possible accumulation of non-biodegradable polymers (95, 443). Although the use of drugs alone for fabricating MNs is still in its early years, this strategy has shown promising results for the few drugs that have been explored so far.

Prausnitz et. al created MNs from montelukast alone by micro-moulding, using 3 different casting methods; casting the molten drug, solvent-casting and drug powder casting followed by solvent washing (92). The MNs successfully penetrated Parafilm® M and pig skin without breaking, as well as maintained stability after 3 months of storage in a desiccant at room temperature. The authors were able to load 1 – 3 mg of montelukast into the MN patch for systemic delivery, with the aim of overcoming the limitations of the current oral formulations given as 4mg and 10 mg daily doses to children and adults respectively which have a bioavailability of approximately 64% (92, 444). Similarly, ArrayPatch, which contains needles made by casting molten itraconazole alone, is a patented MN technology that is being developed by its inventors, with the plans to go into clinical trials in future (443).

While creating MNs from drugs alone may not work for all types of drugs, it was logical to explore the feasibility of creating MNs from PM alone. It can be argued that MNs made from PM alone will dissolve rapidly and be excreted too quickly to exert sufficient therapeutic action. Whist this is plausible, this feasibility study may pave way for further optimisation to create a burst and sustained release MN which could enhance treatment because the antimicrobial effect of aminoglycosides is concentration-dependent (445, 446). As described in 1.7.3, PM is an amino sugar-based antileishmanial drug with a molecular weight of 615 Da. Simple sugars such as maltose (molecular weight 342 Da), have been used as MN materials either as sole materials, in combination with other

materials or as a stabiliser of biologics in MNs (106-108, 149). Sole use of simple sugars as MN materials has been shown to generate brittle MNs with poor skin insertion but the sole use of PM for fabricating MNs has not been investigated.

Micro-moulding using molten PM is unlikely to be suitable, as molten sugars have been reported to very viscous and difficult to use in MN manufacturing (105). Pouring PM powder into the mould is also unlikely to be suitable for micro-moulding due to the high adsorptive nature of PM which could result in non-homogenous distribution of PM in the mould. Therefore, solvent-casting was used in this work to create MNs with needles made from PM alone.

Loading PM into MNs made from chitosan was also explored in this chapter. Chitosan (Figure 4.2) is a biocompatible, biodegradable, and cationic polysaccharide which has been extensively studied for biomedical applications, including for MN fabrication. MNs made from chitosan have been reported to have sufficient mechanical properties for skin insertion and exhibit sustained drug release (123). There are several reports of leveraging the antimicrobial and wound healing properties of chitosan to develop formulations and medical devices for the treatment of infectious diseases and wounds. For example, there are commercially available chitosan-based wound dressings, such as HemCon® and Axiostat® (447, 448). Additionally, MNs were fabricated from chitosan–polyethyleneimine copolymer to encapsulate amphotericin B for synergistic treatment of deep cutaneous fungal infections, which are difficult to be treated by conventional topical formulations, primarily due to the reasons described in chapter 1 (51).

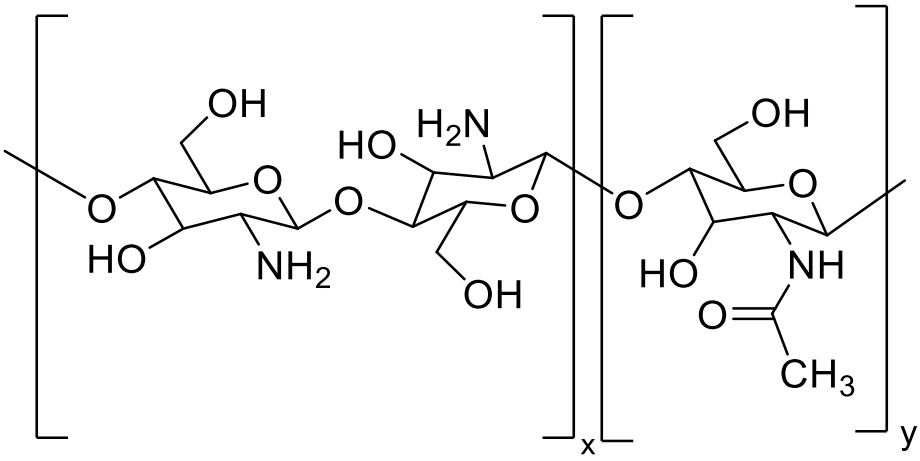

Figure 4.2 Chemical structure of chitosan. Created using ChemDraw (PerkinElmer, USA).

Interestingly, it was recently reported that chitosan has antileishmanial properties (449-451). The exact mechanism of action is unknown, but proposed theories are that chitosan is engulfed by *Leishmania*-infected macrophages and disrupts the cell wall of the parasites (449, 452). In a clinical study, drug-free chitosan-based films facilitated re-epithelialization of CL lesions in the participants (453). Although this study is limited by its sample size (n=10), it demonstrates that chitosan is a promising material for CL treatment. Furthermore, several *in vitro* and *in vivo* studies have shown the synergistic antileishmanial effect of the combination of chitosan with antileishmanial compounds (452, 454-456). As the majority of the *in vivo* studies were focused on the treatment of visceral leishmaniasis, systemic administration was prioritised in the studies. In the CL studies, the formulations, such as nanoparticles, were mainly administered intraperitoneally (457) while the few studies involving topical administration reported partial healing of CL lesions likely due to poor skin penetration (458, 459).

Therefore, exploiting the deep penetrative ability of MNs and the unique intrinsic properties of chitosan could enhance the treatment of CL. This work hypothesises that PM can be loaded into chitosan MNs to achieve adequate skin penetrative ability and sustained release of PM, as well as synergistic antileishmanial effect.

4.1.2 QUANTIFICATION OF PAROMOMYCIN

Drug release and stability tests were needed to be conducted to evaluate the quality of the PM-based MNs fabricated in this work, in addition to the visualisation and mechanical tests conducted earlier. However, it was vital to first develop a protocol that is selective and sensitive enough to quantify PM in the MNs (theoretical amount of PM = 5 µg).

Quantifying PM and other aminoglycosides is challenging due to the lack of a chromophore or a fluorophore, preventing the use of ultraviolet or fluorescence spectroscopy, as well as the highly polar nature of these compounds due to the presence of several amino groups and hydroxyl groups (228, 460, 461). Also, their non-volatility makes them unsuitable for gas chromatography (462).

There is a large body of literature on the quantification of aminoglycosides due to its importance in various applications such as aminoglycoside residue analysis in water, soil and food of animal origin, as well as therapeutic drug monitoring in humans and for drug development (228, 463, 464). However, there is still an obvious need to develop selective and sensitive methods of quantifying aminoglycosides including PM. Several quantification protocols have been reported in the literature, but most were developed to separate and quantify various aminoglycosides in food samples, including PM. There are limited studies on quantifying PM in formulations, in which there is none on quantifying PM in MNs. So, this work also aimed to adapt the PM quantification protocols in the literature to develop a tailored protocol for performance evaluation of the PM-based MNs created in this work.

PM can be quantified using microbiological assays, spectrophotometric methods after derivatisation, immunoassays or using liquid chromatography (LC) coupled to a detector. Microbiological assay is inexpensive and non-complex but lacks selectivity and reproducibility (462, 465, 466). Arshad et. al. used a non-chromatographic spectrophotometric method to quantity gentamicin, an aminoglycoside, by derivatising gentamicin using ninhydrin (318). However, this process has several drawbacks such as

low sensitivity, incomplete chemical reaction, and potential loss of some of the analyte post-derivatisation. Additionally, it was not suitable for this work because the amino groups in chitosan could interfere with the derivatisation.

The use of LC coupled with detectors is an established quantification technique with good selectivity and sensitivity. It is currently the most common method of quantifying aminoglycosides such as PM. This could be because the majority of aminoglycoside reports are based on residue analysis in food and LC-based techniques enable quantification of low quantities of several aminoglycosides simultaneously. The types of LC that have been reported so far are reverse phase liquid chromatography (RPLC) with pre or post column derivatisation, ion pair liquid chromatography (IPLC) and hydrophilic interaction liquid chromatography (HILIC). As this work focuses on PM, Table 4.1 shows some of the LC methods and the LC compatible detectors that have been used for PM quantification.

RPLC with pre or post column derivatisation using reagents such as 1-fluoro-2,4-dinitrobenzene and o-phthalaldehyde (OPA), introduces chromophores or fluorophores to PM for detection by UV or fluorescence spectrometer. For example, Esfandiari et.al. used OPA to derivatise PM to enable fluorescence detection for the quantification of PM in nanoparticles with a limit of detection of 70 ng/mL (256). However, this method is limited by the poor stability of the resulting derivatives, loss of the analyte, complexity, and low efficiency. Also, the addition of an ion pairing reagent is still needed in some cases to improve quantification, such as when Lim et.al. quantified PM in a powder and when Larraneta et. al. quantified gentamicin in a MN patch (146, 467).

Table 4.1 Reported methods of quantifying paromomycin using liquid chromatography and various detectors.

Type of LC	Detector	Mobile phase and flow rate	Derivatising agent	Source/matrix	Reference
IPLC	MS	3.5 mM HFBA in 7:3 % v/v water and acetonitrile mixture. Isocratic flow rate of 0.4 mL/min.	None	i) Human plasma ii) Human skin	(463, 468)
RPLC with an ion pair reagent.	Fluorescence	0.2 M sodium sulphate, 1.2 mM sodium 1-heptanesulfonate and 0.1% acetic acid. Isocratic flow at 1 mL/min.	o-phthalaldehyde	Extracted from a cream	(466)
IPLC	Pulsed amperometric detection	TFA and sodium hydroxide. Isocratic flow at 0.6 mL/min	None	Aqueous PM solution and *ex vivo* human skin	(469)
HILIC	MS	A) 175 mmol/L ammonium formate and 0.3% formic acid. B) methanol and 0.3% formic acid. Gradient flow	None	Honey, milk, and pork. (PM and other AGs)	(470)
RPLC	Fluorescence	Acetonitrile-water (87: 13 % v/v). Isocratic flow at 1 mL/min.	9-fluorenylmethyl chloroformate	PM intramuscular injection and PM microspheres	(471)
HILIC	MS	Acetonitrile, 2 mM ammonium acetate and formic acid (5/95/0.2 v/v/v) and (95/5/0.2 v/v/v) Gradient flow at 0.6 mL/min	None	Human plasma (PM and other AGs)	(472)
IPLC	MS	Methanol:water:TFA (45:55:0.06 v/v) with 5 mM ammonium acetate and 3.0 mg/L ammonium phosphate dibasic.	None	Human plasma	(473)
HILIC	MS	150 mM ammonium acetate with 1% v/v formic acid and acetonitrile. Gradient flow rate of 0.5 mL/min	None	Milk (PM and other AGs)	(474)

IPLC ion pair liquid chromatography, RPLC reverse phase liquid chromatography, HILIC hydrophilic interaction liquid chromatography, MS mass spectrometer, HFBA Heptafluorobutyric acid, TFA Trifluoroacetic acid, PM paromomycin, AG aminoglycoside. Further details about the methods are described in the text outside the table.

IPLC involves the use of a reverse phase column (e.g. C18 column) with a mobile phase containing an ion pairing reagent, such as trifluoroacetic acid and heptafluorobutyric acid. The high polar and polycationic nature of PM results in poor retention in RPLC so the ion pairing reagent enhances interaction between PM and the stationary phase of the column due to its hydrophobic region and ionic region with a charge opposite to that of PM (228).

IPLC, coupled with a mass spectrometer (MS), is the most common type of LC used for PM quantification. For example, protocols that were developed to quantify PM in human plasma after intramuscular administration of PM and application of PM cream had LOQ of 5 ng/mL and 50 ng/mL respectively (463, 473). There is also a report of the use of IPLC coupled with MS to quantify PM in human skin after intramuscular PM administration (468). However, IPLC could not be used in this work due to equipment and policy restrictions because extensive cleansing of the detector is required after the use of ion pairing reagents and these reagents could damage the detector.

HILIC is becoming increasingly popular for the separation and quantification of polar compounds, including PM and other aminoglycosides, mainly because ion pairing reagents are not needed and recent advancements to HILIC columns have improved separation and sensitivity (460, 475, 476). HILIC is a type of LC that uses a polar stationary phase with a mobile phase containing a mixture of an organic solvent and water (475).

IPLC and HILIC enable the detection of PM without derivatisation, and they are generally combined with detectors such as mass spectrometer, pulsed amperometric detection, evaporative light scattering detection or charged aerosol detection. Examples of those used for PM quantification are shown Table 4.1. LC coupled with mass spectrometry (LC-MS) is the most common aminoglycoside quantification technique owing to it being a powerful analytical and highly sensitive tool (464). It is also widely used in pharmaceutical analysis and has been successfully used to quantify drugs released by

MNs (262, 477, 478). In view of these reasons, along with the equipment being available for this work, PM quantification was attempted using LC-MS (HILIC with MS due to the reasons described above).

Zwitterionic HILIC was used in this work because several studies which compared different types of HILIC reported that zwitterionic HILIC is the most suitable HILIC for aminoglycoside quantification (460, 461, 470, 476).

There are few reports of the use of HILIC and MS to quantify PM and other aminoglycosides in food simultaneously (460, 470). However, to the best of the author's knowledge, there is no report of the use of HILIC and MS for the quantification of PM alone in a pharmaceutical formulation or in a skin sample post drug administration.

Therefore, in addition to developing PM-based MNs, this work focused on developing a protocol for quantifying PM in MNs in order to conduct quality assessment tests on the MNs.

4.2 MATERIALS AND METHODS

4.2.1 MATERIALS

Chitosan low molecular weight (50 kDa – 190 kDa, 75-85% deacetylated) and PVP 360 kDa were purchased from Sigma Aldrich, UK. PM sulphate was obtained from Alfa Aesar, UK. PDMS moulds were obtained from Micropoint Technologies Pte Ltd, Singapore (10 x 10 needle array with 500μm high cavities). Formic acid 99% LC-MS grade, Water LC-MS grade and 0.1% v/v formic acid in acetonitrile LC-MS grade were purchased from ThermoFisher Scientific, UK. Ammonium formate for mass spectrometry was purchased from Scientific Laboratory Supplies, UK.

4.2.2 FABRICATION OF PAROMOMYCIN MICRONEEDLES

1g of PM sulphate was dissolved in 5mL of deionised water to make a 20% w/v aqueous solution. 1g of PVP 360 kDa was also dissolved in 5mL of deionised water for the backing layer. Subsequently, PM MNs were created using the commercial mould and methods described in 2.2.2.3, with the needles made from PM and the backing layer made from PVP 360 kDa.

4.2.3 FABRICATION OF PAROMOMYCIN-LOADED CHITOSAN MICRONEEDLES

PM and CS were dissolved separately in 1% v/v glacial acetic acid in water and the solutions were then combined and stirred for 3 hours at room temperature using a magnetic stirrer. The final solution contained 1.25% w/v PM and 2.5% w/v CS. Subsequently, the MNs, denoted herein as CSPM MN, were created using the commercial mould and methods described in 2.2.2.3, with the needles made from chitosan and PM, and the backing layer made from PVP 360 kDa.

PM-free chitosan MNs, denoted herein as CS MN, were also fabricated as a comparator, with the needles made from chitosan and the backing layer from PVP 360 kDa.

4.2.4 PHYSICAL CHARACTERISATION OF MICRONEEDLES

Visualisation, the mechanical properties and the insertion capabilities of CSPM MN and CS MN were evaluated using the methods described in 2.2.4.

4.2.5 METHOD DEVELOPMENT FOR PAROMOMYCIN QUANTIFICATION

The rationale for using HILIC is described in 4.1.2. Due to budget constraints, only one type of column could be used in this study, so it was critical to identify the most appropriate one. In view of this, several ZIC HILIC columns reported for PM quantification were reviewed and an Atlantis Premier BEH Z-HILIC Column was selected, as advised by the instrument's manufacturer (Waters Ltd, USA). Around the time of conducting this study, Waters Ltd had recently reported the first use of this newly released column to quantify PM and other aminoglycosides in food samples (479). The column seemed promising due to the following reasons:

1. The column enabled the use of 20mM ammonium formate in the mobile phase. Several other columns required more than 100mM ammonium formate for optimal peak resolution and sensitivity, but this amount of ammonium formate is close to the maximum tolerance level of mass spectrometers.
2. PM can form complexes with metal surfaces of conventional columns, resulting in peak tailing and low sensitivity over time. The column selected in this study is designed with a surface modification of the column's metal component to reduce interactions between the analyte and column (480, 481).

Thus, this column was used in this study to develop a novel and sensitive protocol for quantifying PM in MNs by reproducing and modifying Waters Ltd quantification protocol for the first time in a non-commercial setting. Several modifications of the protocol were undertaken in this study due to differences in the available LC and MS equipment from those used in Waters Ltd's report. The following sections describe the LC-MS conditions and methods that were investigated.

4.2.5.1 LC APPARATUS AND CONDITIONS

The LC system was a Shimadzu Nexera UPLC (Shimadzu, Japan) and the column was Atlantis Premier BEH Z-HILIC (2.1 x 150 mm, 2.5µm from Waters Ltd, USA) attached to a 2.5µm guard column (Waters Ltd, USA). The column temperature was 50°C while the injection volume was varied to achieve optimum chromatography. A binary mobile phase was used, namely mobile phase A containing 20mM ammonium formate in water (pH 3) and mobile phase B containing 0.1% v/v formic acid in acetonitrile. Initially, a gradient flow was used according to Table 4.2 at a rate of 0.7 mL/min, as per the protocol by Waters Ltd (479), then the protocol was changed to an isocratic flow rate of 0.7 mL/min at 75:25% (A:B) for 10 minutes.

Table 4.2 Gradient flow of the mobile phase for paromomycin quantification

	Time (mins)				
	0	**1**	**5**	**8.1**	**10**
% A	10	75	85	10	10
% B	90	25	15	90	90

4.2.5.2 PREPARATION OF LC MOBILE PHASE A

To prepare 20mM ammonium formate in water (pH 3), 1.26g of ammonium formate was added to 800mL of LC-MS grade water in a 1L volumetric flask. While magnetically stirring the solution at room temperature, formic acid was added dropwise until the pH of the solution was 3 (measured using a pH meter). Then, the solution was made up to 1L using LC-MS grade water and stirred at room temperature.

4.2.5.3 MS APPARATUS AND CONDITIONS

The LC system was coupled to a Triple Quadrupole (QQQ) 8050 Shidmazu MS with electrospray ionisation (ESI) (Shidmazu, Japan). The interface voltage was 5 kV and the interface temperature and desolvation line temperature were 300°C and 150°C respectively. The nebulizing gas flow and desolvation gas flow were 2.5 L/min and 3 L/min respectively. Ionisation was done by ESI in positive mode and PM was detected using multiple reaction monitoring (MRM) mode with mass-to-charge (m/z) 616.3 as the precursor ion and m/z 293.2 and 163.1 as the product ions for qualification and quantification respectively.

4.2.5.4 PREPARATION OF PAROMOMYCIN SOLUTION

Polypropylene vials and containers were used to prepare and inject PM solutions due to the strong affinity of PM to glass. 1 mg/mL of aqueous PM (free base) solution was prepared as the stock solution. This was then diluted with LC-MS grade water to create 100 µg/mL, 10 µg/mL, 1 µg/mL, and 0.1 µg/mL PM solutions as the standards for method development and to create a calibration curve.

4.2.5.5 PREPARATION OF CSPM MN SOLUTION

CSPM MN was added to 10 mL of deionised water and stirred using a magnetic stirrer for 16 hours at room temperature. Then, the resulting solution was transferred to a polypropylene HPLC vial for analysis.

4.2.6 STATISTICAL ANALYSIS

IBM SPSS® Statistics (IBM, USA) was used for statistical tests. Data are presented as mean ± SD of triplicates. Independent samples t-test was used to compare two groups. Differences were regarded as statistically significant if $p < 0.05$.

4.3 RESULTS

4.3.1 FABRICATION OF PAROMOMYCIN MICRONEEDLES

Fabricating MNs with needles made from PM alone was not successful. Less than approximately 40% of the needles remained after removal from the mould due to the brittle nature of the needles. It was challenging to obtain suitable images because the remaining needles were too brittle to handle and several of them further broke upon handling and while viewing under the microscope. Figure 4.3 shows some of the needles with their irregular shapes and large grooves on their surfaces and broken tips likely due to brittleness. Therefore, MNs made from PM alone were not further evaluated since the other objective in this work was to add chitosan to the formulation. However, further insights into these MNs made from PM alone are described in the discussion in 4.4.

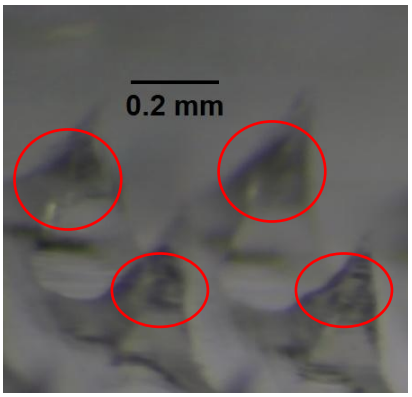

Figure 4.3 Optical microscope images of microneedles made from paromomycin alone. The red circles show the grooves on the needle surfaces from breakage.

4.3.2 FABRICATION OF PAROMOMYCIN-LOADED CHITOSAN MICRONEEDLES

Chitosan (CS) was prepared at 5% w/v and 2.5% w/v for MN fabrication. These concentrations are lower than that used in Chapter 2 due to the viscosity of CS. 5% w/v was too viscous to spread evenly and fill the mould, whereas 2.5% was less viscous, and allowed even spreading on the mould. Hence, 2.5% w/v was selected for MN fabrication. Initially, 2.5% w/v CS solution was used to create both the needles and backing layer, but this formed MNs with weak and fragile backing layers, which broke upon handling. So, PVP 360 kDa was used to create the backing layer of both PM-loaded chitosan MNs (CSPM MN) and drug-free chitosan MNs (CS MN), based on the protocol in Chapter 2.

The resulting CSPM MNs and CS MNs each had 100 pyramidal needles with well-defined tips and layered surfaces similar to the PDMS mould (Figure 4.4). Interestingly, CS MNs appear to have sharper tips than CSPM MN and this was confirmed by measuring the dimensions using ImageJ software (National Institutes of Health, USA) (Table 4.3).

Table 4.3 Dimensions of paromomycin-loaded chitosan microneedles and drug-free chitosan microneedles. Data shown as mean ± SD of triplicates.

MN type	Height (μm)	Base width (μm)	Tip diameter (μm)	Tip to tip spacing (μm)
CSPM MN	381 ± 5	201 ± 1	10 ± 1	493 ± 2
CS MN	388 ± 3	200 ± 3	5 ± 1	493 ± 3

No statistically significant difference was observed between the above listed dimensions of the two groups of microneedles, except the tip diameter. Independent samples t-test

PM-loaded chitosan MNs

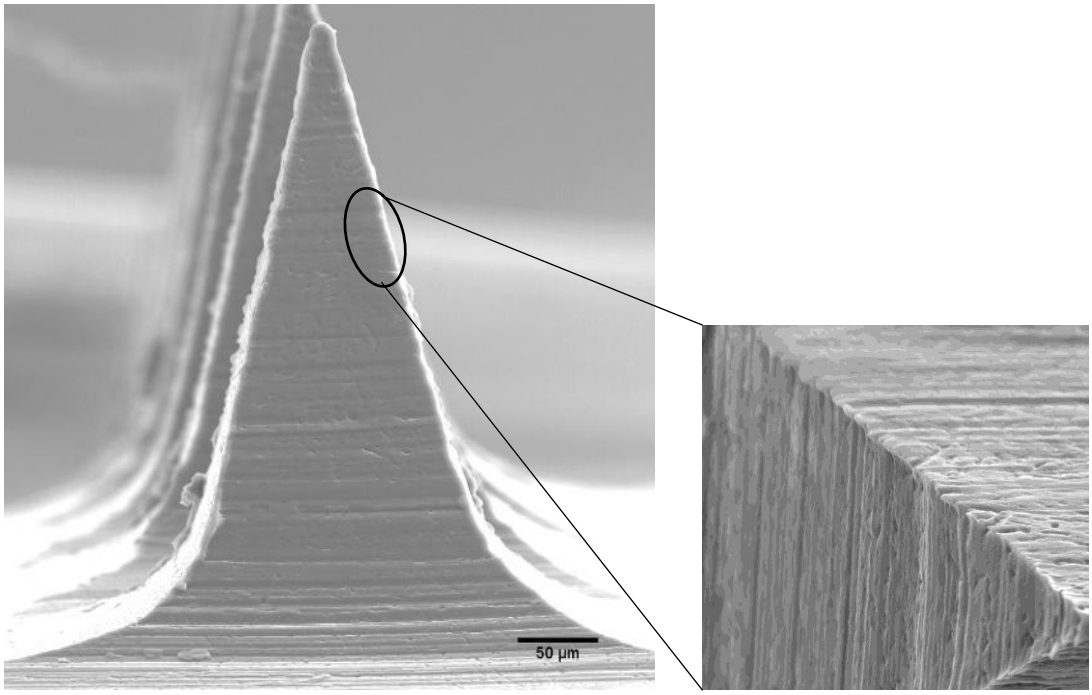

Drug-free chitosan MNs

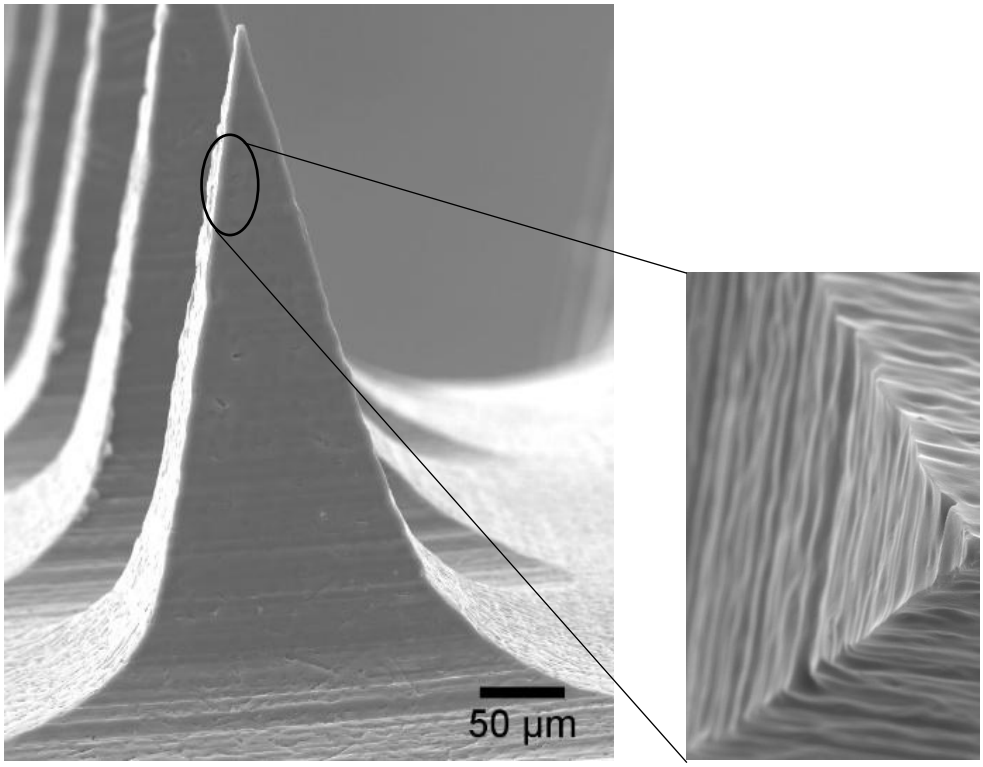

Figure 4.4 SEM images of PM-loaded chitosan microneedles and drug-free chitosan microneedles. Each single microneedle is X500 magnification while the magnified surfaces are X2000. viewed from the top.

4.3.3 EVALUATION OF MECHANICAL PROPERTIES

Figure 4.5 A shows the force-distance curves of the MNs while Figure 4.5 B shows the maximum force required to compress CSPM MNs and CS MNs.

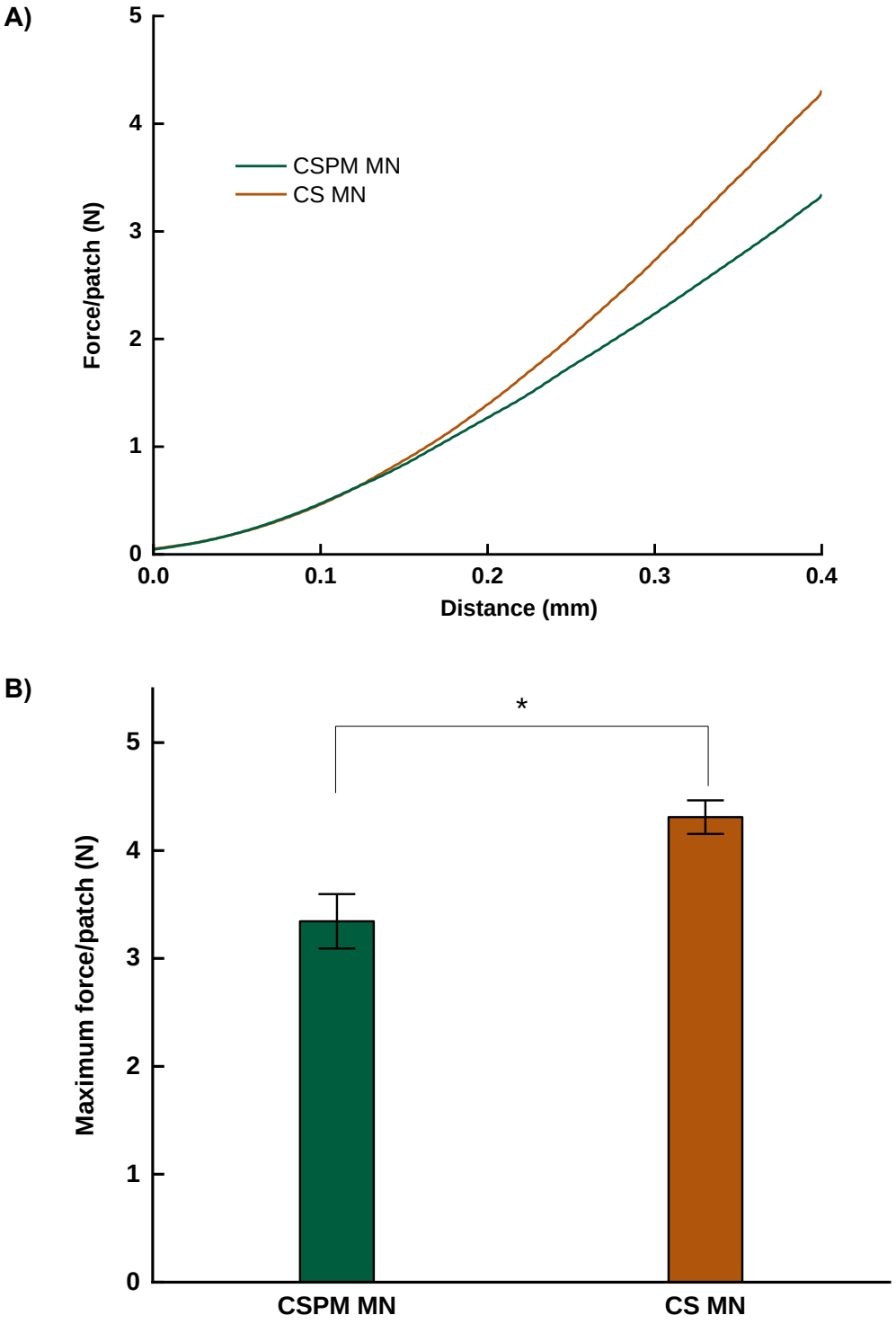

Figure 4.5 A) Force-distance curves of the microneedles after application of an axial force B) Maximum force required to compress the needles to 0.4mm (obtained from the force-distance curves). Data presented as mean ± SD of triplicates. * = p<0.05, ns = p>0.05

There was no sudden drop in the curves of both CSPM MNs and CS MNs and the compression force increased with distance until the end of the experiment for both types of MNs. Also, the needles and backing layer of both types of MNs remained intact. However, CS MNs showed higher resistance to compression than CSPM MNs.

4.3.4 INSERTION TEST

Figure 4.6 shows the penetration efficiency of CSPM MNs and CS MNs after insertion into 8 sheets of Parafilm® M and Figure 4.7 shows the punctured sheets after insertion of CSPM MNs and CS MNs.

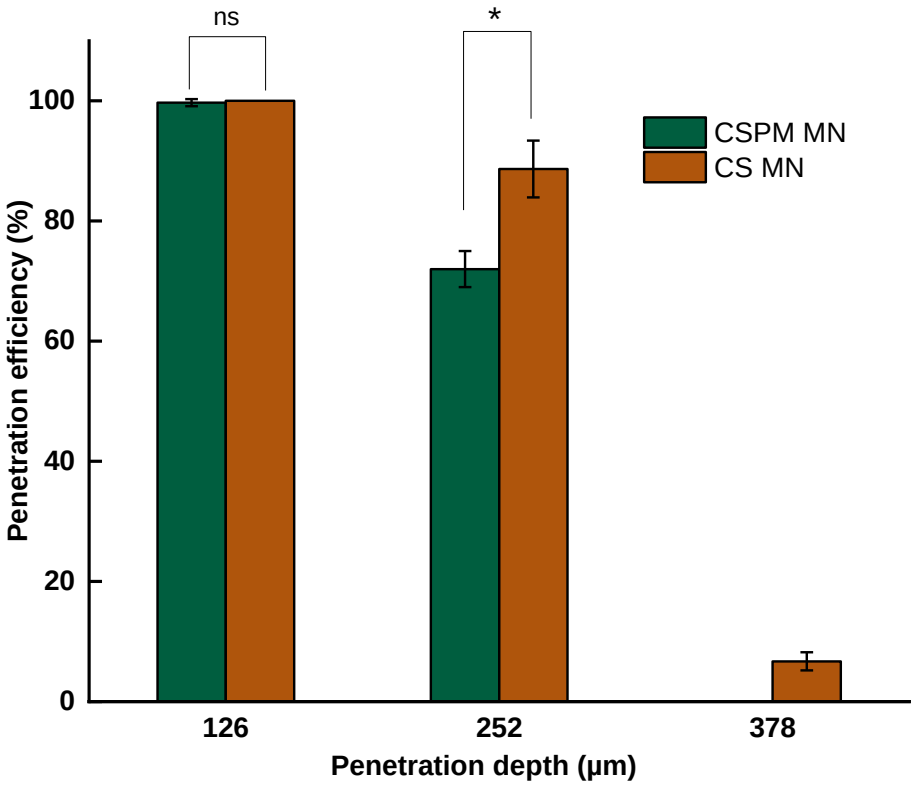

Figure 4.6 Penetration efficiency of paromomycin-loaded chitosan microneedles (CSPM MN) and drug-free chitosan microneedles CS MN) at different depths of Parafilm® M skin simulant. Data presented as mean ± SD of triplicates. * = $p < 0.05$, ns = $p > 0.05$

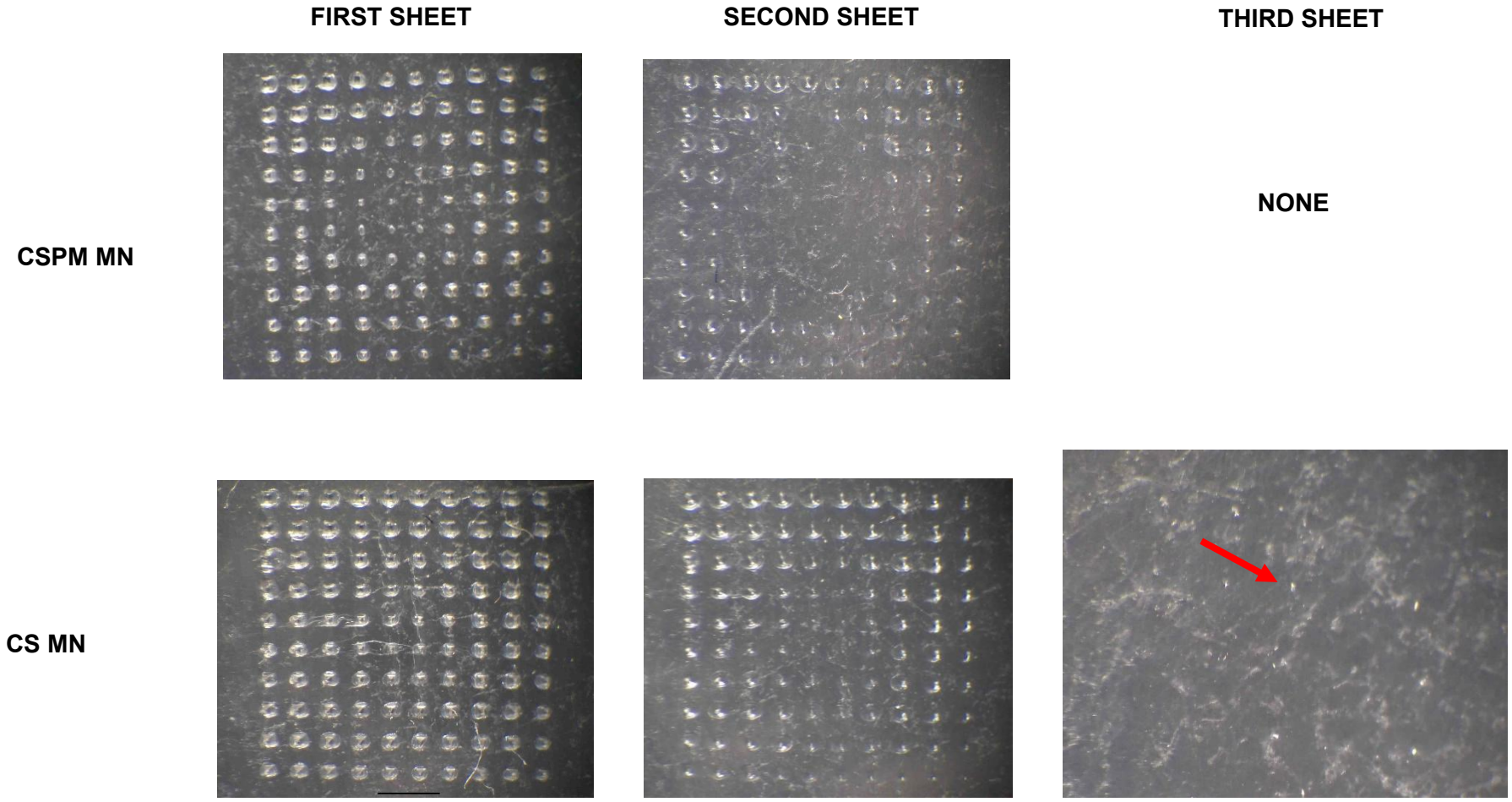

Figure 4.7 Optical microscope images of the first, second and third sheets of Parafilm® M after insertion of paromomycin-loaded chitosan microneedles (CSPM MN) and drug-free chitosan microneedles (CS MN). The holes on the 3rd sheet are not very obvious so the red arrow is pointing towards one of the holes created by CS MN. Magnification X2

The penetration efficiency of the MNs reduced as the depth of the skin model increased, with only CS MN reaching the third layer. CS MN showed 100% penetration efficiency in the first sheet, but this dropped to less than 80% and 15% on average in the second and third sheets respectively. Incorporation of PM into the MNs led to a reduction in penetration efficiency in the second sheet and no penetration in the third sheet.

Both CSPM MNs and CS MNs remained intact after insertion. As post-insertion SEM images of the MNs could not be obtained due to the SEM being faulty for a long period of time, visualisation was done using an optical microscope (details in 2.2.4) (Figure 4.8). It was difficult to obtain clear images of the needle tips, so different magnifications and angles of the MNs were used and the best image was then shown below for each MN type.

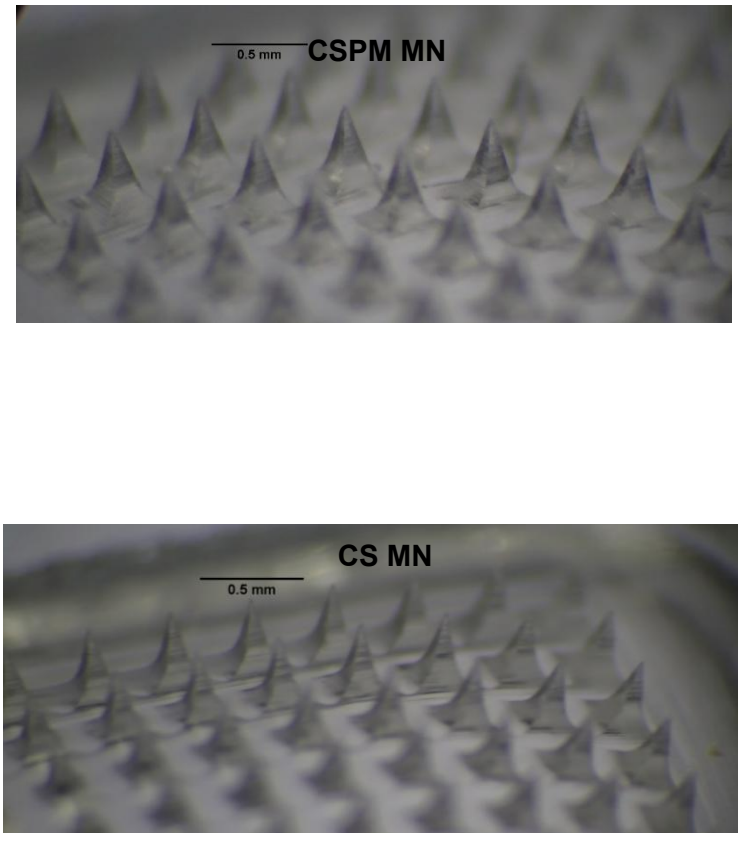

Figure 4.8 Optical microscope images of paromomycin-loaded chitosan microneedles (CSPM MN) and drug-free chitosan microneedles (CS MN) after manual insertion into 8 sheets of Parafilm® M.

4.3.5 PAROMOMYCIN QUANTIFICATION

An initial protocol was selected to quantify PM by LC-MS using mobile phase A (20mM ammonium formate in water (pH 3)), mobile phase B (0.1% v/v formic acid in acetonitrile) and water as the injection solvent.

Initially, 5 µL of PM solutions 100 µg/mL, 10 µg/mL and 1 µg/mL were injected and analysed using the gradient flow shown in Table 4.2. However, after several injections, peak tailing and splitting were evident, as well as an inconsistent retention time between 1 and 3 minutes. Since 75% A and 25 % B is the section of the gradient flow that falls within the retention time of PM, the protocol was changed to an isocratic flow of 75% A and 25 % B to optimise separation, as described in 4.2.5.

The injection volume was reduced to 3 µL and the column was conditioned with 26 mL of the mobile phase, based on the manufacturer's instructions. It was then observed that the retention time became consistent with a well-defined and sharp peak for 100 µg/mL PM, with an intensity around 2 million au (Figure 4.9). However, a tailed and broader peak with an intensity approximately 60,000 au was seen for the more dilute 10 µg/mL solution (Figure 4.11) and a highly irregular peak with an intensity of around 1500 au with significant noise levels was seen for the 1 µg/mL solution (Figure 4.13). Surprisingly, when the analysis was repeated with fresh solutions the next day, the intensity of 10 µg/mL fell to around 27,000 au with longer tailing (Figure 4.15).

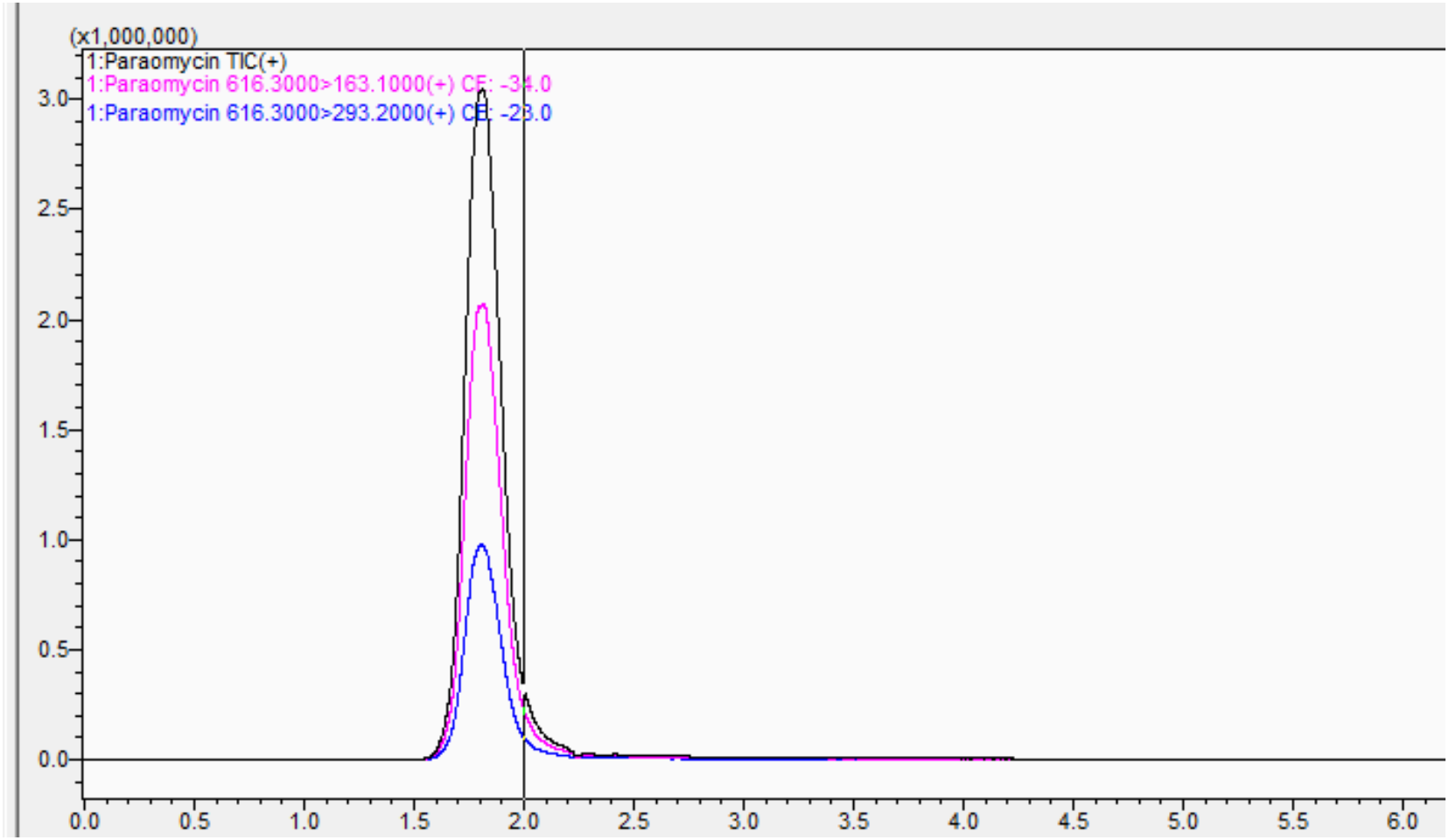

Figure 4.9 LC chromatogram of 100 µg/mL PM solution

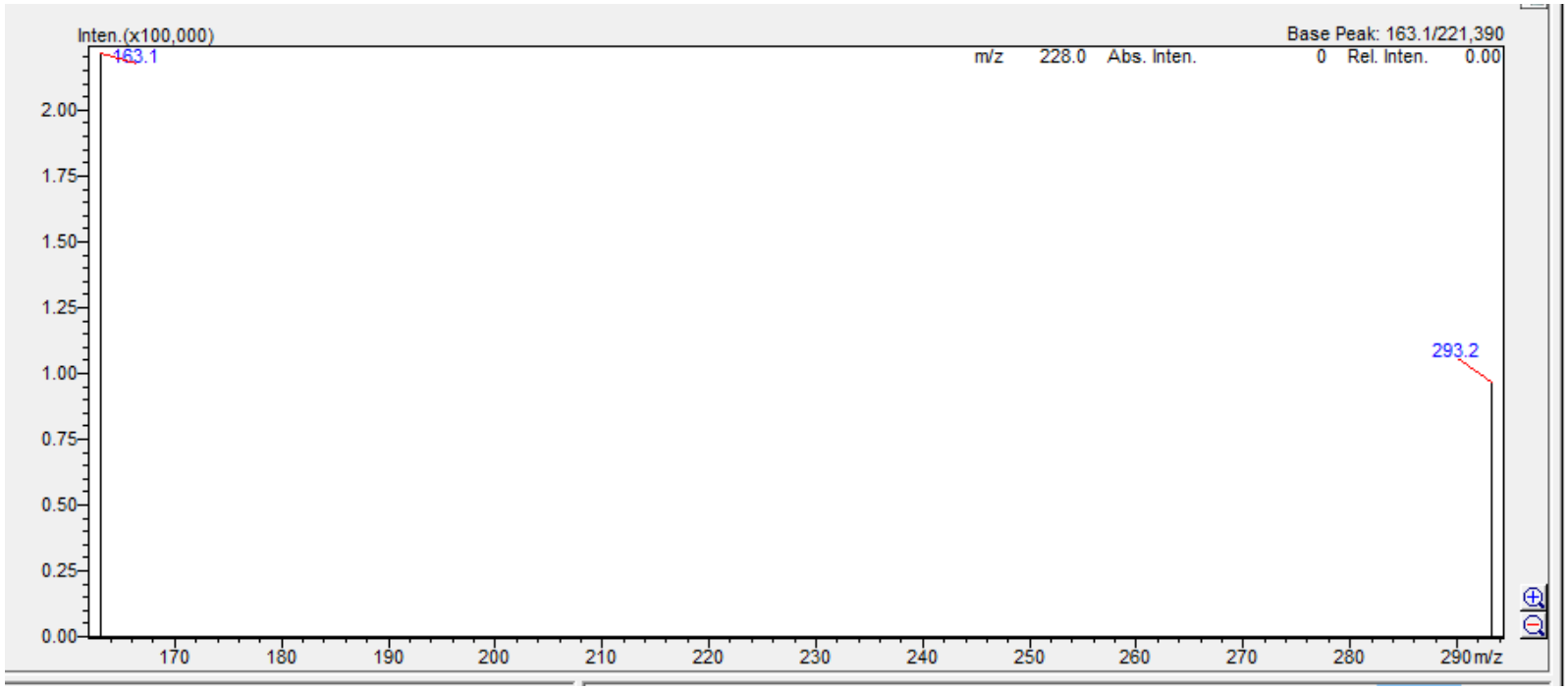

Figure 4.10 MS spectrum of 100 µg/mL PM solution

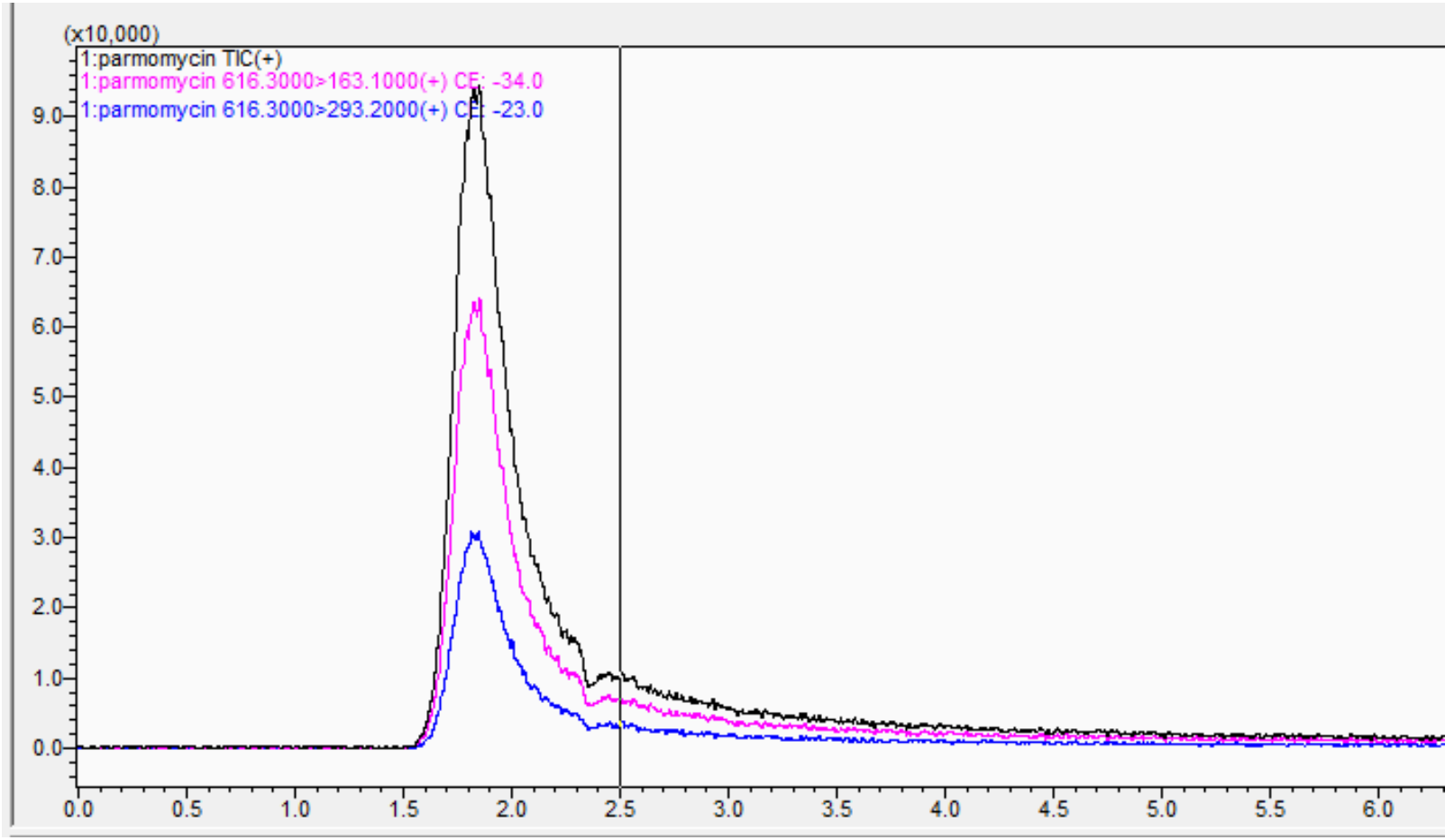

Figure 4.11 LC chromatogram of 10 µg/mL PM solution

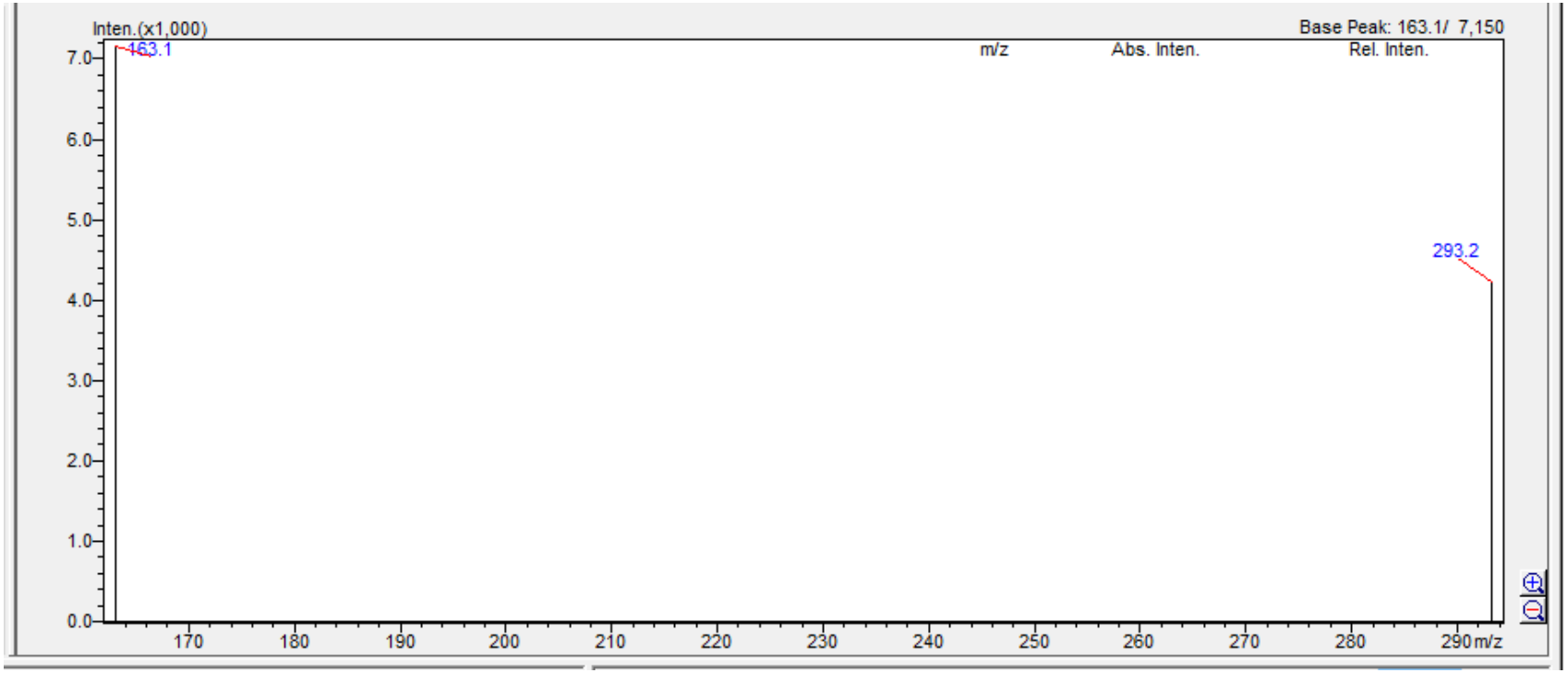

Figure 4.12 MS spectrum of 10 µg/mL PM solution

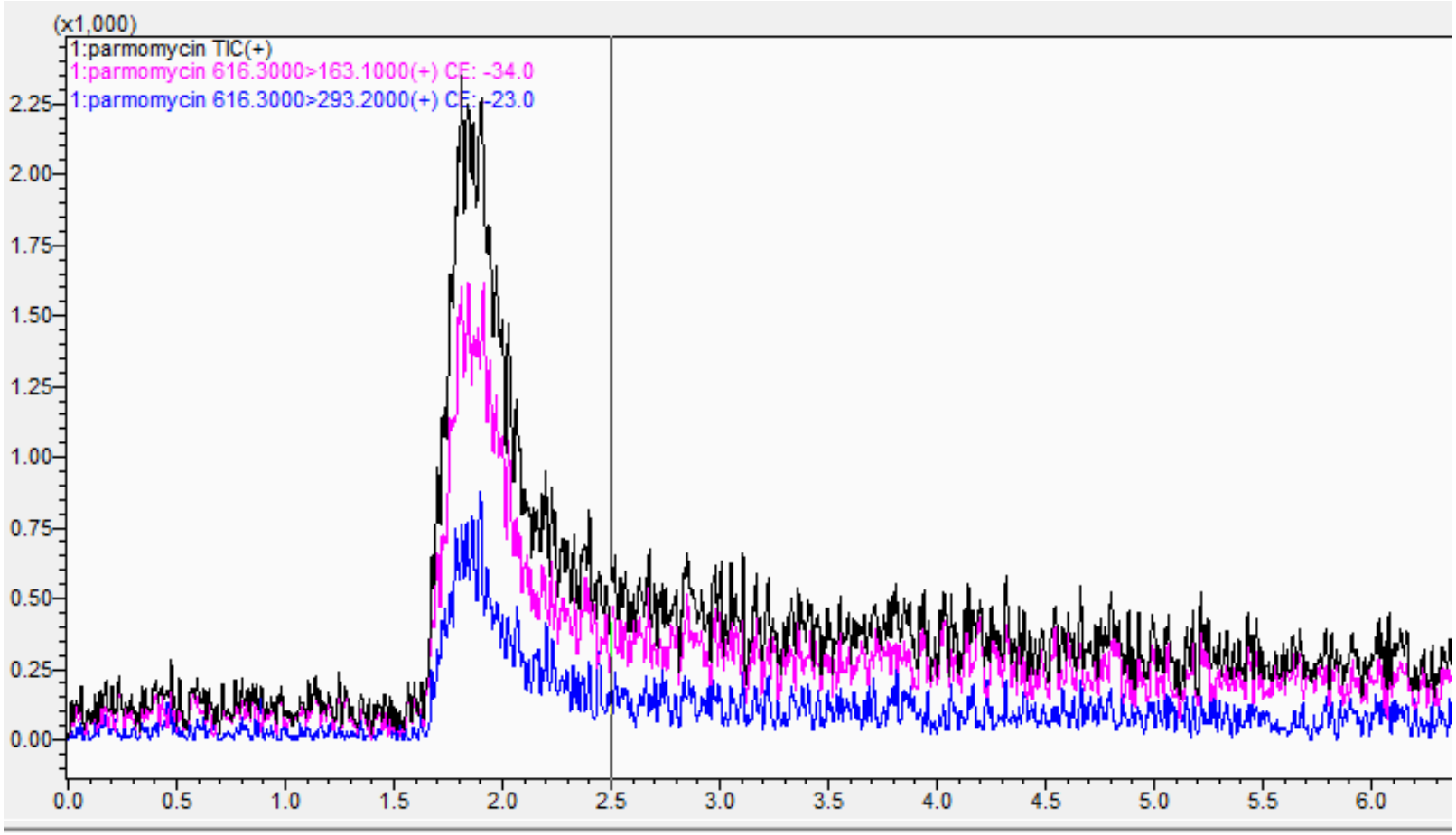

Figure 4.13 LC chromatogram of 1 µg/mL PM solution

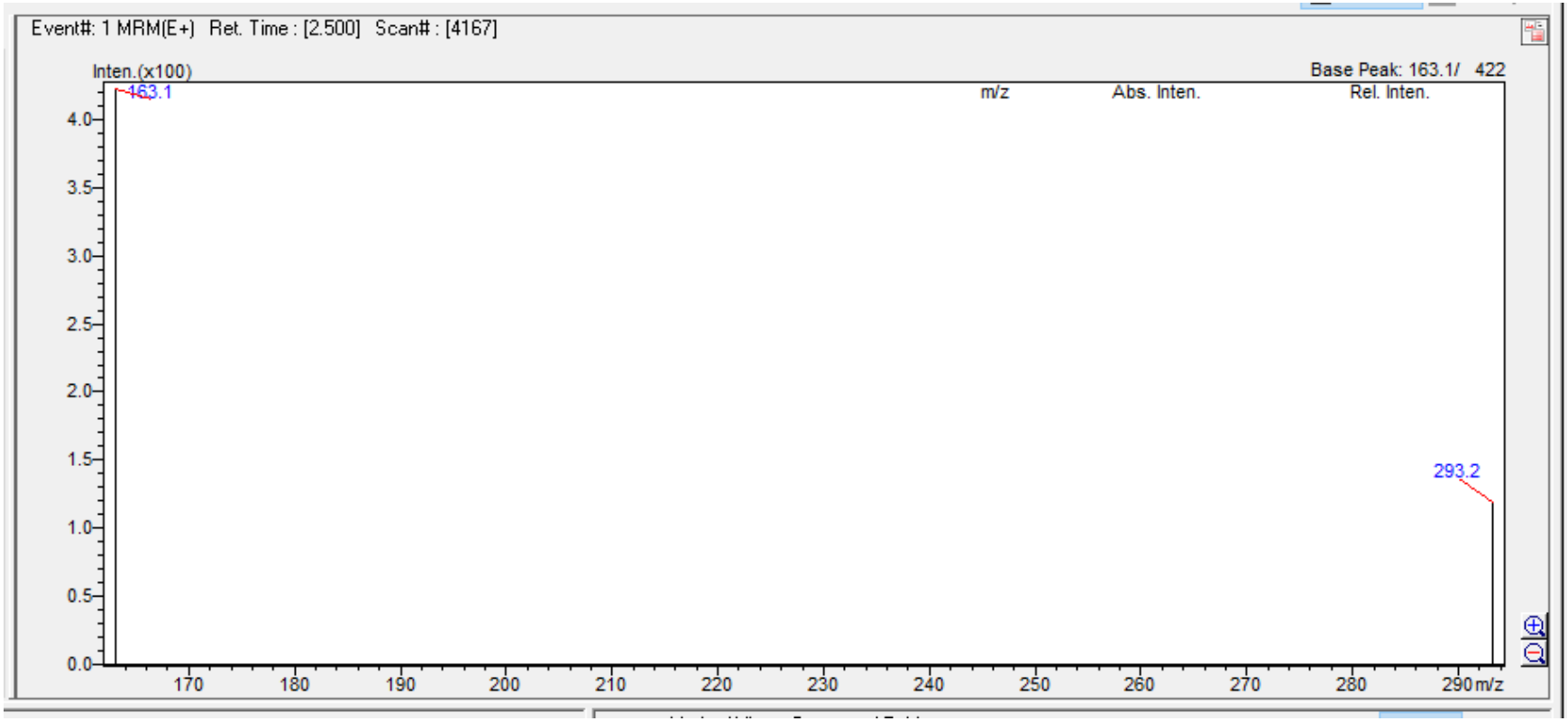

Figure 4.14 MS spectra of 1 µg/mL PM solution

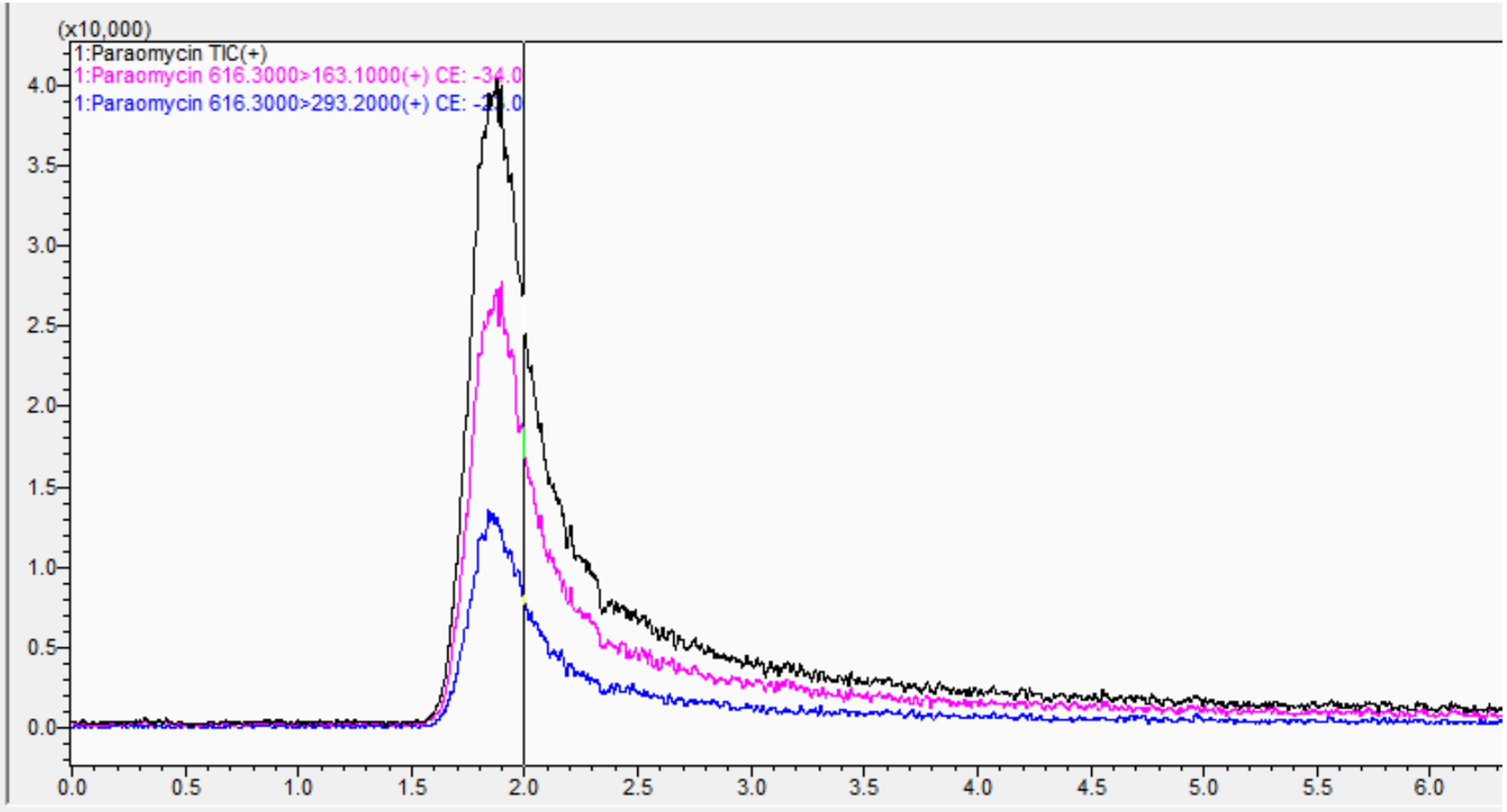

Figure 4.15 LC chromatogram of 10 µg/mL PM solution with reduced intensity

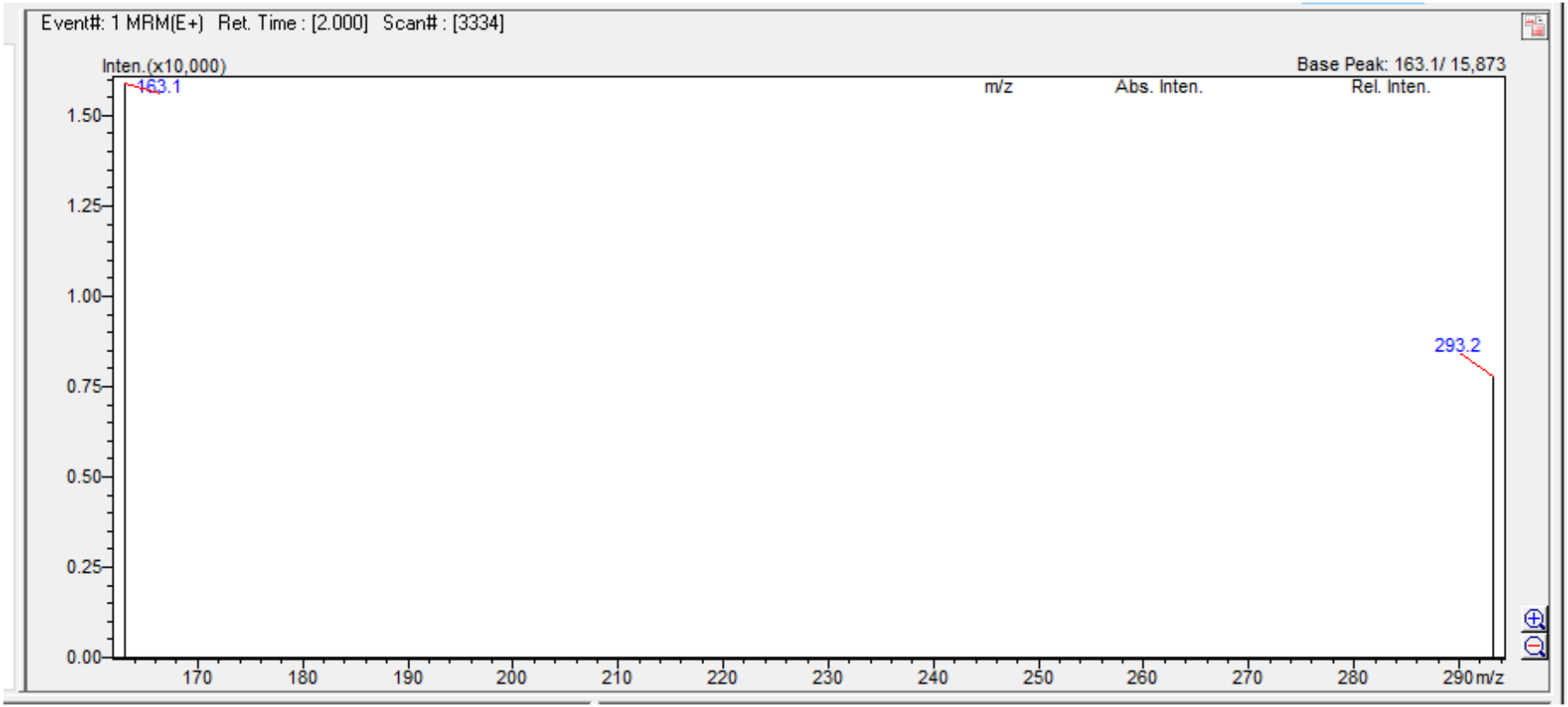

Figure 4.16 MS spectrum of 10 µg/mL PM solution with reduced intensity

Multiple Reaction Monitoring optimisation

10 µg/mL PM solution was injected directly into the MS for Multiple Reaction Monitoring (MRM) optimisation, but there was no marked improvement in the sensitivity in the subsequent HILIC-MS analysis.

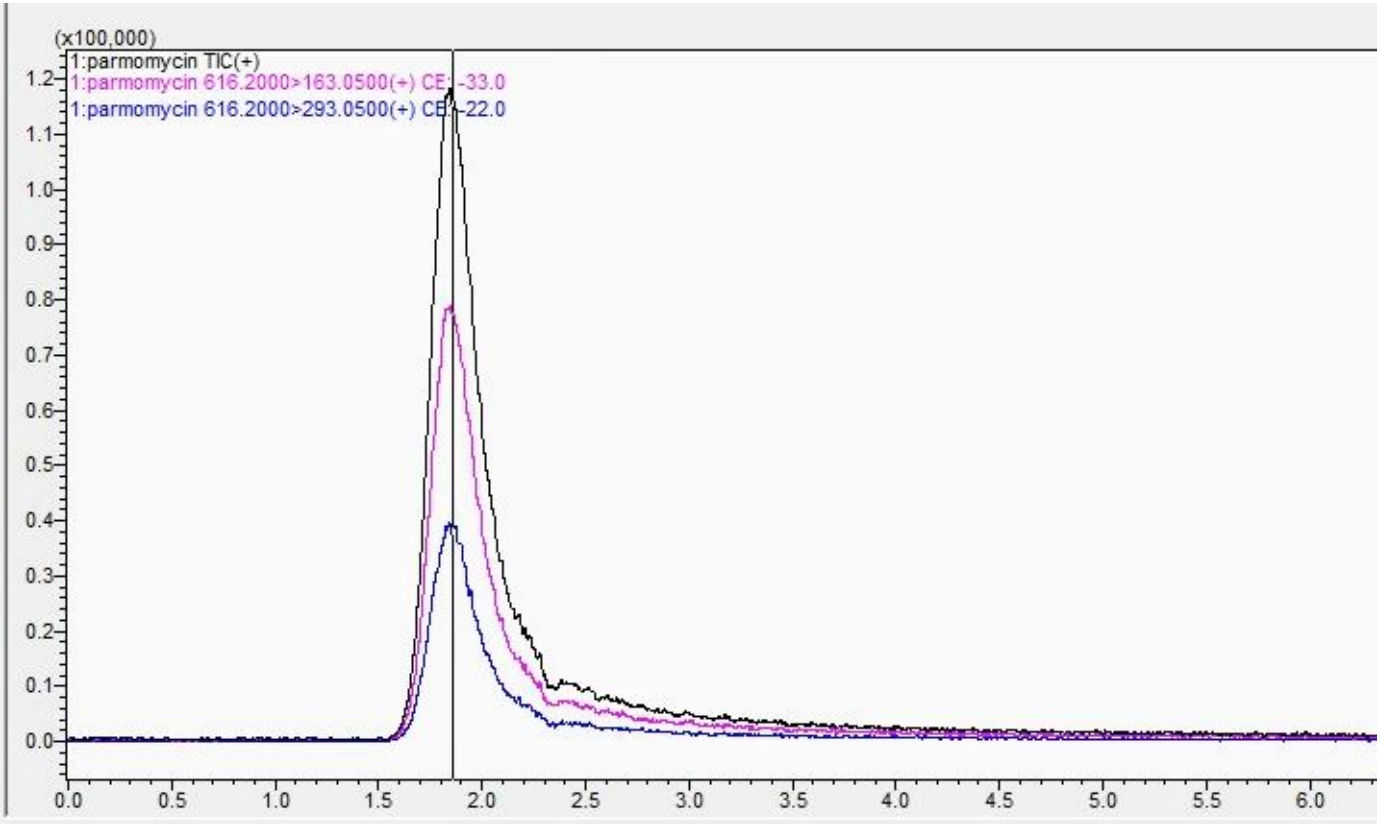

Figure 4.17 LC chromatogram of 10 µg/mL PM solution following Multiple Reaction Monitoring (MRM) optimisation

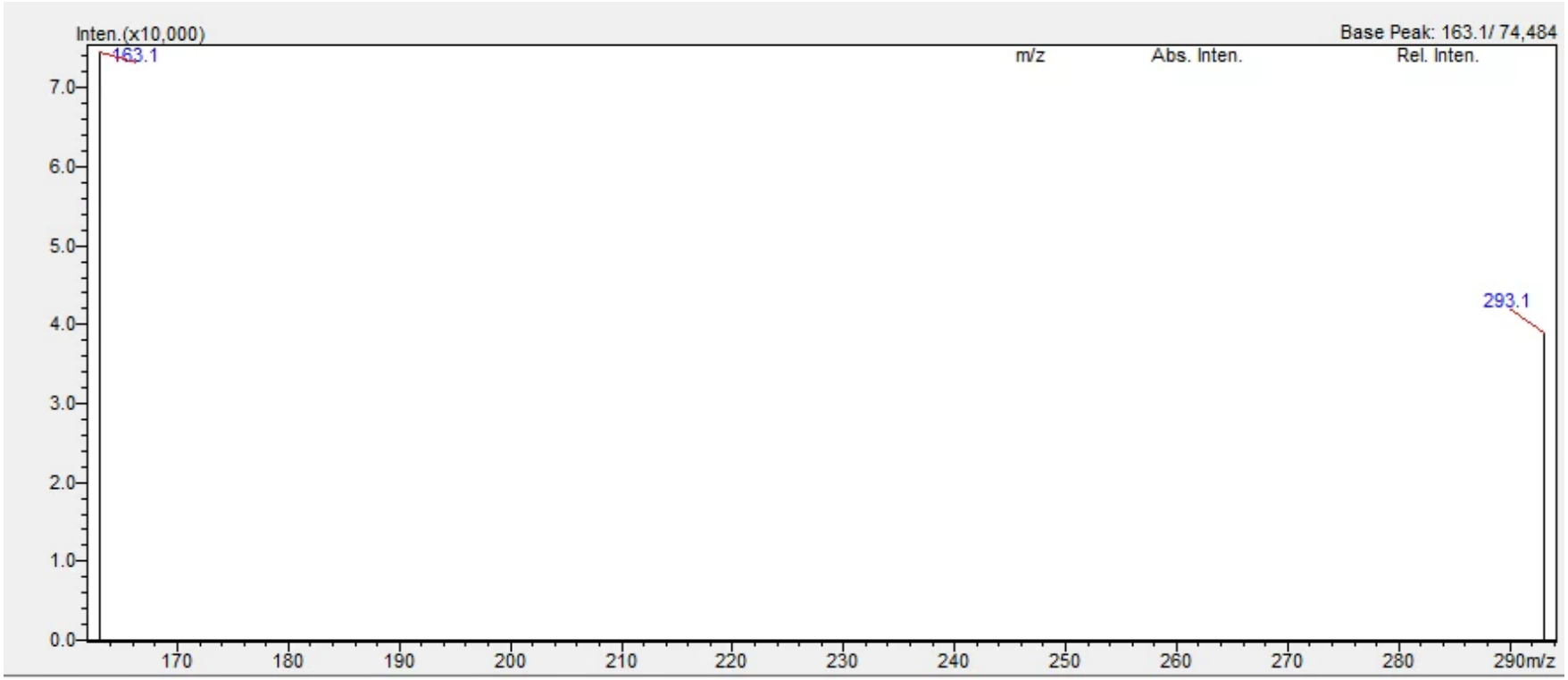

Figure 4.18 MS spectrum of 10 µg/mL PM solution following Multiple Reaction Monitoring (MRM) optimisation

Increase in ammonium formate concentration

In further attempts to improve the resolution of the assay, the concentration of ammonium formate in mobile phase A was increased to 100mM in line with alternative methods in the literature, but without going higher than the tolerance limit of the available MS equipment. All other conditions remained the same.

The analysis involved only 10 µg/mL and 1 µg/mL PM solutions as these were the concentrations with poor separation and reproducibility in the earlier studies. The peak for the 10 µg/mL solution (Figure 4.19) sharpened and gave a shorter retention time of around 1.3 minutes, but with relatively similar intensity as when 20mM ammonium formate was used. There was no improvement in the separation and consistency of the peak for the 1 µg/mL solution, and it was still difficult to distinguish from noise signals.

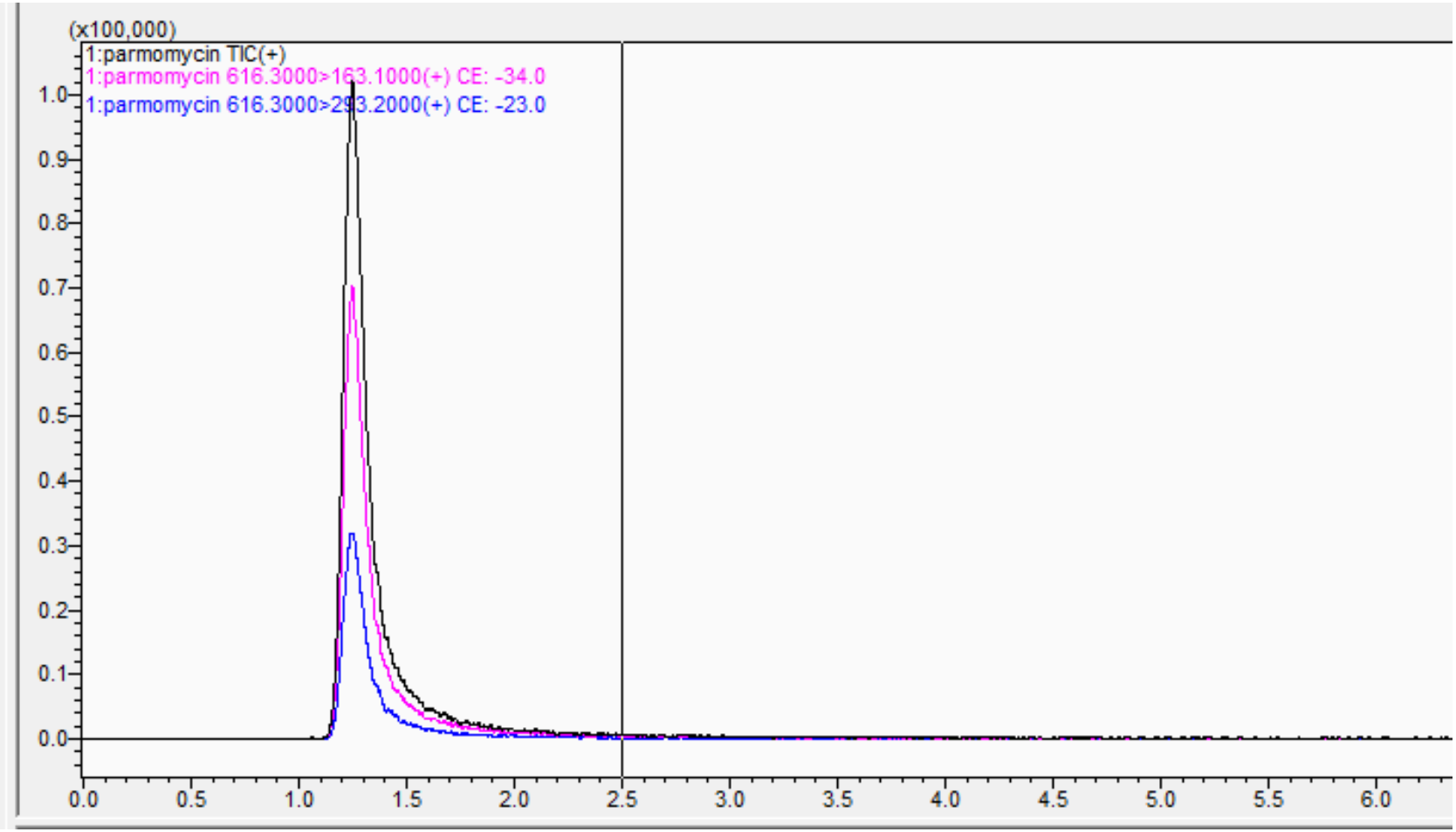

Figure 4.19 LC chromatogram of 10 µg/mL PM solution following an increase in ammonium formate concentration

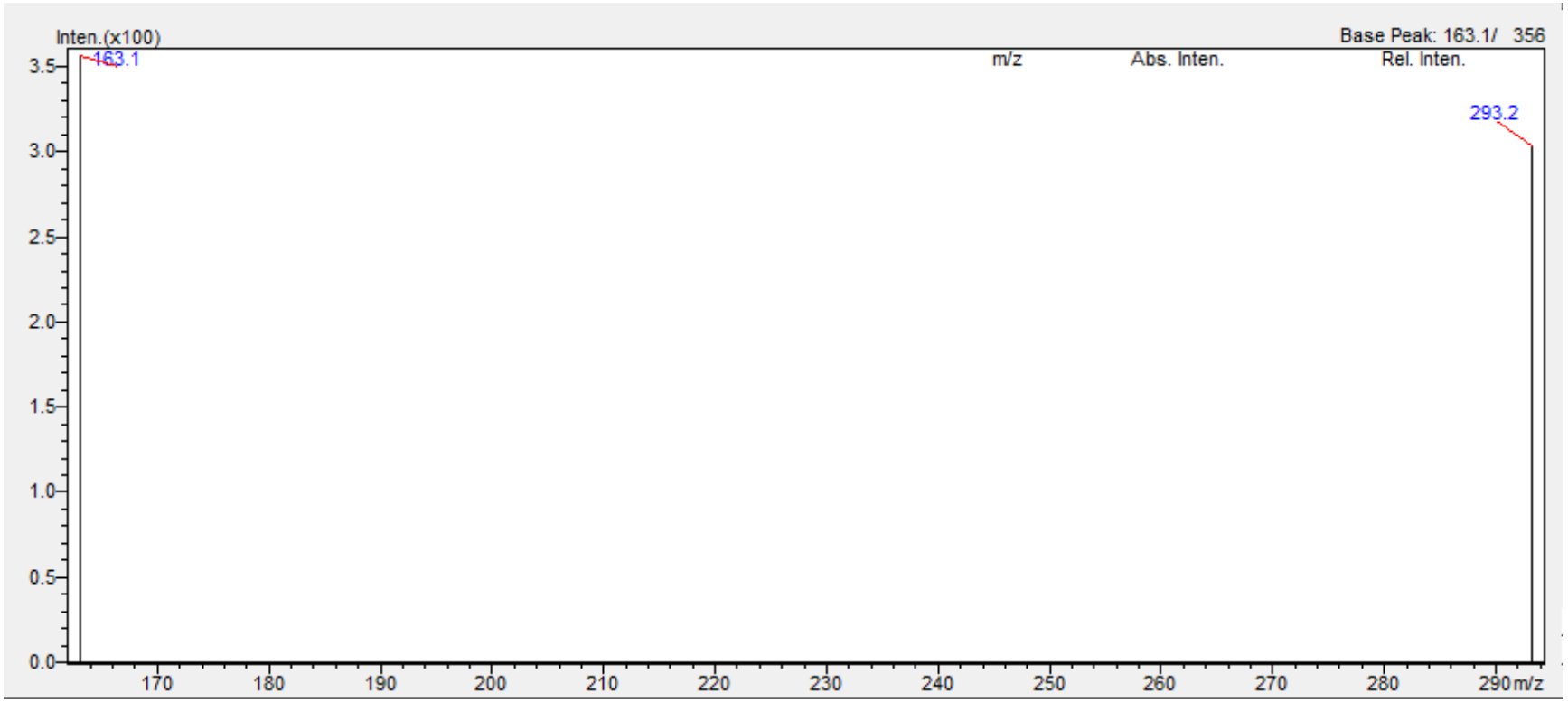

Figure 4.20 MS spectrum of 10 µg/mL PM solution following an increase in ammonium formate concentration

4.3.6 DETECTION OF PM IN CSPM MN

Despite the low intensity of the peaks, a test was conducted to investigate if PM in CSPM MN could be detected using the quantification protocol.

As expected, the amount of PM was too low to detect and reliably quantify (Figure 4.21).

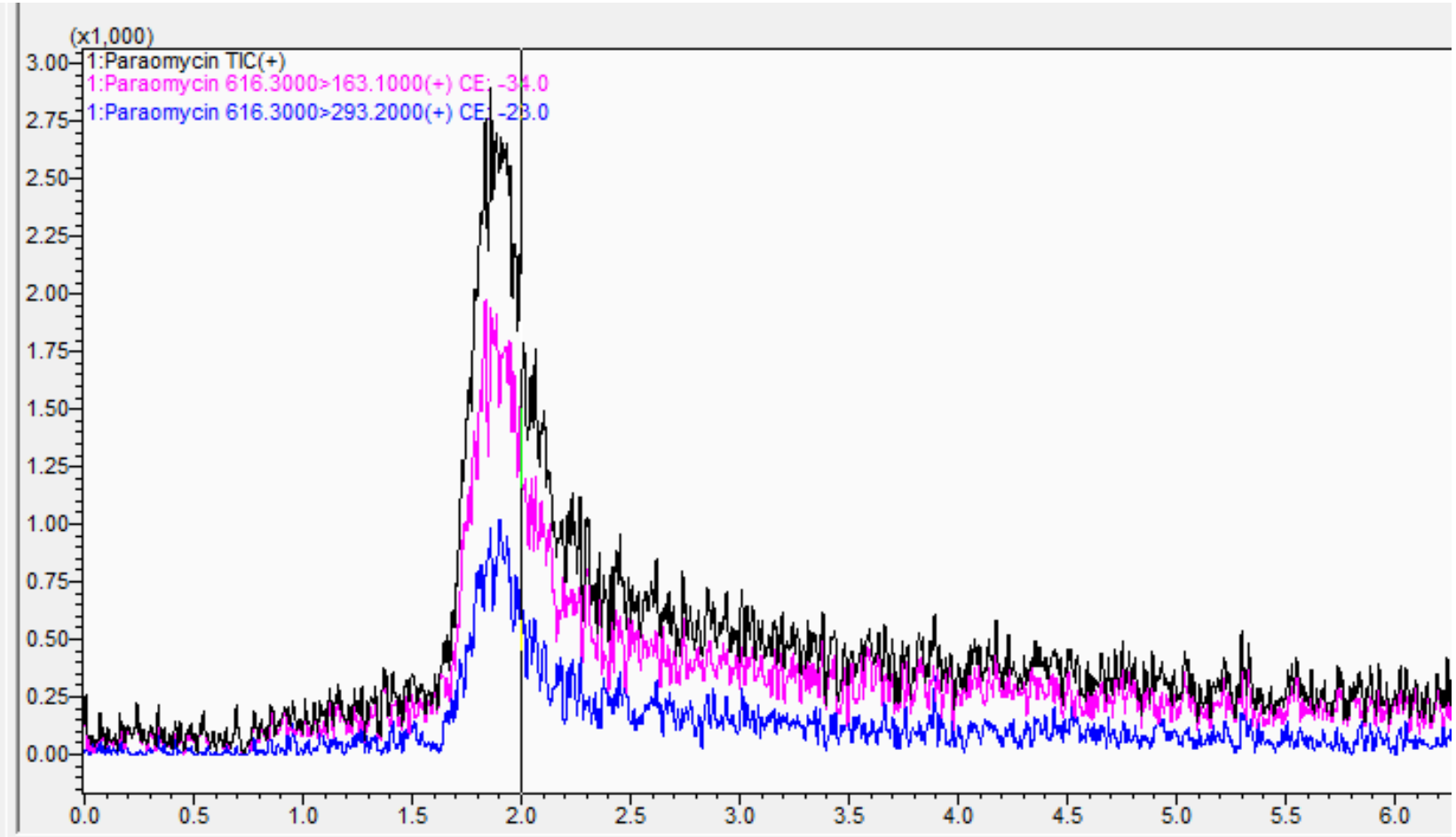

Figure 4.21 LC chromatogram of paromomycin in a sample of paromomycin-loaded chitosan microneedles

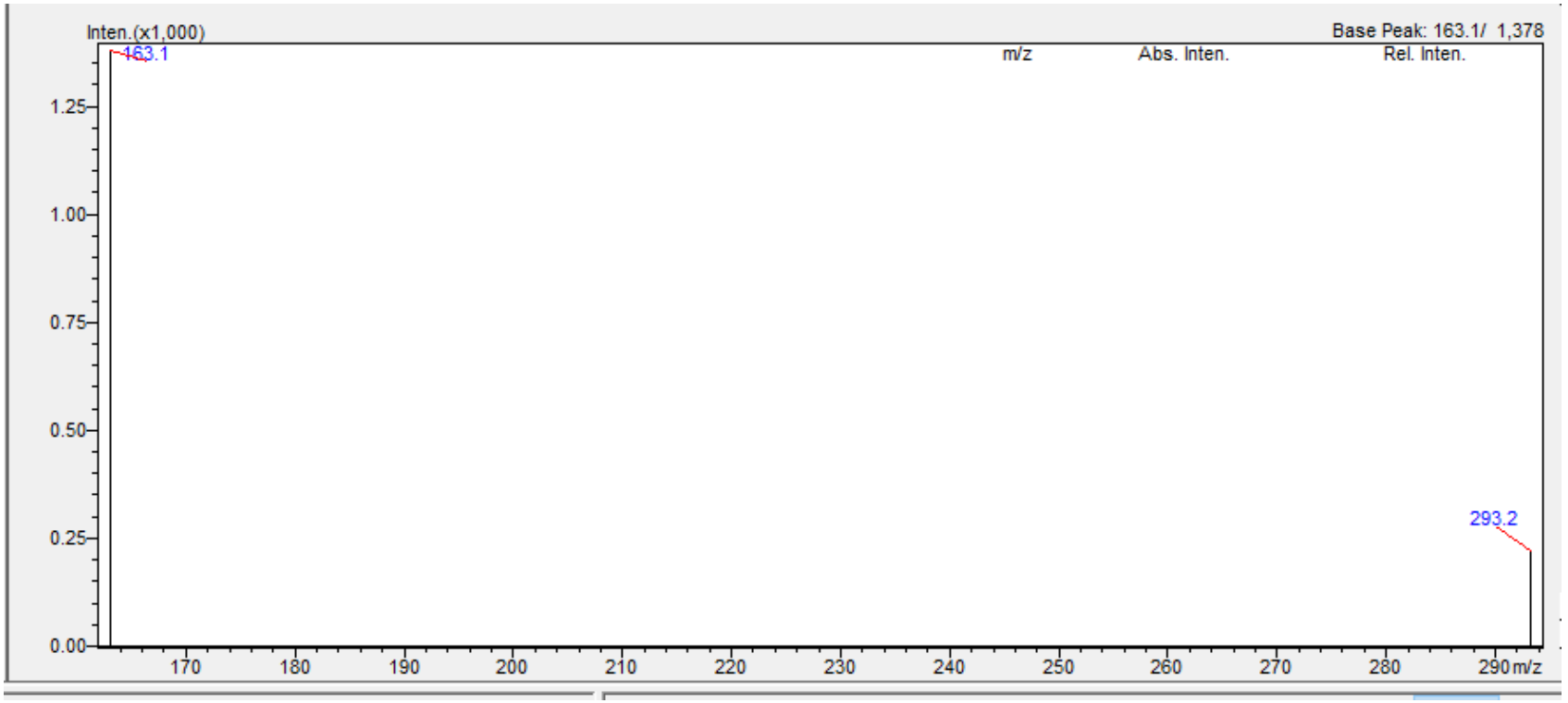

Figure 4.22 MS spectrum of paromomycin in a sample of paromomycin-loaded chitosan microneedles

4.4 DISCUSSION

This chapter describes the first report of fabricating PM-based dissolving MNs of two types for CL treatment; one with needles made from PM alone and another with PM loaded in chitosan needles.

Fabricating dissolving MNs with needles made from PM alone was not successful because the needles were brittle. This is not surprising since PM is an aminoglycoside and thus could have similar behaviour with simple sugars which are known to produce brittle MNs and generally require an additional material to make high-quality MNs (14, 98). Additionally, it is possible that if the PM MNs had formed properly, they may have had poor stability issues due to the hygroscopicity of PM, which is also common issue with MNs made from sugars (98, 105). Overall, the findings of this study suggest the impracticality of fabricating MNs from PM alone through micro-moulding by solvent casting, thereby providing valuable insights to the MN field which seeks to identify other drugs that could be used as sole MN materials. However, since needles formed, although brittle and weak, it is logical to explore strategies to improve the MNs.

One approach to optimise PM for improved mechanical properties could be through chemical modification. For example, the amino groups or hydroxyl groups in PM could be exploited to create a PM prodrug with improved properties. Ideally, the chemical bond dissociates *in situ* to release PM so as not to interfere with the interaction between PM and its target site on *Leishmania* parasites.

Another approach is to include another material, such as a polymer, to enhance the mechanical properties of the MN (98, 107). Since an objective of this work was to develop chitosan MNs containing PM, this was subsequently explored.

PM-loaded chitosan MNs (CSPM MN) and drug-free chitosan MNs (CS MN) were fabricated by micro-moulding using a commercial PDMS mould. Initially the viscosity of chitosan posed an issue during fabrication, but a suitable concentration was then

identified for micro-moulding. CSPM MNs were fabricated using the two-step moulding technique in 2.2.2 to localise PM in the needles alone. This is to enable deposition of the drug into the skin and to create mechanically robust MNs (89, 123). CS MNs were also fabricated using the same method to compare with CSPM MNs. Both MNs formed 100 needles with well-defined tips and pyramidal shapes similar to the mould. This suggests that PM did not hinder the formation of chitosan MNs.

As expected, the heights of CSPM MN and CS MN are less than the height of the mould (500µm). This could be due to water loss during drying, which is commonly seen for MNs made by micro-moulding, as described earlier. It could also be due to incomplete filling of the mould due to the viscosity or high interfacial tension between the mould and the solutions (106, 482). The presence of sharper tips in CS MN than in CSPM MN could be because of the hygroscopic nature of PM which could lead to higher adsorption of atmospheric moisture or greater retention of water in CSPM MN than in CS MN which may have impacted on the final shape of the tips during drying in the mould.

It is imperative that incorporating a drug into MNs does not negatively impact on their ability to overcome resistance from skin during insertion and insert without breaking. In the compression study, a texture analyser applied an axial force to CSPM MN and CS MN to measure the force required to move the probe as a function of distance. The similarity in the shape of the force-distance curves of CSPM MN and CS MN, in terms of showing a continuous curve without a sudden drop suggests that they show the mechanical behaviour that is typical of pyramidal MNs (90). Visualisation under a microscope showed that the MNs did not break within the force range in the experiment, which is consistent with the shape of the curves.

The results also suggest that incorporation of PM reduced the resistance to compression of chitosan MNs. This could be due to the hygroscopicity of PM which may have made CSPM MN more flexible than CS MN due to the plasticising effect of water. In a study by Merlusca et. al, neomycin was incorporated into films made from a blend of chitosan and

PVA which caused a reduction in the mechanical properties of the film (483). Neomycin is an aminoglycoside with a very similar chemical structure as PM except that PM has a hydroxyl group at position 6 in ring 1 of its chemical structure whereas neomycin has an amino group at that position. The authors measured the contact angle between water and the film surface and found that contact angle reduced with the incorporation of neomycin. This then led to their conclusion that the reduction in mechanical properties could be due to the polar nature of neomycin. They also suggested that it could also be due to structural disarrangement of the polymer matrix due to the presence of neomycin.

Studies in the literature which incorporated drugs into MNs have reported that the drug either affected the mechanical properties of the MNs or had negligible effect. For example, amphotericin B had a negligible effect on the mechanical properties of chitosan–polyethyleneimine MNs whereas propranolol reduced the mechanical properties of MNs made from a blend of hyaluronic acid and PVP (51, 142). To date, no studies have predicted the impact of drug loading on the mechanical properties of MNs and so studies tend to empirically examine the influence of drug loading.

The compression study provided direct comparison between the mechanical properties of the CSPM MNs and their resistance to compression with that of CS MNs. However, further studies investigated the skin insertion ability of the MNs to assess whether they could withstand insertion by hand and their ability to maintain their shape after insertion.

Parafilm® M (eight sheets) was used as a skin simulant, with the first sheet corresponding to a penetration depth of 126 μm and the next sheets corresponding to an additional depth of 126 μm, as described in Chapter 2. Both CSPM MNs and CS MNs had approximately 100% penetration efficiency in the first sheet, indicating that they can effectively penetrate the *stratum corneum*, which is about 5-50 μm thick (1, 7, 261).

The penetration efficiencies of the MNs dropped as the depth increased. This is expected due to the elasticity of Parafilm® M in addition to its resistance to insertion. Parafilm® M

mimics the viscoelastic nature of skin which is also shown as the MN penetration depth is less than the needle height.

CS MNs created faint holes in the third sheet but since the penetration efficiency in the third sheet was less than 20%, the penetration depth of CS MN is estimated to be between the second and third sheets (252 - 378μm) (127). CSPM MNs penetrated up to the second sheet, which is less than the penetration depth of CS MNs. This is consistent with the compression test results which showed that CS MNs resisted compression more than CSPM MNs when compressed beyond approximately 0.3 mm. It is also worth noting that tip diameter influences MN skin insertion. Chen et. al compared drug-free chitosan MNs with the same geometry but different tip diameters and reported that MNs with wider tips had lower penetration efficiency and depth than MNs with sharper tips (123). CSPM MNs had wider tips than CS MNs, and the lower penetration efficiency is thus in agreement with the study by Chen et. al. The penetration depths of CS MN and CSPM MN in Parafilm® M are promising because they suggest that the MNs can reach the lower layer of the skin where *Leishmania* parasites reside (7, 29).

Both CSPM MNs and CS MNs did not break after insertion into Parafilm® M, attesting to the reason for CS being one of the common MN materials. It is surprising that CSPM MNs remained intact despite the brittle nature of MNs made from PM alone and the results of the compression study. Although PM reduced the mechanical properties of chitosan MNs, the MNs are able to remain intact post-insertion, suggesting that chitosan is a good material for loading PM in MNs. However, further studies are needed to further evaluate PM-loaded chitosan MNs, especially by using skin that simulates CL-infected skin.

Chitosan MNs are known to exhibit sustained release of the incorporated drug, possibly due to degradation-based drug release (36, 123, 484). This could be beneficial for PM because its highly polar nature makes it prone to rapid clearance, reducing available contact time with the parasites, as described in 1.7. As this is the first report of loading

PM in chitosan MNs, drug release studies are required to evaluate the release mechanism of PM from the MNs. Additionally, stability tests are required to investigate if PM remains stable in the MN after storage. This could be done by measuring the amount of PM before and after storage. However, it was necessary to develop a method of quantifying PM to conduct these tests. The theoretical amount of PM in CSPM MN is 5 µg per MN patch, hence, a quantification method sensitive enough to quantify PM was required.

This work aimed to develop a HILIC-MS assay to quantify PM in MNs for the first time due to the lack of chromophores in PM and the limitations of reverse phase chromatography for PM quantification, as well as the lack of a quantification protocol for PM in MNs in the literature, as further described in 4.1.2.

HILIC is a type of LC which doesn't require the use of ion pairing reagents. It uses a polar stationary phase as in normal phase LC (NPLC) but with a mixture of an organic solvent and water as the mobile phase, resolving the issue of poor solubility of the analyte in the mobile phase of NPLC (475, 485). Several authors have proposed that the retention mechanism in HILIC involves partitioning of the analyte between the mobile phase and hydrophilic layer of the stationary phase, surface adsorption and/or electrostatic interactions between the analyte and the charged stationary phase, depending on the type of HILIC (460, 476, 485, 486).

Amongst the different types of HILIC columns, zwitterionic HILIC has been reported to be the most suitable for the chromatography part of aminoglycoside quantification with mass spectrometry (460, 470, 476). This could be due to its weak interactions with aminoglycosides, in addition to hydrophilic partitioning, which gives a good balance between retention and elution, unlike the strong interactions that typically occur in other HILIC columns (460). Atlantis Premier BEH Z-HILIC column, which was used in this study, is a zwitterionic HILIC column with sulfoalkylbetaine groups covalently bonded to ethylene-bridged hybrid (BEH) particles (Figure 4.23) (487).

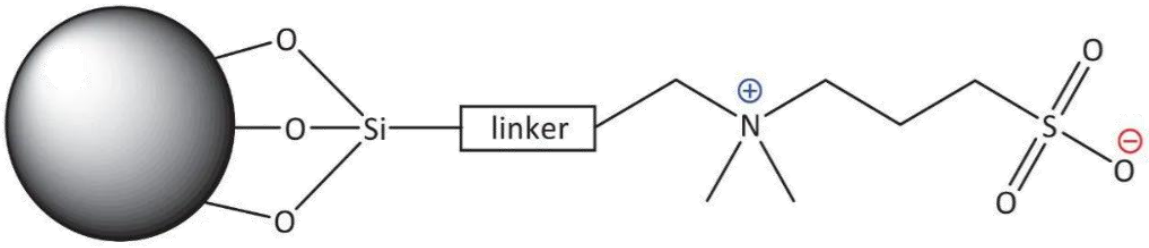

Figure 4.23 Structural representation of the stationary phase of Atlantis Premier BEH Z-HILIC Column. Image reproduced from (487).

In order to develop a HILIC-MS quantification method to quantify PM in MNs, a method reported by Waters Ltd using the Atlantis Premier BEH Z-HILIC column was adapted in this work, as described in 4.2.5. Table 4.4 describes the steps that were conducted to develop a quantification method, along with the outcomes.

Table 4.4 Method development of a HILIC-MS quantification assay for paromomycin in microneedles

Step	Outcome
Binary mobile phase was used at a gradient run, as per Waters Ltd protocol.	Peak tailing, peak splitting and inconsistent retention times were observed.
Switched to an isocratic run to address the shortcomings by focusing the method development on the timeframe that corresponds to the elution of paromomycin.	
The injection volume was reduced from 5 µL to 3 µL and the column was conditioned.	Consistent retention time with a well-defined peak for 100 µg/mL PM solution but low sensitivity and irregular peaks for 10 µg/mL and 1 µg/mL PM solutions.
Multiple Reaction Monitoring optimisation was performed.	No improvement in sensitivity.

Ammonium formate concentration was increased from 20 mM to 100 mM.	The retention time reduced and the 10 µg/mL PM peak sharpened but with no improvement in sensitivity. There were noise signals in the 1 µg/mL PM peak.

A solution of paromomycin-containing microneedles was analysed using the assay, as described in 4.2.5.5 and shown in 4.3.6. This is further discussed later in this discussion section.

Retention time refers to the duration that an analyte resides in a column from injection to elusion. When the retention time is very short, there is a chance of poor separation of the analyte from other components that may be present in the sample. This could in turn affect the selectivity and sensitivity of the quantification method (488). Whereas prolonged retention could lead to peak broadening which also affects the selectivity and sensitivity of the quantification method (488). As explained earlier, HILIC was used in this work to provide optimal elusion of PM due to the chemical structure of PM which makes reverse phase chromatography not ideal without the use of an ion pairing reagent.

The contents of the mobile phase were selected for compatibility with PM and to enable optimal elution for detection and quantification. Acetonitrile, which is commonly used in HILIC, was used in this work because its volatility makes it compatible with MS as it enables desolvation during ionisation and it is a polar aprotic solvent which facilitates partitioning for optimal analyte retention in HILIC, especially as PM has limited solubility in acetonitrile which favours partitioning (460, 475, 488). The buffer, the aqueous mobile phase (mobile phase A) and the aqueous injection solvent reduce the likelihood of PM precipitation and low sensitivity (476).

Low pH was used to enhance the ionisation of PM in the MS, hence improve MS detection, since PM is a basic compound (460, 470, 476, 489). Enhanced ionisation due to low pH could also reduce interactions between PM and the hydrophobic part of the

stationary phase and increase repulsion between PM and the positive ion part of the stationary phase to reduce the risk of peak tailing (479).

Ammonium formate, a MS-compatible volatile buffer, was used to maintain the pH and interfere with any ionic interactions that occur between PM and the negative ion part of the stationary phase which cause prolonged retention (460, 476). Overall, these show the impact of PM compatibility with the mobile phase. Nevertheless, optimisation of the mobile phase composition, such as the buffer concentration, is generally done to provide optimal quantification (461, 476, 488), and this was attempted in this work, in addition to the optimisation of other analytical conditions, as described below and in 4.2.5.

The shapes and intensities of the peaks in this study were not as expected. The reason for poor consistency in peak shapes and retention time is unknown but it may be due to “carry over” of PM from a high injection volume or improper column conditioning. Based on advice from the column’s manufacturer, the column was conditioned, and the analysis was repeated. Subsequently, the peak shape improved, and the retention time was consistent and coincided with the retention time obtained in the report by the manufacturer. However, there was poor detection of 1 µg/mL PM, which was unfortunate given the drug loading into the MNs. Furthermore, it is unusual that the peak intensity of 10 µg/mL PM solution dropped in a subsequent analysis. It could be that the high adsorptive behaviour of PM to metals resulted in loss of PM in the LC system or PM became saturated in the HILIC column after several uses.

The MS detector was run using MRM mode, as described in 4.2.5.3. MRM enables detection and quantification of the selected transition from precursor ions to product ions, resulting to high sensitivity ranging from ng/mL to pg/mL (490). MRM optimisation was employed in this work to identify the optimal MS parameters for maximum sensitivity (470, 490, 491). However, the lack of improvement in the peak intensity suggests that the issue was likely due to the chromatography stage. It is vital to combine LC with MS rather than MS alone, in order to separate PM from other compounds in the sample.

One of the reasons that the Atlantis Premier BEH Z-HILIC column was chosen is because the manufacturer's report showed that it enabled the detection and quantification of PM and other aminoglycosides using 20mM ammonium formate, unlike other zwitterionic HILIC columns reported in the literature which required concentrations above 100mM. The report by the manufacturer was the only one where 20mM ammonium formate was used, at the time of conducting this work. So, the concentration of ammonium formate in this work was increased to investigate if there would be an improvement in sensitivity.

When the concentration of ammonium formate was increased to 100mM, the retention time reduced to about 1 minute and the peak shape became narrower than when using the less concentrated 20mM solution. This is consistent with findings in the literature and the Waters Ltd report (460, 470, 479). This effect could be due to the increased competition between the ammonium ions and PM ions for the stationary phase, resulting in less retention of PM. However, there was no improvement in the sensitivity.

Despite the poor sensitivity of the assay, CSPM MN was dissolved in deionised water and analysed to find out if PM could be detected. A peak corresponding to PM was seen but with excessive noise signals as expected due to the low sensitivity of the assay. This showed that the assay was unsuitable to quantify PM in the MNs developed in this work and for drug release studies.

The multimodal mechanism of HILIC makes method development complex and difficult to predict (461, 476). Potential reasons behind the unusual findings of this work could be poor ionisation, loss of PM in the LC system and/or an inefficient or contaminated column, further details are provided below.

It could be that PM was poorly ionised to give the expected sensitivity. In addition to the MS parameters, LC conditions influence the chromatography and sensitivity (476, 489). Since MRM optimisation and an increase in the buffer concentration did not improve sensitivity in this work, further optimisation strategies could be explored, such as

adjusting the formic acid concentration and/or changing the organic solvent. For example, Yang et.al found that the signal of aminoglycosides improved when they changed the organic solvent from acetonitrile to methanol (470). However, the reason for an increase in sensitivity when methanol is used is not fully known and methanol is generally less preferred due to its viscosity which could result in high back-pressure (488).

As described earlier, the high adsorptive affinity of PM to metals was another reason for selecting the column used in this study, as it was designed to mitigate interactions between the analytes and the column. However, the LC system and its flow path also contain metal tubing (481). There are LC systems that are also designed for metal-sensitive analytes, and such LC system was used in the report by Waters Ltd but not in this work.

It is also possible that the HILIC column used in this work may have been contaminated with excess PM after multiple uses or it showed unexpected poor functionality with the MS detector used in this work. The manufacturers of both the column (Waters Ltd, UK) and MS system (Shidmazu, Japan) were contacted and they were unable to identify the cause of the problem but Waters Ltd suggested trying a different LC technique or column.

Prior to the report by Waters Ltd about the Atlantis Premier BEH Z-HILIC column for aminoglycoside quantification, Yang et.al. compared two other zwitterionic HILIC columns (Obelisc® and ZIC®-HILIC) for the quantification of aminoglycosides in food (470). The authors found that PM could not be eluted from Obelisc® while ZIC®-HILIC gave satisfactory peaks prior to the optimisation of the LC conditions to improve chromatography and sensitivity. In contrast, Diez et. al. conducted a similar comparative study to that of Yang et. al using the same columns and found that Obelisc® gave the best sensitivity especially for PM (460). These differing findings demonstrate that reports of a column or LC conditions working for one study does not guarantee that the same result will be achieved in another study, especially when different LC and MS systems

are used and when the researchers differ in level of expertise. This was also highlighted in a study by Kiontke et. al. which gave insights into LC-MS method transfer and development (489).

Additionally, when Roseboom et. al. attempted zwitterionic HILIC for PM quantification in human plasma, they reported poor elution of PM with broad peaks which resulted in poor sensitivity. However, the use of reverse phase LC with HFBA, an ion pairing reagent, gave high resolution and sensitivity (LOQ 5 ng/mL) (463). Similar findings were seen in another study which compared HILIC with reverse phase LC plus an ion pairing reagent for aminoglycoside quantification (492). Therefore, it may have been useful to test and compare more than one HILIC column and/or try reverse phase LC with an ion pairing reagent but these were not feasible in this study due to the restrictions stated in 4.2.5. Therefore, PM quantification in MNs could not be conducted.

In summary, this chapter describes the first report of loading PM in MNs. MNs made from PM alone were brittle and unfit for use. Chitosan was used as a MN material to encapsulate PM due to its intrinsic antileishmanial activity and suitability as a MN material, as described in the literature. The PM-loaded chitosan MNs seem promising as they showed good mechanical performance and morphology. Further tests are required to confirm the suitability and effectiveness of the MNs for CL treatment, such as drug release and stability tests. However, these could not be conducted due to the lack of a sensitive quantification protocol for PM and attempts to develop a new method were unsuccessful. The method development attempted in this work provides valuable input to the field on the inter-laboratory transferability of LC-MS methods and the use of a new zwitterionic HILIC column with low buffer concentration to quantify PM.

The optimal dose of topical PM required to eliminate *Leishmania* parasites in the skin is underexplored, and this is coupled with *Leishmania* species-dependent therapeutic efficacy of CL treatments and the limited research on CL, a neglected tropical disease. The current PM ointment contains 15% w/w of PM, but this concentration was selected

on an ad hoc basis, primarily based on the optimal concentration of MBCL mentioned in chapter 1 (237).

Physical penetration enhancement methods generally provide the benefit of targeting the lower skin region for CL treatment. A study showed that iontophoresis enabled deposition of a 1% w/v PM solution to the skin region where *Leishmania* parasites typically reside, but further studies are required to identify the optimal amount of PM required for therapeutic efficacy using this method (29). Similarly, MNs enable localisation of the drug in the applied area on the skin and deposit the drug in the target skin region, thereby could enable direct targeting of the parasites (53). Whereas ointments are typically spread on the skin surface and rely on drug movement into the lower region of the skin, which typically results in minimal amount of drug reaching the target site, as described in chapter 1, in addition to the potential for variable dosing of semi-solid formulations when applied on the skin. Furthermore, the formulation strategy used in this work (i.e. using chitosan as the MN material) may provide a dose-sparing effect. These suggest that the PM-loaded MNs in this work may require a lower loading dose than the ointment. Hence, the author of this thesis believes that it is not ideal to base the loading dose of PM-loaded MNs only on the PM concentration in the ointment.

Therefore, due to the limited information on the optimal dose of PM for topical administration to treat CL, a pragmatic approach to PM loading in the MNs made from 2.5 % w/v chitosan solution was used in this work. The theoretical amount of PM in this work is 5 µg (100 needles/patch). The actual loading dose and the total amount of PM that the MNs could release could not be determined in this work due to the unsuccessful attempts to develop a quantification assay for PM, as described earlier.

This work focused on assessing the feasibility of loading PM in MNs but antileishmanial activity tests on the PM-loaded chitosan MNs are required to evaluate PM activity when loaded in MNs, as well as the effect of combining chitosan and PM in MNs. As described earlier in chapter 1, low drug loading is a common limitation of dissolving MNs, but the

use of chitosan may provide a dose-sparing effect, in addition to the potential for MNs to directly target the parasites. Findings from the antileishmanial activity tests could inform patch design to identify the optimal loading dose required for this novel approach of formulating PM. If increased dose loading is required, there are potential strategies to address this. For example, when the patch size of amphotericin-loaded MNs was increased from a patch of 242 needles to 484 needles, the *in vitro* antileishmanial activity increased from 53% to 86% *Leishmania* parasite death (125). Moreover, it is anticipated that a typical drug-loaded MN patch for clinical use could contain around 1000 needles or more, depending on the application (38, 50).

CHAPTER 5 – CONCLUSION

5.1 SUMMARY AND IMPLICATIONS OF THIS THESIS

This thesis aimed to fabricate and evaluate dissolving MNs containing novel compositions. It explored the feasibility of fabricating dissolving MNs from PEOZ, as well as the feasibility of loading PM into dissolving MNs and tailoring the MNs for the treatment of cutaneous leishmaniasis.

Polymers are common materials for fabricating MNs, especially dissolving MNs and hydrogel forming MNs. This is due to the numerous benefits that polymers provide, such as advanced drug release. However, the mechanical properties of polymers typically limit the performance of the MNs, compared to metals, as described in chapter 1. This is usually addressed by blending different polymers and optimising the polymer ratio to achieve optimum mechanical properties. Although several polymers have been reported in the literature for MN fabrication, there is a limited number of miscible polymer blends to develop high-quality MNs. Additionally, there is a need to identify additional polymers that can develop high quality MNs, as this could enable the formulation of various drugs of various physicochemical properties for efficient drug loading. Also, as MN fabrication generally requires tailoring to the desired drug and application rather than a ‘one size fits all’ approach, exploring additional polymers for MN fabrication could in turn maximise the applicability of MNs.

This thesis reports the first use of PEOZ as a material for fabricating dissolving MNs. MNs made from PEOZ of two molecular weights (50 kDa and 200 kDa) were fabricated and characterised and compared with MNs made from polyvinylpyrrolidone (PVP) of two molecular weights (55 kDa and 360 kDa), which were the closest matching molecular weights to PEOZ in the market. PEOZ was explored in this work due to its promising potential shown in various studies for drug delivery, as well as its relatively similar

chemical structure to PVP which is the most common polymer for fabricating dissolving MNs, as described in chapter 1.

Chapter 2 shows the MN fabrication method development that was performed to create an efficient and reliable method of fabricating MNs for this work. The findings of the method development showed the impact of the quality of the PDMS moulds on MN fabrication and the resulting MNs. Thereby, showcasing the importance of ensuring an adequate fabrication process for MN development.

The next study in chapter 2 was the fabrication and characterisation of PEOZ MNs and PVP MNs. This proof-of-concept study suggests that PEOZ 50 kDa may not be a suitable sole material for fabricating dissolving MNs due to its poor performance while PEOZ 200 kDa is a promising material for MN fabrication. The findings were based on microscopic evaluation, compression tests, insertion tests and *in vitro* release tests using sodium fluorescein as a model drug. These findings also suggest that PEOZ has comparable performance to PVP as a MN material, but further investigation is warranted. This study gives novel insights into the feasibility of fabricating dissolving MNs from PEOZ and how the MNs compare with PVP MNs. Overall, this study contributes to the research field that seeks to identify additional MN materials. It also contributes to the current knowledge on the effect of polymer molecular weight on the performance of MNs. Additionally, this study advances the current understanding of the behaviour of PEOZ for drug delivery and showcases further potential applications of PEOZ.

Although fabricating MNs was achievable using PEOZ 50 kDa, its poor morphology and mechanical properties warranted optimisation for MN fabrication. Hence, polymer blending was explored to enhance MNs made from PEOZ 50 kDa. Poly(vinyl alcohol) (PVA) is commonly used to fabricate MNs, in which its blend with PVP is a widely used blend for fabricating dissolving MNs with suitable mechanical properties and tailorable drug release, as described in chapters 1 and 3. It is plausible that the intermolecular interactions between the polymers, favour the mechanical properties of MNs made from

PVA-PVP blends. In view of this, PVA seemed ideal for blending with PEOZ 50 kDa for MN fabrication but miscibility between PVA and PEOZ required investigation.

Therefore, chapter 3 investigated miscibility between PVA and PEOZ using microscopic evaluation, thermal analyses, and Fourier transform infrared spectroscopy (FT-IR). Scanning electron microscopy (SEM) showed phase separation between PVA and PEOZ while the spectra from modulated differential scanning calorimetry (DSC) suggests that the blends exhibit single and broad glass transition temperatures which were around the glass transition temperatures of the polymer that was present in a higher proportion than the other. The findings of the FT-IR analysis suggest that there is no evidence of strong intermolecular interactions between PVA and PEOZ over the range of compositions studied in this thesis. Overall, this study suggests that PVA and PEOZ are not fully miscible, and the potential reason for this and the contributions of this study to the understanding of polymer miscibility are described in chapter 3. Based on the miscibility study, PVA-PEOZ blend was not used for MN fabrication, but suggestions of further studies on the blend are mentioned in chapter 3 and later in this in chapter.

As described earlier, this thesis also explored the feasibility of loading PM into dissolving MNs for the treatment of cutaneous leishmaniasis (CL). The global burden of CL and the limited efficacy of current treatments of CL warrant the need to develop new topical formulations of antileishmanial drugs, especially PM. PM is currently available as an ointment, but its efficacy is hampered by its limited ability to reach the lower region of the skin where *Leishmania* parasites reside and poor retention of PM at the target site due to rapid clearance.

There are numerous benefits that MNs could provide to improve the treatment of early-stage CL. Furthermore, the unique features of MNs meet several aspects of the target product profile of new CL treatments created by the Drugs for Neglected Diseases Initiative (DNDi), as described in 1.7.3. However, there are limited studies on the use of MNs for CL treatment and there is currently no report of using MNs to deposit PM in the

skin for CL treatment. Therefore, this thesis evaluated the feasibility of loading PM into dissolving MNs for CL treatment.

Chapter 4 describes a novel approach of formulating PM by fabricating MNs from PM alone. However, the needles were brittle and broke upon handling. This study contributes to the current knowledge of the sole use of small sugar-based compounds to fabricate MNs, as well as the growing research field focused on fabricating dissolving MNs from drugs alone.

Chapter 4 also describes the fabrication of PM-loaded MNs made from chitosan for CL treatment. Chitosan was selected due to its reported antileishmanial and wound healing properties, in addition to its well-known ability to create MNs. This study showcases a strategic approach to fabricating MNs by tailoring the MN composition to achieve a synergistic therapeutic effect from the drug and the polymer for the intended application. This study showed that loading PM in MNs made from chitosan did not hinder the formation of all the needles in the MN array, but it impacted the mechanical properties of the MNs, which is consistent with several studies in the literature about drug loading in MNs. Nevertheless, the PM-loaded MNs exhibited suitable insertion ability as they penetrated a skin simulant to a depth consistent with the location of *Leishmania* parasites in the skin. Thus, this study provides insights into the potential of utilising dissolving MNs made from chitosan to deposit PM in the lower region of the skin for CL treatment. Additional studies are warranted to further evaluate this drug delivery system for CL treatment.

Studies were also conducted in chapter 4 to develop a sensitive and reproducible assay for quantifying PM in MNs using liquid chromatography and mass spectrometry (LC-MS). This was performed in order to study the drug release of PM from MNs made from chitosan. Quantification of PM is challenging due to the lack of a chromophore or fluorophore in PM. A PM quantification assay using LC-MS was developed by adapting reported methods. The assay was not suitable for use in this study despite conducting

several modifications to the method to improve the sensitivity and reproducibility of the assay. Overall, the findings of this study showcase the challenges of inter-laboratory transfer of LC-MS protocols and gave insights into quantifying PM using zwitterionic HILIC and a mobile phase consisting of a low buffer concentration.

5.2 FUTURE WORK TO SUPPORT CLINICAL TRANSLATION

This thesis showed that PEOZ 200 kDa is a promising material for fabricating dissolving MNs. However, additional studies are required to further evaluate its suitability as a MN material. Firstly, insertion tests using human skin will provide further insights into its penetration ability. Additionally, only pyramidal moulds with a height and base width of 500 µm and 200 µm respectively were used to fabricate the MNs in this work. Studies could be done to further assess the performance of PEOZ 200 kDa when used to fabricate MNs of various dimensions and geometries. It is also logical to assess the effect of drugs of various properties such as molecular weight, on the performance of PEOZ 200 kDa MNs. There is also a need to assess the ability of PEOZ 200 kDa MNs to maintain needle integrity upon storage and maintain the stability of its incorporated drug upon storage. Furthermore, as skin application of dissolving MNs result in deposition of polymers in the skin, skin irritancy tests and toxicology studies are required to provide insights into the safety of the deposition of PEOZ 200 kDa MNs in the skin.

Although PEOZ 50 kDa did not show promising results for MN fabrication, further strategies could be employed. PEOZ is a versatile polymer which could be functionalised to create various PEOZ analogues or crosslinked to obtain a range of swelling abilities (493, 494). Therefore, its versatility could be exploited by modifying or crosslinking PEOZ 50 kDa to enhance the mechanical properties of its resulting MNs, while providing the opportunity to create novel PEOZ-based dissolving MNs which release the incorporated drug in a tailored manner. There is also a potential to use modified PEOZ 50 kDa to fabricate novel hydrogel forming MNs with improved swelling abilities compared to those in the literature.

Additionally, there could be potential applications of PEOZ-PVA blend which could benefit from the phase separation observed in this study. For example, they could be explored for tissue engineering (399, 495), as well as to fabricate porous MNs (described in 1.3.1.5) to extract skin interstitial fluid for diagnosis and drug level monitoring (97).

This thesis also reported an innovative approach to treating CL by loading PM into MNs made from chitosan. Although this drug delivery system is promising for CL treatment, additional tests are warranted to facilitate its use in clinic. Firstly, the skin penetration ability of the MNs requires further evaluation using human skin, both healthy skin and CL-infected skin. This will provide further insights into the suitability of the MNs for CL treatment. It is also logical to compare MN insertion using finger pressing and using an applicator to identify the MN application method that better suits CL-infected skin.

Antileishmanial activity tests using *in vitro* cell culture studies and *in vivo* models are also required to evaluate the activity of PM when loaded into MNs, as well as to assess for potential synergistic effect from chitosan. It is also imperative to assess the stability of the PM-loaded MNs upon storage. This could be done by conducting skin insertion tests after storage, as well as comparing the amount and antileishmanial activity of PM in the MNs before and after storage.

It is envisioned in this work that the reported sustained release behaviour of chitosan MNs will deliver a defined and controlled dose of PM at the target site and sustain delivery for a suitable period to mitigate rapid drug clearance from the tissue for effective activity against *Leishmania* parasites. However, drug release studies are required to evaluate PM release from PM-loaded chitosan MNs. Furthermore, the amount of PM that the MNs deposit into the skin needs to be measured. However, these tests require a sensitive and reproducible assay for quantifying PM. Therefore, it is logical to attempt PM quantification using alternative methods to the one used in this thesis, such as the use of LC-MS and an ion pairing reagent.

Although loading PM into MNs made from chitosan may provide a dose-sparing effect due to the antileishmanial properties of chitosan, it is logical to explore the loading of PM-containing nanocarriers into dissolving MNs for CL treatment. Based on studies in the literature, this strategy could favour increased drug loading in the MNs if there is a requirement for a loading dose higher than the feasible amount in dissolving MNs (91, 496). It could also provide an additional benefit of intracellular uptake into *Leishmania*-infected macrophages in the skin. Intracellular targeting has shown promising results in the literature for CL treatment because drug-containing nanocarriers could be designed to be internalised by macrophages, resulting in enhanced therapeutic effects than the drug alone (254, 256). However, the therapeutic effect of the nanocarriers reported in the literature is generally limited when applied topically for CL treatment due to their limited ability to reach the lower region of the skin where the parasites reside, as described in 1.7.3. Hence, combining the deep penetrative ability of MNs with the increased drug loading and intracellular targeting of nanocarriers is a logical approach to explore for CL treatment.

It is apparent that MNs are promising drug delivery systems, and this thesis has explored the potential to load PM in MNs to leverage the unique features of MNs for CL treatment. It also explored the feasibility of fabricating MNs from PEOZ as a new MN material to maximise the potential of MNs. However, several barriers need to be addressed to facilitate the commercialisation of drug-containing MNs. Standardised characterisation methods and well-defined quality and performance criteria are required to guide the development of MNs and to facilitate regulatory approval of drug-containing MNs. It is likely that thorough analysis of the metabolism and clearance of the polymers used in fabricating MNs will be required by regulatory authorities to ensure patient safety. This is because only a few non-biodegradable polymers are approved by the FDA for intradermal administration (90, 443, 497). Additionally, there is a need for scalable and

reliable manufacturing methods and standardised means of ensuring quality control (38, 439).

It is also vital that the MNs insert into human skin efficiently and consistently to ensure accurate drug dosing. This is likely an essential criterion which will need to be assessed during clinical trials for regulatory approval of drug-loaded MNs. There is also a need for a clearly defined quality threshold for skin insertion to guide MN development, as stated earlier. In addition to blending polymers to achieve robust skin insertion, several attempts have been proposed for adequate skin insertion, such as feedback systems included in the MN patch to assure the patient that sufficient force has been applied to the patch, as well as the use of an applicator that is attached to the MNs (38, 498). Studies have reported that an applicator provides a more efficient and consistent insertion of MNs into human skin than finger pressing but further work is required on the applicator design to ensure that its force does not result in pain (139, 499, 500). Moreover, a broader understanding of the suitable application method will be apparent when larger clinical trials than the current ones in the literature are conducted.

Academic researchers, pharmaceutical companies, regulatory authorities, and public health organisations are working together to address the barriers to MN commercialisation. A notable partnership is PATH's Center of Excellence which is an international multi-disciplinary partnership dedicated to accelerating the commercialisation of drug and vaccine containing MNs (501, 502). Progress is being made as the FDA recently provided regulatory information about MNs for cosmetic use (503) and further work is underway to accelerate the development of regulatory standards for drug and vaccine containing MNs (501).

In conclusion, while the barriers to MN commercialisation are being addressed, proof-of-concept studies like the studies done in this thesis are vital to maximise the potential of MNs and leverage their unique features to enhance the treatment of 'difficult-to-treat' diseases such as cutaneous leishmaniasis.

SUPPLEMENTARY DATA

This section describes preliminary experiments that were conducted but are less relevant to the main experimental chapters.

S1 MICRONEEDLE FABRICATION USING VACUUM

PVP 360 kDa MN fabrication was attempted using a vacuum oven based on methods in the literature (149). The polymer was dissolved in deionised water, as described in 2.2.2.2. The resulting gel was then poured into the custom-made mould from 2.2.2.1, followed by placing the mould in a vacuum oven (Figure S1), and drying at room temperature for 16 hours. However, despite adjustments to the protocol (Figure S1), bubbles were present in the mould, and the resulting MNs had thin needles and a thin backing layer, as well as grooves on the MNs from bubbles, and these suggest that the mould cavities were not completely filled (Figure S2), which in turn suggests that the fabrication method was not suitable for PVP 360 kDa likely due to the viscosity of PVP 360 kDa in water. It is worth noting that the only available vacuum oven was worn out, and this may have influenced the effectiveness of the process. So, centrifugation was used as described in Chapter 2.

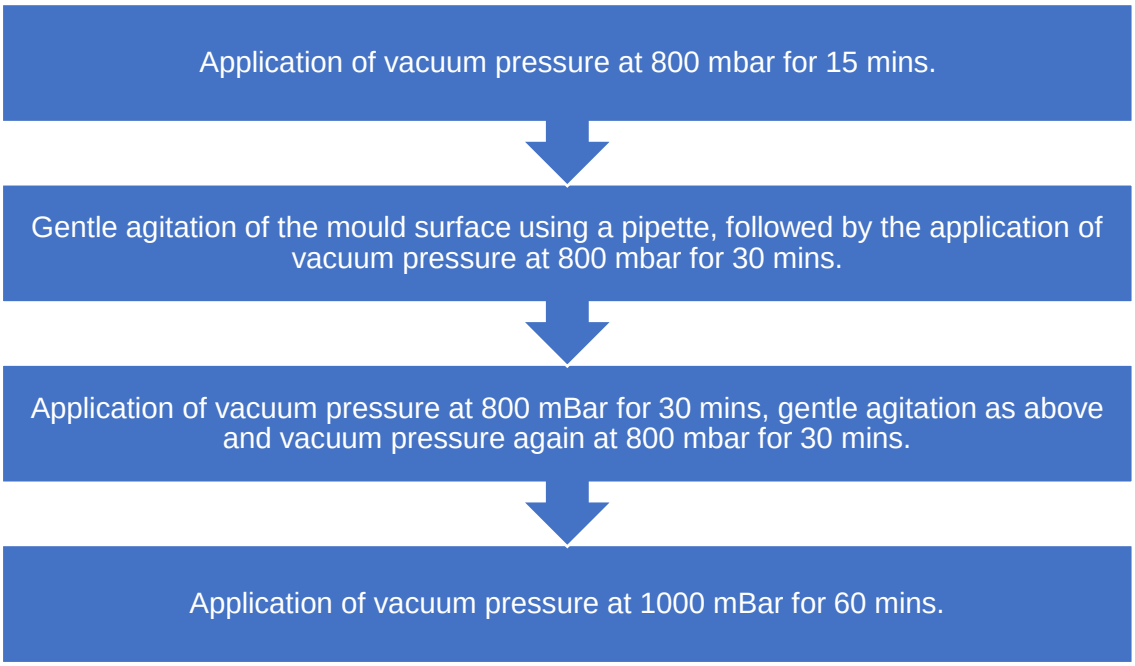

Figure S1 Variations in the protocol for fabricating PVP 360 kDa microneedles using a vacuum oven. The temperature was kept constant at 20°C.

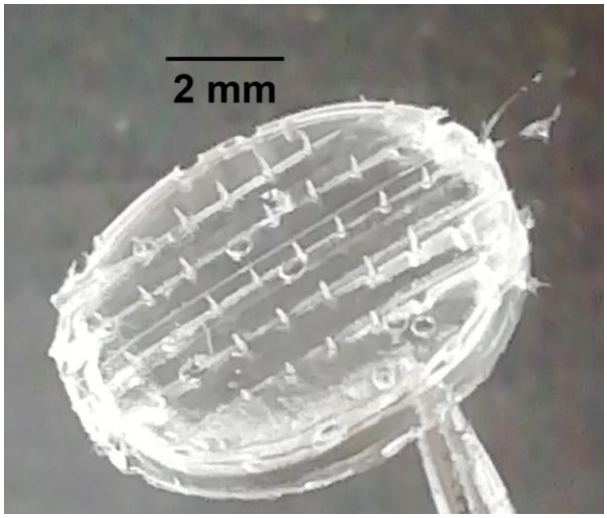

Figure S2 Microneedles containing grooves from bubbles and thin needles and a thin backing layer after fabrication using a vacuum oven. Image taken using a Samsung phone camera (Samsung, South Korea).

S2 SELECTION OF POLYMERS FOR THE BACKING LAYER

Table S1 shows the polymers that were tested to create the backing layers of MNs in this work using methods described in 2.2.2, as well as their respective outcomes. The polymer for the backing layers of the MNs in this work was kept constant so as to compare the polymers used in creating the needles. Although PVP and PVA blend gave a well-defined backing layer, PVP 360 kDa was selected to create the backing layers of the MNs to keep the number of excipients (polymers) used in the MNs to the minimum, as this may reduce the complexity of regulatory approval of the formulation, as described in chapter 4.

Table S1 Polymers which were tested to create the backing layers of the microneedles in this work.

Polymer	Rationale for use	Outcome
PVP 360 kDa	Commonly used in the literature to create MNs, as described in chapters 1 and 2.	Created a robust and well-defined backing layer, as shown in chapters 2 and 4.
PVA 31 kDa – 50 kDa (87-89% hydrolysed)	Commonly used in the literature to create MNs, as described in chapters 1 and 3.	Created a flexible backing layer which flattened upon insertion into 8 sheets of Parafilm M®.
PVP-PVA blend[a]	A common blend used in the literature to create MNs, as described in chapters 1 and 3.	Created a robust and well-defined backing layer.
PEOZ 50 kDa	To enable evaluation of PEOZ as a material for creating MNs	Created a fragile and brittle backing layer, which broke upon removal of the MNs from the mould (Figure S3).

[a] using the same molecular weights of PVP and PVA stated in the previous rows.

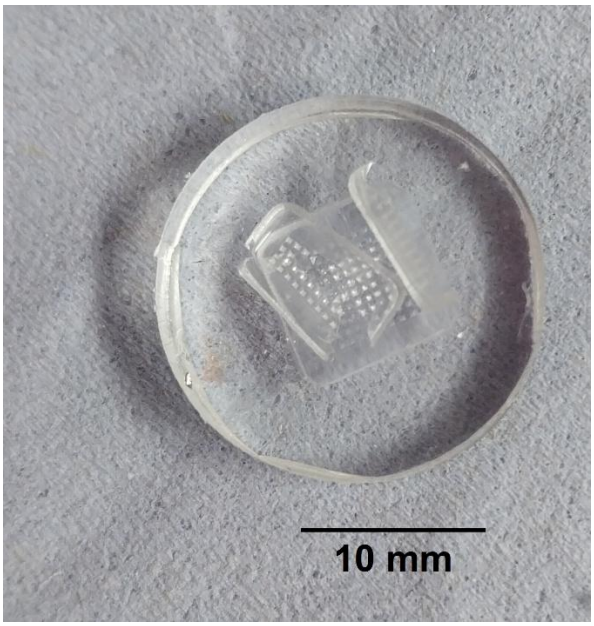

Figure S3 Commercial mould and microneedles with a backing layer made from PEOZ 50 kDa. Image taken using a Samsung phone camera (Samsung, South Korea).

REFERENCES

1. Brown M, Williams AC. The Art and Science of Dermal Formulation Development. 1st ed: CRC Press; 2019.

2. Smythe P, Wilkinson HN. The Skin Microbiome: Current Landscape and Future Opportunities. International Journal of Molecular Sciences. 2023;24(4):3950.

3. Menon GK. New insights into skin structure: scratching the surface. Advanced Drug Delivery Reviews. 2002;54:S3-S17.

4. Benítez JM, Montáns FJ. The mechanical behavior of skin: Structures and models for the finite element analysis. Computers & Structures. 2017;190:75-107.

5. Alkilani AZ, McCrudden MTC, Donnelly RF. Transdermal Drug Delivery: Innovative Pharmaceutical Developments Based on Disruption of the Barrier Properties of the Stratum Corneum. Pharmaceutics [Internet]. 2015; 7(4):[438-70 pp.].

6. Lai-Cheong JE, McGrath JA. Structure and function of skin, hair and nails. Medicine. 2017;45(6):347-51.

7. Van der Maaden K, Jiskoot W, Bouwstra J. Microneedle technologies for (trans)dermal drug and vaccine delivery. Journal of Controlled Release. 2012;161(2):645-55.

8. Bouwstra JA, Ponec M. The skin barrier in healthy and diseased state. Biochimica et Biophysica Acta (BBA) - Biomembranes. 2006;1758(12):2080-95.

9. Taylor K, Aulton M. Aulton's Pharmaceutics : the design and manufacture of medicines. 6th ed: Elsevier; 2021.

10. Van Smeden J, Janssens M, Gooris GS, Bouwstra JA. The important role of stratum corneum lipids for the cutaneous barrier function. Biochimica et Biophysica Acta (BBA) - Molecular and Cell Biology of Lipids. 2014;1841(3):295-313.

11. Baroni A, Buommino E, De Gregorio V, Ruocco E, Ruocco V, Wolf R. Structure and function of the epidermis related to barrier properties. Clinics in Dermatology. 2012;30(3):257-62.

12. Phatale V, Vaiphei KK, Jha S, Patil D, Agrawal M, Alexander A. Overcoming skin barriers through advanced transdermal drug delivery approaches. Journal of Controlled Release. 2022;351:361-80.

13. Wang R, Bian Q, Xu Y, Xu D, Gao J. Recent advances in mechanical force-assisted transdermal delivery of macromolecular drugs. International Journal of Pharmaceutics. 2021;602:120598.

14. Guillot AJ, Cordeiro AS, Donnelly RF, Montesinos MC, Garrigues TM, Melero A. Microneedle-Based Delivery: An Overview of Current Applications and Trends. Pharmaceutics. 2020;12(6).

15. Sabri AH, Cater Z, Gurnani P, Ogilvie J, Segal J, Scurr DJ, et al. Intradermal delivery of imiquimod using polymeric microneedles for basal cell carcinoma. International Journal of Pharmaceutics. 2020;589:119808.

16. Supe S, Takudage P. Methods for evaluating penetration of drug into the skin: A review. Skin Research and Technology. 2021;27(3):299-308.

17. Herbig ME, Evers D-H, Gorissen S, Köllmer M. Rational Design of Topical Semi-Solid Dosage Forms-How Far Are We? Pharmaceutics. 2023;15(7):1822.

18. Guy RH. Drug delivery to and through the skin. Drug Delivery and Translational Research. 2024;14(8):2032-40.

19. Van Bocxlaer K, Croft SL. Pharmacokinetics and pharmacodynamics in the treatment of cutaneous leishmaniasis – challenges and opportunities. RSC Medicinal Chemistry. 2021;12(4):472-82.

20. Paudel KS, Milewski M, Swadley CL, Brogden NK, Ghosh P, Stinchcomb AL. Challenges and Opportunities in dermal/transdermal Delivery. Therapeutic Delivery. 2010;1(1):109-31.

21. Münch S, Wohlrab J, Neubert RHH. Dermal and transdermal delivery of pharmaceutically relevant macromolecules. European Journal of Pharmaceutics and Biopharmaceutics. 2017;119:235-42.

22. Dragicevic N, Maibach H. Combined use of nanocarriers and physical methods for percutaneous penetration enhancement. Advanced Drug Delivery Reviews. 2018;127:58-84.

23. Maibach H, Dragicevic N. Percutaneous Penetration Enhancers Chemical Methods in Penetration Enhancement. 1st ed: Springer Berlin, Heidelberg; 2015.

24. Prausnitz MR, Langer R. Transdermal drug delivery. Nature Biotechnology. 2008;26(11):1261-8.

25. Nogueira IRL, Carneiro G, Yoshida MI, de Oliveira RB, Ferreira LAM. Preparation, characterization, and topical delivery of paromomycin ion pairing. Drug Development and Industrial Pharmacy. 2011;37(9):1083-9.

26. Miller MA, Pisani E. The cost of unsafe injections. Bull World Health Organ. 1999;77(10):808-11.

27. Roussel S, Udabe J, Bin Sabri A, Calderón M, Donnelly R. Leveraging novel innovative thermoresponsive polymers in microneedles for targeted intradermal deposition. International Journal of Pharmaceutics. 2024;652:123847.

28. Ita K. Transdermal iontophoretic drug delivery: advances and challenges. Journal of Drug Targeting. 2016;24(5):386-91.

29. De Sá FAP, Andrade JFM, Miranda TC, Cunha-Filho M, Gelfuso GM, Lapteva M, et al. Enhanced topical paromomycin delivery for cutaneous leishmaniasis treatment: Passive and iontophoretic approaches. International Journal of Pharmaceutics. 2023;648:123617.

30. Escobar-Chavez JJ, Bonilla-Martínez D, Villegas-González MA, Rodríguez-Cruz IM, Domínguez-Delgado CL. The Use of Sonophoresis in the Administration of Drugs Throughout the Skin. Journal of Pharmacy & Pharmaceutical Sciences. 2009;12(1):88-115.

31. Trimzi MA, Ham Y-B. A Needle-Free Jet Injection System for Controlled Release and Repeated Biopharmaceutical Delivery. Pharmaceutics. 2021;13(11):1770.

32. Mitragotri S. Current status and future prospects of needle-free liquid jet injectors. Nature Reviews Drug Discovery. 2006;5(7):543-8.

33. Heather AEB, Jeffrey EG, Yousuf M, Sarika N, Michael SR. Topical and Transdermal Drug Delivery: From Simple Potions to Smart Technologies. Current Drug Delivery. 2019;16(5):444-60.

34. Tobin KV, Fiegel J, Brogden NK. Thermosensitive Gels Used to Improve Microneedle-Assisted Transdermal Delivery of Naltrexone. Polymers. 2021;13(6):933.

35. Patel KK, Brogden NK. Impact of Formulation and Microneedle Length on Transdermal Metronidazole Permeation through Microneedle-Treated Skin. Pharmaceutical Research. 2024;41(2):355-63.

36. Kim Y-C, Park J-H, Prausnitz MR. Microneedles for drug and vaccine delivery. Advanced Drug Delivery Reviews. 2012;64(14):1547-68.

37. Prausnitz MR. Engineering Microneedle Patches for Vaccination and Drug Delivery to Skin. Annual Review of Chemical and Biomolecular Engineering. 2017;8(1):177-200.

38. Forster A, Junger M. Opportunities and challenges for commercializing microarray patches for vaccination from a MAP developer's perspective. Hum Vaccin Immunother. 2022;18(4):2050123.

39. Henry S, McAllister DV, Allen MG, Prausnitz MR. Microfabricated Microneedles: A Novel Approach to Transdermal Drug Delivery. Journal of Pharmaceutical Sciences. 1998;87(8):922-5.

40. Larrañeta E, Lutton REM, Woolfson AD, Donnelly RF. Microneedle arrays as transdermal and intradermal drug delivery systems: Materials science, manufacture and commercial development. Materials Science and Engineering: R: Reports. 2016;104:1-32.

41. Ingrole RSJ, Azizoglu E, Dul M, Birchall JC, Gill HS, Prausnitz MR. Trends of microneedle technology in the scientific literature, patents, clinical trials and internet activity. Biomaterials. 2021;267:120491.

42. Bal SM, Caussin J, Pavel S, Bouwstra JA. In vivo assessment of safety of microneedle arrays in human skin. European Journal of Pharmaceutical Sciences. 2008;35(3):193-202.

43. Arya J, Henry S, Kalluri H, McAllister DV, Pewin WP, Prausnitz MR. Tolerability, usability and acceptability of dissolving microneedle patch administration in human subjects. Biomaterials. 2017;128:1-7.

44. Gill HS, Denson DD, Burris BA, Prausnitz MR. Effect of microneedle design on pain in human volunteers. Clinical Journal of Pain. 2008;24(7):585-94.

45. Bajwa IK, Kaur N, Dsouza JM, Mathew JL. Evaluation of efficacy and safety of intradermal delivery of vaccines through microneedle(s) in human beings: a protocol for a systematic review. Systematic Reviews. 2022;11(1):170.

46. Donnelly RF, Prausnitz MR. The promise of microneedle technologies for drug delivery. Drug Delivery and Translational Research. 2024;14(3):573-80.

47. El-Sahn M, Elliott R, El-Sahn M, Lucas J, Wood Santos T. End-user research into understanding perceptions of and reactions to a microarray patch (MAP) for contraception among women in Ghana, Kenya and Uganda. Frontiers in Reproductive Health. 2024;6.

48. Birchall JC, Clemo R, Anstey A, John DN. Microneedles in Clinical Practice–An Exploratory Study Into the Opinions of Healthcare Professionals and the Public. Pharmaceutical Research. 2011;28(1):95-106.

49. Berger MN, Mowbray ES, Farag MWA, Mathieu E, Davies C, Thomas C, et al. Immunogenicity, safety, usability and acceptability of microarray patches for vaccination: a systematic review and meta-analysis. BMJ Global Health. 2023;8(10):e012247.

50. Li W, Li S, Fan X, Prausnitz MR. Microneedle patch designs to increase dose administered to human subjects. Journal of Controlled Release. 2021;339:350-60.

51. Zan P, Than A, Duong PK, Song J, Xu C, Chen P. Antimicrobial Microneedle Patch for Treating Deep Cutaneous Fungal Infection. Advanced Therapeutics. 2019;2(10):1900064.

52. Ziesmer J, Tajpara P, Hempel N-J, Ehrström M, Melican K, Eidsmo L, et al. Vancomycin-Loaded Microneedle Arrays against Methicillin-Resistant Staphylococcus Aureus Skin Infections. Advanced Materials Technologies. 2021;6(7):2001307.

53. Jamaledin R, Yiu CKY, Zare EN, Niu L-N, Vecchione R, Chen G, et al. Advances in Antimicrobial Microneedle Patches for Combating Infections. Advanced Materials. 2020;32(33):2002129.

54. Sabri AHB, Anjani QK, Gurnani P, Domínguez-Robles J, Moreno-Castellanos N, Zhao L, et al. Fabrication and characterisation of poly(sulfonated) and poly(sulfonic acid) dissolving microneedles for delivery of antibiotic and antifungal agents. International Journal of Pharmaceutics. 2023;644:123292.

55. Anjani QK, Sabri AHB, Hutton AJ, Cárcamo-Martínez Á, Wardoyo LAH, Mansoor AZ, et al. Microarray patches for managing infections at a global scale. Journal of Controlled Release. 2023;359:97-115.

56. Kordyl O, Styrna Z, Wojtyłko M, Michniak-Kohn B, Osmałek T. Microneedle-based arrays – Breakthrough strategy for the treatment of bacterial and fungal skin infections. Microbes and Infection. 2024:105426.

57. Waghule T, Singhvi G, Dubey SK, Pandey MM, Gupta G, Singh M, et al. Microneedles: A smart approach and increasing potential for transdermal drug delivery system. Biomedicine & Pharmacotherapy. 2019;109:1249-58.

58. Osborne J, Hutchinson P. The importance of accurate dosage of topical agents: a method of estimating involved area and application to calcipotriol treatment failures. Journal of the European Academy of Dermatology and Venereology. 2002;16(4):367-73.

59. Rzhevskiy AS, Singh TRR, Donnelly RF, Anissimov YG. Microneedles as the technique of drug delivery enhancement in diverse organs and tissues. Journal of Controlled Release. 2018;270:184-202.

60. Nalluri BN, Anusha SS, Bramhini SR, Amulya J, Sultana AS, Teja CU, et al. In Vitro Skin Permeation Enhancement of Sumatriptan by Microneedle Application. Curr Drug Deliv. 2015;12(6):761-9.

61. Ahmed KS, Shan X, Mao J, Qiu L, Chen J. Derma roller® microneedles-mediated transdermal delivery of doxorubicin and celecoxib co-loaded liposomes for enhancing the anticancer effect. Materials Science and Engineering: C. 2019;99:1448-58.

62. Fernández-García R, Statts L, de Jesus JA, Dea-Ayuela MA, Bautista L, Simão R, et al. Ultradeformable Lipid Vesicles Localize Amphotericin B in the Dermis for the Treatment of Infectious Skin Diseases. ACS Infectious Diseases. 2020;6(10):2647-60.

63. Gupta J, Gill HS, Andrews SN, Prausnitz MR. Kinetics of skin resealing after insertion of microneedles in human subjects. Journal of Controlled Release. 2011;154(2):148-55.

64. Ita K. Transdermal Delivery of Drugs with Microneedles-Potential and Challenges. Pharmaceutics. 2015;7(3):90-105.

65. Tucak A, Sirbubalo M, Hindija L, Rahić O, Hadžiabdić J, Muhamedagić K, et al. Microneedles: Characteristics, materials, production methods and commercial development. Micromachines. 2020;11(11).

66. Koutsonanos DG, Martin MdP, Zarnitsyn VG, Sullivan SP, Compans RW, Prausnitz MR, et al. Transdermal Influenza Immunization with Vaccine-Coated Microneedle Arrays. PLOS ONE. 2009;4(3):e4773.

67. Ryu HR, Jeong H-R, Seon-Woo H-S, Kim JS, Lee SK, Kim HJ, et al. Efficacy of a bleomycin microneedle patch for the treatment of warts. Drug Delivery and Translational Research. 2018;8(1):273-80.

68. Niu L, Chu LY, Burton SA, Hansen KJ, Panyam J. Intradermal delivery of vaccine nanoparticles using hollow microneedle array generates enhanced and balanced immune response. Journal of Controlled Release. 2019;294:268-78.

69. Griss P, Stemme G. Side-opened out-of-plane microneedles for microfluidic transdermal liquid transfer. Journal of Microelectromechanical Systems. 2003;12(3):296-301.

70. Martanto W, Moore JS, Kashlan O, Kamath R, Wang PM, O'Neal JM, et al. Microinfusion Using Hollow Microneedles. Pharmaceutical Research. 2006;23(1):104-13.

71. Martanto W, Moore JS, Couse T, Prausnitz MR. Mechanism of fluid infusion during microneedle insertion and retraction. Journal of Controlled Release. 2006;112(3):357-61.

72. NanoPass. Microneedle Platform [April 2024]. Available from: https://www.nanopass.com/technology/.

73. Jiang X, Lillehoj PB. Microneedle-based skin patch for blood-free rapid diagnostic testing. Microsystems & Nanoengineering. 2020;6(1):96.

74. Chen F, Yan Q, Yu Y, Wu MX. BCG vaccine powder-laden and dissolvable microneedle arrays for lesion-free vaccination. Journal of Controlled Release. 2017;255:36-44.

75. Kim S, Eum J, Yang H, Jung H. Transdermal finasteride delivery via powder-carrying microneedles with a diffusion enhancer to treat androgenetic alopecia. Journal of Controlled Release. 2019;316:1-11.

76. Kim S, Yang H, Eum J, Ma Y, Fakhraei Lahiji S, Jung H. Implantable powder-carrying microneedles for transdermal delivery of high-dose insulin with enhanced activity. Biomaterials. 2020;232:119733.

77. Cárcamo-Martínez Á, Mallon B, Anjani QK, Domínguez-Robles J, Utomo E, Vora LK, et al. Enhancing intradermal delivery of tofacitinib citrate: Comparison between powder-loaded hollow microneedle arrays and dissolving microneedle arrays. International Journal of Pharmaceutics. 2021;593:120152.

78. Li W, Tang J, Terry RN, Li S, Brunie A, Callahan RL, et al. Long-acting reversible contraception by effervescent microneedle patch. Science Advances. 2019;5(11):eaaw8145.

79. Zhu Z, Luo H, Lu W, Luan H, Wu Y, Luo J, et al. Rapidly Dissolvable Microneedle Patches for Transdermal Delivery of Exenatide. Pharmaceutical Research. 2014;31(12):3348-60.

80. Vora LK, Courtenay AJ, Tekko IA, Larrañeta E, Donnelly RF. Pullulan-based dissolving microneedle arrays for enhanced transdermal delivery of small and large biomolecules. International Journal of Biological Macromolecules. 2020;146:290-8.

81. Tas C, Joyce JC, Nguyen HX, Eangoor P, Knaack JS, Banga AK, et al. Dihydroergotamine mesylate-loaded dissolving microneedle patch made of polyvinylpyrrolidone for management of acute migraine therapy. Journal of Controlled Release. 2017;268:159-65.

82. McCrudden MTC, Alkilani AZ, McCrudden CM, McAlister E, McCarthy HO, Woolfson AD, et al. Design and physicochemical characterisation of novel dissolving polymeric microneedle arrays for transdermal delivery of high dose, low molecular weight drugs. Journal of Controlled Release. 2014;180:71-80.

83. Ramalheiro A, Paris JL, Silva BFB, Pires LR. Rapidly dissolving microneedles for the delivery of cubosome-like liquid crystalline nanoparticles with sustained release of rapamycin. International Journal of Pharmaceutics. 2020;591:119942.

84. Permana AD, Paredes AJ, Volpe-Zanutto F, Anjani QK, Utomo E, Donnelly RF. Dissolving microneedle-mediated dermal delivery of itraconazole nanocrystals for improved treatment of cutaneous candidiasis. European Journal of Pharmaceutics and Biopharmaceutics. 2020;154:50-61.

85. Chen W, Tian R, Xu C, Yung BC, Wang G, Liu Y, et al. Microneedle-array patches loaded with dual mineralized protein/peptide particles for type 2 diabetes therapy. Nature Communications. 2017;8(1):1777.

86. Eum J, Kim Y, Um DJ, Shin J, Yang H, Jung H. Solvent-Free Polycaprolactone Dissolving Microneedles Generated via the Thermal Melting Method for the Sustained Release of Capsaicin. Micromachines. 2021;12(2):167.

87. Fonseca DFS, Vilela C, Pinto RJB, Bastos V, Oliveira H, Catarino J, et al. Bacterial nanocellulose-hyaluronic acid microneedle patches for skin applications: In vitro and in vivo evaluation. Materials Science and Engineering: C. 2021;118:111350.

88. Hou A, Quan G, Yang B, Lu C, Chen M, Yang D, et al. Rational Design of Rapidly Separating Dissolving Microneedles for Precise Drug Delivery by Balancing the Mechanical Performance and Disintegration Rate. Advanced Healthcare Materials. 2019;8(21):1900898.

89. Ramöller IK, Tekko IA, McCarthy HO, Donnelly RF. Rapidly dissolving bilayer microneedle arrays – A minimally invasive transdermal drug delivery system for vitamin B12. International Journal of Pharmaceutics. 2019;566:299-306.

90. Lee JW, Park JH, Prausnitz MR. Dissolving microneedles for transdermal drug delivery. Biomaterials. 2008;29(13):2113-24.

91. Rabiei M, Kashanian S, Bahrami G, Derakhshankhah H, Barzegari E, Samavati SS, et al. Dissolving microneedle-assisted long-acting Liraglutide delivery to control type 2 diabetes and obesity. European Journal of Pharmaceutical Sciences. 2021;167:106040.

92. Azizoglu E, Ozer O, Prausnitz MR. Fabrication of pure-drug microneedles for delivery of montelukast sodium. Drug Delivery and Translational Research. 2022;12(2):444-58.

93. Donnelly RF, Singh TRR, Garland MJ, Migalska K, Majithiya R, McCrudden CM, et al. Hydrogel-Forming Microneedle Arrays for Enhanced Transdermal Drug Delivery. Advanced Functional Materials. 2012;22(23):4879-90.

94. Chang H, Zheng M, Yu X, Than A, Seeni RZ, Kang R, et al. A Swellable Microneedle Patch to Rapidly Extract Skin Interstitial Fluid for Timely Metabolic Analysis. Advanced Materials. 2017;29(37):1702243.

95. Donnelly RF, McCrudden MTC, Alkilani AZ, Larraneta E, McAlister E, Courtenay AJ, et al. Hydrogel-Forming Microneedles Prepared from "Super Swelling" Polymers Combined with Lyophilised Wafers for Transdermal Drug Delivery. Plos One. 2014;9(10).

96. Tekko IA, Chen G, Domínguez-Robles J, Thakur RRS, Hamdan IMN, Vora L, et al. Development and characterisation of novel poly (vinyl alcohol)/poly (vinyl pyrrolidone)-based hydrogel-forming microneedle arrays for enhanced and sustained transdermal delivery of methotrexate. International Journal of Pharmaceutics. 2020;586:119580.

97. Eltayib EM, Himawan A, Detamornrat U, Muhtadi WK, Li H, Li L, et al. Porous microneedle arrays as promising tools for the quantification of drugs in the skin: a proof of concept study. Pharmaceutical Development and Technology. 2024;29(3):164-75.

98. Bhatnagar S, Gadeela PR, Thathireddy P, Venuganti VVK. Microneedle-based drug delivery: materials of construction. Journal of Chemical Sciences. 2019;131(9).

99. Kolli CS, Banga AK. Characterization of solid maltose microneedles and their use for transdermal delivery. Pharmaceutical Research. 2008;25(1):104-13.

100. Wang PM, Cornwell M, Hill J, Prausnitz MR. Precise Microinjection into Skin Using Hollow Microneedles. Journal of Investigative Dermatology. 2006;126(5):1080-7.

101. Pradeep Narayanan S, Raghavan S. Fabrication and characterization of gold-coated solid silicon microneedles with improved biocompatibility. The International Journal of Advanced Manufacturing Technology. 2019;104(9):3327-33.

102. Zhao X, Coulman SA, Hanna SJ, Wong FS, Dayan CM, Birchall JC. Formulation of hydrophobic peptides for skin delivery via coated microneedles. Journal of Controlled Release. 2017;265:2-13.

103. Bystrova S, Luttge R. Micromolding for ceramic microneedle arrays. Microelectronic Engineering. 2011;88(8):1681-4.

104. Miyano T, Tobinaga Y, Kanno T, Matsuzaki Y, Takeda H, Wakui M, et al. Sugar Micro Needles as Transdermic Drug Delivery System. Biomedical Microdevices. 2005;7(3):185-8.

105. Donnelly RF, Morrow DIJ, Singh TRR, Migalska K, McCarron PA, O'Mahony C, et al. Processing difficulties and instability of carbohydrate microneedle arrays. Drug development and industrial pharmacy. 2009;35(10):1242-54.

106. Martin CJ, Allender CJ, Brain KR, Morrissey A, Birchall JC. Low temperature fabrication of biodegradable sugar glass microneedles for transdermal drug delivery applications. Journal of Controlled Release. 2012;158(1):93-101.

107. Loizidou EZ, Williams NA, Barrow DA, Eaton MJ, McCrory J, Evans SL, et al. Structural characterisation and transdermal delivery studies on sugar microneedles: Experimental and finite element modelling analyses. European Journal of Pharmaceutics and Biopharmaceutics. 2015;89:224-31.

108. Zhang Y, Jiang G, Yu W, Liu D, Xu B. Microneedles fabricated from alginate and maltose for transdermal delivery of insulin on diabetic rats. Materials Science and Engineering: C. 2018;85:18-26.

109. Pukfukdee P, Banlunara W, Rutwaree T, Limcharoen B, Sawutdeechaikul P, Pattarakankul T, et al. Solid Composite Material for Delivering Viable Cells into Skin Tissues via Detachable Dissolvable Microneedles. ACS Applied Bio Materials. 2020;3(7):4581-9.

110. Migdadi EM, Courtenay AJ, Tekko IA, McCrudden MTC, Kearney M-C, McAlister E, et al. Hydrogel-forming microneedles enhance transdermal delivery of metformin hydrochloride. Journal of Controlled Release. 2018;285:142-51.

111. Nguyen AK, Yang K-H, Bryant K, Li J, Joice AC, Werbovetz KA, et al. Microneedle-Based Delivery of Amphotericin B for Treatment of Cutaneous Leishmaniasis. Biomedical Microdevices. 2019;21(1):8.

112. Park SC, Kim MJ, Baek S-K, Park J-H, Choi S-O. Spray-Formed Layered Polymer Microneedles for Controlled Biphasic Drug Delivery. Polymers. 2019;11(2):369.

113. Kim JS, Choi J-a, Kim JC, Park H, Yang E, Park JS, et al. Microneedles with dual release pattern for improved immunological efficacy of Hepatitis B vaccine. International Journal of Pharmaceutics. 2020;591:119928.

114. Singh P, Carrier A, Chen Y, Lin S, Wang J, Cui S, et al. Polymeric microneedles for controlled transdermal drug delivery. Journal of Controlled Release. 2019;315:97-113.

115. Mao J, Wang H, Xie Y, Fu Y, Li Y, Liu P, et al. Transdermal delivery of rapamycin with poor water-solubility by dissolving polymeric microneedles for anti-angiogenesis. Journal of Materials Chemistry B. 2020;8(5):928-34.

116. Ronnander P, Simon L, Spilgies H, Koch A, Scherr S. Dissolving polyvinylpyrrolidone-based microneedle systems for in-vitro delivery of sumatriptan succinate. European Journal of Pharmaceutical Sciences. 2018;114:84-92.

117. Bhatnagar S, Bankar NG, Kulkarni MV, Venuganti VVK. Dissolvable microneedle patch containing doxorubicin and docetaxel is effective in 4T1 xenografted breast cancer mouse model. International Journal of Pharmaceutics. 2019;556:263-75.

118. Nguyen HX, Bozorg BD, Kim Y, Wieber A, Birk G, Lubda D, et al. Poly (vinyl alcohol) microneedles: Fabrication, characterization, and application for transdermal drug delivery of doxorubicin. European Journal of Pharmaceutics and Biopharmaceutics. 2018;129:88-103.

119. Koyani RD. Synthetic polymers for microneedle synthesis: From then to now. Journal of Drug Delivery Science and Technology. 2020;60:102071.

120. Lee IC, He J-S, Tsai M-T, Lin K-C. Fabrication of a novel partially dissolving polymer microneedle patch for transdermal drug delivery. Journal of Materials Chemistry B. 2015;3(2):276-85.

121. Saha I, Rai VK. Hyaluronic acid based microneedle array: Recent applications in drug delivery and cosmetology. Carbohydrate Polymers. 2021;267:118168.

122. Xu Q, Li X, Zhang P, Wang Y. Rapidly dissolving microneedle patch for synergistic gene and photothermal therapy of subcutaneous tumor. Journal of Materials Chemistry B. 2020;8(19):4331-9.

123. Chen M-C, Ling M-H, Lai K-Y, Pramudityo E. Chitosan Microneedle Patches for Sustained Transdermal Delivery of Macromolecules. Biomacromolecules. 2012;13(12):4022-31.

124. Wei H, Liu S, Tong Z, Chen T, Yang M, Guo Y, et al. Hydrogel-based microneedles of chitosan derivatives for drug delivery. Reactive and Functional Polymers. 2022;172:105200.

125. Zare MR, Khorram M, Barzegar S, Sarkari B, Asgari Q, Ahadian S, et al. Dissolvable carboxymethyl cellulose/polyvinylpyrrolidone microneedle arrays for transdermal delivery of Amphotericin B to treat cutaneous leishmaniasis. International Journal of Biological Macromolecules. 2021;182:1310-21.

126. Fonseca DFS, Costa PC, Almeida IF, Dias-Pereira P, Correia-Sá I, Bastos V, et al. Pullulan microneedle patches for the efficient transdermal administration of insulin envisioning diabetes treatment. Carbohydrate Polymers. 2020;241:116314.

127. Hutton ARJ, Quinn HL, McCague PJ, Jarrahian C, Rein-Weston A, Coffey PS, et al. Transdermal delivery of vitamin K using dissolving microneedles for the prevention of vitamin K deficiency bleeding. International Journal of Pharmaceutics. 2018;541(1):56-63.

128. Moore LE, Vucen S, Moore AC. Trends in drug- and vaccine-based dissolvable microneedle materials and methods of fabrication. European Journal of Pharmaceutics and Biopharmaceutics. 2022;173:54-72.

129. Pamornpathomkul B, Ngawhirunpat T, Tekko IA, Vora L, McCarthy HO, Donnelly RF. Dissolving polymeric microneedle arrays for enhanced site-specific acyclovir delivery. European Journal of Pharmaceutical Sciences. 2018;121:200-9.

130. Bhatnagar S, Kumari P, Pattarabhiran SP, Venuganti VVK. Zein Microneedles for Localized Delivery of Chemotherapeutic Agents to Treat Breast Cancer: Drug Loading, Release Behavior, and Skin Permeation Studies. AAPS PharmSciTech. 2018;19(4):1818-26.

131. Bhatnagar S, Chawla SR, Kulkarni OP, Venuganti VVK. Zein Microneedles for Transcutaneous Vaccine Delivery: Fabrication, Characterization, and in Vivo Evaluation Using Ovalbumin as the Model Antigen. ACS Omega. 2017;2(4):1321-32.

132. Zhao X, Zhang S, Yang G, Zhou Z, Gao Y. Exploring Trehalose on the Release of Levonorgestrel from Implantable PLGA Microneedles. Polymers. 2020;12(1):59.

133. Ng KW, Lau WM, Williams AC. Towards pain-free diagnosis of skin diseases through multiplexed microneedles: biomarker extraction and detection using a highly sensitive blotting method. Drug Delivery and Translational Research. 2015;5(4):387-96.

134. Li QY, Zhang JN, Chen BZ, Wang QL, Guo XD. A solid polymer microneedle patch pretreatment enhances the permeation of drug molecules into the skin. RSC Advances. 2017;7(25):15408-15.

135. Gittard SD, Chen B, Xu H, Ovsianikov A, Chichkov BN, Monteiro-Riviere NA, et al. The effects of geometry on skin penetration and failure of polymer microneedles. Journal of Adhesion Science and Technology. 2013;27(3):227-43.

136. Mishra R, Maiti TK, Bhattacharyya TK. Development of SU-8 hollow microneedles on a silicon substrate with microfluidic interconnects for transdermal drug delivery. Journal of Micromechanics and Microengineering. 2018;28(10):105017.

137. Zhu M, Liu Y, Jiang F, Cao J, Kundu SC, Lu S. Combined Silk Fibroin Microneedles for Insulin Delivery. ACS Biomaterials Science & Engineering. 2020;6(6):3422-9.

138. Wang M, Hu L, Xu C. Recent advances in the design of polymeric microneedles for transdermal drug delivery and biosensing. Lab on a Chip. 2017;17(8):1373-87.

139. Xiu X, Gao G, Liu Y, Ma F. Drug delivery with dissolving microneedles: skin puncture, its influencing factors and improvement strategies. Journal of Drug Delivery Science and Technology. 2022;76:103653.

140. Zhang X, Zhou C, Chen T, Jiang Z, Lu C, Wu C, et al. State-of-the-art strategies to enhance the mechanical properties of microneedles. International Journal of Pharmaceutics. 2024;663:124547.

141. Makvandi P, Kirkby M, Hutton ARJ, Shabani M, Yiu CKY, Baghbantaraghdari Z, et al. Engineering Microneedle Patches for Improved Penetration: Analysis, Skin Models and Factors Affecting Needle Insertion. Nano-Micro Letters. 2021;13(1):93.

142. He J, Zhang Z, Zheng X, Li L, Qi J, Wu W, et al. Design and Evaluation of Dissolving Microneedles for Enhanced Dermal Delivery of Propranolol Hydrochloride. Pharmaceutics. 2021;13(4):579.

143. Economidou SN, Pissinato Pere CP, Okereke M, Douroumis D. Optimisation of Design and Manufacturing Parameters of 3D Printed Solid Microneedles for Improved Strength, Sharpness, and Drug Delivery. Micromachines. 2021;12(2):117.

144. Zhan H, Ma F, Huang Y, Zhang J, Jiang X, Qian Y. Application of composite dissolving microneedles with high drug loading ratio for rapid local anesthesia. European Journal of Pharmaceutical Sciences. 2018;121:330-7.

145. Permana AD, Paredes AJ, Zanutto FV, Amir MN, Ismail I, Bahar MA, et al. Albendazole Nanocrystal-Based Dissolving Microneedles with Improved Pharmacokinetic Performance for Enhanced Treatment of Cystic Echinococcosis. ACS Applied Materials & Interfaces. 2021;13(32):38745-60.

146. González-Vázquez P, Larrañeta E, McCrudden MTC, Jarrahian C, Rein-Weston A, Quintanar-Solares M, et al. Transdermal delivery of gentamicin using dissolving microneedle arrays for potential treatment of neonatal sepsis. Journal of Controlled Release. 2017;265:30-40.

147. Turner JG, White LR, Estrela P, Leese HS. Hydrogel-Forming Microneedles: Current Advancements and Future Trends. Macromolecular Bioscience. 2020:2000307.

148. Teodorescu M, Bercea M. Poly(vinylpyrrolidone) – A Versatile Polymer for Biomedical and Beyond Medical Applications. Polymer-Plastics Technology and Engineering. 2015;54(9):923-43.

149. Dillon C, Hughes H, O'Reilly NJ, McLoughlin P. Formulation and characterisation of dissolving microneedles for the transdermal delivery of therapeutic peptides. International Journal of Pharmaceutics. 2017;526(1):125-36.

150. Sullivan SP, Murthy N, Prausnitz MR. Minimally Invasive Protein Delivery with Rapidly Dissolving Polymer Microneedles. Advanced Materials. 2008;20(5):933-8.

151. Lee IC, Wu Y-C, Tsai S-W, Chen C-H, Wu M-H. Fabrication of two-layer dissolving polyvinylpyrrolidone microneedles with different molecular weights for in vivo insulin transdermal delivery. RSC Advances. 2017;7(9):5067-75.

152. Fonseca DFS, Vilela C, Silvestre AJD, Freire CSR. A compendium of current developments on polysaccharide and protein-based microneedles. International Journal of Biological Macromolecules. 2019;136:704-28.

153. Kang N-W, Kim S, Lee J-Y, Kim K-T, Choi Y, Oh Y, et al. Microneedles for drug delivery: recent advances in materials and geometry for preclinical and clinical studies. Expert Opinion on Drug Delivery. 2020:null-null.

154. Robeson L. Historical Perspective of Advances in the Science and Technology of Polymer Blends. Polymers. 2014;6(5):1251-65.

155. Hoogenboom R. Poly(2-oxazoline)s: A Polymer Class with Numerous Potential Applications. Angewandte Chemie International Edition. 2009;48(43):7978-94.

156. Oleszko-Torbus N, Utrata-Wesołek A, Bochenek M, Lipowska-Kur D, Dworak A, Wałach W. Thermal and crystalline properties of poly(2-oxazoline)s. Polymer Chemistry. 2020;11(1):15-33.

157. Yang L, Wang F, Ren P, Zhang T, Zhang Q. Poly(2-oxazoline)s: synthesis and biomedical applications. Macromolecular Research. 2023;31(5):413-26.

158. Johnson J. Ethicon Introduces ETHIZIA Hemostatic Sealing Patch, Clinically Proven to Stop Disruptive Bleeding 2023 [March 2024]. Available from: https://www.jnj.com/media-center/press-releases/ethicon-introduces-ethiziatm-hemostatic-sealing-patch-clinically-proven-to-stop-disruptive-bleeding.

159. Glassner M, Vergaelen M, Hoogenboom R. Poly(2-oxazoline)s: A comprehensive overview of polymer structures and their physical properties. Polymer International. 2018;67(1):32-45.

160. Jana S, Hoogenboom R. Poly(2-oxazoline)s: a comprehensive overview of polymer structures and their physical properties—an update. Polymer International. 2022;71(8):935-49.

161. Claeys B, Vervaeck A, Vervaet C, Remon JP, Hoogenboom R, De Geest BG. Poly(2-ethyl-2-oxazoline) as Matrix Excipient for Drug Formulation by Hot Melt Extrusion and Injection Molding. Macromolecular Rapid Communications. 2012;33(19):1701-7.

162. Viegas TX, Bentley MD, Harris JM, Fang Z, Yoon K, Dizman B, et al. Polyoxazoline: Chemistry, Properties, and Applications in Drug Delivery. Bioconjugate Chemistry. 2011;22(5):976-86.

163. Abilova GK, Kaldybekov DB, Ozhmukhametova EK, Saimova AZ, Kazybayeva DS, Irmukhametova GS, et al. Chitosan/poly(2-ethyl-2-oxazoline) films for ocular drug delivery: Formulation, miscibility, in vitro and in vivo studies. European Polymer Journal. 2019;116:311-20.

164. Mero A, Pasut G, Via LD, Fijten MWM, Schubert US, Hoogenboom R, et al. Synthesis and characterization of poly(2-ethyl 2-oxazoline)-conjugates with proteins and drugs: Suitable alternatives to PEG-conjugates? Journal of Controlled Release. 2008;125(2):87-95.

165. Sedlacek O, Monnery BD, Mattova J, Kucka J, Panek J, Janouskova O, et al. Poly(2-ethyl-2-oxazoline) conjugates with doxorubicin for cancer therapy: In vitro and

in vivo evaluation and direct comparison to poly[N-(2-hydroxypropyl)methacrylamide] analogues. Biomaterials. 2017;146:1-12.

166. Storti G, Romano G, Gilmore K, Sadowski N, Tiiara A, Luzinov I, et al. Permeability of Skin-Mimicking Cell Coatings by Polymers of Complex Architecture Based on Polyoxazolines. Coatings. 2023;13(6):1007.

167. Simon L, Lapinte V, Lionnard L, Marcotte N, Morille M, Aouacheria A, et al. Polyoxazolines based lipid nanocapsules for topical delivery of antioxidants. International Journal of Pharmaceutics. 2020;579:119126.

168. Trachsel L, Zenobi-Wong M, Benetti EM. The role of poly(2-alkyl-2-oxazoline)s in hydrogels and biofabrication. Biomaterials Science. 2021;9(8):2874-86.

169. Mansfield EDH, Sillence K, Hole P, Williams AC, Khutoryanskiy VV. POZylation: a new approach to enhance nanoparticle diffusion through mucosal barriers. Nanoscale. 2015;7(32):13671-9.

170. Boel E, Smeets A, Vergaelen M, De la Rosa VR, Hoogenboom R, Van den Mooter G. Comparative study of the potential of poly(2-ethyl-2-oxazoline) as carrier in the formulation of amorphous solid dispersions of poorly soluble drugs. European Journal of Pharmaceutics and Biopharmaceutics. 2019;144:79-90.

171. Jiang W, Zhou M, Chen S, Xie J, Chen M, Zhang H, et al. Peptide-Mimicking Poly(2-oxazoline)s Possessing Potent Antifungal Activity and BBB Penetrating Property to Treat Invasive Infections and Meningitis. Journal of the American Chemical Society. 2023;145(47):25753-65.

172. Zhang Y, Li X, Wei B. Environment-Friendly Poly(2-ethyl-2-oxazoline) as an Innovative Consolidant for Ancient Wall Paintings. Nanomaterials. 2018;8(9):649.

173. ClinicalTrials.gov. A Study of Weekly Subcutaneous Injections of SER-214 in Subjects With Parkinson's Disease (PD), to Determine the Safety, Tolerability and Pharmacokinetic (PK) Profile of SER-214 2015 [March 2024]. Available from: https://clinicaltrials.gov/study/NCT02579473.

174. Pan T, Li J, Wang W, inventors; Univ China Pharm (Uycp-C), assignee. Drug delivery system useful for preparation of medicine for preventing and/or treating tumor, comprises pH-sensitive nano drug delivery system coupled with nitric oxide donor and tumor vaccine nanoparticles loaded on microneedle patent CN115581660-A; CN115581660-B.

175. Ross S, Scoutaris N, Lamprou D, Mallinson D, Douroumis D. Inkjet printing of insulin microneedles for transdermal delivery. Drug Delivery and Translational Research. 2015;5(4):451-61.

176. Hirobe S, Azukizawa H, Hanafusa T, Matsuo K, Quan Y-S, Kamiyama F, et al. Clinical study and stability assessment of a novel transcutaneous influenza vaccination using a dissolving microneedle patch. Biomaterials. 2015;57:50-8.

177. Vander Straeten A, Sarmadi M, Daristotle JL, Kanelli M, Tostanoski LH, Collins J, et al. A microneedle vaccine printer for thermostable COVID-19 mRNA vaccines. Nature Biotechnology. 2024;42(3):510-7.

178. Mistilis MJ, Bommarius AS, Prausnitz MR. Development of a Thermostable Microneedle Patch for Influenza Vaccination. Journal of Pharmaceutical Sciences. 2015;104(2):740-9.

179. Gavi TVA. Vaccine Innovation Prioritisation Strategy (VIPS) [April 2024]. Available from: https://www.gavi.org/our-alliance/market-shaping/vaccine-innovation-prioritisation-strategy.

180. Vaxxas Announces and Publishes Successful Phase I Clinical Trial for Measles and Rubella Vaccine Delivered Using its Proprietary High-Density Microarray Skin Patch; Plan for Phase I/II Trial in The Gambia, Africa November 2023 [March 2024]. Available from: https://www.businesswire.com/news/home/20231126169373/en/Vaxxas-Announces-and-Publishes-Successful-Phase-I-Clinical-Trial-for-Measles-and-Rubella-Vaccine-Delivered-Using-its-Proprietary-High-Density-Microarray-Skin-Patch-Plan-for-Phase-III-Trial-in-The-Gambia-Africa.

181. Vaxxas. VAXXAS awarded US$3.67 million (AU$5.4 million) from global charitable foundation, WELLCOME, for human clinical study of typhoid vaccination using needle-free vaccine patch 2023 [March 2024]. Available from: https://www.vaxxas.com/news/articles/vaxxas-awarded-usd3.67-million-aud5.4-million-from-global-charitable-foundation-wellcome-for-human-clinical-study-of-typhoid-vaccination-using-needle-free-vaccine-patch/.

182. Hiraishi Y, Nakagawa T, Quan Y-S, Kamiyama F, Hirobe S, Okada N, et al. Performance and characteristics evaluation of a sodium hyaluronate-based microneedle patch for a transcutaneous drug delivery system. International Journal of Pharmaceutics. 2013;441(1):570-9.

183. Lee KJ, Jeong SS, Roh DH, Kim DY, Choi H-K, Lee EH. A practical guide to the development of microneedle systems – In clinical trials or on the market. International Journal of Pharmaceutics. 2020;573:118778.

184. Dsouza L, Ghate VM, Lewis SA. Derma rollers in therapy: the transition from cosmetics to transdermal drug delivery. Biomedical Microdevices. 2020;22(4):77.

185. Kim M, Yang H, Kim H, Jung H, Jung H. Novel cosmetic patches for wrinkle improvement: retinyl retinoate- and ascorbic acid-loaded dissolving microneedles. International Journal of Cosmetic Science. 2014;36(3):207-12.

186. Yin M, Zeng Y, Liu H-Q, Zhang W, Wang C, Chen C, et al. Dissolving Microneedle Patch Integrated with Microspheres for Long-Acting Hair Regrowth Therapy. ACS Applied Materials & Interfaces. 2023;15(14):17532-42.

187. Aldawood FK, Andar A, Desai S. A Comprehensive Review of Microneedles: Types, Materials, Processes, Characterizations and Applications. Polymers. 2021;13(16):2815.

188. Zhang BL, Yang Y, Zhao ZQ, Guo XD. A gold nanoparticles deposited polymer microneedle enzymatic biosensor for glucose sensing. Electrochimica Acta. 2020;358:136917.

189. Dixon RV, Skaria E, Lau WM, Manning P, Birch-Machin MA, Moghimi SM, et al. Microneedle-based devices for point-of-care infectious disease diagnostics. Acta Pharmaceutica Sinica B. 2021;11(8):2344-61.

190. Erdem Ö, Eş I, Akceoglu GA, Saylan Y, Inci F. Recent Advances in Microneedle-Based Sensors for Sampling, Diagnosis and Monitoring of Chronic Diseases. Biosensors. 2021;11(9):296.

191. Kim Y, Lewis MB, Hwang J, Wang Z, Gupta R, Liu Y, et al. Microneedle patch-based enzyme-linked immunosorbent assay to quantify protein biomarkers of tuberculosis. Biomedical Microdevices. 2024;26(1):15.

192. Gowers SAN, Freeman DME, Rawson TM, Rogers ML, Wilson RC, Holmes AH, et al. Development of a Minimally Invasive Microneedle-Based Sensor for Continuous Monitoring of β-Lactam Antibiotic Concentrations in Vivo. ACS Sensors. 2019;4(4):1072-80.

193. Lee JW, Prausnitz MR. Drug delivery using microneedle patches: not just for skin. Expert Opinion on Drug Delivery. 2018;15(6):541-3.

194. eBioMedicine. Leishmania: an urgent need for new treatments. eBioMedicine. 2023;87.

195. Sangshetti JN, Kalam Khan FA, Kulkarni AA, Arote R, Patil RH. Antileishmanial drug discovery: comprehensive review of the last 10 years. RSC Advances. 2015;5(41):32376-415.

196. Burza S, Croft SL, Boelaert M. Leishmaniasis. The Lancet. 2018;392(10151):951-70.

197. Mann S, Frasca K, Scherrer S, Henao-Martínez AF, Newman S, Ramanan P, et al. A Review of Leishmaniasis: Current Knowledge and Future Directions. Current Tropical Medicine Reports. 2021;8(2):121-32.

198. Sasidharan S, Saudagar P. Leishmaniasis: where are we and where are we heading? Parasitology Research. 2021;120(5):1541-54.

199. Alvar J, Arana B. Leishmaniasis, Impact and Therapeutic Needs. In: Rivas L, Gil C, editors. Drug Discovery for Leishmaniasis: The Royal Society of Chemistry; 2017.

200. Organization WH. Leishmaniasis Fact Sheet [March 2024]. Available from: https://www.who.int/news-room/fact-sheets/detail/leishmaniasis.

201. Curtin JM, Aronson NE. Leishmaniasis in the United States: Emerging Issues in a Region of Low Endemicity. Microorganisms. 2021;9(3):578.

202. Garnier T, Croft SL. Topical treatment for cutaneous leishmaniasis. Curr Opin Investig Drugs. 2002;3(4):538-44.

203. World Health Organization. Report of a meeting of the WHO Expert Committee on the Control of Leishmaniases, Geneva. 2010.

204. Caridha D, Vesely B, van Bocxlaer K, Arana B, Mowbray CE, Rafati S, et al. Route map for the discovery and pre-clinical development of new drugs and treatments for cutaneous leishmaniasis. International Journal for Parasitology: Drugs and Drug Resistance. 2019;11:106-17.

205. Organization WH. Status of endemicity of cutaneous leishmaniasis 2022 2023 [March 2024]. Available from: https://apps.who.int/neglected_diseases/ntddata/leishmaniasis/leishmaniasis.html.

206. Abdoli A, Maspi N, Ghaffarifar F. Wound healing in cutaneous leishmaniasis: A double edged sword of IL-10 and TGF-β. Comparative Immunology, Microbiology and Infectious Diseases. 2017;51:15-26.

207. Bailey MS, Lockwood DNJ. Cutaneous leishmaniasis. Clinics in Dermatology. 2007;25(2):203-11.

208. Serarslan G, Ekiz Ö, Özer C, Sarıkaya G. Dermoscopy in the Diagnosis of Cutaneous Leishmaniasis. Dermatol Pract Concept. 2019;9(2):111-8.

209. Sharquie KE, Hameed AF, Noaimi AA. Panniculitis is a common unrecognized histopathological feature of cutaneous leishmaniasis. Indian Journal of Pathology and Microbiology. 2016;59(1):16-9.

210. Wijesinghe H, Gunathilaka N, Semege S, Pathirana N, Manamperi N, de Silva C, et al. Histopathology of Cutaneous Leishmaniasis Caused by Leishmania donovani in Sri Lanka. Biomed Res Int. 2020;2020:4926819.

211. (DNDi) DfNDi. Cutaneous Leishmaniasis 2023 [March 2024]. Available from: https://dndi.org/diseases/cutaneous-leishmaniasis/facts/.

212. Bennis I, Thys S, Filali H, De Brouwere V, Sahibi H, Boelaert M. Psychosocial impact of scars due to cutaneous leishmaniasis on high school students in Errachidia province, Morocco. Infectious Diseases of Poverty. 2017;6(1):46.

213. Bailey F, Mondragon-Shem K, Haines LR, Olabi A, Alorfi A, Ruiz-Postigo JA, et al. Cutaneous leishmaniasis and co-morbid major depressive disorder: A systematic review with burden estimates. PLOS Neglected Tropical Diseases. 2019;13(2):e0007092.

214. Bennis I, De Brouwere V, Belrhiti Z, Sahibi H, Boelaert M. Psychosocial burden of localised cutaneous Leishmaniasis: a scoping review. BMC Public Health. 2018;18(1):358.

215. Garza-Tovar TF, Sacriste-Hernández MI, Juárez-Durán ER, Arenas R. An overview of the treatment of cutaneous leishmaniasis. Fac Rev. 2020;9:28.

216. Moreno E, Calvo A, Schwartz J, Navarro-Blasco I, González-Peñas E, Sanmartín C, et al. Evaluation of Skin Permeation and Retention of Topical Dapsone in Murine Cutaneous Leishmaniasis Lesions. Pharmaceutics. 2019;11(11):607.

217. Schwartz J, Moreno E, Fernández C, Navarro-Blasco I, Nguewa PA, Palop JA, et al. Topical treatment of L. major infected BALB/c mice with a novel diselenide chitosan hydrogel formulation. European Journal of Pharmaceutical Sciences. 2014;62:309-16.

218. Van Bocxlaer K, McArthur K-N, Harris A, Alavijeh M, Braillard S, Mowbray CE, et al. Film-Forming Systems for the Delivery of DNDI-0690 to Treat Cutaneous Leishmaniasis. Pharmaceutics. 2021;13(4):516.

219. Erber AC, Arana B, Ben Salah A, Bennis I, Boukthir A, Castro Noriega MdM, et al. Patients' preferences of cutaneous leishmaniasis treatment outcomes: Findings from an international qualitative study. PLOS Neglected Tropical Diseases. 2020;14(2):e0007996.

220. Grifferty G, Shirley H, McGloin J, Kahn J, Orriols A, Wamai R. Vulnerabilities to and the Socioeconomic and Psychosocial Impacts of the Leishmaniases: A Review. Res Rep Trop Med. 2021;12:135-51.

221. Bautista-Gomez MM, Doerfler J, Del Mar Castro M. Barriers to cutaneous leishmaniasis care faced by indigenous communities of rural areas in Colombia: a qualitative study. BMC Infect Dis. 2022;22(1):302.

222. Boukthir A, Bettaieb J, Erber AC, Bouguerra H, Mallekh R, Naouar I, et al. Psycho-social impacts, experiences and perspectives of patients with Cutaneous Leishmaniasis regarding treatment options and case management: An exploratory qualitative study in Tunisia. PLOS ONE. 2020;15(12):e0242494.

223. López L, Valencia B, Alvarez F, Ramos AP, Llanos-Cuentas A, Echevarria J, et al. A phase II multicenter randomized study to evaluate the safety and efficacy of combining thermotherapy and a short course of miltefosine for the treatment of uncomplicated cutaneous leishmaniasis in the New World. PLOS Neglected Tropical Diseases. 2022;16(3):e0010238.

224. (DNDi) DfNDi. Target product profile for cutaneous leishmaniasis [April 2024]. Available from: https://dndi.org/diseases/cutaneous-leishmaniasis/target-product-profile/.

225. López L, Vélez I, Asela C, Cruz C, Alves F, Robledo S, et al. A phase II study to evaluate the safety and efficacy of topical 3% amphotericin B cream (Anfoleish) for the treatment of uncomplicated cutaneous leishmaniasis in Colombia. PLoS neglected tropical diseases. 2018;12(7):e0006653.

226. Ibrahim AA, El-Housseiny GS, Aboshanab KM, Yassien MA, Hassouna NA. Paromomycin production from Streptomyces rimosus NRRL 2455: statistical

optimization and new synergistic antibiotic combinations against multidrug resistant pathogens. BMC Microbiol. 2019;19(1):18.

227. Davidson RN, den Boer M, Ritmeijer K. Paromomycin. Transactions of The Royal Society of Tropical Medicine and Hygiene. 2009;103(7):653-60.

228. Farouk F, Azzazy HME, Niessen WMA. Challenges in the determination of aminoglycoside antibiotics, a review. Analytica Chimica Acta. 2015;890:21-43.

229. Serio AW, Keepers T, Andrews L, Krause KM. Aminoglycoside Revival: Review of a Historically Important Class of Antimicrobials Undergoing Rejuvenation. EcoSal Plus. 2018;8(1):10.1128/ecosalplus.ESP-0002-2018.

230. Matos APS, Viçosa AL, Ré MI, Ricci-Júnior E, Holandino C. A review of current treatments strategies based on paromomycin for leishmaniasis. Journal of Drug Delivery Science and Technology. 2020;57:101664.

231. Maarouf M, Lawrence F, Croft SL, Robert-Gero M. Ribosomes of Leishmania are a target for the aminoglycosides. Parasitology Research. 1995;81(5):421-5.

232. Fernández MM, Malchiodi EL, Algranati ID. Differential effects of paromomycin on ribosomes of Leishmania mexicana and mammalian cells. Antimicrob Agents Chemother. 2011;55(1):86-93.

233. Maarouf M, De Kouchkovsky Y, Brown S, Petit PX, Robert-Gero M. In Vivo Interference of Paromomycin with Mitochondrial Activity of Leishmania. Experimental Cell Research. 1997;232(2):339-48.

234. Shalev M, Rozenberg H, Smolkin B, Nasereddin A, Kopelyanskiy D, Belakhov V, et al. Structural basis for selective targeting of leishmanial ribosomes: aminoglycoside derivatives as promising therapeutics. Nucleic Acids Research. 2015;43(17):8601-13.

235. Pokharel P, Ghimire R, Lamichhane P. Efficacy and Safety of Paromomycin for Visceral Leishmaniasis: A Systematic Review. Journal of Tropical Medicine. 2021;2021(1):8629039.

236. Aronson N, Herwaldt BL, Libman M, Pearson R, Lopez-Velez R, Weina P, et al. Diagnosis and Treatment of Leishmaniasis: Clinical Practice Guidelines by the Infectious Diseases Society of America (IDSA) and the American Society of Tropical Medicine and Hygiene (ASTMH). Clinical Infectious Diseases. 2016;63(12):1539-57.

237. El-On J, Jacobs GP, Witztum E, Greenblatt CL. Development of topical treatment for cutaneous leishmaniasis caused by Leishmania major in experimental animals. Antimicrobial Agents and Chemotherapy. 1984;26(5):745-51.

238. El-On J, Halevy S, Grunwald MH, Weinrauch L. Topical treatment of Old World cutaneous leishmaniasis caused by Leishmania major: A double-blind control study. Journal of the American Academy of Dermatology. 1992;27(2):227-31.

239. Arana BA, Mendoza CE, Rizzo NR, Kroeger A. Randomized, controlled, double-blind trial of topical treatment of cutaneous leishmaniasis with paromomycin plus methylbenzethonium chloride ointment in Guatemala. The American journal of tropical medicine and hygiene Am J Trop Med Hyg Am J Trop Med Hyg. 2001;65(5):466-70.

240. Krause G, Kroeger A. Topical treatment of American cutaneous leishmaniasis with paramomycin and methylbenzethonium chloride: a clinical study under field conditions in Ecuador. Transactions of The Royal Society of Tropical Medicine and Hygiene. 1994;88(1):92-4.

241. Ozgoztasi O, Baydar I. A randomized clinical trial of topical paromomycin versus oral ketoconazole for treating cutaneous leishmaniasis in Turkey. International Journal of Dermatology. 1997;36(1):61-3.

242. Asilian A, Jalayer T, Nilforooshzadeh M, Ghassemi RL, Peto R, Wayling S, et al. Treatment of cutaneous leishmaniasis with aminosidine (paromomycin) ointment: double-blind, randomized trial in the Islamic Republic of Iran. Bull World Health Organ. 2003;81(5):353-9.

243. Soto J, Fuya P, Herrera R, Berman J. Topical Paromomycin/Methylbenzethonium Chloride Plus Parenteral Meglumine Antimonate as Treatment for American Cutaneous Leishmaniasis: Controlled Study. Clinical Infectious Diseases. 1998;26(1):56-8.

244. Iddawela D, Vithana SMP, Atapattu D, Wijekoon L. Clinical and epidemiological characteristics of cutaneous leishmaniasis in Sri Lanka. BMC Infect Dis. 2018;18(1):108.

245. Kim DH, Chung HJ, Bleys J, Ghohestani RF. Is Paromomycin an Effective and Safe Treatment against Cutaneous Leishmaniasis? A Meta-Analysis of 14 Randomized Controlled Trials. PLOS Neglected Tropical Diseases. 2009;3(2):e381.

246. 3 Final Report on the Safety Assessment of Benzethonium Chloride and Methylbenzethonium Chloride. Journal of the American College of Toxicology. 1985;4(5):65-106.

247. Horev A, Sagi O, Zur E, Ben-Shimol S. Topical liposomal amphotericin B gel treatment for cutaneous leishmaniasis caused by Leishmania major: a double-blind, randomized, placebo-controlled, pilot study. International Journal of Dermatology. 2023;62(1):40-7.

248. Iraji F, Sadeghinia A. Efficacy of paromomycin ointment in the treatment of cutaneous leishmaniasis: results of a double-blind, randomized trial in Isfahan, Iran. Annals of Tropical Medicine & Parasitology. 2005;99(1):3-9.

249. Faghihi G, Tavakoli-kia R. Treatment of cutaneous leishmaniasis with either topical paromomycin or intralesional meglumine antimoniate. Clinical and Experimental Dermatology. 2003;28(1):13-6.

250. Salah AB, Messaoud NB, Guedri E, Zaatour A, Alaya NB, Bettaieb J, et al. Topical Paromomycin with or without Gentamicin for Cutaneous Leishmaniasis. New England Journal of Medicine. 2013;368(6):524-32.

251. Ben Salah A, Buffet PA, Morizot G, Ben Massoud N, Zâatour A, Ben Alaya N, et al. WR279,396, a Third Generation Aminoglycoside Ointment for the Treatment of Leishmania major Cutaneous Leishmaniasis: A Phase 2, Randomized, Double Blind, Placebo Controlled Study. PLOS Neglected Tropical Diseases. 2009;3(5):e432.

252. Sosa N, Pascale JM, Jiménez AI, Norwood JA, Kreishman-Detrick M, Weina PJ, et al. Topical paromomycin for New World cutaneous leishmaniasis. PLoS Negl Trop Dis. 2019;13(5):e0007253.

253. Azim M, Khan SA, Ullah S, Ullah S, Anjum SI. Therapeutic advances in the topical treatment of cutaneous leishmaniasis: A review. PLOS Neglected Tropical Diseases. 2021;15(3):e0009099.

254. Kharaji MH, Doroud D, Taheri T, Rafati S. Drug Targeting to Macrophages With Solid Lipid Nanoparticles Harboring Paromomycin: an In Vitro Evaluation Against L. major and L. tropica. AAPS PharmSciTech. 2016;17(5):1110-9.

255. Carneiro G, Santos DCM, Oliveira MC, Fernandes AP, Ferreira LS, Ramaldes GA, et al. Topical delivery and in vivo antileishmanial activity of paromomycin-loaded liposomes for treatment of cutaneous leishmaniasis. Journal of Liposome Research. 2010;20(1):16-23.

256. Esfandiari F, Motazedian MH, Asgari Q, Morowvat MH, Molaei M, Heli H. Paromomycin-loaded mannosylated chitosan nanoparticles: Synthesis, characterization and targeted drug delivery against leishmaniasis. Acta Tropica. 2019;197:105072.

257. Ferreira LS, Ramaldes GA, Nunan EA, Ferreira LAM. In Vitro Skin Permeation and Retention of Paromomycin from Liposomes for Topical Treatment of the Cutaneous Leishmaniasis. Drug Development and Industrial Pharmacy. 2004;30(3):289-96.

258. Bavarsad N, Fazly Bazzaz BS, Khamesipour A, Jaafari MR. Colloidal, in vitro and in vivo anti-leishmanial properties of transfersomes containing paromomycin sulfate in susceptible BALB/c mice. Acta Tropica. 2012;124(1):33-41.

259. Arya J, Prausnitz MR. Microneedle patches for vaccination in developing countries. Journal of Controlled Release. 2016;240:135-41.

260. S. Saeed M, K. Al-Sudany N, Naif A, S. Al Chalabi Q. Treatment of cutaneous leishmaniasis with radiofrequency microneedling. Journal of Pakistan Association of Dermatologists. 2023;33(4):1263-9.

261. Larrañeta E, Moore J, Vicente-Pérez EM, González-Vázquez P, Lutton R, Woolfson AD, et al. A proposed model membrane and test method for microneedle insertion studies. International Journal of Pharmaceutics. 2014;472(1):65-73.

262. Rojekar S, Vora LK, Tekko IA, Volpe-Zanutto F, McCarthy HO, Vavia PR, et al. Etravirine-loaded dissolving microneedle arrays for long-acting delivery. European Journal of Pharmaceutics and Biopharmaceutics. 2021;165:41-51.

263. Li W, Chen JY, Terry RN, Tang J, Romanyuk A, Schwendeman SP, et al. Core-shell microneedle patch for six-month controlled-release contraceptive delivery. Journal of Controlled Release. 2022;347:489-99.

264. Lopez-Ramirez MA, Kupor D, Marchiori L, Soto F, Rueda R, Reynoso M, et al. Combinatorial microneedle patch with tunable release kinetics and dual fast-deep/sustained release capabilities. Journal of Materials Chemistry B. 2021;9(9):2189-99.

265. Wu D, Quan YS, Kamiyama F, Kusamori K, Katsumi H, Sakane T, et al. Improvement of transdermal delivery of sumatriptan succinate using a novel self-dissolving microneedle array fabricated from sodium hyaluronate in rats. Biol Pharm Bull. 2015;38(3):365-73.

266. Thakur RRS, Tekko IA, Al-Shammari F, Ali AA, McCarthy H, Donnelly RF. Rapidly dissolving polymeric microneedles for minimally invasive intraocular drug delivery. Drug Delivery and Translational Research. 2016;6(6):800-15.

267. Costa P, Sousa Lobo JM. Modeling and comparison of dissolution profiles. European Journal of Pharmaceutical Sciences. 2001;13(2):123-33.

268. Celebioglu A, Uyar T. Design of polymer-free Vitamin-A acetate/cyclodextrin nanofibrous webs: antioxidant and fast-dissolving properties. Food & Function. 2020;11(9):7626-37.

269. Larrañeta E, Stewart S, Fallows SJ, Birkhäuer LL, McCrudden MTC, Woolfson AD, et al. A facile system to evaluate in vitro drug release from dissolving microneedle arrays. International Journal of Pharmaceutics. 2016;497(1):62-9.

270. Zhuang J, Rao F, Wu D, Huang Y, Xu H, Gao W, et al. Study on the fabrication and characterization of tip-loaded dissolving microneedles for transdermal drug delivery. European Journal of Pharmaceutics and Biopharmaceutics. 2020;157:66-73.

271. Men Z, Lu X, He T, Wu M, Su T, Shen T. Microneedle patch-assisted transdermal administration of recombinant hirudin for the treatment of thrombotic diseases. International Journal of Pharmaceutics. 2022;612:121332.

272. Koh KJ, Liu Y, Lim SH, Loh XJ, Kang L, Lim CY, et al. Formulation, characterization and evaluation of mRNA-loaded dissolvable polymeric microneedles (RNApatch). Scientific Reports. 2018;8(1):11842.

273. Zhu S, Zhang B, Wang Y, He Y, Qian G, Deng L, et al. A bilayer microneedle for therapeutic peptide delivery towards the treatment of diabetes in db/db mice. Journal of Drug Delivery Science and Technology. 2021;62:102336.

274. Bediz B, Korkmaz E, Khilwani R, Donahue C, Erdos G, Falo LD, et al. Dissolvable Microneedle Arrays for Intradermal Delivery of Biologics: Fabrication and Application. Pharmaceutical Research. 2014;31(1):117-35.

275. Smith E, Lau WM, Abdelghany TM, Vukajlovic D, Novakovic K, Ng KW. Vac-and-fill: A micromoulding technique for fabricating microneedle arrays with vacuum-activated, hands-free mould-filling. International Journal of Pharmaceutics. 2024;650:123706.

276. Lohmann L. LTS to support Micron Biomedical as strategic CDMO partner to scale up Micron´s Microarray Patch technology [April 2024]. Available from: https://www.ltslohmann.com/en/press-releases/lts-to-support-micron-biomedical-as-strategic-cdmo-partner-to-scale-up-microns-microarray-patch-technology/.

277. Jang M, Baek S, Kang G, Yang H, Kim S, Jung H. Dissolving microneedle with high molecular weight hyaluronic acid to improve skin wrinkles, dermal density and elasticity. International Journal of Cosmetic Science. 2020;42(3):302-9.

278. Leone M, Romeijn S, Slütter B, O'Mahony C, Kersten G, Bouwstra JA. Hyaluronan molecular weight: Effects on dissolution time of dissolving microneedles in the skin and on immunogenicity of antigen. European Journal of Pharmaceutical Sciences. 2020;146:105269.

279. Chen BZ, Ashfaq M, Zhang XP, Zhang JN, Guo XD. In vitro and in vivo assessment of polymer microneedles for controlled transdermal drug delivery. Journal of Drug Targeting. 2018;26(8):720-9.

280. Mangang KN, Thakran P, Halder J, Yadav KS, Ghosh G, Pradhan D, et al. PVP-microneedle array for drug delivery: mechanical insight, biodegradation, and recent advances. Journal of Biomaterials Science, Polymer Edition. 2023;34(7):986-1017.

281. Khataei S, H.Al-Musawi M, Asadi K, Ramezani S, Abbasian M, Ghorbani M. Effect of molecular weight and content of polyvinylpyrrolidone on cell proliferation, loading capacity and properties of electrospun green tea essential oil-incorporated polyamide-6/polyvinylpyrrolidone nanofibers. Journal of Drug Delivery Science and Technology. 2023;82:104310.

282. Chi Y, Huang Y, Kang Y, Dai G, Liu Z, Xu K, et al. The effects of molecular weight of hyaluronic acid on transdermal delivery efficiencies of dissolving microneedles. European Journal of Pharmaceutical Sciences. 2022;168:106075.

283. Davis SP, Landis BJ, Adams ZH, Allen MG, Prausnitz MR. Insertion of microneedles into skin: measurement and prediction of insertion force and needle fracture force. Journal of Biomechanics. 2004;37(8):1155-63.

284. Ranamukhaarachchi SA, Stoeber B. Determining the factors affecting dynamic insertion ofmicroneedles into skin. Biomedical Microdevices. 2019;21(4):100.

285. Yan Q, Weng J, Shen S, Wang Y, Fang M, Zheng G, et al. Finite Element Analysis for Biodegradable Dissolving Microneedle Materials on Skin Puncture and Mechanical Performance Evaluation. Polymers. 2021;13(18):3043.

286. Sabri AH, Kim Y, Marlow M, Scurr DJ, Segal J, Banga AK, et al. Intradermal and transdermal drug delivery using microneedles – Fabrication, performance evaluation

and application to lymphatic delivery. Advanced Drug Delivery Reviews. 2020;153:195-215.

287. Römgens AM, Bader DL, Bouwstra JA, Baaijens FPT, Oomens CWJ. Monitoring the penetration process of single microneedles with varying tip diameters. Journal of the Mechanical Behavior of Biomedical Materials. 2014;40:397-405.

288. Chen W, Wang C, Yan L, Huang L, Zhu X, Chen B, et al. Improved polyvinylpyrrolidone microneedle arrays with non-stoichiometric cyclodextrin. Journal of Materials Chemistry B. 2014;2(12):1699-705.

289. Xiong S, Ye S, Ni P, Zhong M, Shan J, Yuan T, et al. Polyvinyl-alcohol, chitosan and graphene-oxide composed conductive hydrogel for electrically controlled fluorescein sodium transdermal release. Carbohydrate Polymers. 2023;319:121172.

290. Yoo J-W, Giri N, Lee CH. pH-sensitive Eudragit nanoparticles for mucosal drug delivery. International Journal of Pharmaceutics. 2011;403(1):262-7.

291. Jakka D, Matadh AV, Shivakumar HN, Maibach H, Murthy SN. Polymer Coated Polymeric (PCP) microneedles for sampling of drugs and biomarkers from tissues. European Journal of Pharmaceutical Sciences. 2022;175:106203.

292. Stein S, Bogdahn M, Rosenbaum C, Weitschies W, Seidlitz A. Distribution of fluorescein sodium and triamcinolone acetonide in the simulated liquefied and vitrectomized Vitreous Model with simulated eye movements. European Journal of Pharmaceutical Sciences. 2017;109:233-43.

293. Railic M, Crean AM, Vucen S. Unravelling Microarray Patch Performance: The Role of In Vitro Release Medium and Biorelevant Testing. Molecular Pharmaceutics. 2024;21(10):5028-40.

294. Bagde A, Dev S, Madhavi K. Sriram L, Spencer SD, Kalvala A, Nathani A, et al. Biphasic burst and sustained transdermal delivery in vivo using an AI-optimized 3D-printed MN patch. International Journal of Pharmaceutics. 2023;636:122647.

295. Anand O, Yu LX, Conner DP, Davit BM. Dissolution Testing for Generic Drugs: An FDA Perspective. The AAPS Journal. 2011;13(3):328-35.

296. Cai B, Söderkvist K, Engqvist H, Bredenberg S. A New Drug Release Method in Early Development of Transdermal Drug Delivery Systems. Pain Research and Treatment. 2012;2012(1):953140.

297. FDA. Transdermal and Topical Delivery Systems - Product Development and Quality Considerations 2019 [cited Jan 2025. Available from: https://www.fda.gov/regulatory-information/search-fda-guidance-documents/transdermal-and-topical-delivery-systems-product-development-and-quality-considerations.

298. Shah VP, Simona Miron D, Ștefan Rădulescu F, Cardot J-M, Maibach HI. In vitro release test (IVRT): Principles and applications. International Journal of Pharmaceutics. 2022;626:122159.

299. Ng S-F, Rouse J, Sanderson D, Eccleston G. A Comparative Study of Transmembrane Diffusion and Permeation of Ibuprofen across Synthetic Membranes Using Franz Diffusion Cells. Pharmaceutics. 2010;2(2):209-23.

300. FDA. Guidance for Industry: Nonsterile Semisolid Dosage Forms; Scale-Up and Post-Approval Changes: Chemistry, Manufacturing, and Controls; In Vitro Release Testing and In Vivo Bioequivalence Documentation [Jan 2025]. Available from: https://www.fda.gov/drugs/drug-approvals-and-databases/dissolution-methods-database.

301. Sheshala R, Anuar NK, Abu Samah NH, Wong TW. In Vitro Drug Dissolution/Permeation Testing of Nanocarriers for Skin Application: a Comprehensive Review. AAPS PharmSciTech. 2019;20(5):164.

302. Kulkarni M, Potdar S, Date AA, Marfatiya A. In Vitro Release Testing of Acyclovir Topical Formulations Using Immersion Cells. ASSAY and Drug Development Technologies. 2021;19(2):75-84.

303. Wang B, Zhang S, Zhao X, Lian J, Gao Y. Preparation, characterization, and in vivo evaluation of levonorgestrel-loaded thermostable microneedles. Drug Delivery and Translational Research. 2022;12(4):944-56.

304. Paredes AJ, Volpe-Zanutto F, Permana AD, Murphy AJ, Picco CJ, Vora LK, et al. Novel tip-loaded dissolving and implantable microneedle array patches for sustained release of finasteride. International Journal of Pharmaceutics. 2021;606:120885.

305. Garland MJ, Migalska K, Tuan-Mahmood T-M, Raghu Raj Singh T, Majithija R, Caffarel-Salvador E, et al. Influence of skin model on in vitro performance of drug-loaded soluble microneedle arrays. International Journal of Pharmaceutics. 2012;434(1):80-9.

306. Shen J, Burgess DJ. In vitro–in vivo correlation for complex non-oral drug products: Where do we stand? Journal of Controlled Release. 2015;219:644-51.

307. Silva ACQ, Pereira B, Lameirinhas NS, Costa PC, Almeida IF, Dias-Pereira P, et al. Dissolvable Carboxymethylcellulose Microneedles for Noninvasive and Rapid Administration of Diclofenac Sodium. Macromolecular Bioscience. 2023;23(1):2200323.

308. Yu X, Li M, Zhu L, Li J, Zhang G, Fang R, et al. Amifostine-loaded armored dissolving microneedles for long-term prevention of ionizing radiation-induced injury. Acta Biomaterialia. 2020;112:87-100.

309. Noyes AA, Whitney WR. THE RATE OF SOLUTION OF SOLID SUBSTANCES IN THEIR OWN SOLUTIONS. Journal of the American Chemical Society. 1897;19(12):930-4.

310. Miller-Chou BA, Koenig JL. A review of polymer dissolution. Progress in Polymer Science. 2003;28(8):1223-70.

311. Mario G, Gabriele G. Mathematical Modelling and Controlled Drug Delivery: Matrix Systems. Current Drug Delivery. 2005;2(1):97-116.

312. Du H, Liu P, Zhu J, Lan J, Li Y, Zhang L, et al. Hyaluronic Acid-Based Dissolving Microneedle Patch Loaded with Methotrexate for Improved Treatment of Psoriasis. ACS Applied Materials & Interfaces. 2019;11(46):43588-98.

313. Li S, Xia D, Prausnitz MR. Efficient Drug Delivery into Skin Using a Biphasic Dissolvable Microneedle Patch with Water-Insoluble Backing. Advanced Functional Materials. 2021;31(44):2103359.

314. Xie Y, Wang H, Mao J, Li Y, Hussain M, Zhu J, et al. Enhanced in vitro efficacy for inhibiting hypertrophic scar by bleomycin-loaded dissolving hyaluronic acid microneedles. Journal of Materials Chemistry B. 2019;7(42):6604-11.

315. Paarakh MP, Jose PA, Setty CM, Christoper GVP. RELEASE KINETICS – CONCEPTS AND APPLICATIONS. International Journal of Pharmacy Research & Technology. 2019.

316. Ofokansi KC, Kenechukwu FC. Formulation Development and Evaluation of Drug Release Kinetics from Colon-Targeted Ibuprofen Tablets Based on Eudragit RL 100-Chitosan Interpolyelectrolyte Complexes. ISRN Pharm. 2013;2013:838403.

317. Pourtalebi Jahromi L, Ghazali M, Ashrafi H, Azadi A. A comparison of models for the analysis of the kinetics of drug release from PLGA-based nanoparticles. Heliyon. 2020;6(2):e03451.

318. Arshad MS, Zafar S, Rana SJ, Nazari K, Chang M-W, Ahmad Z. Fabrication of gentamicin sulphate laden stimulus responsive polymeric microarray patches for the treatment of bacterial biofilms. Journal of Drug Delivery Science and Technology. 2023;84:104504.

319. Liu H, Zhang S, Zhou Z, Xing M, Gao Y. Two-Layer Sustained-Release Microneedles Encapsulating Exenatide for Type 2 Diabetes Treatment. Pharmaceutics. 2022;14(6):1255.

320. Peng K, Vora LK, Domínguez-Robles J, Naser YA, Li M, Larrañeta E, et al. Hydrogel-forming microneedles for rapid and efficient skin deposition of controlled release tip-implants. Materials Science and Engineering: C. 2021;127:112226.

321. Higuchi T. Mechanism of sustained-action medication. Theoretical analysis of rate of release of solid drugs dispersed in solid matrices. Journal of Pharmaceutical Sciences. 1963;52(12):1145-9.

322. Dash S, Murthy PN, Nath L, Chowdhury P. Kinetic modeling on drug release from controlled drug delivery systems. Acta Pol Pharm. 2010;67(3):217-23.

323. Siepmann J, Peppas NA. Modeling of drug release from delivery systems based on hydroxypropyl methylcellulose (HPMC). Advanced Drug Delivery Reviews. 2001;48(2):139-57.

324. Paul DR. Elaborations on the Higuchi model for drug delivery. International Journal of Pharmaceutics. 2011;418(1):13-7.

325. Siepmann J, Peppas NA. Higuchi equation: Derivation, applications, use and misuse. International Journal of Pharmaceutics. 2011;418(1):6-12.

326. Lee PI. Modeling of drug release from matrix systems involving moving boundaries: Approximate analytical solutions. International Journal of Pharmaceutics. 2011;418(1):18-27.

327. Trucillo P. Drug Carriers: A Review on the Most Used Mathematical Models for Drug Release. Processes. 2022;10(6):1094.

328. Kalia YN, Guy RH. Modeling transdermal drug release. Advanced Drug Delivery Reviews. 2001;48(2):159-72.

329. Zarei Chamgordani N, Asiaei S, Ghorbani-Bidkorpeh F, Babaee Foroutan M, Dahmardehei M, Moghimi HR. A Long-Lasting Triamcinolone-Loaded Microneedle Patch for Prolonged Dermal Delivery. Iran J Pharm Res. 2024;23(1):e138857.

330. Park J-H, Allen MG, Prausnitz MR. Polymer Microneedles for Controlled-Release Drug Delivery. Pharmaceutical Research. 2006;23(5):1008-19.

331. Yadav PR, Han T, Olatunji O, Pattanayek SK, Das DB. Mathematical Modelling, Simulation and Optimisation of Microneedles for Transdermal Drug Delivery: Trends and Progress. Pharmaceutics. 2020;12(8):693.

332. Yadav PR, Hingonia P, Das DB, Pattanayek SK. Modeling of Dissolving Microneedle-Based Transdermal Drug Delivery: Effects of Dynamics of Polymers in Solution. Molecular Pharmaceutics. 2024;21(10):5104-14.

333. Siepmann J, Siepmann F. Mathematical modeling of drug delivery. International Journal of Pharmaceutics. 2008;364(2):328-43.

334. Mircioiu C, Voicu V, Anuta V, Tudose A, Celia C, Paolino D, et al. Mathematical Modeling of Release Kinetics from Supramolecular Drug Delivery Systems. Pharmaceutics. 2019;11(3):140.

335. Chavoshi S, Rabiee M, Rafizadeh M, Rabiee N, Shamsabadi AS, Bagherzadeh M, et al. Mathematical modeling of drug release from biodegradable polymeric microneedles. Bio-Design and Manufacturing. 2019;2(2):96-107.

336. wyffels L, Verbrugghen T, Monnery BD, Glassner M, Stroobants S, Hoogenboom R, et al. μPET imaging of the pharmacokinetic behavior of medium and high molar mass

89Zr-labeled poly(2-ethyl-2-oxazoline) in comparison to poly(ethylene glycol). Journal of Controlled Release. 2016;235:63-71.

337. Li H-Z, Chen S-C, Wang Y-Z. Thermoplastic PVA/PLA Blends with Improved Processability and Hydrophobicity. Industrial & Engineering Chemistry Research. 2014;53(44):17355-61.

338. Teodorescu M, Bercea M, Morariu S. Biomaterials of PVA and PVP in medical and pharmaceutical applications: Perspectives and challenges. Biotechnology Advances. 2019;37(1):109-31.

339. Maldonado-Santoyo M, Ortíz-Estrada C, Luna-Bárcenas G, Sanchez IC, Cesteros LC, Katime I, et al. Miscibility behavior and hydrogen bonding in blends of poly(vinyl phenyl ketone hydrogenated) and poly(2-ethyl-2-oxazoline). Journal of Polymer Science Part B: Polymer Physics. 2004;42(4):636-45.

340. Zhang Y, Li X, Guo S, Wei B. Blending poly(2-ethyl-2-oxazoline) with hydrophobic polymers as a hybrid adhesive with enhanced water-resistant properties. Journal of Applied Polymer Science. 2021;138(47):51404.

341. Tamahkar E. Bacterial cellulose/poly vinyl alcohol based wound dressings with sustained antibiotic delivery. Chemical Papers. 2021;75(8):3979-87.

342. Rivera-Hernández G, Antunes-Ricardo M, Martínez-Morales P, Sánchez ML. Polyvinyl alcohol based-drug delivery systems for cancer treatment. International Journal of Pharmaceutics. 2021;600:120478.

343. De Jaeghere W, De Beer T, Van Bocxlaer J, Remon JP, Vervaet C. Hot-melt extrusion of polyvinyl alcohol for oral immediate release applications. International Journal of Pharmaceutics. 2015;492(1):1-9.

344. Zhang XP, Wang BB, Li WX, Fei WM, Cui Y, Guo XD. In vivo safety assessment, biodistribution and toxicology of polyvinyl alcohol microneedles with 160-day uninterruptedly applications in mice. European Journal of Pharmaceutics and Biopharmaceutics. 2021;160:1-8.

345. Parada LG, Cesteros LC, Meaurio E, Katime I. Miscibility and specific interactions in blends of poly(vinyl acetate-co-vinyl alcohol) with poly(ethyloxazoline). Macromolecular Chemistry and Physics. 1997;198(8):2505-17.

346. Sudhamani SR, Prasad MS, Udaya Sankar K. DSC and FTIR studies on Gellan and Polyvinyl alcohol (PVA) blend films. Food Hydrocolloids. 2003;17(3):245-50.

347. Jose J, Shehzad F, Al-Harthi MA. Preparation method and physical, mechanical, thermal characterization of poly(vinyl alcohol)/poly(acrylic acid) blends. Polymer Bulletin. 2014;71(11):2787-802.

348. Rajashekara, Shubha, Subhranshu, Navya. Preparation , Characterization and Spectroscopic Investigations of PEOX-PVOH Blend Films. Sensors & Transducers. 2017;210(3):32-7.

349. Aoi K, Takasu A, Tsuchiya M, Okada M. New chitin-based polymer hybrids, 3. Miscibility of chitin-graft-poly(2-ethyl-2-oxazoline) with poly(vinyl alcohol). Macromolecular Chemistry and Physics. 1998;199(12):2805-11.

350. Oh NG, Hwang SY, Na YH. Fabrication of a PVA-Based Hydrogel Microneedle Patch. ACS Omega. 2022;7(29):25179-85.

351. Limpan N, Prodpran T, Benjakul S, Prasarpran S. Influences of degree of hydrolysis and molecular weight of poly(vinyl alcohol) (PVA) on properties of fish myofibrillar protein/PVA blend films. Food Hydrocolloids. 2012;29(1):226-33.

352. Aruldass S, Mathivanan V, Mohamed AR, Tye CT. Factors affecting hydrolysis of polyvinyl acetate to polyvinyl alcohol. Journal of Environmental Chemical Engineering. 2019;7(5):103238.

353. Park J-C, Ito T, Kim K-O, Kim K-W, Kim B-S, Khil M-S, et al. Electrospun poly(vinyl alcohol) nanofibers: effects of degree of hydrolysis and enhanced water stability. Polymer Journal. 2010;42(3):273-6.

354. Mitani E, Ozaki Y, Sato H. Two types of CO···HO hydrogen bonds and OH···OH (dimer, trimer, oligomer) hydrogen bonds in PVA with 88% saponification/PMMA and PVA with 99% saponification/PMMA blends and their thermal behavior studied by infrared spectroscopy. Polymer. 2022;246:124725.

355. Chen S, Yang H, Huang K, Ge X, Yao H, Tang J, et al. Quantitative Study on Solubility Parameters and Related Thermodynamic Parameters of PVA with Different Alcoholysis Degrees. Polymers. 2021;13(21):3778.

356. Marin E, Rojas J, Yhors C. A review of polyvinyl alcohol derivatives: Promising materials for pharmaceutical and biomedical applications. African Journal of Pharmacy and Pharmacology. 2014;8:674-84.

357. Stavropoulou A, Papadokostaki KG, Sanopoulou M. Thermal properties of poly(vinyl alcohol)–solute blends studied by TMDSC. Journal of Applied Polymer Science. 2004;93(3):1151-6.

358. Lewandowska K. Miscibility and thermal stability of poly(vinyl alcohol)/chitosan mixtures. Thermochimica Acta. 2009;493(1):42-8.

359. Freire TF, Quinaz T, Fertuzinhos A, Quyền NT, de Moura MFSM, Martins M, et al. Thermal, Mechanical and Chemical Analysis of Poly(vinyl alcohol) Multifilament and Braided Yarns. Polymers. 2021;13(21):3644.

360. Mohsin M, Hossin A, Haik Y. Thermal and mechanical properties of poly(vinyl alcohol) plasticized with glycerol. Journal of Applied Polymer Science. 2011;122(5):3102-9.

361. Boonsuk P, Kaewtatip K, Chantarak S, Kelarakis A, Chaibundit C. Super-tough biodegradable poly(vinyl alcohol)/poly(vinyl pyrrolidone) blends plasticized by glycerol and sorbitol. Journal of Applied Polymer Science. 2018;135(26):46406.

362. D'souza OJ, Hiremani VD, Gasti T, Goudar N, L VS, Masti SP, et al. Fabrication and Study of Poly (vinyl alcohol) Film Functionalized with Basella alba Stem Extract. Journal of Polymers and the Environment. 2022;30(7):2888-904.

363. Sau S, Pandit S, Kundu S. Crosslinked poly (vinyl alcohol): Structural, optical and mechanical properties. Surfaces and Interfaces. 2021;25:101198.

364. Lilleby Helberg RM, Dai Z, Ansaloni L, Deng L. PVA/PVP blend polymer matrix for hosting carriers in facilitated transport membranes: Synergistic enhancement of CO2 separation performance. Green Energy & Environment. 2020;5(1):59-68.

365. Colombo A, Gherardi F, Goidanich S, Delaney JK, de la Rie ER, Ubaldi MC, et al. Highly transparent poly(2-ethyl-2-oxazoline)-TiO2 nanocomposite coatings for the conservation of matte painted artworks. RSC Advances. 2015;5(103):84879-88.

366. Ozkose UU, Altinkok C, Yilmaz O, Alpturk O, Tasdelen MA. In-situ preparation of poly(2-ethyl-2-oxazoline)/clay nanocomposites via living cationic ring-opening polymerization. European Polymer Journal. 2017;88:586-93.

367. Shan X, Williams AC, Khutoryanskiy VV. Polymer structure and property effects on solid dispersions with haloperidol: Poly(N-vinyl pyrrolidone) and poly(2-oxazolines) studies. International Journal of Pharmaceutics. 2020;590:119884.

368. Kim JH, Min BR, Kang YS. Thermodynamic Model of the Glass Transition Behavior for Miscible Polymer Blends. Macromolecules. 2006;39(3):1297-9.

369. Thomas S, Abolhasani M, Grohens Y, Jyotishkumar P. Characterization of polymer blends : miscibility, morphology and interfaces. John Wiley & Sons, Incorporated; 2015.

370. Su S. Prediction of the Miscibility of PBAT/PLA Blends. Polymers. 2021;13(14):2339.

371. Cornelis H, Derveaux E, Singh A, Smet M, Adriaensens P, Van den Mooter G. A Miscibility Study of p(MMA-co-HEMA)-Based Polymer Blends by Thermal Analysis and Solid-State NMR Relaxometry. Molecular Pharmaceutics. 2024;21(11):5529-38.

372. Muralisrinivasan NS. Polymer blends and composites : chemistry and technology. 1 ed: John Wiley & Sons, Incorporated; 2017. p. 157-60.

373. Muthuraj R, Misra M, Mohanty AK. Biodegradable compatibilized polymer blends for packaging applications: A literature review. Journal of Applied Polymer Science. 2018;135(24):45726.

374. Huggins ML. Some Properties of Solutions of Long-chain Compounds. The Journal of Physical Chemistry. 1942;46(1):151-8.

375. Flory PJ. Thermodynamics of High Polymer Solutions. The Journal of Chemical Physics. 1942;10(1):51-61.

376. Russell TH, Edwards BJ, Khomami B. Characterization of the Flory-Huggins interaction parameter of polymer thermodynamics. Europhysics Letters. 2014;108(6):66003.

377. Marsac PJ, Shamblin SL, Taylor LS. Theoretical and Practical Approaches for Prediction of Drug–Polymer Miscibility and Solubility. Pharmaceutical Research. 2006;23(10):2417-26.

378. Kim SD, Chakravarti S, Tian J, Bell P. The phase behavior and the Flory–Huggins interaction parameter of blends containing amorphous poly(resorcinol phthalate-block-carbonate), poly(bisphenol-A carbonate) and poly(ethylene terephthalate). Polymer. 2010;51(10):2199-206.

379. Xavier P, Rao P, Bose S. Nanoparticle induced miscibility in LCST polymer blends: critically assessing the enthalpic and entropic effects. Physical Chemistry Chemical Physics. 2016;18(1):47-64.

380. Thakral S, Thakral NK. Prediction of Drug–Polymer Miscibility through the use of Solubility Parameter based Flory–Huggins Interaction Parameter and the Experimental Validation: PEG as Model Polymer. Journal of Pharmaceutical Sciences. 2013;102(7):2254-63.

381. Pajula K, Taskinen M, Lehto V-P, Ketolainen J, Korhonen O. Predicting the Formation and Stability of Amorphous Small Molecule Binary Mixtures from Computationally Determined Flory−Huggins Interaction Parameter and Phase Diagram. Molecular Pharmaceutics. 2010;7(3):795-804.

382. Miquelard-Garnier G, Roland S. Beware of the Flory parameter to characterize polymer-polymer interactions: A critical reexamination of the experimental literature. European Polymer Journal. 2016;84:111-24.

383. Glova AD, Falkovich SG, Dmitrienko DI, Lyulin AV, Larin SV, Nazarychev VM, et al. Scale-Dependent Miscibility of Polylactide and Polyhydroxybutyrate: Molecular Dynamics Simulations. Macromolecules. 2018;51(2):552-63.

384. Pannuzzo M, Horta BAC, La Rosa C, Decuzzi P. Predicting the Miscibility and Rigidity of Poly(lactic-co-glycolic acid)/Polyethylene Glycol Blends via Molecular Dynamics Simulations. Macromolecules. 2020;53(10):3643-54.

385. Fekete E, Földes E, Damsits F, Pukánszky B. Interaction-structure-property relationships in amorphous polymer blends. Polymer Bulletin. 2000;44(4):363-70.

386. Büki L, Gönczy E, Fekete E, Hellmann GP, Pukánszky B. Miscibility-property correlations in blends of glassy amorphous polymers. Macromolecular Symposia. 2001;170(1):9-20.

387. Ethier J, Antoniuk ER, Brettmann B. Predicting polymer solubility from phase diagrams to compatibility: a perspective on challenges and opportunities. Soft Matter. 2024;20(29):5652-69.

388. Costa GP, Choi P, Stoyanov SR, Liu Q. The temperature dependence of the Hildebrand solubility parameters of selected hydrocarbon polymers and hydrocarbon solvents: a molecular dynamics investigation. Journal of Molecular Modeling. 2024;30(7):196.

389. Biernat M, Dąbczyński P, Biernat P, Rysz J. Phase Separation in PCDTBT:PCBM Blends: from Flory-Huggins Interaction Parameters to Ternary Phase Diagrams. Chinese Journal of Polymer Science. 2020;38(9):1025-33.

390. Utracki LA. Thermodynamics of Polymer Blends. In: Utracki LA, editor. Polymer Blends Handbook. Dordrecht: Springer Netherlands; 2003. p. 123-201.

391. Venkatram S, Kim C, Chandrasekaran A, Ramprasad R. Critical Assessment of the Hildebrand and Hansen Solubility Parameters for Polymers. Journal of Chemical Information and Modeling. 2019;59(10):4188-94.

392. Greenhalgh DJ, Williams AC, Timmins P, York P. Solubility parameters as predictors of miscibility in solid dispersions. Journal of Pharmaceutical Sciences. 1999;88(11):1182-90.

393. Lindvig T, Michelsen ML, Kontogeorgis GM. A Flory–Huggins model based on the Hansen solubility parameters. Fluid Phase Equilibria. 2002;203(1):247-60.

394. Emerson JA, Toolan DTW, Howse JR, Furst EM, Epps TH, III. Determination of Solvent–Polymer and Polymer–Polymer Flory–Huggins Interaction Parameters for Poly(3-hexylthiophene) via Solvent Vapor Swelling. Macromolecules. 2013;46(16):6533-40.

395. Panayiotou C. Polymer–polymer miscibility and partial solvation parameters. Polymer. 2013;54(6):1621-38.

396. Hansen CM. The Universality of the Solubility Parameter. Product R&D. 1969;8(1):2-11.

397. Meaurio E, Sanchez-Rexach E, Zuza E, Lejardi A, Sanchez-Camargo AdP, Sarasua J-R. Predicting miscibility in polymer blends using the Bagley plot: Blends with poly(ethylene oxide). Polymer. 2017;113:295-309.

398. Katopodis K, Kapourani A, Vardaka E, Karagianni A, Chorianopoulou C, Kontogiannopoulos KN, et al. Partially hydrolyzed polyvinyl alcohol for fusion-based pharmaceutical formulation processes: Evaluation of suitable plasticizers. International Journal of Pharmaceutics. 2020;578:119121.

399. Schoolaert E, Merckx R, Becelaere J, Everaerts M, Van Guyse JFR, Sedlacek O, et al. Immiscibility of Chemically Alike Amorphous Polymers: Phase Separation of Poly(2-ethyl-2-oxazoline) and Poly(2-n-propyl-2-oxazoline). Macromolecules. 2020;53(17):7590-600.

400. David DJ, Sincock TF. Estimation of miscibility of polymer blends using the solubility parameter concept. Polymer. 1992;33(21):4505-14.

401. Bayer G, Shayganpour A, Zia J, Bayer IS. Polyvinyl alcohol-based films plasticized with an edible sweetened gel enriched with antioxidant carminic acid. Journal of Food Engineering. 2022;323:111000.

402. Ibrahim MM, El-Zawawy WK, Nassar MA. Synthesis and characterization of polyvinyl alcohol/nanospherical cellulose particle films. Carbohydrate Polymers. 2010;79(3):694-9.

403. Lai W-C, Liau W-B. Study of the miscibility and crystallization behavior of poly(ethylene oxide)/poly(vinyl alcohol) blends. Journal of Applied Polymer Science. 2004;92(3):1562-8.

404. Çaykara T, Demirci S. Preparation and Characterization of Blend Films of Poly(Vinyl Alcohol) and Sodium Alginate. Journal of Macromolecular Science, Part A. 2006;43(7):1113-21.

405. Bhat V, Shivakumar HR, Sheshappa RK, Ganesh S, Prasad P, Guru GS, et al. Miscibility and Thermal Behavior of Pullulan/Polyacrylamide Blends. Journal of Macromolecular Science, Part A. 2011;48(11):920-6.

406. Fang L, Goh SH. Miscible chitosan/tertiary amide polymer blends. Journal of Applied Polymer Science. 2000;76(12):1785-90.

407. Rahman MS, Al-Marhubi IM, Al-Mahrouqi A. Measurement of glass transition temperature by mechanical (DMTA), thermal (DSC and MDSC), water diffusion and density methods: A comparison study. Chemical Physics Letters. 2007;440(4):372-7.

408. Leyva-Porras C, Cruz-Alcantar P, Espinosa-Solís V, Martínez-Guerra E, Piñón-Balderrama CI, Compean Martínez I, et al. Application of Differential Scanning Calorimetry (DSC) and Modulated Differential Scanning Calorimetry (MDSC) in Food and Drug Industries. Polymers. 2020;12(1):5.

409. Verdonck E, Schaap K, Thomas LC. A discussion of the principles and applications of Modulated Temperature DSC (MTDSC). International Journal of Pharmaceutics. 1999;192(1):3-20.

410. Foreman J. SSR, Marcozz C. L. Exploring the Sensitivity of Thermal Analysis Techniques to the Glass Transition [March 2024]. Available from: https://www.tainstruments.com/pdf/literature/TA082.pdf.

411. Nuño-Donlucas S, Cesteros LC, Puig JE, Katime I. Effect of the Acrylic acid Content on Miscibility and Mechanical Properties of Mixtures of Poly[ethylene-co-(acrylic acid)] and Poly(2-ethyl-2-oxazoline). Macromolecular Chemistry and Physics. 2001;202(5):663-71.

412. Nyamweya N, Hoag SW. Assessment of Polymer-Polymer Interactions in Blends of HPMC and Film Forming Polymers by Modulated Temperature Differential Scanning Calorimetry. Pharmaceutical Research. 2000;17(5):625-31.

413. Newman A, Zografi G. Commentary: Considerations in the Measurement of Glass Transition Temperatures of Pharmaceutical Amorphous Solids. AAPS PharmSciTech. 2019;21(1):26.

414. Hill DJT, Whittaker AK, Wong KW. Miscibility and Specific Interactions in Blends of Poly(4-vinylphenol) and Poly(2-ethoxyethyl methacrylate). Macromolecules. 1999;32(16):5285-91.

415. Gordon M, Taylor JS. Ideal copolymers and the second-order transitions of synthetic rubbers. i. non-crystalline copolymers. Journal of Applied Chemistry. 1952;2(9):493-500.

416. Soradech S, Kengkwasingh P, Williams AC, Khutoryanskiy VV. Synthesis and Evaluation of Poly(3-hydroxypropyl Ethylene-imine) and Its Blends with Chitosan Forming Novel Elastic Films for Delivery of Haloperidol. Pharmaceutics. 2022;14(12):2671.

417. Urakawa O, Yasue A. Glass Transition Behaviors of Poly (Vinyl Pyridine)/Poly (Vinyl Phenol) Revisited. Polymers. 2019;11(7):1153.

418. Lopez E, Koh YP, Zapata-Hincapie JA, Simon SL. Composition-dependent glass transition temperature in mixtures: Evaluation of configurational entropy models. Polymer Engineering & Science. 2022;62(8):2435-45.

419. Abiad MG, Carvajal MT, Campanella OH. A Review on Methods and Theories to Describe the Glass Transition Phenomenon: Applications in Food and Pharmaceutical Products. Food Engineering Reviews. 2009;1(2):105-32.

420. An L, He D, Jing J, Wang Z, Yu D, Jiang B, et al. Effects of molecular weight and interaction parameter on the glass transition temperature of polystyrene mixtures and its blends with polystyrene/poly (2,6-dimethyl-p-phenylene oxide). European Polymer Journal. 1997;33(9):1523-8.

421. Schugmann M, Foerst P. Systematic Investigation on the Glass Transition Temperature of Binary and Ternary Sugar Mixtures and the Applicability of Gordon–Taylor and Couchman–Karasz Equation. Foods. 2022;11(12):1679.

422. Lim D-S, Kim E-B, Lee H-Y, Kwon Y-N, Kim J-H, Lee J-C, et al. Highly miscible bio-based poly(lactic acid)/acetylated cellulose ether ultrafiltration membranes with improved water permeances. Journal of Membrane Science. 2024;711:123195.

423. Lin AA, Kwei TK, Reiser A. On the physical meaning of the Kwei equation for the glass transition temperature of polymer blends. Macromolecules. 1989;22(10):4112-9.

424. Miwa Y, Usami K, Yamamoto K, Sakaguchi M, Sakai M, Shimada S. Direct Detection of Effective Glass Transitions in Miscible Polymer Blends by Temperature-Modulated Differential Scanning Calorimetry. Macromolecules. 2005;38(6):2355-61.

425. De Oliveira W, Glasser WG. Multiphase materials with lignin. XII. Blends of poly(vinyl chloride) with lignin–caprolactone copolymers. Journal of Applied Polymer Science. 1994;51(3):563-71.

426. Zheng Q, Zhang Y, Montazerian M, Gulbiten O, Mauro JC, Zanotto ED, et al. Understanding Glass through Differential Scanning Calorimetry. Chemical Reviews. 2019;119(13):7848-939.

427. Ford JL, Mann TE. Fast-Scan DSC and its role in pharmaceutical physical form characterisation and selection. Advanced Drug Delivery Reviews. 2012;64(5):422-30.

428. Schick C. Differential scanning calorimetry (DSC) of semicrystalline polymers. Analytical and Bioanalytical Chemistry. 2009;395(6):1589-611.

429. Sonaglioni D, Tombari E, Capaccioli S. Fast differential scanning calorimetry: new solutions in data treatment and applications to molecular glass-formers. Thermochimica Acta. 2023;719:179385.

430. McGregor C, Bines E. The use of high-speed differential scanning calorimetry (Hyper-DSC™) in the study of pharmaceutical polymorphs. International Journal of Pharmaceutics. 2008;350(1):48-52.

431. Knopp MM, Löbmann K, Elder DP, Rades T, Holm R. Recent advances and potential applications of modulated differential scanning calorimetry (mDSC) in drug development. European Journal of Pharmaceutical Sciences. 2016;87:164-73.

432. Song M, Hammiche A, Pollock HM, Hourston DJ, Reading M. Modulated differential scanning calorimetry: 4. Miscibility and glass transition behaviour in poly(methyl methacrylate) and poly(epichlorohydrin) blends. Polymer. 1996;37(25):5661-5.

433. De Melo-Diogo D, Costa EC, Alves CG, Lima-Sousa R, Ferreira P, Louro RO, et al. POxylated graphene oxide nanomaterials for combination chemo-phototherapy of breast cancer cells. European Journal of Pharmaceutics and Biopharmaceutics. 2018;131:162-9.

434. Sreekumar PA, Al-Harthi MA, De SK. Effect of glycerol on thermal and mechanical properties of polyvinyl alcohol/starch blends. Journal of Applied Polymer Science. 2012;123(1):135-42.

435. El-Sayed S, Mahmoud KH, Fatah AA, Hassen A. DSC, TGA and dielectric properties of carboxymethyl cellulose/polyvinyl alcohol blends. Physica B: Condensed Matter. 2011;406(21):4068-76.

436. Pötschke P, Paul DR. Formation of Co-continuous Structures in Melt-Mixed Immiscible Polymer Blends. Journal of Macromolecular Science, Part C. 2003;43(1):87-141.

437. Izutsu K-i, Yoshida H, Abe Y, Yamamoto E, Sato Y, Ando D. Application of the Thermal Analysis of Frozen Aqueous Solutions to Assess the Miscibility of Hyaluronic

Acid and Polymers Used for Dissolving Microneedles. Pharmaceutics. 2024;16(10):1280.

438. Permana AD, McCrudden MTC, Donnelly RF. Enhanced Intradermal Delivery of Nanosuspensions of Antifilariasis Drugs Using Dissolving Microneedles: A Proof of Concept Study. Pharmaceutics. 2019;11(7):346.

439. Creelman B, Frivold C, Jessup S, Saxon G, Jarrahian C. Manufacturing readiness assessment for evaluation of the microneedle array patch industry: an exploration of barriers to full-scale manufacturing. Drug Delivery and Translational Research. 2022;12(2):368-75.

440. Yan X, Cayla A, Devaux E, Salaün F. Microstructure Evolution of Immiscible PP-PVA Blends Tuned by Polymer Ratio and Silica Nanoparticles. Polymers (Basel). 2018;10(9).

441. Panapitiya N, Wijenayake S, Nguyen D, Karunaweera C, Huang Y, Balkus K, et al. Compatibilized Immiscible Polymer Blends for Gas Separations. Materials. 2016;9(8):643.

442. Um IC, Park YH. The effect of casting solvent on the structural characteristics and miscibility of regenerated silk fibroin/Poly(vinyl alcohol) blends. Fibers and Polymers. 2007;8(6):579-85.

443. Sartawi Z, Blackshields C, Ariamanesh A, Farag FF, Griffin B, Crean A, et al. Glass Microneedles: A Case Study for Regulatory Approval Using a Quality by Design Approach. Advanced Materials. 2023;35(52):2305834.

444. Aurobindo Pharma-Milpharm Ltd. Montelukast 10 mg film-coated tablets summary of product characteristics. Electronic Medicines Compendium [Internet]. 2021 [cited 2024 Jan 18]. Available from: https://www.medicines.org.uk/emc/product/1222/smpc.

445. Lacy MK, Nicolau DP, Nightingale CH, Quintiliani R. The pharmacodynamics of aminoglycosides. Clin Infect Dis. 1998;27(1):23-7.

446. Coser EM, Ferreira BA, Branco N, Yamashiro-Kanashiro EH, Lindoso JAL, Coelho AC. Activity of paromomycin against Leishmania amazonensis: Direct correlation between susceptibility in vitro and the treatment outcome in vivo. International Journal for Parasitology: Drugs and Drug Resistance. 2020;14:91-8.

447. Thambiliyagodage C, Jayanetti M, Mendis A, Ekanayake G, Liyanaarachchi H, Vigneswaran S. Recent Advances in Chitosan-Based Applications—A Review. Materials. 2023;16(5):2073.

448. Iqbal Y, Ahmed I, Irfan MF, Chatha SAS, Zubair M, Ullah A. Recent advances in chitosan-based materials; The synthesis, modifications and biomedical applications. Carbohydrate Polymers. 2023;321:121318.

449. Riezk A, Raynes JG, Yardley V, Murdan S, Croft SL. Activity of Chitosan and Its Derivatives against Leishmania major and Leishmania mexicana in vitro. Antimicrobial Agents and Chemotherapy. 2020;64(3):e01772-19.

450. Esboei BR, Mohebali M, Mousavi P, Fakhar M, Akhoundi B. Potent antileishmanial activity of chitosan against Iranian strain of Leishmania major (MRHO/IR/75/ER): In vitro and in vivo assay. J Vector Borne Dis. 2018;55(2):111-5.

451. Salah-Tazdaït R, Tazdaït D, Harrat Z, Eddaikra N, Abdi N, Mameri N, editors. Antiparasite Activity of Chitosan. Proceedings of 2015 International Conference on Chemical, Metallurgy and Environmental Engineering, Istanbul, Turkey; 2015.

452. AlMohammed HI, Khudair Khalaf A, E. Albalawi A, Alanazi AD, Baharvand P, Moghaddam A, et al. Chitosan-Based Nanomaterials as Valuable Sources of Anti-Leishmanial Agents: A Systematic Review. Nanomaterials. 2021;11(3):689.

453. Abdollahimajd F, Moravvej H, Dadkhahfar S, Mahdavi H, Mohebali M, Mirzadeh H. Chitosan-based biocompatible dressing for treatment of recalcitrant lesions of cutaneous leishmaniasis: A pilot clinical study. Indian journal of dermatology, venereology and leprology. 2019;85(6):609-14.

454. Singh PK, Pawar VK, Jaiswal AK, Singh Y, Srikanth CH, Chaurasia M, et al. Chitosan coated PluronicF127 micelles for effective delivery of Amphotericin B in experimental visceral leishmaniasis. International Journal of Biological Macromolecules. 2017;105:1220-31.

455. Ribeiro TG, Franca JR, Fuscaldi LL, Santos ML, Duarte MC, Lage PS, et al. An optimized nanoparticle delivery system based on chitosan and chondroitin sulfate molecules reduces the toxicity of amphotericin B and is effective in treating tegumentary leishmaniasis. Int J Nanomedicine. 2014;9:5341-53.

456. Loiseau PM, Pomel S, Croft SL. Chitosan Contribution to Therapeutic and Vaccinal Approaches for the Control of Leishmaniasis. Molecules. 2020;25(18).

457. Zadeh Mehrizi T, Shafiee Ardestani M, Haji Molla Hoseini M, Khamesipour A, Mosaffa N, Ramezani A. Novel Nanosized Chitosan-Betulinic Acid Against Resistant Leishmania Major and First Clinical Observation of such parasite in Kidney. Scientific Reports. 2018;8(1):11759.

458. Riezk A, Van Bocxlaer K, Yardley V, Murdan S, Croft SL. Activity of Amphotericin B-Loaded Chitosan Nanoparticles against Experimental Cutaneous Leishmaniasis. Molecules. 2020;25(17):4002.

459. Malli S, Pomel S, Ayadi Y, Deloménie C, Da Costa A, Loiseau PM, et al. Topically Applied Chitosan-Coated Poly(isobutylcyanoacrylate) Nanoparticles Are Active Against Cutaneous Leishmaniasis by Accelerating Lesion Healing and Reducing the Parasitic Load. ACS Applied Bio Materials. 2019;2(6):2573-86.

460. Díez C, Guillarme D, Staub Spörri A, Cognard E, Ortelli D, Edder P, et al. Aminoglycoside analysis in food of animal origin with a zwitterionic stationary phase and

liquid chromatography–tandem mass spectrometry. Analytica Chimica Acta. 2015;882:127-39.

461. Glinka M, Wojnowski W, Wasik A. Determination of aminoglycoside antibiotics: Current status and future trends. TrAC Trends in Analytical Chemistry. 2020;131:116034.

462. Stead DA. Current methodologies for the analysis of aminoglycosides. Journal of Chromatography B: Biomedical Sciences and Applications. 2000;747(1):69-93.

463. Roseboom IC, Thijssen B, Rosing H, Mbui J, Beijnen JH, Dorlo TPC. Highly sensitive UPLC-MS/MS method for the quantification of paromomycin in human plasma. Journal of Pharmaceutical and Biomedical Analysis. 2020;185:113245.

464. Amponsah SK, Boadu JA, Dwamena DK, Opuni KFM. Bioanalysis of aminoglycosides using high-performance liquid chromatography. Admet dmpk. 2022;10(1):27-62.

465. Organization WH. Paromomycin sulfate The International Pharmacopoeia 2022 [April 2024]. 11th:[Available from: https://digicollections.net/phint/2022/index.html#d/b.6.1.263.

466. Pick J, Olson LL, Ellis WY, Lim P. Development and validation of a method to extract and quantitate paromomycin and gentamicin from an Aquaphilic® cream formulation. Journal of Pharmaceutical and Biomedical Analysis. 1997;16(1):131-7.

467. Olson LL, Pick J, Ellis WY, Lim P. A chemical assessment and HPLC assay validation of bulk paromomycin sulfate. Journal of Pharmaceutical and Biomedical Analysis. 1997;15(6):783-93.

468. Roseboom IC, Thijssen B, Rosing H, Alves F, Younis BM, Musa AM, et al. Development and validation of an ultra-high performance liquid chromatography coupled to tandem mass spectrometry method for the quantification of the antileishmanial drug paromomycin in human skin tissue. Journal of Chromatography B. 2022;1211:123494.

469. Pujol-Brugués A, Calpena-Campmany AC, Riera-Lizandra C, Halbaut-Bellowa L, Clares-Naveros B. Development of a liquid chromatographic method for the quantification of paromomycin. Application to in vitro release and ex vivo permeation studies. Spectrochimica Acta Part A: Molecular and Biomolecular Spectroscopy. 2014;133:657-62.

470. Yang B, Wang L, Luo C, Wang X, Sun C. Simultaneous Determination of 11 Aminoglycoside Residues in Honey, Milk, and Pork by Liquid Chromatography with Tandem Mass Spectrometry and Molecularly Imprinted Polymer Solid Phase Extraction. Journal of AOAC INTERNATIONAL. 2019;100(6):1869-78.

471. Khan W, Kumar N. Characterization, thermal stability studies, and analytical method development of Paromomycin for formulation development. Drug Testing and Analysis. 2011;3(6):363-72.

472. Oertel R, Neumeister V, Kirch W. Hydrophilic interaction chromatography combined with tandem-mass spectrometry to determine six aminoglycosides in serum. Journal of Chromatography A. 2004;1058(1):197-201.

473. Ravis WR, Llanos-Cuentas A, Sosa N, Kreishman-Deitrick M, Kopydlowski KM, Nielsen C, et al. Pharmacokinetics and absorption of paromomycin and gentamicin from topical creams used to treat cutaneous leishmaniasis. Antimicrob Agents Chemother. 2013;57(10):4809-15.

474. Moreno-González D, Hamed AM, García-Campaña AM, Gámiz-Gracia L. Evaluation of hydrophilic interaction liquid chromatography–tandem mass spectrometry and extraction with molecularly imprinted polymers for determination of aminoglycosides in milk and milk-based functional foods. Talanta. 2017;171:74-80.

475. Kahsay G, Song H, Van Schepdael A, Cabooter D, Adams E. Hydrophilic interaction chromatography (HILIC) in the analysis of antibiotics. Journal of Pharmaceutical and Biomedical Analysis. 2014;87:142-54.

476. Kumar P, Rubies A, Companyó R, Centrich F. Hydrophilic interaction chromatography for the analysis of aminoglycosides. Journal of Separation Science. 2012;35(4):498-504.

477. Beccaria M, Cabooter D. Current developments in LC-MS for pharmaceutical analysis. Analyst. 2020;145(4):1129-57.

478. Singh P, Zeng X, Chen X, Yang Y, Chen Y, Cui S, et al. Quantitation of polymeric-microneedle-delivered HA15 in tissues using liquid chromatography-tandem mass spectrometry. Journal of Pharmaceutical and Biomedical Analysis. 2020;185:113230.

479. Waters Corporation Jinchuan Yang PDR. Analysis of Aminoglycosides in Foods Using a Zwitterionic Stationary Phase and Liquid Chromatography Tandem Mass Spectrometry 2022 [September 2022]. Available from: https://www.waters.com/nextgen/hr/en/library/application-notes/2021/analysis-of-aminoglycosides-in-foods-using-a-zwitterionic-stationary-phase-and-liquid-chromatography-tandem-mass-spectrometry.html.

480. DeLano M, Walter TH, Lauber MA, Gilar M, Jung MC, Nguyen JM, et al. Using Hybrid Organic–Inorganic Surface Technology to Mitigate Analyte Interactions with Metal Surfaces in UHPLC. Analytical Chemistry. 2021;93(14):5773-81.

481. Lioupi A, Virgiliou C, Walter TH, Smith KM, Rainville P, Wilson ID, et al. Application of a hybrid zwitterionic hydrophilic interaction liquid chromatography column in metabolic profiling studies. Journal of Chromatography A. 2022;1672:463013.

482. McGrath MG, Vucen S, Vrdoljak A, Kelly A, O'Mahony C, Crean AM, et al. Production of dissolvable microneedles using an atomised spray process: Effect of microneedle composition on skin penetration. European Journal of Pharmaceutics and Biopharmaceutics. 2014;86(2):200-11.

483. Merlusca IP, Matiut DS, Lisa G, Silion M, Gradinaru L, Oprea S, et al. Preparation and characterization of chitosan–poly(vinyl alcohol)–neomycin sulfate films. Polymer Bulletin. 2018;75(9):3971-86.

484. Chiu Y-H, Chen M-C, Wan S-W. Sodium Hyaluronate/Chitosan Composite Microneedles as a Single-Dose Intradermal Immunization System. Biomacromolecules. 2018;19(6):2278-85.

485. Dejaegher B, Vander Heyden Y. HILIC methods in pharmaceutical analysis. Journal of Separation Science. 2010;33(6-7):698-715.

486. Alpert AJ. Hydrophilic-interaction chromatography for the separation of peptides, nucleic acids and other polar compounds. Journal of Chromatography A. 1990;499:177-96.

487. Waters Corporation Thomas H. Walter Kenneth D. Berthelette Amit Patel Bonnie A. Alden Justin McLaughlin Jessica Field Nicole Lawrence Steve Shiner. Introducing Atlantis BEH Z-HILIC: A Zwitterionic Stationary Phase Based on Hybrid Organic/Inorganic Particles [Internet]. 2021 [January 2024]. Available from: https://www.waters.com/nextgen/us/en/library/application-notes/2021/introducing-atlantis-beh-z-hilic-a-zwitterionic-stationary-phase-based-on-hybrid-organic-inorganic-particles.html.

488. Sargent M. Guide to achieving reliable quantitative LC-MS measurements. First ed: RSC Analytical Methods Committee; 2013.

489. Kiontke A, Oliveira-Birkmeier A, Opitz A, Birkemeyer C. Electrospray Ionization Efficiency Is Dependent on Different Molecular Descriptors with Respect to Solvent pH and Instrumental Configuration. PLOS ONE. 2016;11(12):e0167502.

490. Sherwood CA, Eastham A, Lee LW, Risler J, Mirzaei H, Falkner JA, et al. Rapid Optimization of MRM-MS Instrument Parameters by Subtle Alteration of Precursor and Product m/z Targets. Journal of Proteome Research. 2009;8(7):3746-51.

491. Chinthakindi S, Kannan K. A liquid chromatography–tandem mass spectrometry method for the analysis of primary aromatic amines in human urine. Journal of Chromatography B. 2021;1180:122888.

492. Mokh S, Jaber F, Kouzayha A, Budzinski H, Al Iskandarani M, Mokh S. Optimization and Comparisons for Separation, Detection and Quantification of 12 Aminoglycosides Using 2 Chromatographic Conditions by LC-MS/MS. American Journal of Analytical Chemistry. 2014;5:982-94.

493. Boerman MA, Roozen E, Sánchez-Fernández MJ, Keereweer AR, Félix Lanao RP, Bender JCME, et al. Next Generation Hemostatic Materials Based on NHS-Ester Functionalized Poly(2-oxazoline)s. Biomacromolecules. 2017;18(8):2529-38.

494. Hoogenboom R. The future of poly(2-oxazoline)s. European Polymer Journal. 2022;179:111521.

495. Akoumeh R, Elzein T, Martínez-Campos E, Reviriego F, Rodríguez-Hernández J. Fabrication of porous films from immiscible polymer blends: Role of the surface structure on the cell adhesion. Polymer Testing. 2020;91:106797.

496. Peng K, Vora LK, Tekko IA, Permana AD, Domínguez-Robles J, Ramadon D, et al. Dissolving microneedle patches loaded with amphotericin B microparticles for localised and sustained intradermal delivery: Potential for enhanced treatment of cutaneous fungal infections. Journal of Controlled Release. 2021;339:361-80.

497. F.D.A. FDA-Approved Dermal Fillers [April 2024]. Available from: https://www.fda.gov/medical-devices/aesthetic-cosmetic-devices/fda-approved-dermal-fillers.

498. Vicente-Pérez EM, Quinn HL, McAlister E, O'Neill S, Hanna L-A, Barry JG, et al. The Use of a Pressure-Indicating Sensor Film to Provide Feedback upon Hydrogel-Forming Microneedle Array Self-Application In Vivo. Pharmaceutical Research. 2016;33(12):3072-80.

499. Leone M, Van Oorschot BH, Nejadnik MR, Bocchino A, Rosato M, Kersten G, et al. Universal Applicator for Digitally-Controlled Pressing Force and Impact Velocity Insertion of Microneedles into Skin. Pharmaceutics. 2018;10(4):211.

500. Nguyen TT, Park JH. Human studies with microneedles for evaluation of their efficacy and safety. Expert Opinion on Drug Delivery. 2018;15(3):235-45.

501. RWG. Microneedle Array Patch Regulatory Working Group [April 2024]. Available from: https://www.microneedleregulatory.org/.

502. PATH. Microarray Patch Resources [April 2024]. Available from: https://www.path.org/who-we-are/programs/mdht/mapresources/.

503. FDA. Microneedling Devices [April 2024]. Available from: https://www.fda.gov/medical-devices/aesthetic-cosmetic-devices/microneedling-devices.